UNIVERSIDAD NACIONAL AUTÓNOMA DE MÉXICO

Instituto de Geología

POSGRADO EN CIENCIAS DE LA TIERRA

Petrogénesis y Extrusión de rocas de Alta Presión (facies esquisto azul-eclogita) en la porción oeste del Complejo Acatlán, Ixcamilpa de Guerrero, Pue., sur de México

T E S I S

QUE COMO REQUISITO PARCIAL PARA OBTENER EL GRADO DE:
DOCTOR E N C I E N C I A S DE LA TIERRA

P R E S E N T A

Ramos Arias Mario Alfredo

JURADO:
Dr. Fernando Ortega Gutiérrez
Dr. John Duncan Keppie
Dr. Luigi Solari Lovati
Dr. Peter Schaaf
Dr. Michelangelo Martini

UNAM POSGRADO Ciencias de la Tierra

C.U. MÉXICO D.F., Octubre 2011

A Ximena….

…….tus ojos son la luz y brújula en la tempestad…

…..tu risa el destello feliz en mi alma.

Debo agradecer en primer lugar al Instituto de Geología y al Posgrado en Ciencias de la Tierra por la enriquecedora estadía científica a lo largo de estos años, contribución importante en mi desarrollo académico y humano, además del reconocimiento a la UNAM, como institución de nobleza, rincón de México donde impera la igualdad y libertad.

Gracias a CONACyT, por la beca otorgada, esperando que hoy y en el futuro retribuir la confianza e inversión en el capital humano mexicano.

De igual forma, gracias al programa PAPIIT, vía mi asesor de tesis, ya que me permitió completar las campañas, preparación de muestras y estudios pertinentes.

Guardo especial gratitud hacia el Dr. Duncan, por compartir su conocimiento, metodología y amistad, gracias por dejarme apreciar la Tectónica de Placas desde su perspectiva, sueño de mi infancia, plasmado en realidad desde el campo, en las aulas, los mapas, los modelos y los artículos, para mí todo ello es tesoro invaluable. Agradezco los enriquecedores comentarios de los sinodales: Dr. Fernando, Dr. Luigi, Dr. Peter, Dr. Michelangelo, me ha permitido dimensionar mi trabajo.

A mis compañeros de barranca: Carlos, Rosalva, Gonzalo, Judith, Fabián, gracias por unirse a las jornadas de cañadas con agua y tardes a 40°, en los sepias y verdes de Ixcamilpa, por su amena compañía y charlas de enorme valor.

Gracias por el soporte técnico para la obtención de fechamientos, parte columnar del trabajo, a: Dr. V. Valencia, Dr. L. Solari y M. en C. C. Ortega, en la técnica U-Pb en Tucson y Juriquilla. Y Dr. J. Lee, y Dra. A. Ortega por las mesetas de Ar-Ar en Queens University y Ensenada. De igual manera a los amigos del LUGIS y separación de minerales: Consuelo, Teo, Vianney y Daniel, por la paciencia y ayuda en la obtención de minerales. A Carlos Linares, JL Arce y Karina, por el apoyo en la preparación de láminas pulidas, obtención y análisis de datos durante las sesiones de microsonda en el LUP, y con ello realizar la geotermobarometría.

Especial gratitud y cariño a mis amigos: a Ross, por tu entendimiento y compañía en los días de guardia obscura; a Carlos, por la crítica con humor y trabajo duro. A Berlaine, por ser el ancla objetiva en todos los aspectos. Gracias Judith, por tu bondad y enorme calidad humana, me permite recordar que siempre hay luz en las personas; a Val, por tu comprensión y solidaridad; a Sandra y Fabián, por tardes de risa, momentos amenos y de empatía. A Daniel y Gonzalo, noches de futbol y días de camaradería. En el inicio del ciclo, a Carlitos, Josué, Oris, Emilio y Miguel, compartimos bastantes momentos de alegría. A Ceci, con tu gusto y dedicación, solo me queda imitarte. Gracias Lau, por la vertiginosa amistad, compartir tu familiaridad y contagiar la buena actitud. A Mar, por tu amistad incondicional. A mis amigos viejos: Ale, Isma, Mauro, Kary, Carlos, va por ustedes también desde el exilio.

Mi sangre es la sangre de hombres y mujeres que labraron la tierra, que adoraron al sol y que amaron la lluvia, contemplaron conmovidos las nubes abrazando montañas. Ancestros que sintieron la arena bajo sus pies, subían los cerros, usaban cada árbol y matorral, jugaban con el viento y cantaban ecos en las barrancas. En el crepúsculo, al asomar las estrellas y el conejo de la luna tal vez tuvieron el mismo sentimiento de cuan pequeña es la vida de un hombre en la inmensidad del mundo… pienso al unísono que igual de inmensos son los sueños en el corazón humano.

Gracias a mi familia por igual, ellos son el eslabón con mis ancestros, son la tradición oral, son el respeto por la naturaleza, el amor al trabajo, a los semejantes y a la tierra en que nací. Hacia ellos dedico mi esfuerzo. Amigos y familia son mi patria… ayer, hoy y mañana me vuelvo uno.

Índice **Pag.**

Índice de Tablas **Pag.**

Índice de Figuras

Capítulo 4

Capítulo 5

Resumen

Las rocas de alta presión son críticas para las reconstrucciones paleogeográficas, ya que ocurren comúnmente en un ambiente de subducción; por lo tanto, el conocimiento de su geometría, geodinámica y geocronología son esenciales para interpretaciones tectónicas. Cartográficamente existen dos cinturones metamórficos con rocas de alta presión en el Complejo Acatlán: uno intermedio llamado Piaxtla-Mimilulco, y otro más occidental denominado Ixcamilpa-Olinalá, éste último ha sido interpretado como una cuenca tras-arco del Ordovícico medio-tardío, posicionada en el margen sur del Océano Iapetus, la cual fue sujeta a subducción y fue emplazada debajo de Laurencia durante la colisión con Gondwana, hacia el Silúrico temprano.

No obstante, nueva cartografía geológico-estructural ha revelado que las rocas metamórficas de alto grado en Ixcamilpa ocurren en un *klippe* con vergencia hacia el W-NW, formado durante polifase de deformación, este conjunto de rocas incluye:

(a) Ensamble Piaxtla (Neoproterozoico-Ordovícico), consiste en meta-sammitas, meta-pelitas y cuerpos de meta-basitas, que han sido deformados bajo condiciones metamórficas de facies de esquisto azul-eclogita anfibolita, y que fueron afectadas por retrogresión posicionándoles en facies de anfibolita-esquisto verde.

(b) Los meta-sedimentos y meta-basitas son intrusionados por granitoides megacristalinos (Cámbrico-Ordovícico) y son afectados por la deformación en conjunto con los metasedimentos;

(c) este ensamble de alto grado sobreyace en forma de cabalgadura con vergencia hacia el W sobre la Unidad Zumpango (Carbonífero) conformada por rocas cuarcíticas, meta-sammitas y cenizas volcánicas.

Análisis de zircones detríticos por LA-ICPMS en el sistema U-Pb ha arrojado picos poblacionales con las siguientes edades:

(i) 435-490 Ma, probablemente derivados de los granitoides distribuidos en el Complejo Acatlán,

(ii) 500-700 Ma, comúnmente derivados del bloque de Yucatán y orógenos brasileños,

(iii) 800-900 Ma, con procedencia del Arco Goiás en el este de Amazonia, y

(iv) 950-1300 Ma, con la fuente más probable de Oaxaquia o Amazonia;

(v) para la Unidad Zumpango, los zircones detríticos más jóvenes son de 310-360 Ma, y se interpretan como proveniencia local del Complejo Acatlán.

El depósito de rocas con fuentes neoproterozoicas-ordovícicas se infiere que tiene lugar en el margen sur del Océano Réico adyacente a Oaxaquia/Amazonia, mientras que las rocas carboníferas fueron depositadas en el margen oeste de Pangea.

Por otra parte, se han efectuado fechamientos por el método $^{40}Ar/^{39}Ar$ para minerales inmersos en la fábrica de la deformación de las rocas de alto grado, los cuales han dejado mesetas de 344-339 Ma para anfíbol, 318 ± 4 Ma para glaucofano, y 329-325 ± 2 Ma para muscovita; el intervalo de 20 Ma para dichas mesetas $^{40}Ar/^{39}Ar$, se interpreta en términos de extrusión dúctil progresiva. La etapa terminal del emplazamiento es el posicionamiento de las rocas de alta presión sobre la Unidad Zumpango durante el Misisípico; al final de este periodo, se produce un clivaje penetrativo en facies de sub-esquisto verde. Subsecuentemente las unidades de alto y bajo grado son replegadas conjuntamente, configurando pliegues métricos/kilométricos sub-verticales, con el tren de eje de pliegues hacia el SW, la estructura mayor a su vez es afectada por un fallamiento frágil-transtensivo del Cenozoico, posicionando a las unidades en su configuración actual.

Las rocas del área de Ixcamilpa tienen equivalencias litológicas, geoquímicas y geocronológicas con aquellas otras del cinturón intermedio Piaxtla-Mimilulco. Los protolitos ígneos máficos para ambos cinturones definen firmas geoquímicas subalcalinas-toleíticas y parecen estar ligados a un magmatismo bimodal; en suma, las fábricas de deformación en condiciones de alta presión han sido fechadas en tiempos Misisípicos. Cabe mencionar que el límite oriental del cinturón intermedio consiste de una estructura de cizalla normal dúctil desarrollada entre los ~337 Ma (sección Las Minas-Patlanoaya) y la estructura en Ixcamilpa es la raíz de una napa, este hecho es consistente con una zona de extrusión dúctil con cima en fallamiento normal y base con falla inversa.

La subducción tiene lugar en el margen noroeste de Gondwana, donde muy posiblemente los protolitos de rift-margen pasivo ordovícicos adyacentes a Oaxaquia, entraron en la zona de subducción y subsecuentemente extruido en la parte superior de la corteza en tiempos carboníferos. El presente trabajo provee de nuevos datos que permiten hacer reevaluaciones sobre la reconstrucción paleo-geográfica, donde una zona de extrusión dúctil está limitada en ambos lados por unidades similares (unidades, Zumpango, Progreso, Salada). Es posible que las rocas de alto grado se hayan emplazado en la corteza superior en una zona de extrusión dúctil y su naturaleza no marcaría del todo una sutura oceánica.

Abstract

High pressure rocks are critics for paleogeographic reconstructions, because occur mainly in subduction settings; by this, knowledge of its geometry, geodynamic, and geochronology are essentials for tectonic interpretations. Cartographically exist two metamorphic belts with high pressure rocks in Acatlán Complex: one intermeddle named Piaxtla –Mimilulco, and other western named Ixcamilpa-Olinalá. The last one has been interpreted like a back arc basin of middle-late Ordovician, positioned in the southern limit of Iapetus Ocean, which was subject to subduction and was emplaced beneath Laurentia during collision with Gondwana until early Silurian.

However, new geologic-structural cartography has revealed that high pressure metamorphic rocks in Ixcamilpa area occur in one klippe with top to the W-NW, formed during deformation polyphase, this assemblage of rocks include:

a)Piaxtla Suite (Neoproterozoic-Ordovician), consist of meta-psammites, meta-pelites and meta-basites bodies, that has been deformed together under metamorphic conditions of blueschist- eclogite amphibolites facies and were overprinted by retrogression metamorphism in amphibolites-greenschist facies.

b) meta-sediments and meta-basites are intruded by megacrystic granitoids (Cambric- Ordovician) and were deformed together with meta-sediments;

c) This assemblage in high/middle grade thrust with top to the W at Zumpango Unit (Carboniferous) conformed by quartzitic, meta-psammitic and volcanic ash rocks.

Detrital zircon analyses by LA-ICPMS in U-Pb have yield peaks with ages in:

(i) 435-490 Ma, derived probably from granitoids distributed in Acatlán Complex,

(ii) 500-700 Ma, derived mainly from Yucatán Block and brasilian orogens,

(iii) 800-900 Ma, proceed from Goiás Arc in east Amazonia, and

(iv) 950-1300 Ma, with probably source from Oaxaquia or Amazonia;

(v) for Zumpango Unit, youngest detrital zircons are 310-360 Ma, and were interpreted like local provenance from Acatlán Complex.

The deposit of rocks with Neoproterozoic -Ordovician source were inferred placed into southern margin of Rheic Ocean juxtapose to Oaxaquia/Amazonia, and the carboniferous rocks were deposited in western margin of Pangea.

By other hand, were obtained ages by $^{40}Ar/^{39}Ar$ method for minerals in deformation fabric for high grade rocks, which yield plateaus of 344-339 Ma in amphibole, 318 ± 4 Ma in glaucophane, and 329-325 ± 2 Ma in muscovite; the interval of 20 Ma for this plateaus is interpreted in terms of progressive ductile extrusion. The last stage of emplacement is the placed of high pressure rocks over Zumpango Unit during Mississippian; at end of this period, it's produced penetrative cleavage in sub-greenschist facies. The next step is the refolding of high and low grade rocks, building metric/ kilometric upright folds, with fold axis in average trend at SW, major structure is affected by brittle-transtensive faulting of Cenozoic, which positioned the units in actual configuration.

The rocks of Ixcamilpa area have lithological, geochemical and geochronological equivalences with those from intermeddle belt Piaxtla-Mimilulco. The mafic igneous protoliths in both belts define geochemical signatures sub-alkaline tholeiite and are related to bimodal magmatism; in addition, the fabrics of deformation in high pressure conditions have been dated in Mississippian times. Oriental boundary of intermeddle belt consist of ductile shear zone structure development between ~337 Ma (Las Minas-Patlanoaya section) and the structure in Ixcamilpa is a nape, this fact is consistent with one ductile extrusion zone with normal faulting at top and thrust at base.

The subduction have placed in northwestern margin of Gondwana, where possibly the protoliths of Ordovician rift- passive margin are juxtaposed to Oaxaquia, get inside subduction zone, and subsecuently extruded into upper crust during Carboniferous. Present work provide of new data that allow make reevaluations about paleogeographic reconstruction, where one ductile extrusion zone its limited in both sides by similar units (Zumpango, Progreso, Salada). Then, it's possible that high pressure rocks have been emplaced into upper crust in one ductile extrusion zone and its nature don't mark one oceanic suture strictly.

Capítulo 1

Introducción:

Conceptos y generalidades de extrusión de rocas de Alta Presión,
Extrusión de rocas de alta presión en el Complejo Acatlán

El Complejo Acatlán se constituye como un bloque relicto de rocas paleozoicas dentro de los basamentos cristalinos en el sur de México, forma parte del Terreno Mixteca (Campa y Coney, 1983; Sedlock et al., 1993; Keppie et al., 2004a). Contiene una diversidad de litologías con grado metamórfico y deformación variables. Dentro de este conjunto de rocas polideformadas existen ensambles de rocas en alta presión en facies de esquisto azul y de eclogita-anfibolita con retrogresión en facies de esquisto verde. Las rocas de alta presión y el rol que juegan dentro de las zonas de subducción es un tópico con enorme controversia en la comunidad geológica; la presencia de rocas que fueron sepultadas más allá de los 40 km y que en este momento se encuentran en condiciones superficiales, establece uno de los mayores paradigmas para la geología.

Desde los trabajos pioneros hace ya más de 30 años (Ortega Gutiérrez, 1974; 1978) hasta los estudios recientes, el Complejo Acatlán se erige como uno de los laboratorios naturales en los cuales la tectónica de placas presenta el testimonio de las zonas de subducción; dado su complejidad merece reclamar relevancia y un lugar dentro de los debates geológicos del mundo.

Conceptos y Generalidades de Extrusión de Rocas de Alta Presión

Hacia 1961, Miyashiro ya había publicado su célebre trabajo de paridad de cinturones en zonas de subducción, desde entonces se han efectuado revisiones extensas para el metamorfismo de alta presión, pasando el umbral de los 10 Kbar, el cual denota un sepultamiento superior a los ~30 km. Existe una variedad de escenarios tectónicos donde se tiene reportada la extrusión de rocas de alta presión, los cuales incluyen ambientes de: i) rift oceánico y continental; ii) zonas de fallas transforme (Ring et al., 1999); y iii) **zonas de subducción oceánica y colisión continental**, estos últimos, constituyen los ambientes tectónicos más significativos y complejos, ya que exponen una gran variedad de rocas exhumadas desde diferentes niveles corticales (Liou et al., 2004; Ernst y Liuo 2008 y Ernst, 2008).

La frontera que delimita la formación de rocas metamórficas de alta y ultra-alta presión es la curva de equilibrio entre cuarzo y coesita-diamante en un rango de presión entre los 2.8-5 GPa; ello implica que el metamorfismo de ultra-alta presión debió ocurrir en un rango de ~80-150 km de profundidad, donde la corteza continental con ~2.8 g/cm^3 de densidad es subducida dentro del material mantélico de ~3.3g/cm^3 (Liou et al., 2004). Mientras que el metamorfismo de alta presión ocurrirá en profundidades de un orden de 40 a 100 km (Figura 1.1).

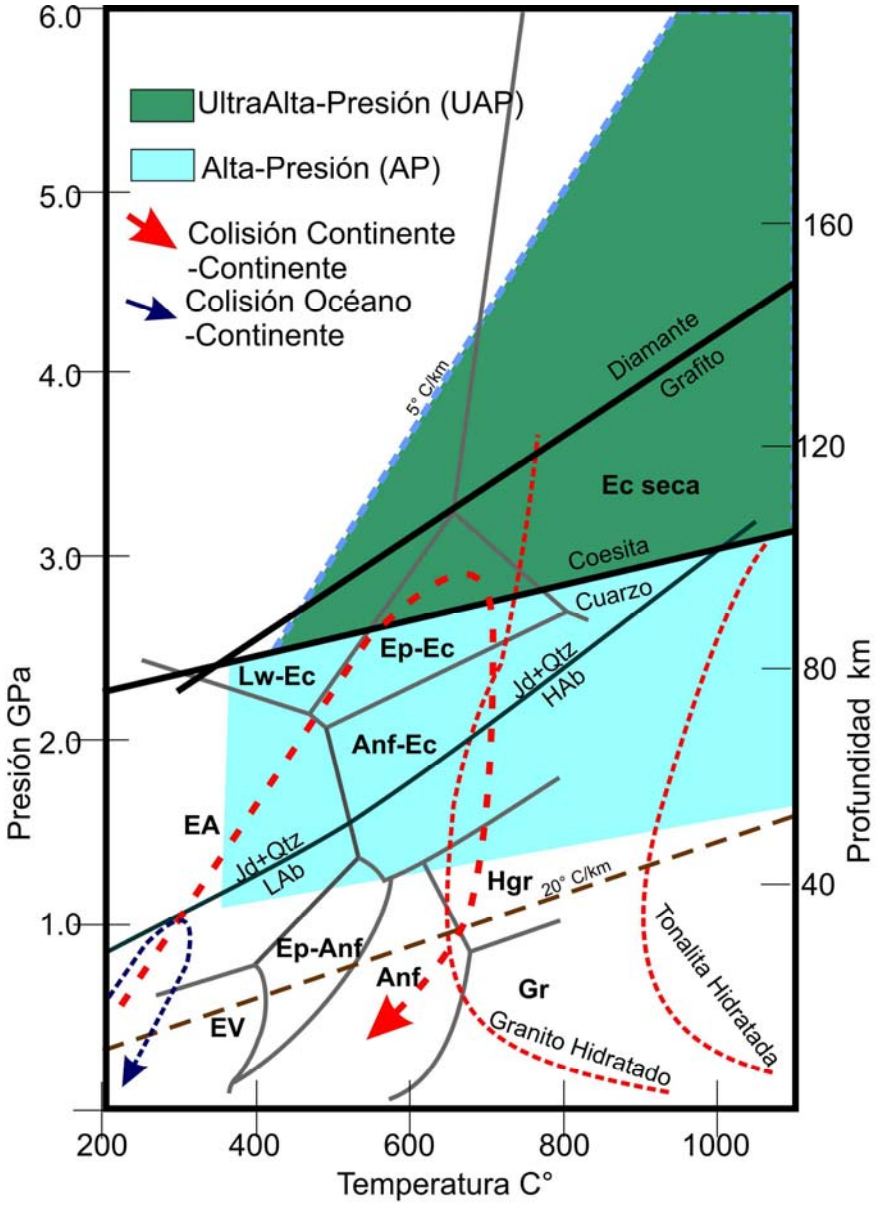

Figura 1.1. Diagrama P vs T con campos de facies metamórficas y líneas de estabilidad mineral, Jd+Qtz=Ab, Coesita-Cuarzo, Diamante-Grafito; curvas de fusión de granito hidratado, tonalita hidratada; gradiente de temperatura a 20 °C/km y 5 C°/km, y ejemplos de trayectorias para colisiones continentales (rojo) y colisión Oceano-Continente (azul). Tomado de Liou et al. (2004); Ernst y Liou (2008) más referencias y abreviaciones: Lw: Lawsonita, Ec: Eclogita, Ep: Epidota, Anf: Anfibolita, EV: Esquisto verde, EA: Esquisto Azul, Jd: Jadeita, Qtz: Cuarzo, HAb: Albita Alta, LAb: Albita Baja, Gr: Granulita, HGr: Granulita Alta.

La extrusión de rocas, es un término ampliamente relacionado a procesos volcánicos; no obstante, la base del concepto de extrusión implica expeler, expulsar o exhumar rocas que se encuentran en el interior de la corteza. La extrusión de rocas metamórficas de alta presión es un problema poco entendido, y evidentemente requiere la remoción de las masas rocosas sobreyacientes, o bien, el transporte de las rocas de alta presión a través de estos mismos cuerpos superiores hacia posiciones someras (Platt,

1993). Se pensaba que mecanismos como las napas o fallas laterales con transpresión por si solas podían traer de vuelta a la superficie dichos ensambles metamórficos, aunado al acortamiento horizontal y engrosamiento vertical cortical; no obstante, estos mecanismos pueden ser acompañados o asistidos por otros procesos (Platt, 1993; Grujic et al., 1996; Chemeda et al., 1996; Hynes, 2002; Godin et al., 2006).

La **extrusión** de rocas metamórficas es un proceso que sincroniza el movimiento de bloques rocosos en profundidad dentro del flujo de canal de subducción; se activa principalmente por las **fuerzas de flotabilidad,** ya que existen contrastes de densidad entre piezas corticales subducidas y la zona del manto sub-litosférico, con movimientos de masa simultáneos y superficiales en la corteza como son la **exhumación**, **el levantamiento y la erosión**. La arquitectura primordial es una zona restringida por dos límites de falla (Figura 1.2): una **superior con componente de cizalla normal** y otra **inferior con componente de cizalla inversa** (Platt, 1993; Grujic et al., 1996; Chemeda et al., 1996; Hynes, 2002). El sistema de fallas inversas imbrican y engrosan la base de la corteza (***underthrusting***), inclusive en la base de zonas de falla puede incorporarse volúmenes de material mantélico (***underplating)***; en consecuencia se produce **el flujo de canal** que asciende hasta la superficie como una extrusión dúctil.

El **flujo en canal de subducción** es un sistema donde un material rocoso confinado entre dos placas relativamente rígidas, superior e inferior, se comporta físicamente como fluido viscoso; dicho fluido es deformado por una cizalla, inducida mediante un esfuerzo deviatórico. En otras palabras, se trata de una masa de baja competencia que fluye verticalmente debido a gradientes laterales de presión litostática más de presión horizontal; y que traducido a un contexto tectónico, predominan fuerzas de gravedad y convergencia asociadas a las masas continentales con desarrollo directo en una zona de subducción (Turcotte y Schubert, 2002; Gerya y Stöckhert, 2002; Godin et al. 2006).

Ahora bien, el flujo consiste de la suma de dos componentes de cizalla: simple y pura, expresados como la velocidad del flujo en un canal de subducción:

Velocidad= ω_c (Flujo Couette) + ω_p (Flujo Poisseuile)

la primera explica una vorticidad uniforme dentro del canal, mientras que la segunda explica un mayor flujo en el núcleo del canal, a su vez que en las partes exteriores va en decremento (Figura 1.2) (Mancktelow, 1995; Godin et la., 2006; Jessup et al., 2006).

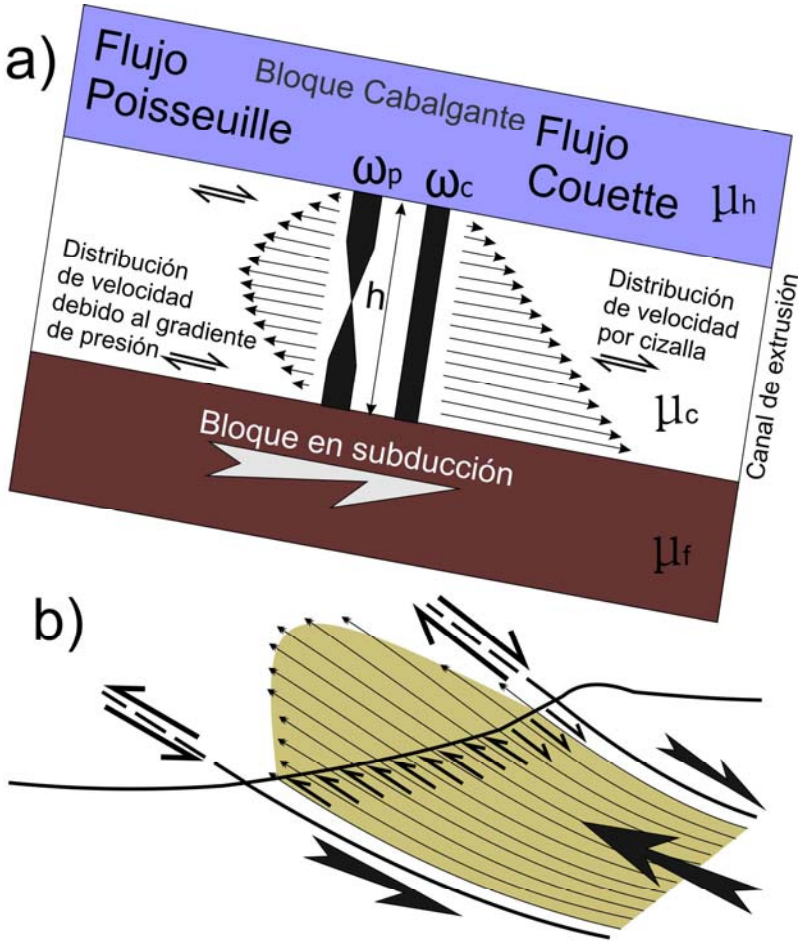

Figura 1.2. a) Diagrama que muestra el patrón de flujo en un canal de extrusión de amplitud h. La viscosidad del material en el canal decrece en el centro (μh>μc<μf), por lo tanto, la distribución interna de velocidades se muestran en diferencia relativa con respecto el bloque de techo; es importante remarcar, que existe una baja velocidad interna en la parte superior del canal de extrusión, a la postre, esta diferencia producirá una zona de cizalla normal. Es representado el flujo Couette como producto de la cizalla (esencialmente cizalla simple) y el Flujo Poiseuille como la cizalla pura, que en su conjunto denotan la vorticidad. b) Extrusión de un bloque dúctil, fallamiento discreto en los bordes, facilita la extrusión, combinación de cizalla simple y cizalla pura, el flujo interno tiene diferencias desde la cima a la base dado que existen distintos campos de velocidades (tomado de Grujic et al., 2002; Godin et al., 2006 y más referencias).

El flujo del material en el canal de subducción se puede visualizar como un modelo geodinámico, que sincroniza procesos de movimiento dúctil en el núcleo de un orógeno de colisión (corteza inferior/intermedia), en conjunto con el flujo y extensión en la parte somera (corteza superior); es decir, el flujo se traslada desde corteza profunda en un régimen estructural eminentemente dúctil hasta condiciones de corteza superior en un régimen dúctil-frágil (Ring et al., 1999).

El motor principal del flujo en la extrusión, son las **fuerzas de flotabilidad** (Platt, 1993). El fenómeno de la ruptura o delaminación cortical constituye la explicación más sencilla, donde la fuerza con que se jala a la placa en subducción puede reducirse notablemente al ser arrancada la placa en subducción, con efecto inmediato en el levantamiento desde medios relativamente más densos. Éste es un mecanismo funcional para explicar la exhumación de piezas corticales subducidas dentro del manto; sin embargo, el contexto del ambiente de subducción tiene implicaciones más complejas.

Si se observa que muchos bloques de rocas de alta presión se encuentran en contigüidad de bloques de bajo/nulo grado metamórfico, es muy probable que los bloques de alta presión pudieron haber sido emplazados mediante **diapirismo** (Miyashiro, 1961). Los cuerpos serpentiníticos tendrían un comportamiento mecánico análogo a lodos de baja densidad sometidos a cargas hidrostáticas o litostáticas, con tendencia a fluir hacia gradientes de presión más bajos.

A menudo se encuentran diapiros serpentiníticos en la parte del ante-arco asociados con esquisto azul, yuxtapuestos con el piso oceánico (ejemplo: Las Marianas). La presencia de material mantélico en niveles someros, indicaría que la hidratación de cuñas orogénicas es un mecanismo significativo para disparar la flotabilidad negativa. Existen muchos otros casos de rocas en facies de esquisto azul–eclogita ensamblados como piezas ofiolíticas, intercaladas con cuerpos ultramáficos hidratados; para Ernst (1975), se trata de una evidencia clara del ambiente de subducción de placa oceánica que hidrata al manto.

La **flotabilidad** por hidratación del manto puede entenderse si se piensa que la exhumación de rocas mantélicas y de alta presión en la cuña de acreción se debe al incremento de volumen y la caída de la densidad causada por la **serpentinización** (Miyashiro, 1961, 1972). De igual forma, la presencia de **sedimentos en la subducción** es otro factor que contribuye con la flotabilidad; dado que tienen menor densidad relativa con respecto al manto, es posible que se desacoplen de la placa en subducción desde profundidades de ~100 km, y por tanto regresar y emplazarse en la litósfera por debajo del tras-arco (el tras-arco es el lugar tectónico donde existe corteza débil, atenuada y/o adelgazada). El ascenso del material sedimentario asemejaría a una

pluma que se distribuye lateralmente cientos de kilómetros, resultando en un desequilibrio mecánico y contribuyendo al adelgazamiento litosférico y levantamiento de otras piezas en posiciones más someras (Currie et al., 2007).

Algunos modelos ponderan la contribución de la flotabilidad, flujo interno del canal y expulsión tipo émbolo ó pistón, considerándoles procesos que actúan de manera sincrónica en casi todos los ambientes de extrusión. La predominancia relativa de cada modelo obedece al papel que juega la geometría, la densidad del material y el grosor cortical, tanto de corteza como de manto; de igual manera, la edad, ángulo de la placa en subducción y velocidad de convergencia pueden considerarse como factores cambiantes a lo largo de la historia geodinámica del orógeno.

Para Warren et al. (2008), es posible reconocer tres estilos en la extrusión: **(i)** El primero por flotabilidad; es favorecido principalmente por el contraste entre la alta densidad del manto litosférico y baja densidad cortical, en el instante mismo en que son introducidas piezas corticales en el canal de subducción (Figura 1.3a). **(ii)** Un segundo modelo explica esencialmente la circulación de material dentro del canal; debido a la tracción de la placa en subducción, se incorpora material al canal y regresa hacia posiciones someras, completando un ciclo de ingresar y desocupar volumen de rocas dentro del espacio confinado entre las placas (Figura 1.3b). **(iii)** El último estilo de extrusión es identificado como un émbolo o pistón, donde una corteza continental y el manto subyacente funcionan como contrafuerte magnificado, obligando a regresar a la superficie a una placa en subducción relativamente más débil (Figura 1.3c).

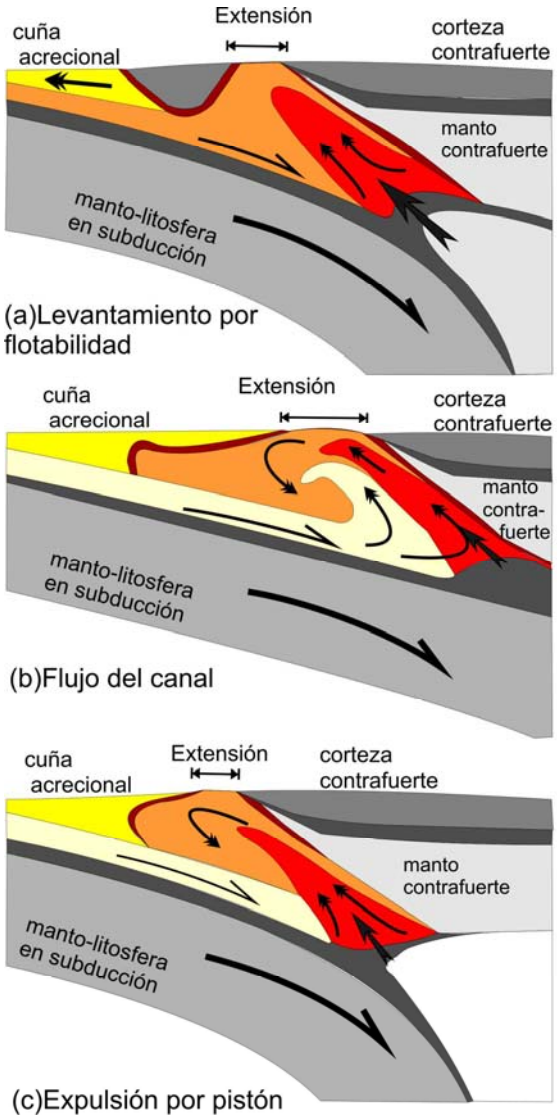

Figura 1.3. Modelos de extrusión de rocas de alta presión tomados de Warren et al., 2008: a) M1: Levantamiento por flotabilidad; la energía de flotabilidad se acumula en la base del canal, en conjunto con el material continental que se ha desacoplado de la placa en subducción, el levantamiento comienza cuando existe la etapa de rollback de la placa en subducción ya que la corteza superior tiene una debilidad, la extrusión es asistida por la remoción de capas sobreyacientes por la circulación dentro del canal, el cual extiende y adelgaza la corteza superior, traslada la energía a la cuña acrecional, naturalmente se pliega el interior del orógeno y es posible que la exhumación ocurra sin mucha erosión. b) M2: Flujo de material dentro del canal; este proceso es manejado por el flujo del material, la circulación desde altas profundidades e incorporando niveles someros; es dirigido esencialmente por la tracción de la placa en subducción. La flotabilidad actúa en la base del canal por lo que el material regresa a posiciones someras una vez que ha sido desacoplado de la placa en subducción. c) M3 expulsión por pistón; una corteza continental relativamente rígida se encuentra en la base del canal, actúa como contrafuerte, por lo que expele el material de alta presión en el canal.

La capacidad de flujo en el canal tiende a reducirse notablemente en zonas someras por la denudación y el enfriamiento, con efecto inmediato en las propiedades viscosas del material. El enfriamiento ocurre durante el ascenso de la placa o cuña de extrusión, por lo cual la deformación se particiona en fallas discretas y no como zonas de cizalla dúctil extensas (Godin et la., 2006).

La contraparte del proceso de acreción por debajo de la raíz cortical es la **extensión;** la existencia de este mecanismo controla el balance de fuerzas asociadas con el contraste de elevación en la superficie (reacciones isostáticas); se posiciona en la parte superior donde ocurre el emplazamiento y se manifiesta mediante un núcleo metamórfico (*core complex*), o bien, **fallamiento lístrico dúctil,** por lo que se efectúa una partición

de la deformación dependiendo del nivel estructural. La extensión cortical, podría ser acompañada por fusión (leucosomas), si es el caso de una descompresión súbita del terreno metamórfico.

Por otra parte, la generación de **fallas laterales** facilita de manera importante el reacomodo de bloques corticales someros; se asume que existen regiones en la corteza que modificaron su régimen de fallamiento, al pasar de fallas con movimientos inversos a fallas con rampas laterales (Housman y England 1986); ejemplos conocidos es el arreglo de fallas conjugado en el Tíbet, produciéndose una extensión ESE-WNW aunque la compresión regional en el orógeno sea N-S, permitiendo un sistema de reacomodo tectónico.

También se asume que la sobrepresiones y movimientos son propiciados por una componente de esfuerzos deviatóricos focalizados (Burov et al., 2001 y más referencias); y que en algunas zonas son bastante magnificados actuando como un pistón, de tal forma que es posible reproducir sobrepresiones de corteza inferior en condiciones corticales más someras-intermedias y frías (de entre 20 a 40 km). También se piensa que con base en el posicionamiento de la isograda de estabilidad de **coesita-diamante**, existen dos niveles corticales en los cuales el flujo de canal tiene a lugar, es decir, dos celdas de flujo independiente: Uno somero con circulación del complejo acrecional (ensambles metamórficos de alta presión), y otro profundo, donde la circulación en presiones altas es propicia para la formación de rocas eclogíticas de presión ultra-alta (Agard et al. 2009). No obstante, la interacción en la frontera entre estos dos niveles es poco entendida y debatible, ya que existen lentes de rocas de ultra-presión rodeados de rocas formadas en condiciones intermedias-someras.

Recientemente, autores como Liou et al. (2004), seguidos por Ernst et al. (2008), Ernst y Liou (2008), han revisado los cinturones metamórficos de alta y ultra-alta presión relacionándolos con los **ambientes tectónicos** en los que estos ocurren y clasificándolos en dos tipos dependiendo de las características del protolito:

a) **Márgenes de colisión Continente-Continente (Tipo Himalaya)**: incluye complejos basales continentales y sedimentos volcaniclásticos sobreyacientes

provenientes de una amplia variedad de ambientes tectónicos; el basamento carece de características oceánicas y tiene una mayor extensión. La extrusión proviene desde las raíces orogénicas en campos de presión alta/ultra-alta; se activa por imbricación de las raíces corticales en la zona sub-continental (>80-150 km). Si se toma a los Himalayas como un ejemplo clásico de colisiones continentales, las montañas se construyen mediante *underthrusting* y el levantamiento ocurre en un intervalo de 11 Ma, donde la placa Índica subduce por debajo de la placa Asiática (Figura 1.4a).

b) **Márgenes de colisión Océano-Continente (Tipo Pacífico)**: consiste en rocas formando complejos acrecionales, con protolitos eminentemente oceánicos, incluyendo paquetes de pedernales, meta-basitas de origen MORB y fragmentos de montes marinos, que además suelen ser acompañados de turbiditas de trinchera. La extrusión se genera en una zona de subducción de la zona sub-continental, con la presencia de una cuenca de ante-arco, granitos, tonalitas trondhjemitas y el mismo arco volcánico. El material oceánico se desacopla de la placa oceánica en subducción y regresa a la superficie desde profundidades de entre 40 a 50 km hasta posicionarse en los 15-20 km. Es muy posible que los sedimentos depositados sobre las cuencas de ante-arco, directamente sobre la placa en subducción, vayan hacia abajo y consecuentemente pueden ser arrancados o despegados en el vértice del flujo donde las placas superior e inferior están en contacto (Figura 1.4b).

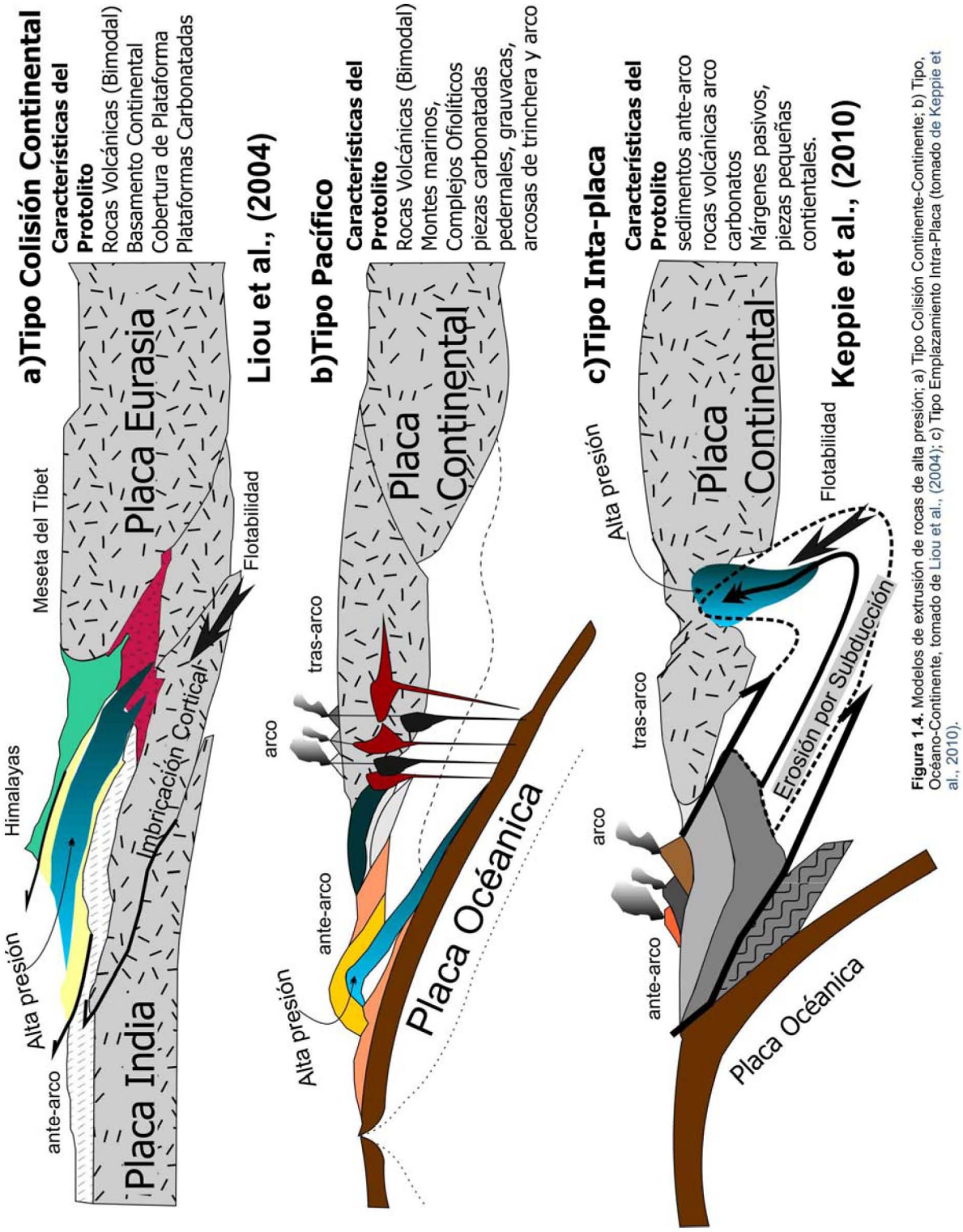

Figura 1.4. Modelos de extrusión de rocas de alta presión; a) Tipo Colisión Continente-Continente; b) Tipo, Océano-Continente, tomado de Liou et al., (2004); c) Tipo Emplazamiento Intra-Placa (tomado de Keppie et al., 2010).

Para el modelo Tipo Pacífico, Keppie et al. (2008b, 2010a 2010b), han propuesto una variante, donde el material de la corteza superior puede ser removido mediante **erosión por subducción**. En seguida, éste material se desacopla de la placa en subducción y

regresa por **flotabilidad**, emplazándose en la misma **placa superior** esencialmente por **extrusión** (Figura 1.4c). La erosión por subducción es un proceso que juega un papel importante, afectando la corteza continental localizada en márgenes continentales activos (von Huene y Scholl 1991), aseveración corroborada por los modelos numéricos de Stöckhert y Gerya, (2005); Gerya y Stöckhert, (2006); Castro y Gerya, (2007); Keppie et al., (2010).

Sin embargo, es necesaria la distinción entre los dos modelos; primordialmente, la extrusión de las rocas de alta presión en la **placa superior** significa tener un **registro geológico similar** en ambos lados del cinturón de extrusión, por lo que no es una sutura oceánica *sensu stricto.* Es decir, en el modelo de emplazamiento en la corteza superior, el material removido durante las etapas iniciales por la erosión-subducción es el **ante-arco, arco, tras-arco**, o bien, **márgenes pasivos** en el reinicio del ciclo orogénico; dichos elementos tectónicos regresan por flotabilidad y se emplazan en la misma placa cabalgante. Se asume que no existe una aloctonía del complejo acrecional, con la ausencia de una secuencia ofiolítica que delate su naturaleza oceánica. En el caso de ser una colisión Tipo Pacífico, existirían distintos registros faunísticos, cronológicos e inclusive paleomagnéticos para ambos lados en convergencia (Figura 1.4c).

Extrusión de Rocas de Alta Presión en el Complejo Acatlán.

En el Complejo Acatlán, existen dos cinturones de rocas de alto grado/presión: uno en la parte media denominado **Piaxtla-Mimilulco** y otro hacia el oeste **Ixcamilpa-Olinalá** (Figura 2.1). Ambos cinturones fueron inicialmente interpretados como suturas oceánicas por Ortega-Gutiérrez (1981); Ortega-Gutiérrez et al. (1999), destacando que rocas de alta presión fueron extruidas a lo largo de la zona de Falla de Caltepec (límite entre terrenos Mixteco y Zapoteco) y transportados hacia el oeste en una estructura de napa durante tiempos ordovícicos. La napa fue replegada en estructuras sinformes durante el Pérmico, en las cuales las rocas de alta presión están expuestas. Mientras que para Talavera Mendoza et al. (2005) y Vega-Granillo et al. (2007, 2009), existen relictos de cinco bloques oceánicos, incluidas cuencas y arcos, dentro de historias geológicas de colisión entre Gondwana y Laurencia involucrando los océanos Iapetus y Réico (Figura 1.5). Por su parte, Keppie et al. (2008a) han propuesto que el cinturón de Piaxtla-Mimilulco fué extruido en la placa superior, y que por sus características no pertenece a

una sutura oceánica en sentido estricto. Dicha propuesta es respaldada por la similitud del registro geológico en ambos lados del cinturón de alta presión, criterio aplicable a la distinción para terrenos de alta presión emplazados en un margen Tipo Pacífico con la variante de Intraplaca (figura 1.4 b, c; Figura 1.6). (Keppie et al., 2010).

El término de **Ensamble ó *Suite* Piaxtla**, fué emitido inicialmente por Ramírez-Espinoza (2001) como reemplazo del término original de **Formación Xayacatlán** (Ortega-Gutiérrez, 1978), el cual agrupaba una diversidad de rocas de alto grado metamórfico en el Complejo Acatlán. Las rocas del cinturón Ixcamilpa-Olinalá fueron incluidas en la *Suite* Piaxtla por Ramírez-Espinoza (2001), Talavera-Mendoza et al. (2005), Keppie et al. (2008a, 2010) y Vega-Granillo et al. (2007, 2009). En el presente trabajo, las rocas de **alta presión de Ixcamilpa** siguen formando parte del **Ensamble Piaxtla**, esencialmente porque fué analizada la naturaleza del protolito (geocronología, geoquímica y metamorfismo), el cual tendría equivalencias litológicas con las demás rocas de alto grado a lo largo del Complejo Acatlán. No obstante, pudieron subdividirse unidades con características independientes y cartografiables, dado que existen contrastes litológicos, además de la "aparición" de minerales metamórficos, aunado a que existen límites y estilos estructurales; con tales distinciones fue posible mejorar la resolución cartográfica del Ensamble Piaxtla.

El cinturón de **Ixcamilpa-Olinalá**, ha sido interpretado estructuralmente de dos maneras (Figura 1.5):

(i) Como un *klippe* compuesto por una cuenca ante-arco del Ordovícico medio-tardío en el margen sur del Océano Iapetus que fué subducida por debajo de Laurencia y extruida en el canal de subducción durante el Ordovícico tardío-Silúrico temprano (Vega-Granillo et al., 2009); esta interpretación fue basada en la presencia de zircones detríticos con una edad aproximada de ~477 Ma, a su vez de la existencia de magmatismo granítico ordovícico, que en conjunto denotan una presencia de un arco, el cual se erigió simultáneo al metamorfismo durante una subducción hacia el cierre del Oceáno Iapetus en un periodo entre los 458–443 Ma; en seguida se sobrepone otro evento metamórfico, inferido por una meseta de fengita para el sistema $^{40}Ar/^{39}Ar$ en 323 ± 6 Ma, interpretado como otro evento de subducción durante el cierre del Océano Réico (Talavera-Mendoza et al., 2005; Vega-Granillo et al., 2007, 2009) (Figura 1.5).

O bien, **(ii)** una serie de bloques limitados por fallas del Cenozoico temprano, evidentes en el área de Olinalá, aunque inicialmente fueron deformados dúctilmente durante el Devónico tardío-Carbonífero temprano (Ortega-Obregón et al., 2009).

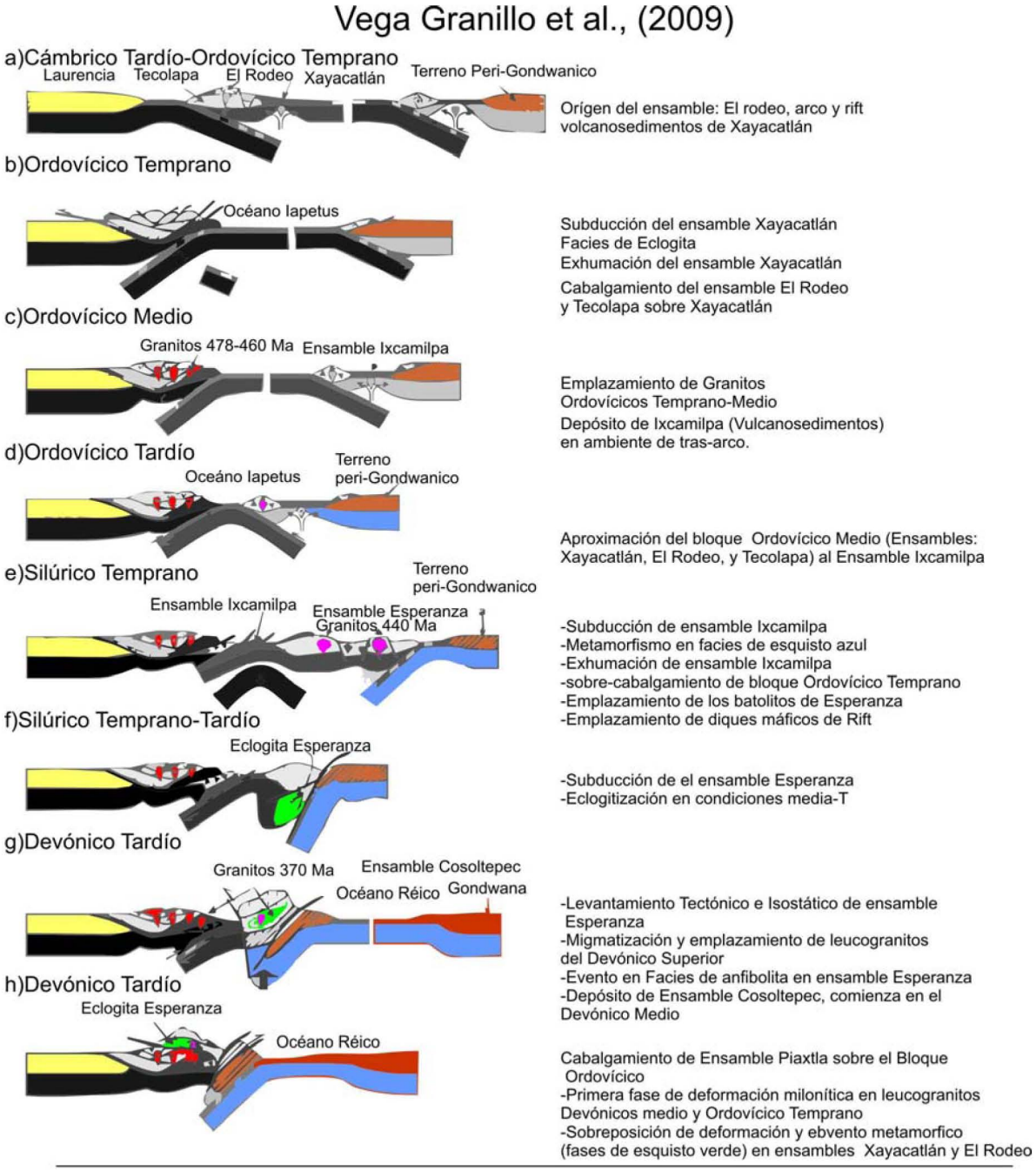

Figura 1.5. Modelos tectónicos para la generación de rocas de alta-presión en el Complejo Acatlán. (Tomado de Vega Granillo et al., 2009)

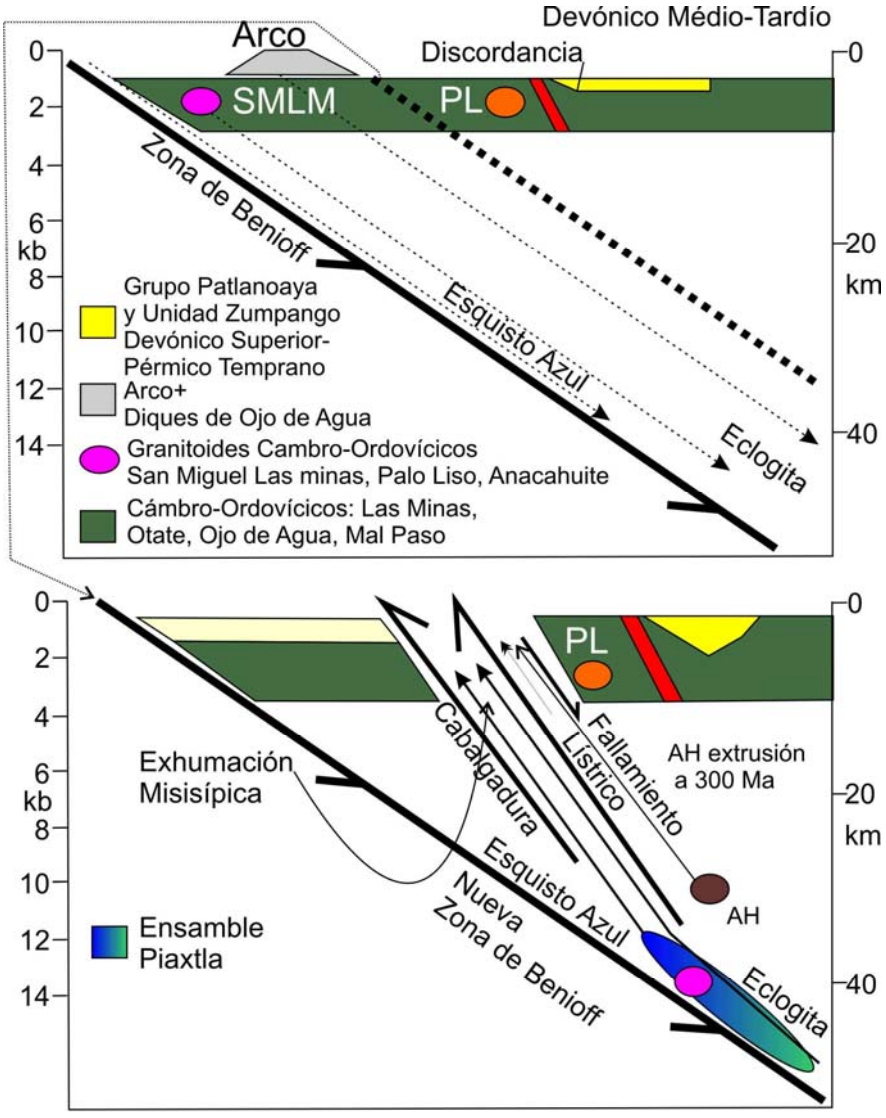

Figura 1.6 Modelo W-E que muestra: a) erosión por subducción del margen pasivo y rocas del arco de la placa superior, durante Devónico medio-superior: seguida de b) metamorfismo de alta presión y extrusión en la placa superior. (modificado de Keppie et al., 2010a)

Dada la existencia de interpretaciones contrastantes, es necesario entender en primer término la temporalidad, naturaleza y origen del protolito; para posteriormente describir y desglosar la geometría y evolución estructural, resolviendo el tiempo para el metamorfismo de alta presión, y de esta manera catalogar el ambiente tectónico en el cuál ocurrió su emplazamiento. La revisión del registro geológico en el área de Ixcamilpa incluye:

El **Capítulo 2** (Ramos Arias y Keppie, 2010), que pretende precisar la **geocronología del protolito** mediante mapas detallados geológico-estructurales del oeste del Complejo Acatlán, y acotar de manera clara el depósito de secuencias meta-

sedimentarias intrusionadas por cuerpos ígneos máficos y graníticos. Se construye una correlación de rocas del área de Ixcamilpa, en primer lugar con el área de Olinalá al sur, y posteriormente con aquellas otras zonas al norte y este del Complejo Acatlán donde afloran rocas de alta presión (Piaxtla-Asís, Mimilulco-Las Minas); a su vez que se discuten las procedencias potenciales y afinidades detríticas en un contexto regional y paleogeográfico.

El **Capítulo 3** (Ramos Arias et al., 2011), describe la **geometría, cinemática y temporalidad de la deformación**; si bien, rocas en facies de esquisto azul ya habían sido reportadas con anterioridad en el Complejo Acatlán, el presente trabajo ofrece avances en la descripción del metamorfismo en congruencia con eventos de deformación. Se discute el posicionamiento espacio-temporal de la fábrica de foliación y plegamiento, así como el inherente grado metamórfico alcanzado dentro del contexto y arquitectura de la extrusión de rocas de alta presión a lo largo del Complejo Acatlán; lo cual permite correlacionar y discutir características pertenecientes a algún ambiente tectónico en particular.

De forma complementaria se presenta el **Capítulo 4** (Keppie et al., 2010)**,** el cual expone la estructura y metamorfismo en facies de esquisto azul en la zona de San Miguel Las Minas-Patlanoaya, en la porción norte del Complejo Acatlán, con ello se pretende comparar la naturaleza y **temporalidad** del metamorfismo de alta presión de Ixcamilpa con las localidades inmersas en el cinturón intermedio de **Piaxtla-Mimilulco.**

Por último, se presenta el **Capítulo 5**, el cuál engloba la **correlación y discusión** de la naturaleza del protolito de las rocas de alta presión en Ixcamilpa, el contexto en el cuál la geocronología es consistente con la fábrica en la **historia de deformación y metamorfismo** a lo largo del Complejo Acatlán; así como las **implicaciones tectónicas y paleogeográficas** que le manifiesten perteneciente de algún modelo de extrusión para rocas metamórficas de alta presión.

Capítulo 2

U-Pb Neoproterozoic-Ordovician protolith age constraints for high-medium pressure rocks thrust over low-grade metamorphic rocks in the Ixcamilpa area, Acatlán Complex, southern México.

Canadian Journal Earth Sciences, Vol. 48, p. 45-61, (2011)

Ramos-Arias M. A. [1]

Keppie J. D.[1]

[1]Departamento de Geología Regional, Instituto de Geología, Universidad Nacional Autónoma de México, 04510 México, D.F., México.

ABSTRACT

High grade and high pressure rocks in Acatlán Complex (southern Mexico) are inferred to have been emplaced either during the convergence and collision between Laurentia and Gondwana or during subduction on the western margin of Pangea. In the Ixcamilpa area, such rocks occur in a synformal nappe and are subdivided into: (i) the Neoproterozoic-Ordovician Piaxtla Suite (metapsammite, meta-pelite and amphibolite) that passes structurally upwards from blueschist through eclogite to amphibolite facies; intruded by (ii) Cambro-Ordovician megacrystic granitoids; both of which were thrust westwards over (iii) Carboniferous Zumpango Unit consisting of clastic and meta-volcanic rocks. LA-ICPMS U-Pb zircon geochronology yielded age population peaks at: (i) 435-490 probably derived from Acatlán granitoids, (ii) 500-700 Ma likely derived from the Yucatan Peninsula and Brasiliano orogens, (iii) 800-900 Ma with provenance in the Goiás arc of eastern Amazonia, and (iv) 950-1300 Ma sourced either Oaxaquia, Amazonia or Laurentia: the younger ca. 310-360 Ma ages are limited to the Zumpango Unit and likely have a local provenance. The overall similarity of the Piaxtla rocks in the

Ixcamilpa area and those in the Piaxtla-Mimilulco median belt suggests that Ixcamilpa nappe roots in the median belt, which is interpreted as an extrusion zone within the Acatlán Complex. Since neither high pressure belt represents a closed ocean, deposition of the Neoproterozoic-Ordovician rocks is inferred to have taken place on the southern margin of Rheic Ocean adjacent to Oaxaquia/Amazonia, whereas the Carboniferous rocks were deposited on the western margin of Pangea synchronous with extrusion of the HP rocks.
Keywords: U-Pb zircon, High pressure, Nappe, Acatlán Complex, Southern Mexico.

Introduction

High pressure (HP) rocks are commonly inferred to represent the remnants of an ocean basin extruded back up the subduction zone; their protoliths range from ophiolites and oceanic arcs to bimodal volcanic and continental margin deposits (Liou et al. 2004). In southern Mexico, two HP belts occur within the Paleozoic rocks of the Acatlán Complex: the median Piaxtla-Mimilulco and Ixcamilpa-Olinalá (Fig.2.1). Whereas Paleozoic ophiolitic, passive margin, bimodal rift-related volcanic, and arc protoliths have been identified in the Piaxtla-Mimilulco belt (Meza-Figueroa et al. 2003; Proenza et al. 2004; Murphy et al. 2006), and amphibolite-greenschist facies rocks in the Olinalá area have yielded Ediacaran-Ordovician and Carboniferous protolith ages (Talavera-Mendoza et al. 2005; Ortega-Obregón et al. 2009), detrital zircons from only one blueschist sample (ca. 477 Ma and Precambrian ages) and one megacrytsic granitoid (1043 ± 50 Ma) in the Ixcamilpa area have been dated (Talavera-Mendoza et al. 2005). In this paper, we define eight units in the Ixcamilpa area and present U-Pb LAICPMS zircon analyses in order to constrain their ages: structural and geochemical data will be presented in subsequent papers.

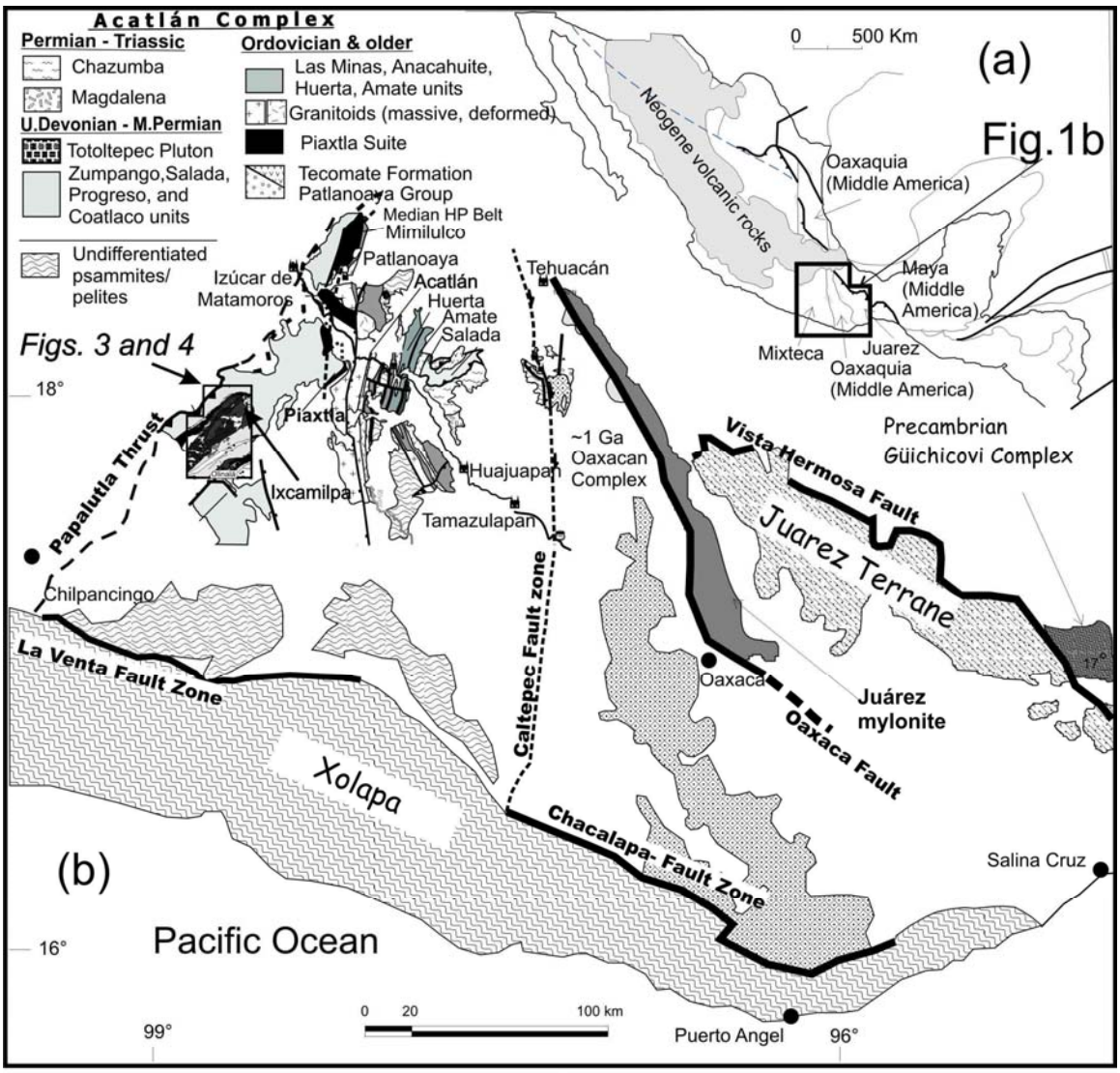

Figure 2.1 Acatlán Complex in the context of the Southern Mexican Terranes (modified after Keppie et al. 2008a).

The Acatlán Complex is bounded by three tectonic boundaries (Fig. 2.1): (i) on its eastern side, the Permian, Caltepec dextral ductile shear (Elías–Herrera and Ortega-Gutiérrez 2002) juxtaposes the Acatlán Complex against ca. ~1 Ga Oaxacan Complex; (ii) to the south, the sinistral transtensional, Cenozoic, Chacalapa–La Venta Fault places it against the Mesozoic-Cenozoic Xolapa Complex (Tolson, 2005); and (iii) its western margin, the Late Cretaceous Papalutla thrust places Acatlán Complex over Cretaceous Morelos-Guerrero Platform(Cerca et al., 2006). To the north, the Acatlán Complex is covered by volcanic and volcaniclastic sequences of Cenozoic Transmexican Volcanic Belt.).

The Paleozoic rocks of the Acatlán Complex may be subdivided into two assemblages of contrasting metamorphic grade and geochronology (Keppie et al. 2008a and references therein) has provided constraints on the geological record. The low grade sequence is composed of:

(a) a Neoproterozoic-Ordovician clastic sequence intruded by ca. 480-440 Ma bimodal, rift-related igneous rocks; and

(b) a latest Devonian-Permian shallow marine sequence (>906 m) consisting of meta-psammites, meta-pelites and tholeiitic mafic volcanic rocks.

The HP metamorphic rocks consist of:

(i) a Neoproterozoic-Ordovician rift-shelf intruded by bimodal rift-related intrusions that are similar to the low grade rocks;

(ii) periarc ultramafic rocks, and

(iii) arc and MORB rocks. The Ordovician granitoids contain concordant inherited zircons that range in age from ca. 900 to 1300 Ma, suggesting a source in the Oaxacan Complex.

Concordant ages of detrital zircons in both the low- and high-grade Cambro-Ordovician metasedimentary rocks indicate a provenance in local Ordovician plutons and/or ca. 1 Ga Oaxacan basement, and distal northwestern Gondwana sources with an unique source in the 900-750 Ma Goiás magmatic arc within the Brasiliano orogen. The 900-750 Ma ages allow distinction between Laurentian and Amazonian sources (Keppie et al. 2008a).

The HP belts in the Acatlán Complex have generally been inferred to occur in synformal keels of a single nappe rooted in the Caltepec shear zone (Ortega-Gutiérrez et al. 1999; Talavera-Mendoza et al. 2005; Vega-Granillo et al. 2007, 2009). On the other hand, Ramos-Arias et al. (2008) has shown that the eastern margin of the Piaxtla-Mimilulco belt is a listric normal shear zone, which led Keppie et al. (2008a) to propose that the median Piaxtla-Mimilulco HP belt was extruded into the Acatlán Complex. In the Olinalá area, Ortega-Obregón et al. (2009) suggested that the faults bounding the high-grade rocks have normal and/or transcurrent displacements rather than being thrusts as proposed by Talavera-Mendoza et al. (2005). These HP rocks were traditionally interpreted to be oceanic remnants of either Iapetus alone (Ortega-Gutiérrez 1981; Ortega-Gutiérrez et al. 1999), or three oceans, an unnamed ocean marginal to

Laurentia, Iapetus and Rheic oceans (Talavera Mendoza et al. 2005; Vega-Granillo et al. 2007, 2009) (Fig. 2.2a). Alternatively, Keppie et al. (2008a) infer emplacement of HP rocks into the western margin of Pangea that were derived from protoliths formed along the southern Rheic Ocean passive margin. Clearly the origin of the HP rocks in the Ixcamilpa area has important implications for paleogeographic reconstructions.

GEOLOGICAL SETTING OF THE IXCAMILPA AREA

The western part of the Acatlán Complex in the Olinalá and Ixcamilpa areas was initially studied by Hermanns (1994), Farfán (1998), Ramírez-Espinoza (2001), Torres de León (2001), and de la Cruz (2004). Subsequently, Talavera-Mendoza et al. (2005) and Vega-Granillo et al. (2007, 2009) sampled the western Acatlán Complex for geochronology. The meta-sediments associated with blueschists near Ixcamilpa yielded large zircon populations with age peaks at ~477 Ma, ~603, ~708 Ma, ~946,,~1128 Ma, ~1821 Ma, and a few ~3115– 2550 Ma grains. These blueschists yielded a $^{40}Ar/^{39}Ar$ plateau age for phengite of 322 ± 4 Ma (Vega-Granillo et al. 2007). Talavera-Mendoza et al. (2005) also dated the Tecolapa tonalitic granite using zircon LA-ICPMS analyses, which yielded a major age population at ca. 1043 ± 50 Ma interpreted as the intrusive age with a few younger ages inferred to be due to Pb-loss. Similarly, the Ocotitlan megacrystic granite, lying in the area just to the south of the Ixcamilpa area, yielded discordia intercept ages of 1165 ± 30 Ma and 597 ± 57 Ma that were interpreted as the age of intrusion and the time of Pb-loss, respectively (Talavera-Mendoza et al., 2005). However, the Ocotitlan granite was redated by Ortega-Obregon et al. (2009a) and yielded a population of concordant Ordovician (464 ± 4 Ma) zircons interpreted as the intrusive age: older ages were attributed to inheritance. These data were integrated into the following geological history for the whole Acatlán Complex (Fig. 2.2a) (Talavera-Mendoza et al. 2005, 2006; Vega-Granillo et al. 2007, 2009):

a) ~1.0-1.2 Ga intrusion of Tecolapa granitoids that were correlated with the Grenville Orogenic Belt along the eastern margin of Laurentia;
b) ~480-470 Ma magmatism inferred to have been a peri-Laurentian island arc built on Grenvillian basement that was post-dated the first stage of eclogite metamorphism;
c) ~470-460 Ma imbrication of HP ophiolitic and basin rocks into a suture between peri-Laurentia arc and eastern Laurentia shield;

d) magmatism above a new subduction zone, the latter producing ~460-440 Ma blueschist metamorphism at Ixcamilpa related to convergence within Iapetus;
e) Silurian magmatism and HP metamorphism at ~419 Ma in the Organal area inferred to mark closure of Iapetus;
f) Devonian deposition of clastic rocks on the passive margin of Amazonia bordering the Rheic Ocean;
g) ~300 Ma deposition of clastic sediments followed by low grade deformation during final continental collision of Laurentia and Gondwana.

This tectonic evolution contrasts with that proposed by Nance et al. (2006, 2007), Murphy et al. (2006), Middleton et al. (2007), Keppie et al. (2008a), Morales-Gámez et al. (2008, 2009a and b), and Ramos-Arias et al. (2008); Keppie et al. (2008a) who proposed the following geological history (Fig. 2.2b):

a) Deposition of Cambrian and Ordovician sedimentary rocks intruded by Ordovician bimodal tholeiites and megacrystic granitoids in a rift-passive margin setting along the southern margin of Rheic Ocean (Oaxaquia-Amazonia);
b) Devono-Carboniferous convergence on the western margin of Pangea accompanied by subduction erosion of the Ordovician rift-passive margin, late Paleozoic forearc and arc followed by Early Carboniferous extrusion of HP rocks into the Acatlán Complex: this was synchronous with deposition of Devono-Carboniferous peri-arc sedimentary sequences intrusion of tholeiitic dykes;
c) Permian arc magmatism in a dextral transtensional regime on the western margin of Pangea synchronous with clastic deposition.

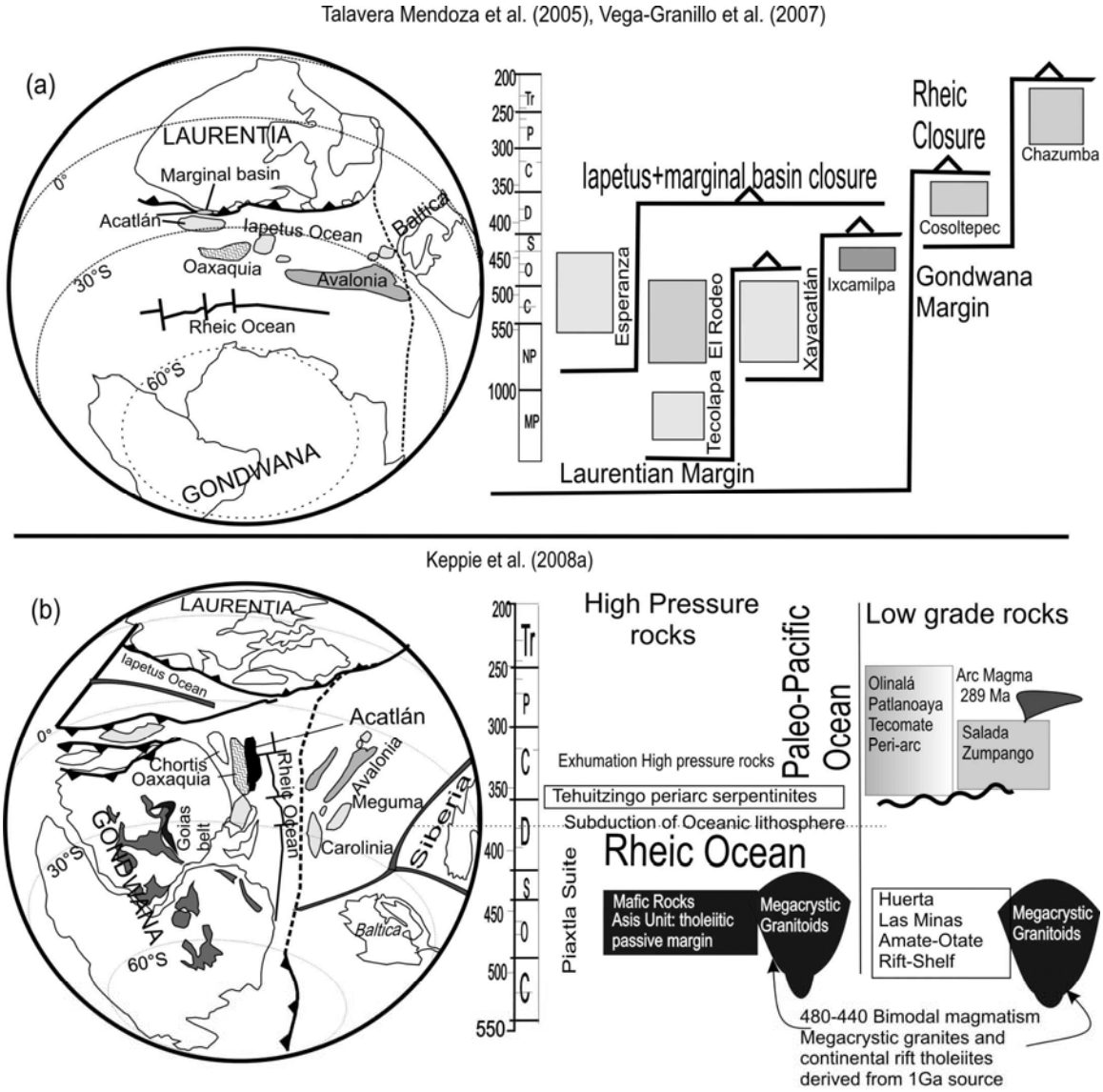

Figure 2.2 Comparison of sequence of events for the Acatlán Complex: (a) modified after Talavera-Mendoza et al. (2005) and Vega-Granillo et al. (2007); and (b) after Keppie et al. (2008a). Ch=Chortis, Ca= Carolinia, Me=Meguma.

LITHOLOGICAL UNITS

The rocks of the Acatlán Complex in the Ixcamilpa area have been subdivided into several fault-bounded blocks either by steeply dipping, Cenozoic, transtensional brittle faults or upper Paleozoic thrust zones (Fig. 2.3): (i) high-pressure (HP) and high-medium grade rocks of the Neoproterozoic-Ordovician Piaxtla Suite; (ii) Ordovician megacrystic granitoids; and (iii) sub-greenschist facies rocks of the Carboniferous Zumpango Unit. The high-medium grade rocks are floored by a WNW-vergent thrust

zone (Encinera thrust) that places them on top of the low-grade Zumpango Unit, which is itself thrust over the Cretaceous Morelos platform along the Laramide Papalutla thrust in the northwestern corner of the area. The ≤500 m thick, Encinera thrust zone is best exposed on the Tecolapa-Papalutla road and in the Barranca Grande, and consists of phyllonites with a discrete, anastomosing, micaceous schistosity. The map pattern and structural data (to be published elsewhere) indicate that the Encinera thrust is gently folded by a synform, which is truncated along its eastern margin by a steeply dipping Cenozoic brittle fault. In the Ixcamilpa area, the Piaxtla Suite is subdivided into six tectonic slices (Fig. 2.3).

The Zumpango rocks and the high-medium grade rocks may be traced directly southwards into the Olinalá area where they occur in the Northern and North-Central fault blocks, respectively (Ortega-Obregon et al. 2009)(Fig. 2.4). The rocks in the North-Central block were assigned to two units: the Tlaxco Amphibolite (subdivided into four fault slices in the Ixcamilpa area), and the Zacango Unit (gneisses and schists). The eastern Zumpango belt may be a northern continuation of the Central block of Ortega-Obregón et al. (2009).

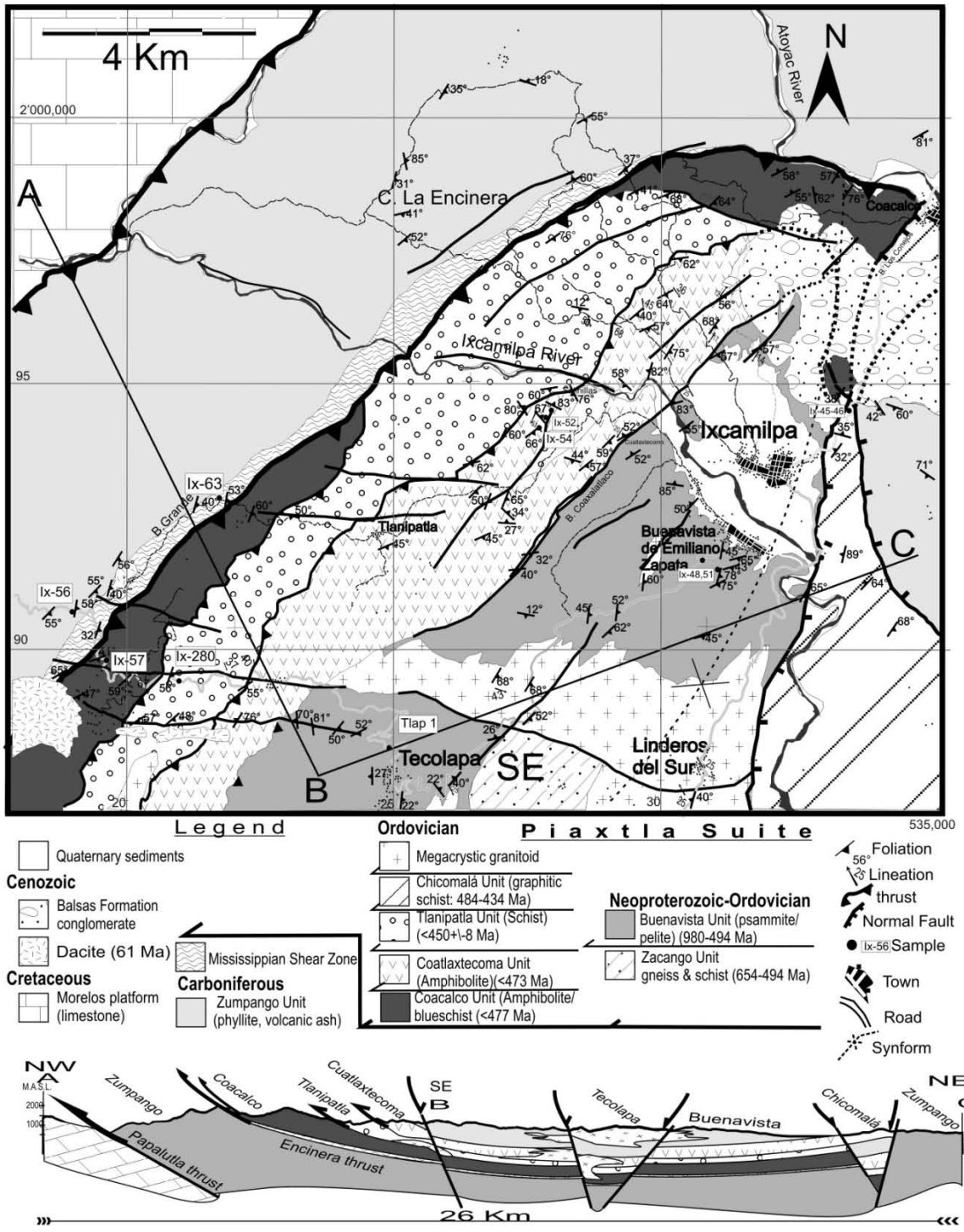

Figure 2.3 Geologic map and cross-sections of the Ixcamilpa area showing the truncated synformal structure, Ixcamilpa area, western Acatlán Complex.

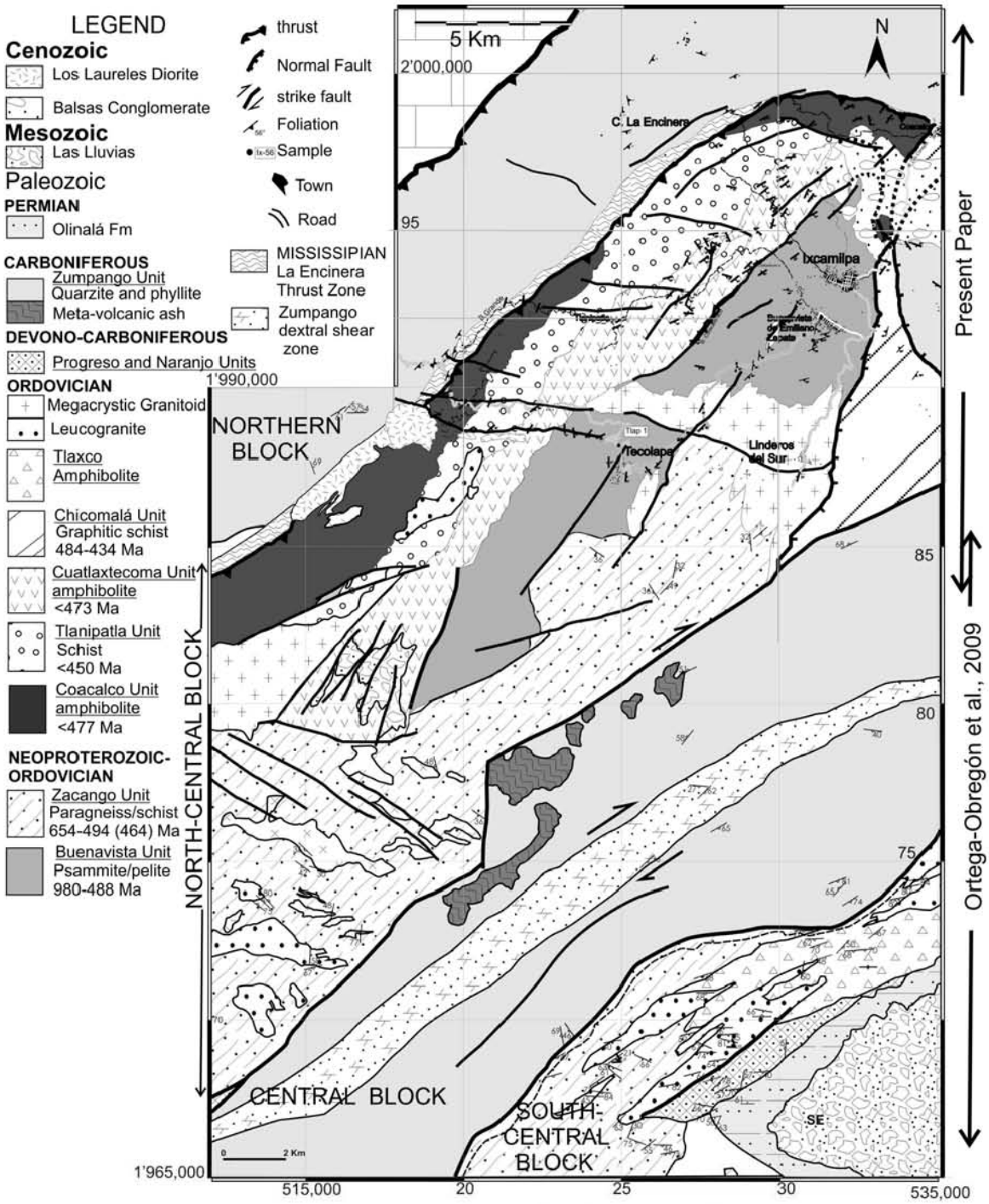

Figure 2.4 Combined geological maps of the Ixcamilpa and Olinalá areas (this paper and Ortega-Obregón et al. 2009) showing the youngest U-Pb ages of detrital and igneous zircons.

Neoproterozoic-Ordovician Piaxtla Suite

Using a combination of lithology and metamorphic grade, the Piaxtla Suite in the Ixcamilpa area has been subdivided into six units that occur in tectonic slices bounded by ductile shear zones (Fig. 2.3). From bottom to top these are:

Coacalco Unit: amphibolite (blueschist)

In the Ixcamilpa area, there are two tectonic slices of the Coacalco Unit consisting of amphibolite that are bounded on the northern and northwestern sides by the Encinera thrust zone. One slice is parallel to the Encinera thrust, whereas the other crops out within the Piaxtla Suite. The amphibolites are characterized by bands of amphibole and plagioclase and locally blue glaucophane showing evidence of corrosion and reaction rims, plagioclase (albite) with aligned epidote and amphibole inclusions that locally coexist with rotated, zoned garnets. These bands are interleaved with other lepidoblastic domains containing chlorite, white mica, cataclastically deformed clinozoisite, blue amphibole fibers, and accessory rutile-titanite, iron oxides and zircon.

Tlanipatla Unit (meta-sediments + amphibolite)

The Tlanipatla Unit occurs in a NE-trending slice extending from the Atoyac River to Tecolapa. It is best exposed on Tecolapa-Papalutla road and in the Ixcamilpa River. It is generally bounded by shear zones either with the Coacalco or Zumpango units on the west and the Cuatlaxtecoma Unit on the east. It is mainly composed of polydeformed psammitic and pelitic metasedimentary rocks with amphibolite lenses. This unit is cut by megacrystic granite near the southern margin of the map (Figs. 2.2 and 2.3). The metasedimentary rocks are characterized by a composite, penetrative mica fabric with local garnet porphyroblasts surrounded by lepidoblastic mica and chlorite interleaved with stretched quartz-feldspars ribbons. Accessory iron oxides and zircon are also present.

Cuatlaxtecoma Unit (amphibolite)

The Cuatlaxtecoma Unit occurs in a NE-trending slice bordered by the Tlanipatla and Buenavista units. It extends from 3 km northeast of Coacalco to west of Tecolapa. The best outcrops are in Barranca Cuatlaxtecoma, 2.5 km northwest of Buenavista and in Barranca El Toro. It consists mainly of amphibolites interfingered with

metasedimentary rocks and intruded by mylonized granitic dikes, all of which are folded together. The amphibolites are mainly characterized by bands of aligned amphibole, plagioclase (albite) and garnet with accessory rutile-titanite, Fe-Ti oxides, and zircon separated by bands of white mica-chlorite and local zoisite-clinozoisite. Some amphibolitic lenses contain relicts of small corroded pyroxene that may indicate peak metamorphic conditions in the eclogite facies. Rotated garnet porphyroblasts with a folded internal foliation are present and many garnets have pressure shadows containing plagioclase and quartz surrounded by lepidoblastic chlorite. The amphiboles show cataclastic deformation and have chlorite reaction rims indicating retrograde metamorphism. The metasedimentary rocks consist of bands of quartz and micaceous/chlorite.

Zacango Unit

This unit was described by Ortega-Obregón et al. (2009) and consists of paragneisses, meta-psammites and minor schists, in which the metamorphic grade varies from upper to lower amphibolite facies. It is intruded by amphibolite dikes and megacrystic granitoids. In the Ixcamilpa area, the best outcrops are on the Linderos del Sur-Tecolapa road. The unit is bounded to the north by a brittle fault that juxtaposes it against the Tecolapa megacrystic granite. Brittle normal faults also form the western and southern contacts, where it is juxtaposed against the Buenavista and Zumpango units, respectively (Ortega-Obregón et al. 2009). The meta-psammites consist of quartz and white mica with some feldspar inclusions, and locally contain garnet and large crystals of amphibole. The poly-deformed, amphibolites consist of lepidoblastic amphibole, epidote, plagioclase and chlorite.

Buenavista Unit (meta-sediments + hypabyssal intrusions)

The Buenavista Unit consists of psammitic and pelitic metasedimentary rocks intruded by megacrystic granitoids, leucogranite and mafic dikes, all of which were deformed together. It forms a NE-trending slice extend from Buenavista to Tecolapa villages that is best exposed along the road south of Buenavista and in the nearby barranca. This unit is bounded by the Cuatlaxtecoma and Chicomalá units. The meta-psammites consist of white mica and bands of stretched quartz. The granitic dikes

contain bands of stretched quartz and cataclastic K-feldspars domains. Mafic dikes contain corroded hornblende relicts that have been rotated and cataclastically deformed. Lepidoblastic chlorite and albite bands also occur. Zoisite-clinozoisite, rutile, titanite, zircons and Fe oxides are accessory minerals. Locally in the north, amphibolitic lenses contain garnet with corrosion bays and exhibiting cataclastic flow are preserved suggesting that Buenavista Unit may have been metamorphosed in the amphibolite facies and subsequently retrogressed in the greenschist facies.

Chicomalá Unit (graphitic schist)

The Chicomalá Unit is exposed in an irregular-shaped, fault block exposed east of Ixcamilpa. The main outcrops are on the Coacalco-Ixcamilpa road, and in the Barranca Chicomalá, 3 km SE from Ixcamilpa. It consists of interbedded graphitic schist and meta-quartzite cut by pegmatites and rare mafic-intermediate dikes. The meta-pelitic layers have abundant graphite, white mica, and stretched quartz bands. Mafic bodies contain chlorite pseudomorphs patches after amphibole, plagioclase and white mica. This mineral association suggests peak metamorphism in the amphibolite facies, with retrogressive metamorphism in the greenschist facies. Abundant quartz veins are deformed with the host rocks. Quartz-feldspar pegmatites contain accessory zircon, pyrite, and rutile.

Ordovician Megacrystic Tecolapa Granitoid

The E-trending, megacrystic Tecolapa granitoid pluton cuts across the Buenavista and Zacango units near the southern margin of the area. K-feldspar megacrystic granite is cut by leucogranite dikes. Both are mylonitic, and leucogranite dikes display recumbent isoclinal folds. Good outcrops occur on the Ventanas Iyotcingo-Tecolapa road. The megacrystic granite is characterized by oblate and rotated, K-feldspar porphyroclasts that have been deformed by cataclastic flow. They are surrounded by a foliation consisting of stretched quartz and white mica.

Carboniferous Zumpango Unit

In the Ixcamilpa area, the sub-greenschist Zumpango Unit occurs in two NE-trending fault blocks that border the high-grade rocks (Figs. 2.2 and 2.3). The Zumpango Unit was defined by Ortega-Obregón et al. (2009) in the Olinalá area where it occurs in the Central and Northern fault blocks. In the Ixcamilpa area, the Northern block is bounded by two thrusts: (i) on the northwestern margin, the Laramide Papalutla thrust places the Zumpango Unit on top of the Cretaceous Morelos Platform; and (ii) on the southeastern margin, the upper Paleozoic Encinera thrust places the high-medium grade units on top of the Zumpango Unit. In the Central block, the Zumpango Unit is juxtaposed on its western margin against the Chicomalá Unit along N-trending brittle fault, and is unconformably overlain by Cenozoic clastic sediments on the eastern side.

The Zumpango Unit consists mainly of quartzite interbedded with meta-arkose, phyllite and white volcanic ash layers that are locally hydrothermally altered, and intruded by deformed quartz veins. The quartzites exhibit domains of stretched quartz crystals separated by solution cleavage bands consisting of micaceous (sericite?) and chlorite fibers. The ash layers preserve some altered K-feldspar and plagioclase phenocrysts set in a fine grained groundmass containing accessory iron oxides and zircons.

U-Pb GEOCHRONOLOGY

In order to constrain the ages of the various units, twelve samples were collected for U-Pb LA-ICPMS isotopic analysis of zircon from the various units in the Ixcamilpa area: 9 metasedimentary rocks and 2 amphibolites and 1 granitoid (Fig. 2.3, Table 1). Sample preparation, analytical methods and choice of youngest and best ages are as described by Gehrels et al. (2006) and Solari et al. (2009) and are given in detail in the caption to Table 1 (data repository $_{Anexo}$).

Piaxtla Suite

Detrital zircon from meta-psammite (sample Ix 57) in the **Coacalco Unit** yielded Neoproterozoic ages between 793-874 Ma, 916-1048 Ma and 1160-1275 Ma. The youngest concordant detrital zircon is 874 ± 8 Ma and is the same within error as the

mean of five youngest zircons is 899 ± 23 Ma: the latter age is used in this paper (Fig. 2.5 A, B).

The sample of **Tlanipatla garnet mica schist** (Ix 280) yielded a large detrital zircon population with ages in the range of 413-496 Ma (peak at ~434 Ma), with a few zircons at ca. 730-943 Ma and between ca. 1400 and 1725 Ma. The youngest concordant detrital zircon is 437 ± 7 Ma, and the calculated mean of the nineteen youngest zircons is Ordovician 457 ± 12 Ma: the latter is regarded as more robust (Fig. 2.5 C, D).

The amphibolite (Ix 52) in the **Cuatlaxtecoma Unit** yielded very few zircons with single ages ranging from 388 to 563 Ma, and 1070 to 1464 Ma (Table 1). The younger ages are either discordant and/or have large errors and so are not meaningful. The youngest concordant zircon is 1195 ± 45 Ma. Another sample from this unit, a meta-psammite (Ix 54), yielded major age population peaks at ca. 950 and 1190 Ma, several Ordovician and Cambrian-Ediacaran ages, and a few old ages of ca. 1500 Ma, ca. 1875 and 2780 Ma. The youngest concordant, single detrital zircon is Ordovician 471± 3 Ma and the mean of the three youngest zircons is 473 ± 16 Ma: the latter is probably the more robust age (Fig. 2.5G, H).

The meta-psammite sample (Ix 48) from the **Buenavista Unit** yielded detrital zircons ranging in age from ca. 710 to 1630 Ma. The youngest concordant detrital zircon is 956 ± 13 Ma and the mean of four youngest grains is 976 ± 100 Ma. The main population peak has an age of 1205 Ma. A second meta-psammite sample (Ix 51) has detrital zircons ranging from ca. 850 to 1840 Ma with the main peak at ca. 1220 Ma and lesser peaks at 1360 and 1550 Ma. The youngest concordant detrital zircon is 978 ± 30 Ma and the mean of three youngest zircons is 982± 19 Ma (Fig. 2.6A, B, C, D). Thus the youngest zircons are similar within error.

The meta-psammite sample (Ix 46) of the **Chicomalá Unit** yielded one concordant detrital zircon with an age of 493 ± 13 Ma that is within error the same as the mean of the eight youngest zircons yielded an age of 482 ± 14 Ma: the latter is used in this paper (Fig. 2.6E and F). There is also a population of ca. 1050-1270 Ma zircons and a few Paleoproterozoic and Archean ages. The youngest concordant zircon in the amphibolite sample (Ix 45) of the Chicomalá Unit is 446 ± 10 Ma and is within error the same as the mean of four youngest zircons is 434 ± 33 Ma: the latter is used

in this paper (Fig. 2.6F and H). Older grains have ages ca. ~1 Ga (997-1006 Ma) and between 1100 and 1207 Ma.

The youngest concordant zircon in the granodiorite sample (Tlap 1) from **Tecolapa granitoid pluton** yielded 488 ± 7 Ma. This is within the error of the mean of the three youngest zircons gave an age of 501 ± 44 Ma resulting in an intrusive age straddling the Cambro-Ordovician boundary (Fig. 2.7a).

Zumpango Unit

Zircons in an ash layer (Ix 56) from the **Zumpango Unit** in the northwestern part of the area yielded a mean age of 373 ± 65 Ma for the five youngest zircons, whereas the youngest concordant zircon is 374 ± 9 Ma: the latter is taken to be the crystallization age of the ash. On the other hand, the youngest detrital concordant zircon in a meta-psammite sample (Ix 190) from the eastern part of the area yielded an age of 310 ± 3 Ma and a mean of the three youngest zircons is 362 ± 39 Ma. Given the low errors on the age of the single detrital zircon, the 310 Ma probably provides an older limit on the time of deposition of this specific meta-psammite. Older ages in the meta-psammite gave ages between ca. 458 and 560 Ma, with older population peaks at ca. 909 to 1250 Ma (Fig. 2.7B-E).

The phyllonite sample (Ix 63) from the **Encinera thrust zone** yielded detrital ages in the range 322-383 Ma, 504-671 Ma and 900-1100 Ma. The youngest concordant zircon is 322 ± 5 Ma and provides a maximum age for mylonitization in the shear zone. (Fig. 2.8F, G).

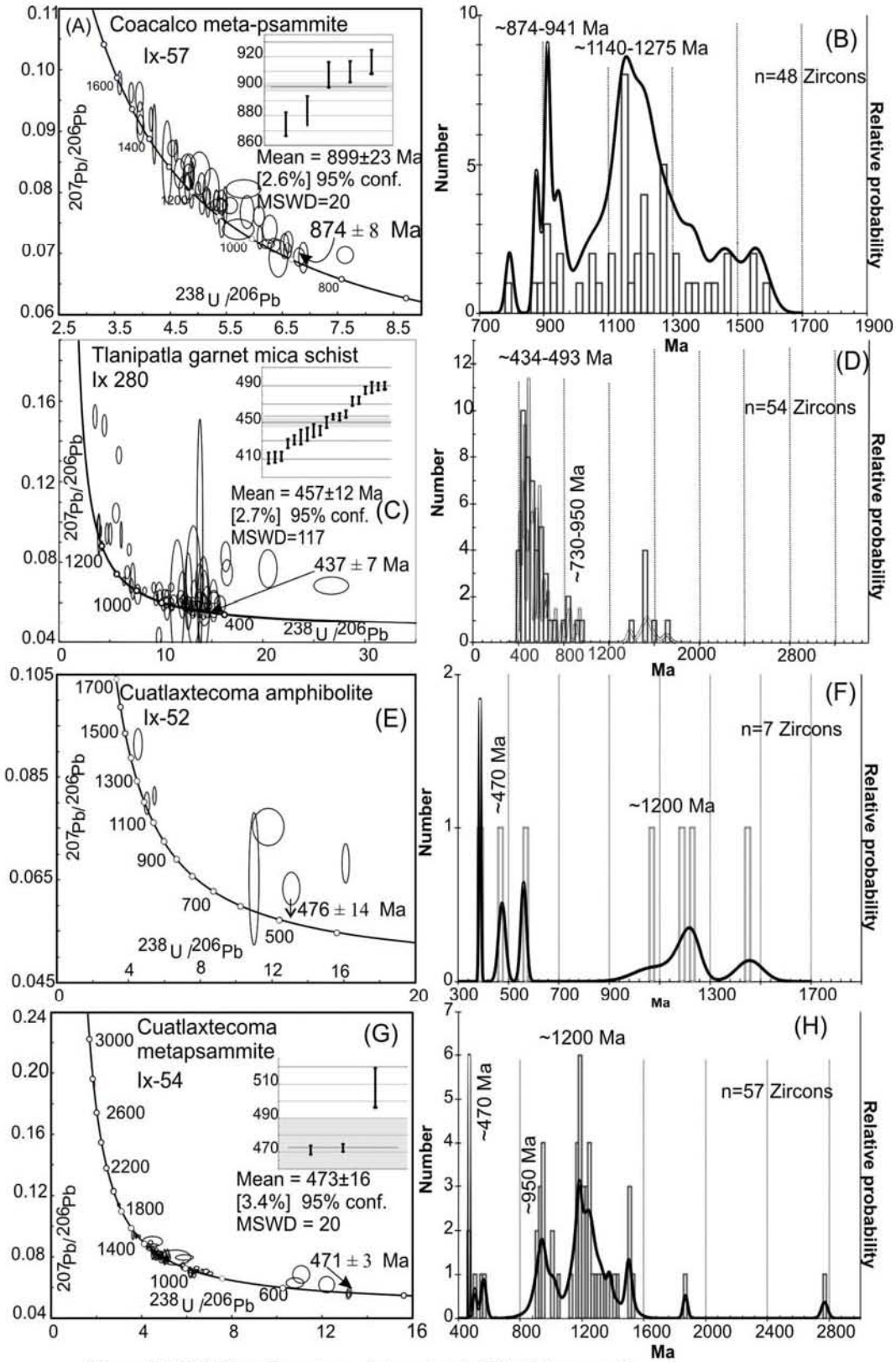

Figure 2.5 U-Pb Tera-Wasserburg plots and probability histograms of:
(A-B) Coacalco meta-psammite; (C-D) Tlanipatla garnet-mica schist;
(E-H) Cuatlaxtecoma amphibolite and meta-psammite.

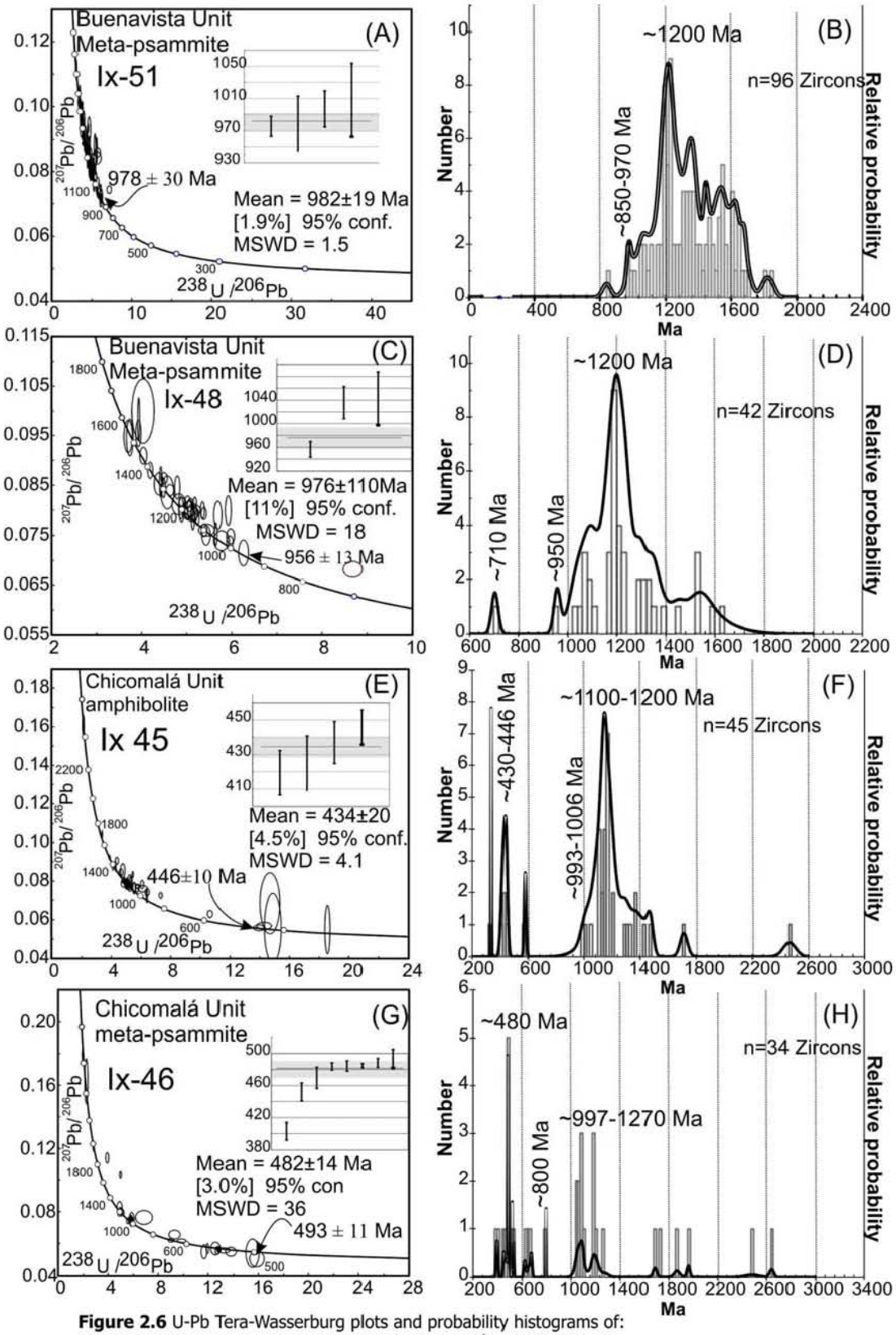

Figure 2.6 U-Pb Tera-Wasserburg plots and probability histograms of: (A-D) Buenavista meta-psammites; (E-H) Chicomalá amphibolite and meta-psammite.

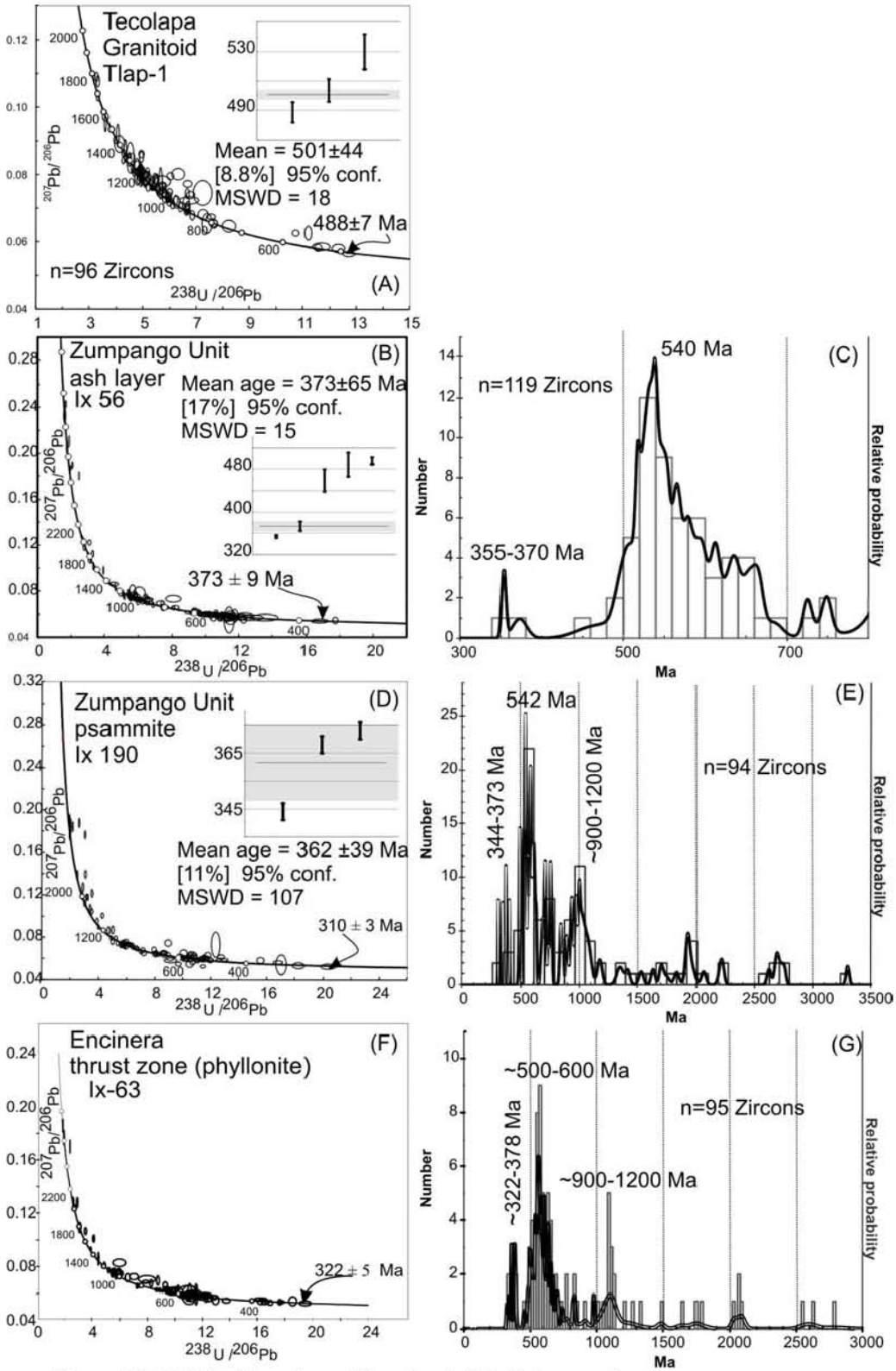

Figure 2.7 U-Pb Tera-Wasserburg plots and probability histograms of: (A) Tecolapa Megacrystic Granitoid; (B) white ash layer in northwestern Zumpango area; (C-D) meta-psammitic bands in eastern Zumpango outcrops; (E-F) detrital zircons in the Encinera thrust zone.

CONSTRAINTS ON AGES OF UNITS

The time for deposition of the eight metasedimentary units is constrained between the youngest detrital zircon and the age of cross-cutting intrusions (amphibolites and granitoids). The Tecolapa megacrystic granite yielded a mean intrusive age of 501 ± 44 Ma, which straddles the Cambro-Ordovician boundary. This age is within the range of other, mainly Ordovician, megacrystic granitoids in the Acatlán Complex (Talavera-Mendoza et al., 2005; Miller et al. 2007; Keppie et al., 2008a). The Mesoproterozoic ages in the Tecolapa pluton are attributed to inheritance (c.f. Talavera-Mendoza et al., 2005), and may indicate a source in the underlying Oaxacan Complex. The Tecolapa pluton cuts the Buenavista and Zacango units and so provides a younger limit on their deposition. The youngest detrital zircons in these two units are 980 Ma and 654 Ma (Ortega-Obregon et al. 2009), respectively, which limit their time of deposition within the Neoproterozoic and Cambrian.

The Tlanipatla and Cuatlaxtecoma units are cut by megacrystic granites. Although these specific granites have not been dated, they are probably of Ordovician age based on their similarity to the Teticic (461 ± 1 Ma) and Ocotitlán (464 ± 4 Ma) granitoids occurring 3-5 kilometers to the south of the Ixcamilpa area (Ramírez-Espinoza 2001; Ortega Obregón et al. 2009), and other Ordovician granites in the Acatlán Complex (Keppie et al., 2008a). The Tlanipatla Unit is likely younger than 457 ± 12 Ma, whereas the Cuatlaxtecoma Unit is probably younger than 473 ± 16 Ma and both are younger than undated, but probably Middle-Late Ordovician, cross-cutting megacrystic granites. Deposition of the Chicomalá Unit during the Ordovician is constrained between 482 ±14 Ma (the youngest detrital zircons) and 436 ± 20 Ma zircons in the cross-cutting amphibolitic dikes. A meta-psammite interleaved with blueschists (Coacalco Unit) previously yielded Ordovician detrital zircon ages (peak at ca. 477 Ma: Talavera-Mendoza et al. 2005): unfortunately a younger limit is not available, but its depositional age is likely similar to all the other units in the area.

Deposition of one of the ash layers in the Zumpango Unit is taken to be 356 ± 15 Ma (i.e. Mississippian). On the other hand, the youngest detrital zircon in Ix 190 gave an age of 310 ± 3 Ma suggesting that deposition of the Zumpango Unit probably ranges up at least into the Pennsylvanian. An ash layer in the Zumpango Unit in the Olinalá area yielded a concordant age of 327 ± 2 Ma with young detrital zircons in psammite ranging

from ca. 350 to 385 Ma, and a detrital muscovite yielded a 338 ± 2 Ma Ar-Ar plateau age (Ortega-Obregon et al. 2009). Taking all the age data from the Zumpango Unit into account suggest that its deposition may have lasted throughout the Carboniferous.

CORRELATIONS

(i) Olinalá

The rocks in most of the Ixcamilpa area may be traced laterally into those of northern, north-central and central blocks in the Olinalá area mapped by Ortega-Obregon et al. (2009)(Fig. 2.4). Thus, the Zumpango (northern block) and Zacango (north-central block) units are common to both maps (note that the Chicomalá Unit was included in the Zacango Unit by Ortega-Obregon et al. 2009). The mafic Tlaxco Unit in the north-central block of Ortega-Obregon et al. (2009) was subdivided into two mappable units: Cuatlaxtecoma and Coacalco units. An older age constraint (473 ± 7 Ma) for the Tlaxco Unit only comes from samples in the south-central block (Ortega-Obregon et al. 2009).

The Tlaxco mafic rocks and the megacrystic granitoids in the south-central block were inferred to be part of a bimodal Ordovician suite, in which the mafic rocks are rift tholeiites and the granitoids have a calc-alkaline signature reflecting the source (Ortega-Obregon et al., 2010). Although no chemical analyses were performed on the bimodal volcanic rocks in the Zumpango Unit by Ortega-Obregon et al. (2010), they inferred that they were part of the rift tholeiites in the Progreso and Naranjo units.

(ii) Mimilulco-Piaxtla HP belt

High-grade rocks in the Ixcamilpa area have very similar lithologies and protolith ages to those of the Piaxtla Suite in the Asis area, which consists of 700-470 Ma paragneisses cut by bimodal rift tholeiites and ca. 470-420 Ma megacrystic granitoids (Fig. 2.9) (Murphy et al. 2006; Middleton et al. 2007). The rocks in the Asis area were inferred to represent a subducted part of the rift-passive margin of Oaxaquia, and the similarity suggests this interpretation is also applicable to the Ixcamilpa high-grade rocks. This raises the question: are the Ixcamilpa rocks an offset part of the median Mimilulco-Piaxtla belt or a separate belt? One scenario suggests that the Ixcamilpa belt represents a laterally displaced portion of the Mimilulco-Piaxtla belt: this would require a *sinistral* displacement. However, such a scenario seems unlikely given the following

facts: (i) the western boundary of the Piaxtla Suite in the northern Acatlán Complex is a *dextral* Permian fault (Barley 2006); (ii) the NE-trending, Laramide faults, one of which is cut by the ~61 Ma Los Laureles Dacite) in the Olinalá area also have *dextral-normal* kinematics (Ortega-Obregon et al., 2009); and (iii) the N-trending fault near the eastern margin of the Ixcamilpa area is a *normal* fault (Fig. 2.3). On the other hand, the high-medium grade rocks in the Ixcamilpa area are preserved above a synformally folded west-vergent thrust (kinematic data to be published elsewhere). The base of the similar HP rocks in the Tehuitzingo area (Piaxtla-Mimilulco belt) is also a west-vergent thrust (Galáz et al. 2009), which raises a more likely scenario that the Ixcamilpa rocks represent a klippe derived from the median HP belt.

Given the close correlation of the Ixcamilpa and Piaxtla belts, the high-medium grade rocks in the Ixcamilpa belt probably represent part of the Piaxtla Suite. The term, Piaxtla Suite, was used by Ortega-Gutierrez et al. (1999) for HP rocks in the Acatlán Complex as a replacement for the original term, Xayacatlán Formation (Ortega-Gutierrez 1978). Amphibolite facies rocks in the Piaxtla Suite were regarded as retrograde HP rocks, and although this may apply to some areas, some of the rocks in the Ixcamilpa area appear to have peak metamorphism in the amphibolite facies, e.g. Buenavista, Zacango and Chicomalá units. Ortega-Gutierrez et al. (1999), Ramirez-Espinoza (2001), Talavera-Mendoza et al. (2005) and Vega-Granillo et al. (2007, 2009) included these latter rocks in the Xayacatlán Formation, and given the difficulty in determining whether the amphibolite facies rocks are prograde or retrograde HP rocks, we propose that they also be included in the Piaxtla Suite.

(iii) Northern and Eastern Acatlan

It is remarkable that the lower Paleozoic sequence of events in the high-medium grade rocks rocks of the Ixcamilpa-Olinalá and Asis areas are very similar to those in the low grade rocks of the northern and eastern Acatlán Complex (Fig. 2.9: Keppie et al. 2008a). Thus, Neoproterozoic-Ordovician clastic rocks in the Patlanoaya and Xayacatlán areas are cut by Ordovician bimodal mafic tholeiites and megacrystic granites (Ramos-Arias et al. 2008; Keppie et al. 2008b; Morales-Gamez et al. 2008). Furthermore, similar Late Paleozoic rocks are present in all areas: (Devono-Carboniferous clastic rocks cut by rift tholeiites unconformably overlain by Permian arc-related rocks (Ramos-Arias et al.

2008; Keppie et al. 2008a; Morales-Gamez et al. 2008, 2009a). These observations led Keppie et al. (2008a) and Ortega-Obregon et al. (2009, 2010) to suggest that the high grade rocks of Piaxtla Suite represent subducted slices of the rift-passive and marginal arc complex that were subsequent extruded into the upper plate.

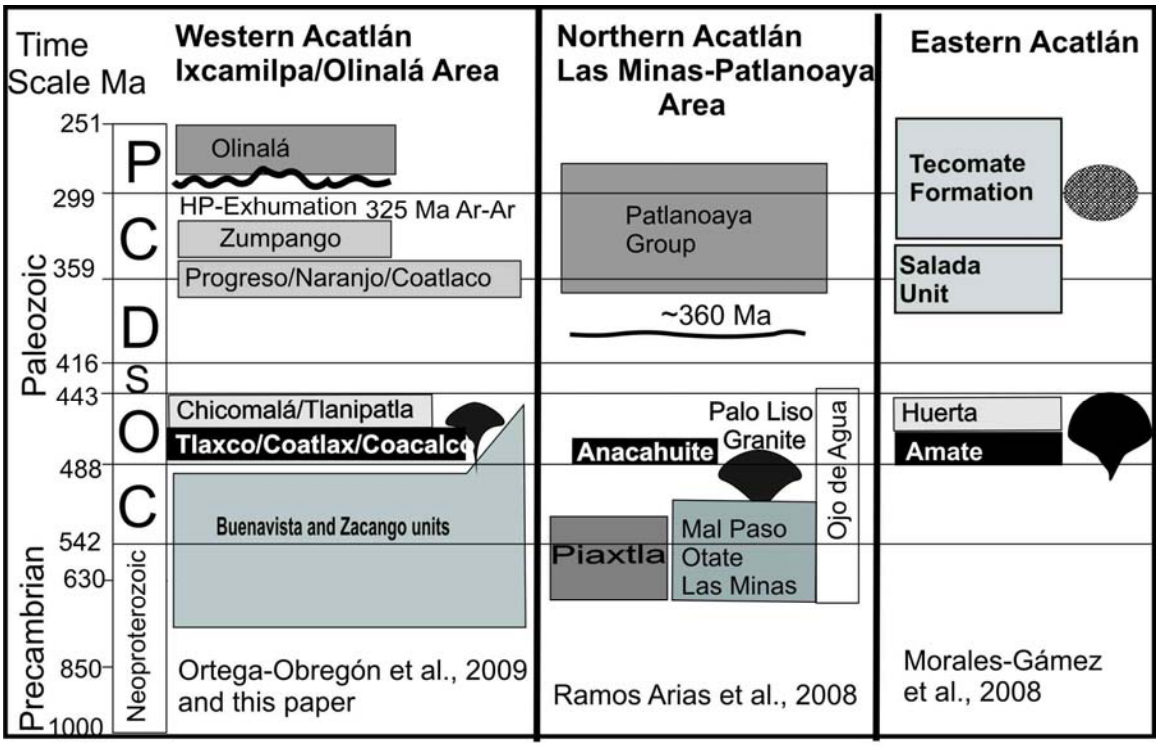

Figure 2.8 Space-Time correlation diagram for Ixcamilpa, Las Minas-Patlanoaya and Xayacatlán areas.

DETRITAL ZIRCON PROVENANCE

Detrital zircon provenance has been extensively used in the Acatlán Complex with differing conclusions with respect to lower Paleozoic rocks: (i) Talavera-Mendoza et al. (2005) and Vega-Granillo et al. (2007, 2009) favoured a Laurentian provenance, whereas (ii) Keppie et al. (2008a and b) and Nance et al (2006, 2007) preferred an Amazonian source (Fig. 2.9). This difference in opinion is understandable given the similar age ranges in the potential source regions (Laurentia and Amazonia). However, Keppie et al. (2008a) identified a small, but distinct, population of ca. 800-900 Ma concordant zircons with low uncertainties errors that they argued could only be derived from Goiás arc on the eastern side of Amazonia (Pimentel et al. 2000; Laux et al. 2004). In this study concordant 800-900 Ma zircons have been found in the Coacalco and Tlanipatla (Table 1), and the Zacango units (Ortega-Obregón et al. 2009). Similarly, the

500-700 Ma detrital zircon populations in Tlanipatla and Cuatlaxtecoma units (Table 1) were most likely derived from the Yucatan and Brasiliano orogens (Keppie et al. 2008a; Martens et al. 2010). Inter-sample variability in the ages of detrital zircon populations is interpreted as a function of the drainage system and differences in exposure in the source regions.

Although the 950-1300 Ma detrital zircons in the lower Paleozoic rocks of the Ixcamilpa area may be derived from either Laurentia or Amazonia, they fall in the range of events in Oaxaquia (Keppie and Ortega-Gutierrez 2009), and so a local source is regarded as most likely (Fig. 2.10). This is consistent with the inference that the Acatlán Complex is underlain by the Oaxacan Complex in the Ordovician (Keppie et al. 2008a), which is reinforced by the large population of 950-1300 Ma inherited zircons in the Cambro-Ordovician Tecolapa megacrystic granitoid. On the other hand, Permo-Carboniferous rocks deposited after the formation of Pangea could have been derived from either Laurentia or Amazonia, and so are not useful in paleogeographic reconstructions. The 435-490 Ma detrital zircons correspond to the age of bimodal magmatism in Acatlán Complex, and so a local source in these Ordovician plutons seems most probable.

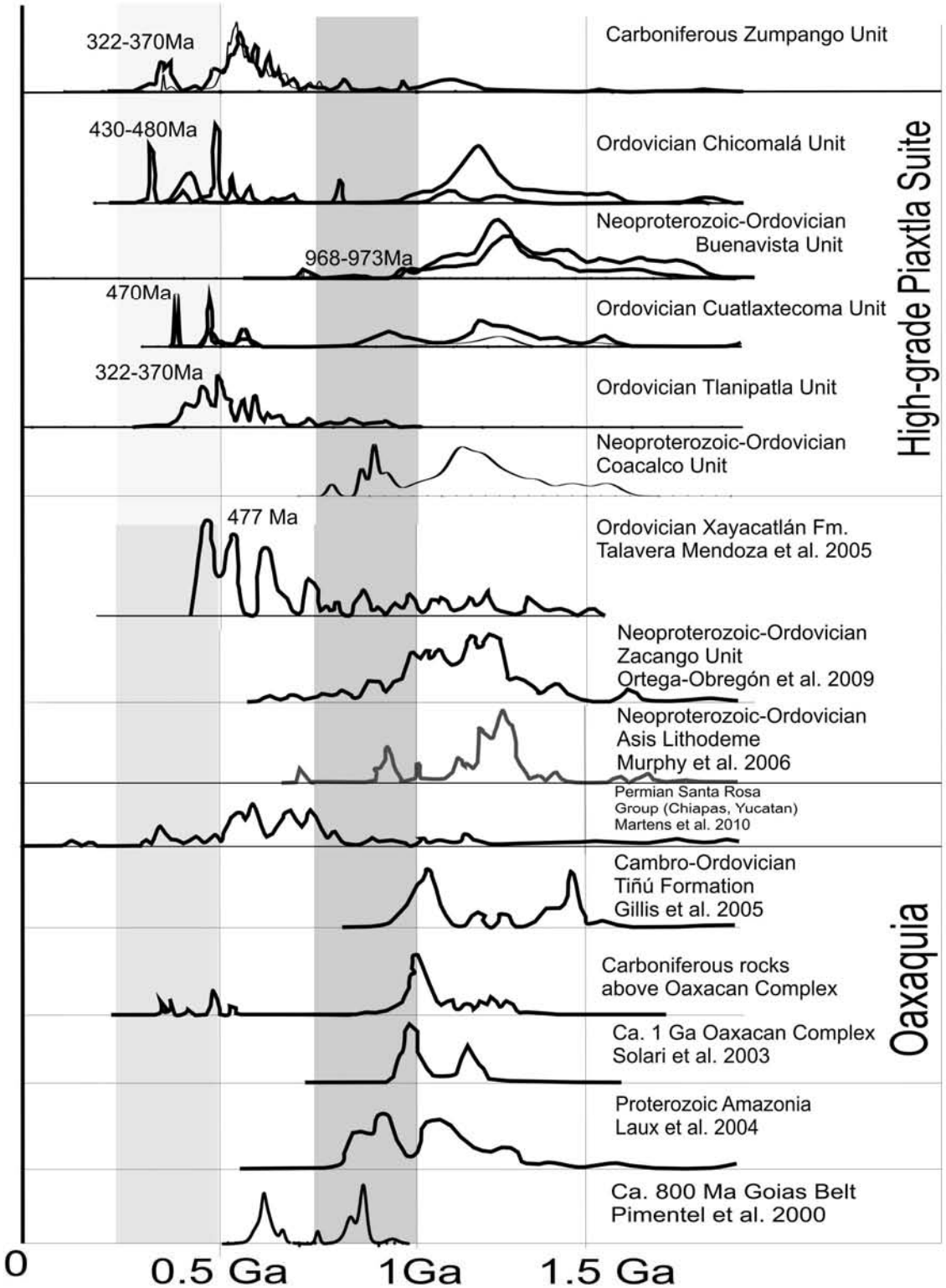

Figure 2.9 Comparative detrital zircon histograms from Ixcamilpa area with other areas in the Acatlán Complex: data from Ortega Obregón et al. (2009); Talavera-Mendoza et al. (2005), the Oaxacan Complex (Gillis et al. 2005), Maya Mountains (Martens et al. 2010), and the Goias magmatic arc in eastern Amazonia (Pimentel et al. 2000; Laux et al. 2004).

DISCUSSION

New mapping and U-Pb geochronology of the various units has permitted considerable revision of the geological map of the Ixcamilpa area. Data presented in this paper generally confirm the sequence of events recorded by Ortega-Obregon et al. (2009) in the Olinalá area (see Geological Setting), which includes:

(i) deposition of Neoproterozoic-Ordovician clastic rocks intruded by, and partially synchronous with, intrusion of Cambrian-Ordovician bimodal igneous rocks in a rift environment (Piaxtla Suite) (Fig. 2.10a); and

(ii) high-medium grade metamorphism associated with westerly-vergent thrusting and polyphase deformation during the Carboniferous that was synchronous with deposition of clastic rocks (Zumpango Unit)(Fig. 2.10b). The Carboniferous age of the HP metamorphism provided by the 322 ± 4 Ma sericite age (Vega-Granillo et al. 2009) is consistent with new $^{40}Ar/^{39}Ar$ data for glaucophane and white mica (authors' unpublished data).

Subdivision of the high-medium grade rocks indicates that the Coacalco blueschists form the sole of the basal Encinera thrust, and are structurally overlain by retrograde eclogites and amphibolite-facies rocks. Such a sequence is typical of HP pressure belts elsewhere in the world (e.g. Japan and the western Alps: Ernst 1975). The correlations made on this paper with HP rocks in the median belt within the central Acatlán Complex (Fig. 2.9) suggest that the Ixcamilpa belt represents a western *klippe* of the Mimilulco-Piaxtla belt preserved above a synformally folded thrust. In this case, there is only zone of extruded Neoproterozoic-Ordovician rocks in the Acatlán Complex (Piaxtla-Mimilulco belt). Keppie et al. (2008a) proposed that these HP rocks were extruded into the upper plate above the subduction zone and do not mark an oceanic suture. This simplifies paleogeographic reconstructions for the Acatlán Complex during the Paleozoic. Thus, detrital zircon ages in the Neoproterozoic-Ordovician rocks of the Ixcamilpa area suggests derivation from, and deposition along the passive margin of, Oaxaquia-Amazonia (e.g. Keppie et al. 2008a): this is uniquely indicated by the ~800-900 Ma zircons present in some of the units, which do not occur in Laurentia (Fig. 2.9). The ages of Piaxtla protoliths are consistent with their being deposited on the rift margin of Oaxaquia-Amazonia (Fig. 2.10) (Keppie et al. 2008a).

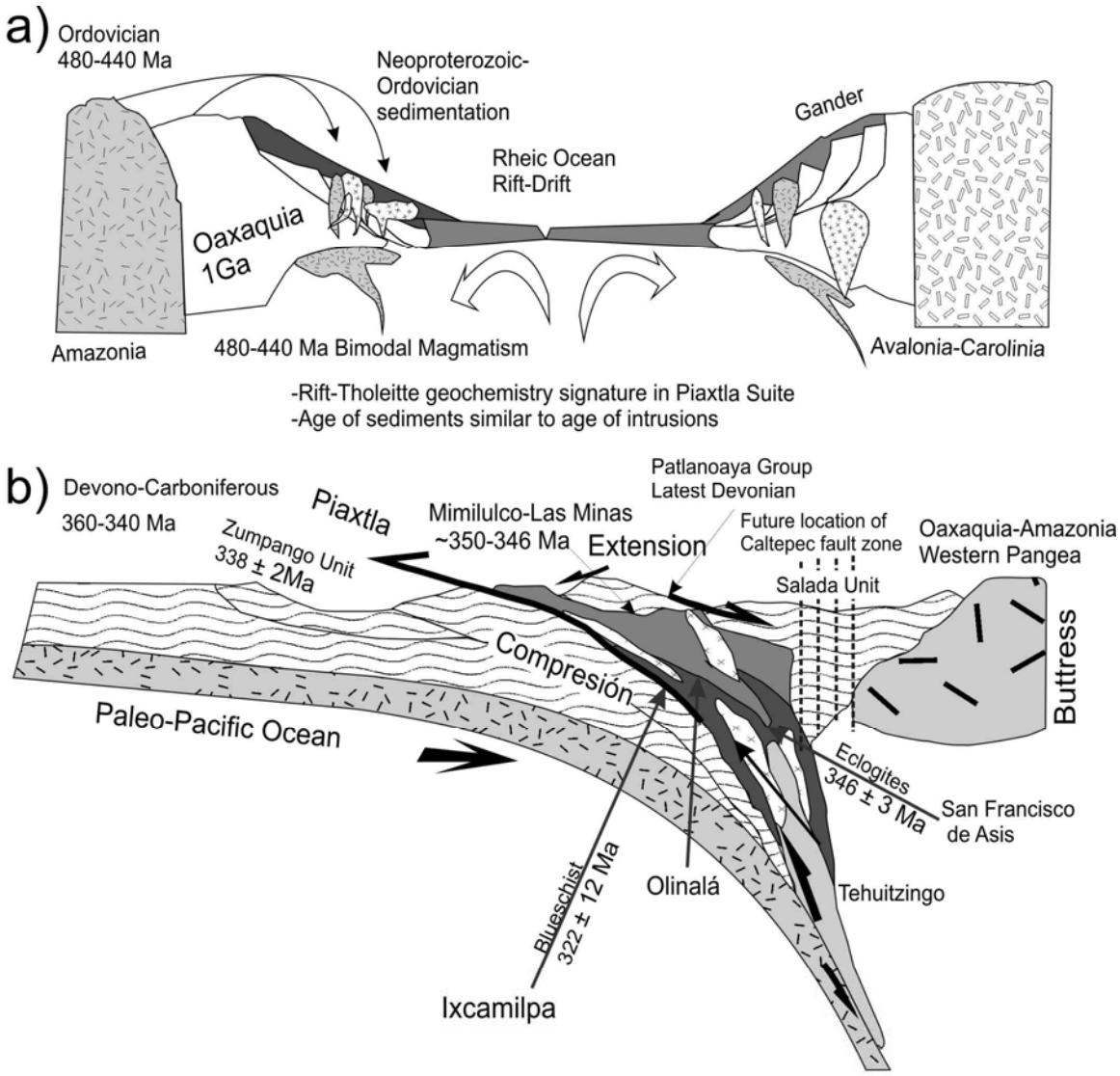

Figure 2.10 (a) Inferred Ordovician paleogeography for the Piaxtla Suite and Ordovician bimodal rift-related intrusions in the Acatlán Complex, and possible provenance of detrital zircons from Amazonia and Peri-Gondwana terranes (modified after Keppie et al. 2008a); b) Carboniferous extrusion tectonic setting (modified after Keppie et al. 2008a), Ar-Ar and U-Pb ages are extracted from Middleton et al. (2006); Elías Herrera et al. (2006); Vega Granillo et al. (2007); Ramos-Arias et al. (2008); Ortega Obregón et al. (2009).

Table Caption

Table 1. LA-ICPMS, U-Pb isotopic analyses of zircon.

The twelve samples were crushed, and heavy minerals were separated using a Wilfley table, and then passed through a Franz magnetic separator at the Instituto de Geología, Universidad Nacional Automona de México (UNAM). Zircon was extracted using heavy liquids and hand picking, and then mounted in epoxy and polished. They were photographed in both transmitted and reflected light and analyzed zircons were

examined by SEM-CL (cathodo-luminiscence). Individual, homogeneous grains were selected for analysis by Laser Ablation Inductively Coupled Plasma-Mass Spectrometry (LA-ICPMS), ten samples at the Arizona Laser Chron Center, and two samples at the Centro de Geociencias (UNAM) in Juriquilla, Queretaro.

U-Pb data are quoted with 2σ uncertainties in old zircons (>1.3 Ga), analyses with >20% discordance or >10% reverse discordance were considered unreliable and were rejected (Gehrels et al., 2006). The low precision in measuring ^{207}Pb in young grains (with $^{206}Pb/^{238}U$ ages of <800 Ma) results in large uncertainties in the $^{207}Pb/^{206}Pb$ ages (Gehrels et al., 2006). This makes the geological significance of concordance and discordance difficult to assess, and thus these data were not rejected. For ages <800 Ma, the best age is the $^{206}Pb/^{238}U$ age, whereas for ages >800 Ma the the $^{207}Pb/^{206}Pb$ age is taken. Samples analyzed at Centro de Geociencias (Juriquilla, Queretaro, Mexico) were corrected following Solari et al. (2009) that produced accuracies better than 0.5%, and precisions in the range of 2-3% 2σ uncertainties in the $^{206}Pb/^{238}U$ ratios in analyses of reference material zircons.

Jeffries et al. (2003) regarded a single, high-precision, zircon analysis with $^{206}Pb/^{238}U$, $^{207}Pb/^{238}U$, and $^{206}Pb/^{207}Pb$ ratios that are the same within small uncertainties as concordant to date the time of intrusion and/or extrusion in igneous rocks or the maximum age of deposition. On the other hand, Gehrels et al. (2006) proposed that a cluster of three or more zircons with similar $^{206}Pb/^{238}U$ ages is robust. We use one or both of these criteria in assessing the age data. U-Pb data were plotted on Tera-Wasserburg diagrams (Figs. 2.5-7) using IsoPlot 3.00 of Ludwig (1991) and as relative age probability curves, which add probability distributions from all analyses from a given sample into a unique composite probability distribution (Figs. 2.5-7). The age probability plots are constructed from the $^{206}Pb/^{238}U$ age for young zircon grains (<1.3 Ga) and the $^{206}Pb/^{207}Pb$ age for older zircon grains (>1.3 Ga).

Capítulo 3

A Carboniferous high-pressure klippe in the western Acatlán Complex of southern México: implications for the tectonothermal development and paleogeography of Pangea.

International Geology Review, DOI:10.1080/00206814.2011.580634, (2011)

Mario A. Ramos-Arias[a*], J. Duncan Keppie[a], James K.W. Lee[b], and Amabel Ortega-Rivera[c]

[a] *Departamento de Geología Regional, Instituto de Geología, Universidad Nacional Autónoma de México, 04510 México, D.F., México.*

[b] *Department of Geological Sciences and Geological Engineering, Queen's University, Kingston, Ontario, Canada, K7L 3N6*

[c] *Instituto de Geología, Universidad Nacional Autónoma de México, Estación Regional del Noroeste, Apartado Postal 1039, Hermosillo, Sonora 83000, México*

Abstract

High-pressure (HP) rocks are critical for palinspastic restorations because they mark inferred subducted/extruded oceanic crust; knowledge of their geometric, geodynamic, and age relationships provide essential constraints on paleogeographic reconstructions. The westernmost HP belt (Ixcamilpa) in the Acatlán Complex of southern Mexico has been inferred to be a mid-Late Ordovician backarc basin on the southern Iapetan margin that was subducted beneath eastern Laurentia and extruded up the subduction zone in the Early Silurian. Reexamination of Ixcamilpa HP rocks has revealed that they comprise lower Paleozoic rift-passive margin protoliths, and occur in a W-vergent klippe (not a suture) formed during polyphase deformation. Peak metamorphic conditions of blueschist-amphibole eclogite facies evidence retrogression through epidote amphibolite to greenschist facies. $^{40}Ar/^{39}Ar$ dating of various rocks yielded plateau ages of 344-339 Ma for calcic amphibole, 318 ± 4 Ma for glaucophane,

and 329-325 ± 2 Ma for muscovite (excess argon), which clearly indicate a Carboniferous age for this tectonothermal event. We interpret the 20 my range in amphibole ages as reflecting progressive unroofing. The terminal stage of progressive thrusting placed the HP rocks above the Middle Mississippian Zumpango Unit, during which a single penetrative sub-greenschist fabric was produced. Subsequent Permian or Laramide deformation refolded all the rocks about NE-trending upright folds. We postulate that the root zone of the HP nappe lies to the east in the median HP belt, which has a structure consistent with an extrusion zone. Inasmuch as similar units of the Acatlán Complex bound this HP root zone on either side, it is inferred to have been extruded into the upper plate above the subduction zone, and thus is not an oceanic suture. Our new data provide constraints for a Carboniferous paleogeographic reconstruction, whereby subduction erosion of passive margin rocks took place on the western margin of Pangea and were subsequently extruded into the upper (Acatlán) plate.

Keywords: high-pressure, klippe, Acatlán Complex, Mexico, Carboniferous, assembly of Pangea

*Corresponding author (email: alfredogeo@yahoo.com.mx)

Introduction

Belts of high-pressure (HP) rocks have recently been subdivided into Continental collision- and Pacific-types (Liou et al., 2004), and are generally interpreted as marking the location of former oceans that were subducted to produce HP metamorphism and then extruded back up the subduction zone (e.g. Ernst et al., 1997, 2008). However, Keppie et al. (2010) have recently proposed that some HP rocks were extruded into the upper plate. The two modes of extrusion may be distinguished by comparing the rocks on either side of the HP belt, in order to determine whether they have different or similar geological records and paleomagnetic signatures, respectively. The origin of HP belts, either extruded up along the subduction channel (continental collision- and Pacific-types) or into the upper plate is critical for making paleogeographic reconstructions.

Two HP belts occur in the Acatlán Complex of southern México: the median Piaxtla-Mimilulco and the Ixcamilpa-Olinalá belts (Fig. 3.1). These HP belts were traditionally interpreted to mark oceanic sutures (Ortega-Gutiérrez, 1981), an interpretation subsequently adopted by Ortega-Gutiérrez et al. (1999), Talavera Mendoza et al. (2005) and Vega-Granillo et al. (2007, 2009), who inferred that they

were the remnants of one to five ocean basins within the Iapetus and Rheic oceans. In contrast, Keppie et al. (2008a) proposed that the median Piaxtla-Mimilulco HP belt was extruded into the upper plate, and so does not mark an oceanic suture, a proposal consistent with the similarity of rocks on either side. The Ixcamilpa-Olinalá HP belt has been interpreted in two ways: (i) as a klippe composed of a mid-Late Ordovician backarc basin on the southern margin of the Iapetus Ocean that was subducted beneath Laurentia and extruded back up the subduction channel during the Late Ordovician-Early Silurian (Vega-Granillo et al., 2009) based on the presence of ca. 477 Ma detrital zircons of presumed arc provenance associated with inferred subduction-related metamorphism at ca. 458–443 Ma and a 323 ± 6 Ma $^{40}Ar/^{39}Ar$ phengite age related to closure of the Rheic Ocean (Talavera-Mendoza et al., 2005; Vega-Granillo et al., 2007, 2009); or (ii) as a series of Early Cenozoic fault-bounded blocks in the Olinalá area initially deformed in the late Devonian-earliest Carboniferous during extrusion into the Acatlán Complex (Ortega-Obregon et al., 2009). Resolution of these contrasting interpretations of the structural geometry, the age of HP metamorphism and their tectonic setting led us to further investigate the Ixcamilpa area. In this paper, we present structural, petrological, geochemical, and geochronological data which indicate that the HP rocks in the Ixcamilpa area represent a klippe rooted in the median HP belt and emplaced during the Mississippian. This conclusion has important implications for the paleogeography of the Acatlán Complex and its relationship to the amalgamation of Pangea.

Geological Setting

The Acatlán Complex is bounded by three tectonic boundaries: (i) on the eastern side, the Permian, Caltepec dextral ductile shear (Elías–Herrera and Ortega-Gutiérrez, 2002) juxtaposes the Acatlán Complex against the ca. 1 Ga Oaxacan Complex; (ii) to the south, the sinistral transtensional, Cenozoic Chacalapa–La Venta Fault places it against the Mesozoic-Cenozoic Xolapa Complex (Tolson, 2005; Torres de León, 2005); and (iii) to the west, the Late Cretaceous Papalutla thrust places Acatlán Complex on top of the Cretaceous Morelos-Guerrero Platform (De Cserna et al., 1980 and Cerca et al., 2006).

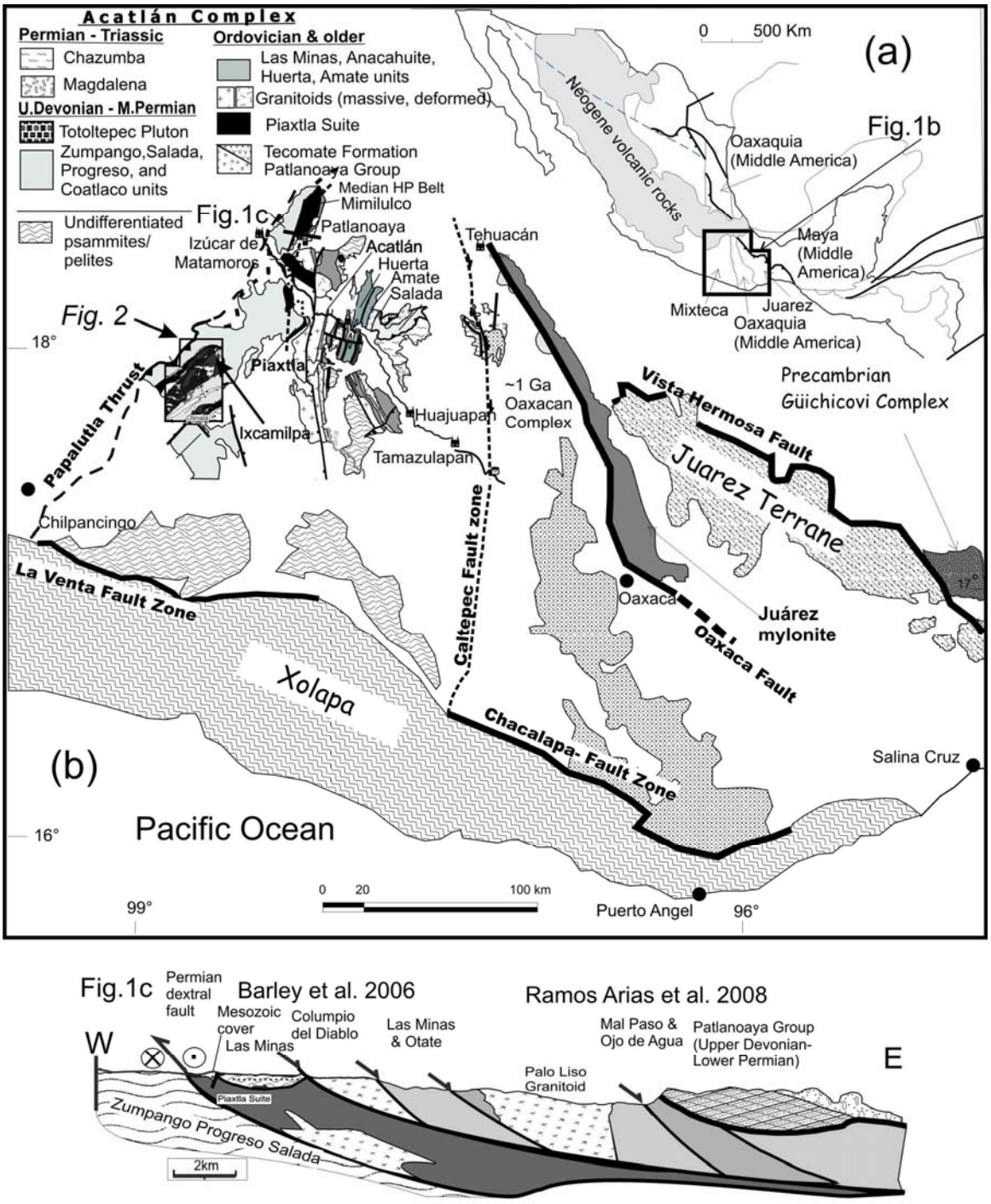

Figure 3.1 Acatlán Complex in the context of tectonostratigraphic terranes in Southern México (modified after Ortega Gutiérrez et al., 1999; Keppie 2004).

The northern margin of the Acatlán Complex is covered by volcanic and volcaniclastic sequences of the Cenozoic Trans-Mexican Volcanic Belt (Fig. 3.1b).

The Acatlán Complex may be subdivided into two parts separated by the N-S, Piaxtla-Mimilulco HP belt. The western part of the Acatlán Complex in the Olinalá and Ixcamilpa areas were initially studied by Hermanns (1994), Farfán (1998), Ramírez-

Espinoza (2001), Torres de León (2001), and De la Cruz (2004). Subsequently, Talavera-Mendoza et al. (2005) and Vega-Granillo et al. (2007, 2009) sampled the western Acatlán Complex for geochronology, and Ortega-Obregon et al. (2009) and Ramos and Keppie (2011) have recently published detailed geological maps of the Olinalá and Ixcamilpa areas, respectively, accompanied by zircon U-Pb geochronological data. The rocks of the Piaxtla Suite in the Ixcamilpa area preserve metamorphic grades from blueschist through amphibolite eclogite to greenschist facies and were subdivided into a series of tectonic slices (Fig. 3.2) by Ramos-Arias and Keppie (2011).

These recent data indicate that the rocks are of Neoproterozoic-Paleozoic age: (i) the pre-Silurian Piaxtla Suite (metapsammites, metapelites and rift-related tholeiitic amphibolites) exists in five tectonic slices that pass structurally upwards from blueschist through amphibolite eclogite to amphibolite facies: the youngest detrital zircons range from Neoproterozoic to Ordovician; intruded by (ii) Ordovician megacrystic granitoids; structurally overlying (iii) Carboniferous Zumpango Unit consisting of clastic (youngest detrital zircon age = 310 ± 3 Ma) and volcanic rocks (356 ± 15 Ma and 327 ± 2 Ma). Ages of other detrital zircon populations (and potential sources in parentheses) yield peaks of 435-490 Ma (Acatlán granitoids), 500-700 a (Yucatan-Brasiliano), 800-900 Ma (Goiás arc, eastern Amazonia), and 950-1300 Ma (Oaxaquia, Amazonia or Laurentia).

Published constraints on the timing of deformation were provided by $^{40}Ar/^{39}Ar$ plateau ages for phengite of 322 ± 4 Ma in the Ixcamilpa area (Vega-Granillo et al., 2007), and 342 ± 2 Ma (amphibole), 361 ± 3 Ma (muscovite), 331 ± 5 Ma (muscovite) in the Olinalá area, and indicate cooling through 550ºC and 350ºC, respectively (Ortega-Obregon et al., 2009). Vega-Granillo et al. (2007, 2009) inferred that the HP metamorphism was associated with subduction-related igneous rocks dated at ca. 458–443 Ma, and attributed the Mississippian age to subsequent overprinting. However, the calc-alkaline granitic arc rocks of supposed arc affinities have recently been shown to be part of a bimodal suite associated with rift-related tholeiitic rocks (Keppie et al., 2008b; Ortega-Obregon et al., 2010). The data provided in this paper indicate that the HP and associated rocks of the Piaxtla Suite occur in a W-vergent klippe metamorphosed and

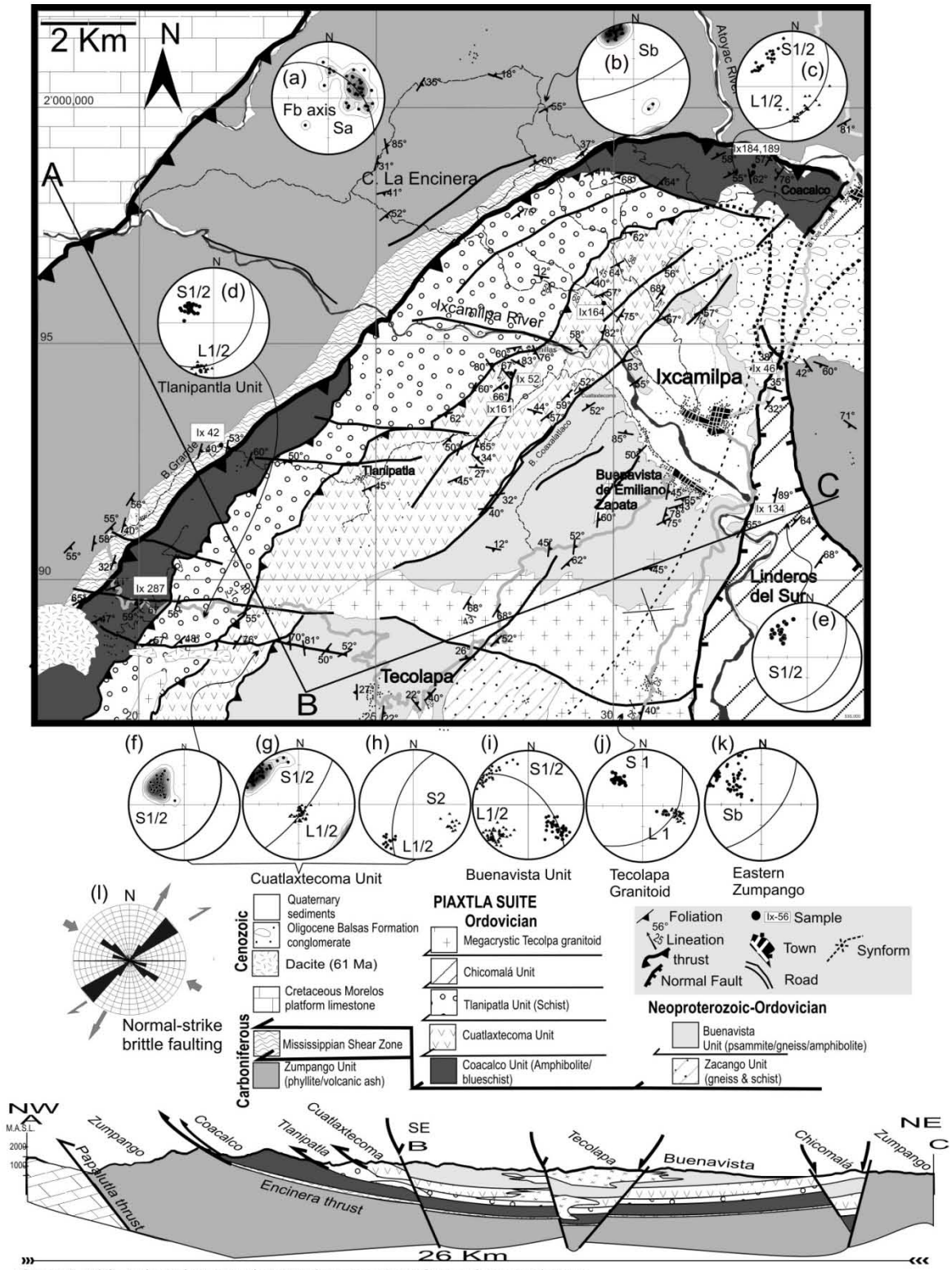

Figure 3.2 (a) Geological-Structural Map and cross-section of Ixcamilpa area showing general disposition of the structures and Cenozoic faults structures.

emplaced during the Mississippian that was subsequently overprinted by Cenozoic sub-vertical faults.

Thus, incorporation of the most recent data led Ortega-Obregon et al. (2009, 2010) and Ramos-Arias and Keppie (2011) to derive the following geological history for the Ixcamilpa-Olinalá area:

1. Neoproterozoic to Lower-Middle Ordovician deposition of clastic rocks;
2. Ordovician intrusion of bimodal granitoids and amphibolites;
3. Lower-middle Mississippian deposition of clastic rocks associated with mafic and felsic lavas and minor intrusions that was synchronous with Late Devonian-Middle Mississippian deformation and metamorphism;
4. Lower Permian low-grade deformation;
5. Middle-Upper Permian deposition of the Olinalá Formation;
6. Late Paleocene-Early Eocene normal-transcurrent faulting on ENE-trending faults and ENE-trending open folds during the Laramide Orogeny;
7. Intrusion of a 61 Ma diorite (Lower Paleocene).

Structure

Ramos-Arias and Keppie (2011) assigned the HP and associated rocks of Ixcamilpa area to the Piaxtla Suite and subdivided them into several tectonic slices (Fig. 3.2)(from bottom to top): (i) Coacalco Unit (glaucophane schist, amphibolite, and metasedimentary rocks); (ii) Tlanipantla Unit (metapsammites, metapelites and a few amphibolites); (iii) Cuatlaxtecoma Unit (amphibolite, metasedimentary rocks cut by granitic dikes); (iv) Zacango Unit (paragneiss, metapsammite and metapelite); (v) Buenavista Unit (metapsammite, metapelite and a few amphibolites); and (vi) Chicomala Unit (graphitic schist, meta-quartzite cut by pegmatite and rare mafic dikes). Also within the high grade rocks is the Ordovician megacrystic Tecolapa metagranitoid, which is cut by metaleucogranite dikes. All of these units are thrust over the Zumpango Unit, a sub-greenschist facies unit consisting of quartzite, meta-arkose, phyllite and white volcanic ash.

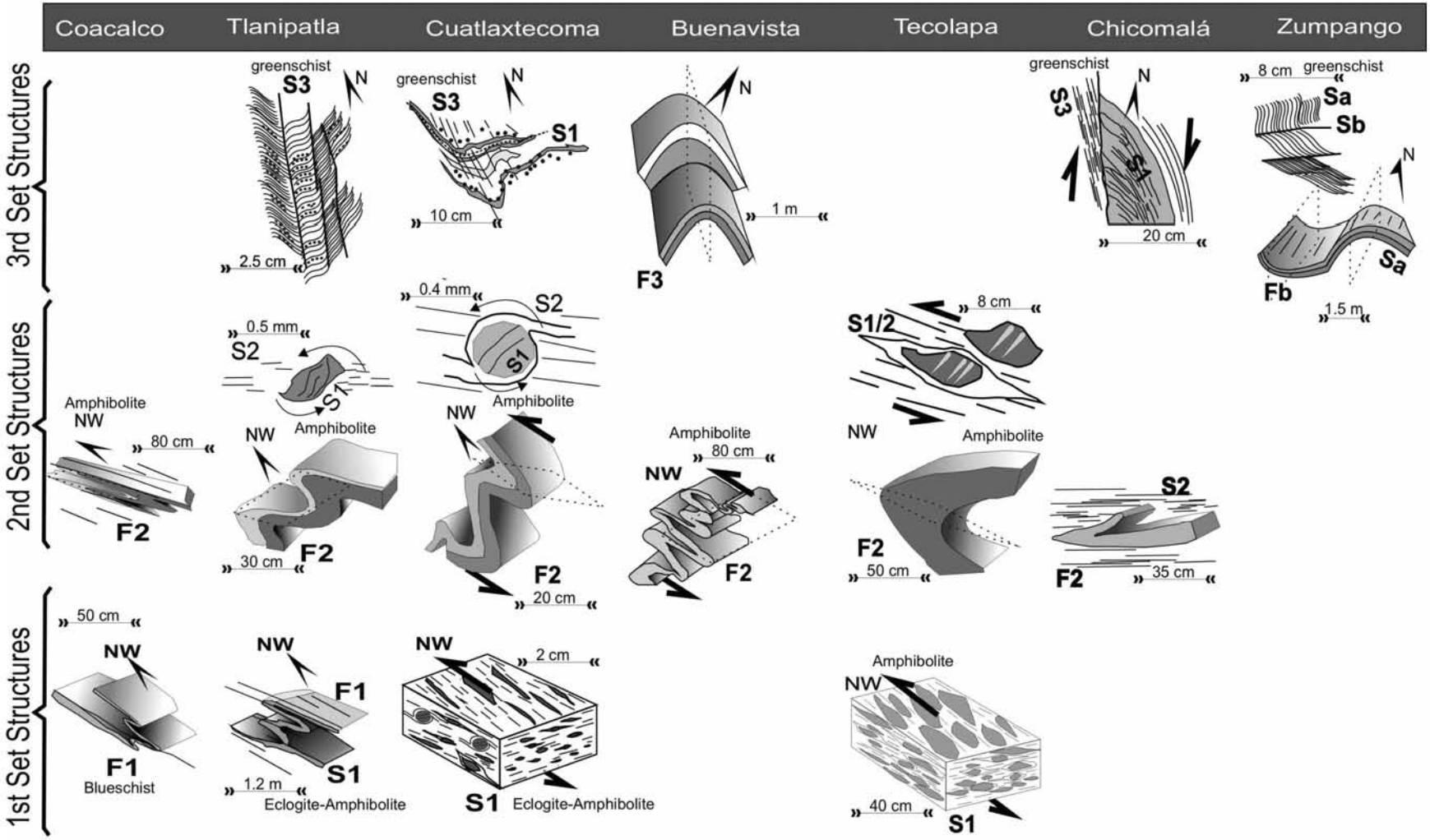

Figure 3.3 Summary of the geometry and spatial orientation of ductile structures in the HP rocks and Zumpango unit of Ixcamilpa area.

Mesoscopic-microscopic structure in the Piaxtla Suite

The rocks of the Piaxtla Suite in the Ixcamilpa area display ductile polyphase deformation (Fig. 3.3).

1st Set of Structures. In the polydeformed psammitic and pelitic meta-sedimentary rocks of the **Tlanipatla Unit**, intrafolial isoclinal folds, F_1, are associated with stretched quartz-feldspars ribbons (L_1). The earliest structures in the meta-psammites of the **Zacango Unit** consist of stretched quartz/feldspar and white mica bands, S_1, locally containing porphyroblasts of garnet. In the mafic dikes within the **Chicomalá Unit,** chlorite pseudomorphs after aligned amphibole, plagioclase and white mica, with chlorite- and mica-fish shape indicating thrusting with top-to-the-NW. Abundant quartz veins that may cut remnants of bedding, S_0, were deformed together with metasedimentary rocks in isoclinal recumbent folds, F_1.

In the mafic rocks of the **Coacalco, Buenavista and Cuatlaxtecoma units,** the S_1 foliation is defined by aligned sub-idiomorphic glaucophane, amphibole, and plagioclase with oriented amphibole defining a mineral lineation, L_1. In the mafic rocks of the **Coacalco Unit,** bands of glaucophane alternate with epidote and white mica domains parallel to S_1. In the **Cuatlaxtecoma Unit**, bands of garnet surrounded by relicts of amphibole, epidote, and chlorite, plagioclase alternate with white mica-chlorite lepidoblastic domains are subparallel to L_1 and S_1, and are generally parallel to the transposed S_2 foliation.

Metagranitic dikes that cut the **Buenavista Unit** contain bands of stretched quartz and cataclastic K-feldspars defining solution cleavage domains, S_1, which are subparallel to axial planes of tight-isoclinal F_1 folds.

2nd Set of Structures. The S_1 foliation is deformed by close-isoclinal asymetric folds (F_2) that have axial planes defined by another penetrative foliation (S_2). In the **Coacalco** Unit, an intense penetrative axial planar foliation is defined by aligned glaucophane partly replaced by chlorite in corrosion and reaction rims. The glaucophane is accompanied by poikiloblastic plagioclase (albite) containing internal aligned epidote, NaCa-amphibole, and phengite. Some amphiboles have a cataclastic flow texture.

In places within the **Cuatlaxtecoma Unit**, zoned garnet porphyroblasts contain cores with S-shaped trails of amphibole and clinozoicite surrounded by a clear idiomorphic rim, around which the S_2 foliation is deformed. This is interpreted as syntectonic garnet growth followed by static growth and then flattening.

In the **Buenavista and Cuatlaxtecoma units,** S_1 is transposed into a S_2 solution cleavage resulting in a $S_{1/2}$ foliation defined by bands of mica, quartz-feldspar and epidote-mica-chlorite. This transposed foliation is overgrown by poikiloblastic plagioclase containing inclusions of quartz, apatite, epidote, amphibole and plagioclase**.** Aligned amphibole defines a mineral lineation, L_2.

F_2 folds in the **Cuatlaxtecoma Unit** fall in Classes 1C, 2 and 3 of Ramsay (1967) (Fig. 3.5) suggesting flexural folding with superimposed flattening (Ramsay, 1967; Davis and Reynolds, 2000). The Hansen method (Marshak and Mitra, 1998) was used to determine the kinematics of the curvilinear F_2 folds in the Cuatlaxtecoma and Buenavista units, and at two localities yielded a top to the NW sense of movement (Fig. 3.4a,b). At some localities $L_{1/2}$ plots on great circles coincident with the foliation and the plunge varies from gently SW to down-dip (Fig. 3.4f and g): this is interpreted as the result of rotation towards the northwesterly slip direction indicated by associated δ and σ at these localities indicate top-to-the-NW (Fig. 3.4c and d)..

In the **meta-sedimentary** rocks of the Piaxtla Suite (**Tlanipatla, Zacango and Chicomalá units)**, isoclinal, recumbent F_2 folds have an axial planar foliation, $S_{1/2}$, defined by aligned chlorite and white mica, and rarely, clinozoizite. Stretched quartz defines the $L_{1/2}$ lineation. Fold geometry indicates that the F_2 folds fall in the 1C and 2 classes of Ramsay (1967) (Fig. 3.5).

*3rd Set of Structures***.** $S_{1/2}$ is folded by mesoscopic and megascopic, upright, open, NE-trending F_3 folds in both the mafic and meta-sedimentary rocks. F_3 is locally accompanied by a crenulation cleavage defined by sericite and an SC' fabric indicating dextral movement in a ductile-brittle regime (Fig. 3.6).

Mesoscopic-microscopic structure in the Ordovician megacrystic granitoids

The Ordovician megacrystic Tecolapa Granitoid and cross-cutting leucogranitic dikes are mylonitic. The dikes contain a S_1 foliation consisting of stretched quartz and K-feldspar, which is deformed by recumbent, close, Class 2 folds, F_2, indicating a combination of flexural folding and flattening (Fig. 3.5). Oblate and rotated K-feldspar porphyroclasts display σ and δ shapes indicating a top-to–the-NW sense of thrusting. These porphyroclasts have an oblate shape with a mean K ratio of 0.29, where K = (long axis/medium axis)/(medium axis/short axis): some of the scatter around this value may be due to initial shape variation (Fig. 3.7). The oblate porphyroclasts are

surrounded by a foliation consisting of stretched and aligned quartz L_2 and white mica. The combination of K-feldspar lamellae, quartz ribbons, and quartz veins within the K-feldspars suggest deformation took place at temperatures intermediate between recrystallization of quartz and brittle cracking of K-feldspars at >ca.450° C (Passchier, 1996; Blekinsop 2002; Vernon and Clarke, 2008).

Mesoscopic-microscopic structure in the Mississippian Zumpango Unit

The sub-greenschist facies **Zumpango Unit** is composed of interbedded meta-arkose, quartzite, phyllite and white volcanic ash layers intruded by deformed quartz veins. The ash layers preserve some altered K-feldspar and plagioclase phenocrysts set in a fine grained groundmass containing accessory iron oxides clay matrix and zircons. Hydrothermal alteration is visible adjacent normal faults. The quartzites contain a solution cleavage, Sa, consisting of alternating bands of stretched and recrystallized quartz, sericite and chlorite, indicative of sub-greenschist facies metamorphism. The Sa cleavage is deformed by open, upright, SW-plunging, folds (Fb), which locally have an axial planar crenulation cleavage (Sb) that is not associated with new mineral growth (Fig. 3.6).

Major structure

The penetrative $S_{1/2}$ foliation in the Piaxtla rocks is generally oriented 045/65°SE *(Fig. 3.2 and 3.3).* The $S_{1/2}$ foliation in the Coacalco unit is 040-045/ 35° and the $L_{1/2}$ amphibole lineation plunges 40-50°SE (Fig. 3.2c). The strongly penetrative $S_{1/2}$ foliation in the metasediments of Tlanipatla Unit is oriented at 045/35-40°SE and quartz stretching lineation plunges to 20°SW (Fig. 3.2d). In the Cuatlaxtecoma Unit, the S_2 foliation is oriented 045/60-75°SE, with an amphibole mineral lineation plunging at 70-85°SE, and a quartz stretching lineation in discrete shear zones plunging to 20°SW (Figures 3.2 f, g, h). In the Buenavista Unit, the $S_{1/2}$ foliation is distributed along a π-circle, whose pole is the F_3 fold axis plunging at 15°SW (Fig. 3.2i). The orientation of $S_{1/2}$ foliation and $L_{1/2}$ quartz stretching lineation in Tecolapa Granitoid are oriented at 040-050/40° and 100/30-45°SE respectively (Fig. 3.2j). The $S_{1/2}$ in the Chicomala Unit is generally oriented at 045/40°SE (Fig. 3.2e).

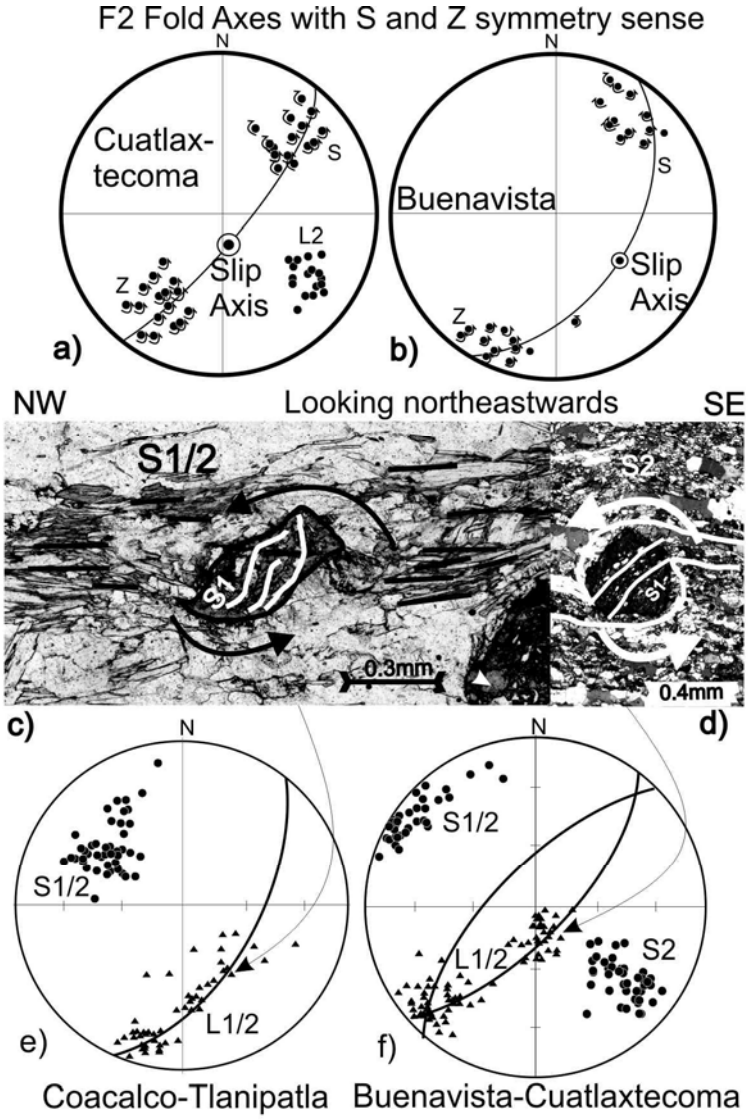

Figure 3.4 Structures in high-grade rocks: (a-b) Hansen method stereoplots applied to recumbent asymmetric folds in the Cuatlaxtecoma, and Buenavista units showing a top to NW vergence; (c-d) NE-looking microphotographs of porphyroclasts with σ and δ shape indicating top-to–the-NW movement. (f-g) Orientation of $S_{1/2}$ fabric and associated lineation, $L_{1/2}$.

The Sa foliation in the western part of the Zumpango Unit is distributed along a great circle with a pole (≡Fb fold axis) oriented at 230/40°SE (Fig. 3.2a), and lies on the subvertical, ENE-trending Sb crenulation cleavage (Fig. 3.2b). In the eastern part of the Zumpango Unit, the Sa solution cleavage is oriented at 045/30-40°SE (Fig. 3.2k).

The **Encinera Thrust** places the high-grade Piaxtla Suite above the low-grade Zumpango Unit. The mylonitic shear zone is 100-300 m wide with anastomosing, penetrative solution cleavage accompanied by late hydrothermal alteration. Within the mylonitic fabric, some σ blocks and a mica lineation indicate oblique thrust-dextral movement to N-NW. The metamorphic grade increases from west to east up to the

contact with Coacalco Unit, where Sa and S_2 are parallel. The Encinera Thrust and Piaxtla Suite have a synformal shape with a large open fold plunging ~200/15-20°SW (Figs. 2 and 3).

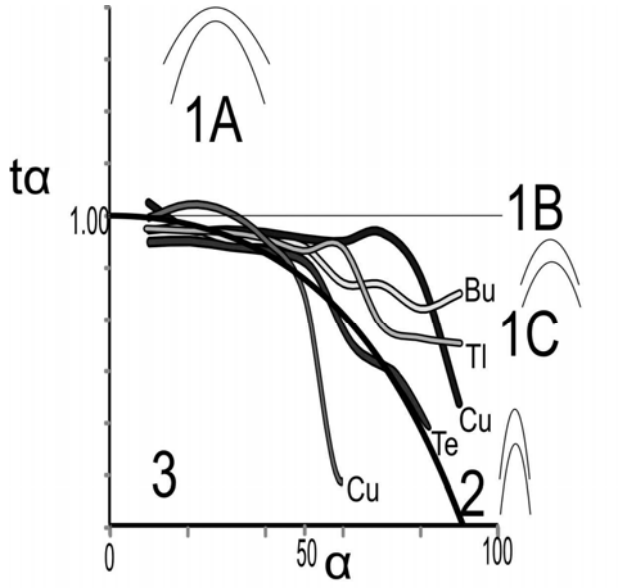

Figure 3.5 Isogon analyses for F_2 folds of Tlanipatla, Cuatlaxtecoma, Buenavista and Tecolapa units.

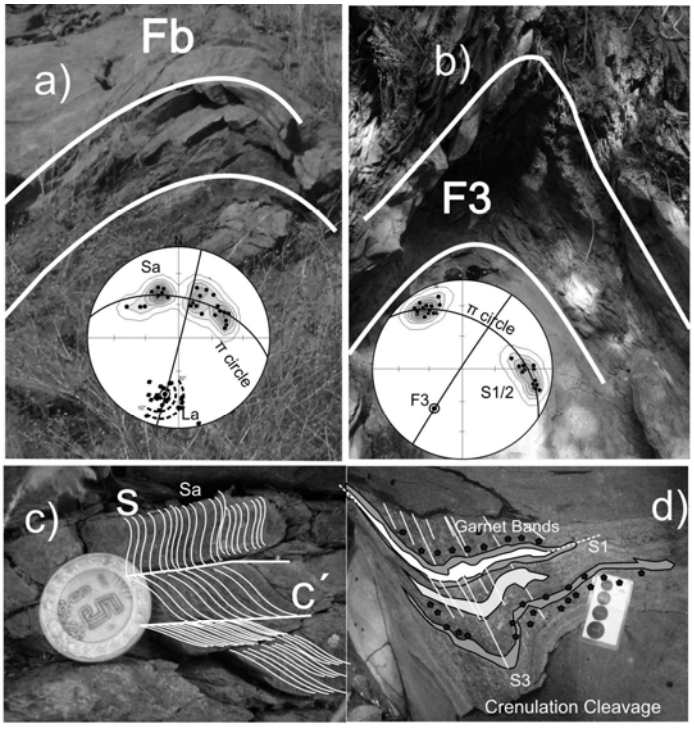

Figure 3.6 Upright open folding with orientations in: (a) low grade Zumpango Unit; (b) high grade Buenavista unit; (c) SC´ fabric and (d) crenulations in Zumpango and Cuatlaxtecoma units.

The ***Papalutla Thrust*** consists of a NE-trending shear zone, 200-400 m wide dipping at 45°SE with metre-size folds and a discrete mylonitic fabric consisting mainly of Cretaceous limestones and clastic rocks of the Zumpango Unit. Cerca et al. (2006) has determined the kinematics as top-to-the-NW.

N-S and E-W normal faults and NE-SW transcurrent-normal faults deform the Paleozoic rocks in the Ixcamilpa Area (Fig. 3.2l). In the east, the Chicomalá Unit is faulted against the Zumpango Unit along a N-trending, antithetic normal fault, which is unconformably overlain by Oligocene clastic sediments of the Balsas Formation. The NE-trending faults cut the ca. 61 Ma Los Laureles Dacite (Ortega Obregón et al., 2009; Ramos-Arias and Keppie, 2011). These two observations bracket some of the faulting in the Paleogene and so may have been contemporaneous with Laramide Orogeny.

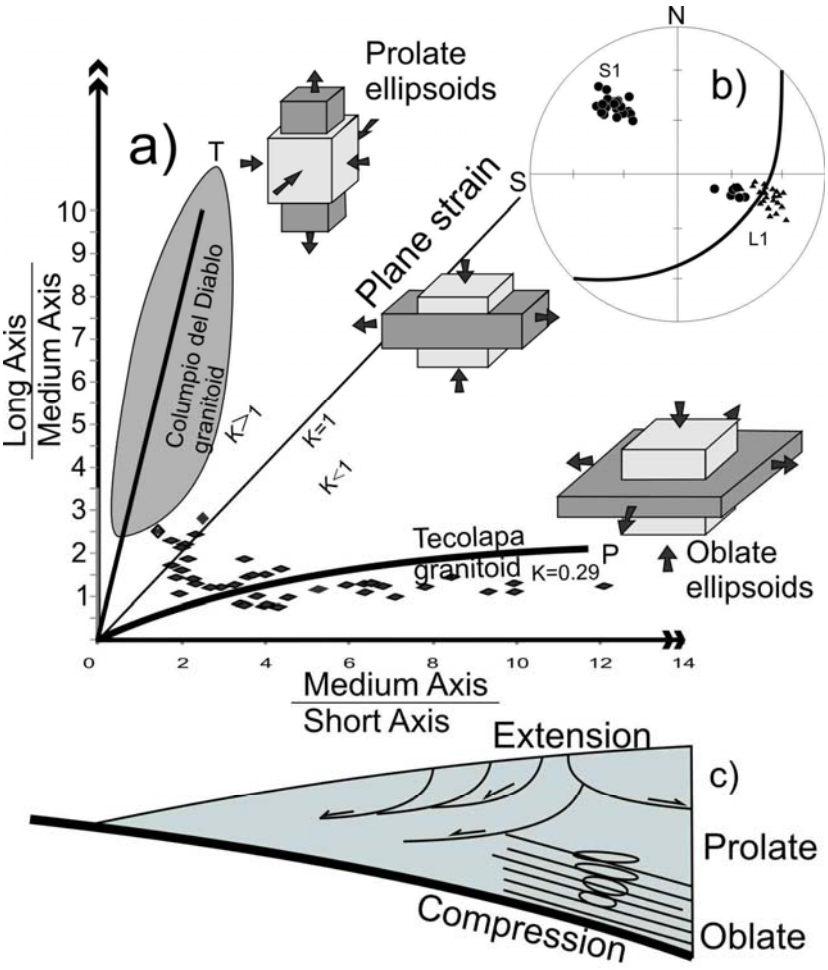

Figure 3.7 Shape analyses in megacrystic granite Tecolapa: (a) Flinn diagram showing that ellipsoids are oblate (S tectonite) compared with the prolate ellipsiods of the Columpio del Diablo Granitoid (Ramos Arias et al. 2008), and the shape of tensional and compressional ellipsoids of Hudleston (1999); (b) $S_{1/2}$ and $L_{1/2}$ with σ kinematic figures indicating a top to NW movement; (c) inferred compressional and tensional strain in the crust during subduction (after Ring et al. 1999).

Metamorphic grade

Seventy thin sections of the Piaxtla Suite were examined using transmitted and reflected light microscopy, to determine the pressure-temperature (P-T) conditions experienced by the high pressure/grade blueschists and garnetiferous amphibolites in the Coaclaco and Cuatlaxtecoma units (Piaxtla Suite). This was followed by electron-microprobe mineral analyses of 5 polished sections with a total of 490 WDS (wavelength dispersive spectrometer) analyses at LUP, Instituto de Geofísica, UNAM, to obtain major elements in oxides (Table 1). P-T trajectories were constructed by combining semi-quantitative and quantitative estimates of the P-T conditions of metamorphism. Semi-quantitative estimates were obtained using a simplified grid of the NCFMASH system for metabasites in the blueschist-eclogite fields (Will et al., 1998 and references therein). Quantitative P-T estimates were obtained using conventional geobarometers and geothermometers that use several experimental and/or theoretical calibrations for multi-phase equilibrium (Table 2).

Blueschist of the Coacalco Unit

Two types of glaucophane occur in the **Coacalco Unit**: idiomorphic and subidiomophic porphyroblasts with corroded embayments of chlorite and needles of Na-amphibole (glaucophane, winchite and barroisite). The glaucophane generally defines the lepidoblastic S_2 fabric, however decussate crystals also occur. The S_2 fabric is also defined by epidote, chlorite fibers and phengite (Fig. 3.8a-c). In some cases, the glaucophane is zoned (Fig. 3.8d). The analyses were used in the phengite geobarometer of Massone and Schyerer (1988) (Table 3 shows Si values) and glaucophane-albite (Gln-Ab) geothermometer of Blundy and Holland (1990). These yielded a peak pressure during F_1 of 12.2 Kbar at 290-396°C for the stable assemblage Ep+Gln+Chl+Ab, where Ep = epidote, Gln = glaucophane, Chl = chlorite, and Ab = albite. This was followed during F_2 by NaCa amphibole growth at peak temperatures between 486 and 566°C at a lower pressure of 6-6.7 Kb (Holland and Blundy 1994; Brown, 1977). A further stage during F_3 is indicated by Ca amphibole that is stable with Ab, for which analyses indicate temperatures and pressures of 399-419°C and 5-5.6 Kb (Spear, 1980; Brown, 1977). Applying the geothermometer of Cathelineau (1988) in chlorite yields temperatures of 330-335°C for progressive deformation during F_3. These P-T determinations indicate that the Coacalco blueschists started in the blueschist field, and retrogressed through epidote

amphibole facies, and finally into greenschist facies (see Coacalco paths, *Co*, in Table 2 and Fig. 3.10).

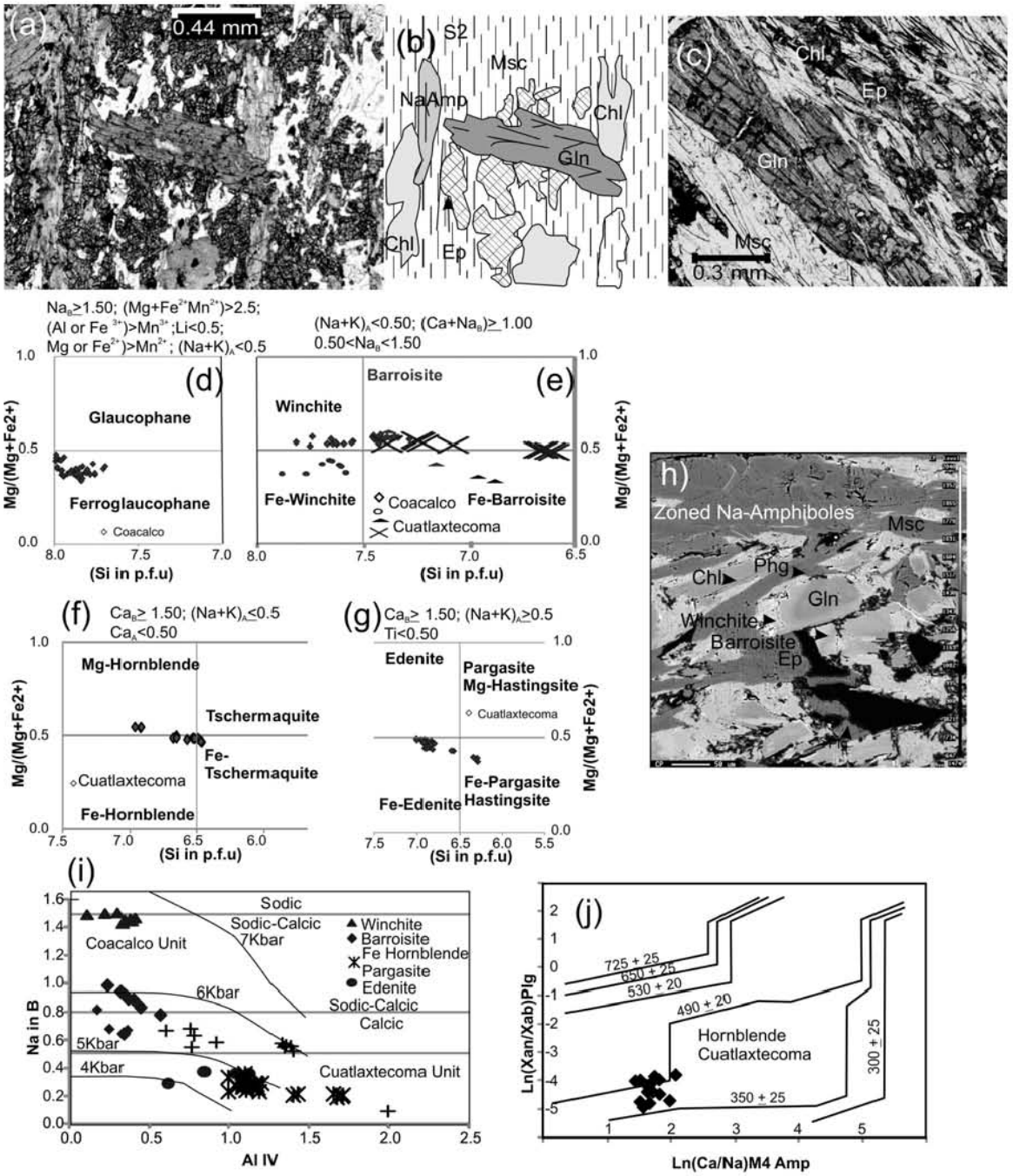

Figure 3.8 Textures and chemistry of amphiboles in the Coacalco Unit: (a-c) microphotographs showing glaucophane surrounded by a lepidoblastic fabric; (d,e) chemistry plotted on Na and NaCa amphibole discrimination diagrams (after Leake et al. 2003); (f-g) chemistry plotted on Ca discrimination diagrams for amphiboles; (h) microphotograph of the Coacalco Unit showing zoning in Na amphibole, and the lepidoblastic texture of NaCa amphiboles, epidote, albite, chlorite, phengite assemblage; (i) pressure estimates based on crossite content in amphibole (after Brown, 1977); and (j) temperature estimates for paired CaAmp-Ab (after Spear, 1980).

Garnet amphibolites of the Cuatlaxtecoma Unit

In the **Cuatlaxtecoma Unit**, thermobarometry of garnet was applied using: (i) core-rim compositions in syntectonic zoned garnet, in which the core is assumed to be in equilibrium with foliated poikiloblastic inclusions of amphibole, chlorite and plagioclase; and (ii) the rim and matrix NaCa and Ca amphiboles inside pressure shadows adjacent to garnet, plagioclase, chlorite and epidote (Fig 9), where prograde and retrograde metamorphism associated with shear deformation may be determined (Spear, 1995 and references therein).

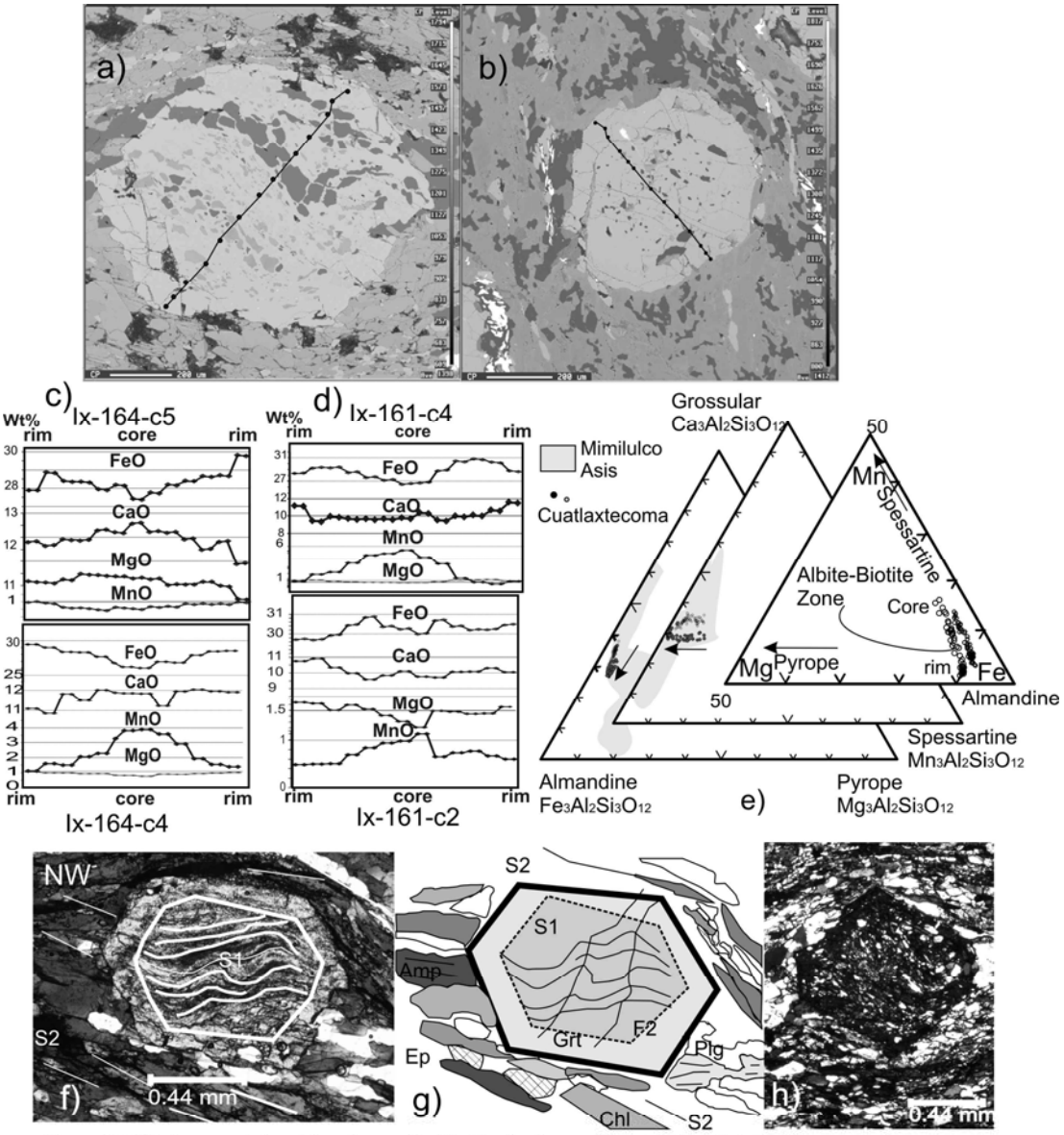

Figure 3.9 Textures and chemistry of garnet in the Cuatlaxtecoma Unit, Piaxtla Suite: (a-b) microphotographs; (c-d) cross-sectional compositions; (e) ternary chemical diagrams: note that the garnets are depleted in Mn, have increasing almandine compositions from core to rim, and fall in Ab-Bt field of Banno et al., (1986); (f-g-h) microphotographs of garnet showing an internal foliation, S_1, deformed by F_2, and a clear static rim surrounded by a lepidoblastic texture that is bowed around the garnet.

Data from core-to-rims transects in different syntectonic garnet porphyroblasts in amphibolites of the Cuatlaxtecoma Unit yield an average composition $Alm_{58-60}Prp_{2.7-3.3}Grs_{32-3.3}Sps_{3.3-6.0}$ (where Alm = almandine, Prp = pyrope, Grs = grossularite, and Sps = spessartine), show prograde zoning with depleted Mn, increasing Alm compositions, and plot in the biotite-albite (Bt-Ab) zone of Banno, (1986)(Fig. 3.9e). The garnet cores are considered to be metastable with foliated inclusions of NaCa Amphibole +Plagioclase+Chlorite+Quartz. This latter mineral assemblage is surrounded by lepidoblastic NaCa and Ca-amphibole, albite poikiloblasts, abundant chlorite fibers accompanied by minor phengite (Phg), and epidote (Zo). Secondary chlorite corona surrounding amphibole and garnet occur in association with accessory pyrite, chalcopyrite, and unstable rutile, and ilmenite.

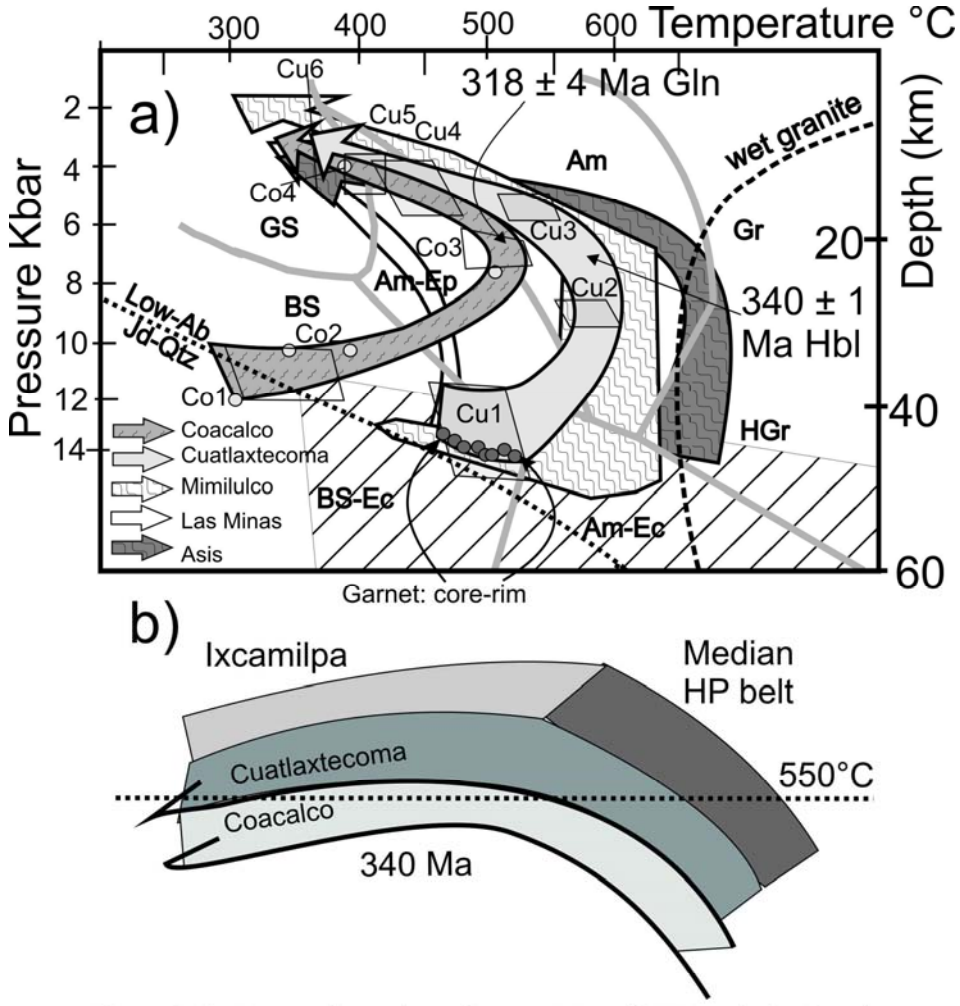

Figure 3.10 Metamorphic grades and interpretation: (a) P-T-t paths for Coacalco (Co) and Cuatlaxtecoma (Cu) units constructed on the basis geothermobarometry from the mineral chemistry summarized in Table 2. Other P-T paths plotted for comparison are from: Meza Figueroa et al. (2003) for Mimilulco; Keppie et al., (2010) for Las Minas; Middleton et al. (2007) for Asis; and (b) model to explain the isograd distribution in the Acatlán Complex during the Carboniferous.

Grn+Amp pairs analyzed from core to rim, and Grn + external Amp, yielded temperatures between 440 and 550 °C using the geothermometer of Graham and Powell (1984) (Table 4). Pressures of 9.2-16.7 Kb during F_1 were obtained using the phengite geobarometer of Massone and Schyerer (1988).

Applying the Amp+Ab geothermometer and Amp geobarometer (Spear, 1980; Brown, 1977; Holland and Blundy; 1994), the lepidoblastic NaCa and Ca amphibole formed during F_2 yielded temperatures of 520-547°C and 560-609°C and pressures decreasing from 9.5 Kb to 5.88 Kb. A further stage during F_3 is indicated by analyses of hornblende-amphibole, which indicate a lower pressure of <4.5Kb. Finally, chlorite needles give a temperature of 356-364°C (Kranidiotis and MacLean, 1987; Cathelineau, 1988).

These data indicate peak conditions for the Grn+Ep+Chl+Amp+Plg +Qtz assemblage in the amphibole eclogite field (Liou et al., 2004; Ernst and Liou, 2008) (Fig 10a). This is consistent with the absence of jadeite and omphacite due to replacement to albite, which indicates retrogression into the Ep-Amp field in greenschist facies (see Cuatlaxtecoma paths *Cu*, in Table 2 and Fig. 3.10).

^{40}Ar-^{39}Ar Geochronology

Six samples were collected for $^{40}Ar/^{39}Ar$ analyses – three for amphibole and three for muscovite. The amphiboles were separated from: (a) two amphibolite samples of the Cuatlaxtecoma Unit (Ix 52: Lat 18°2´15´´, Long 98°44.9´44´´; Ix 164: Lat 18°3´1.2´´, Long 98°43´2,75´´); and (b) glaucophane from the Coacalco Unit (Ix-189: Lat 18°4´48.75´´, Long 98°41´43.76´´). Muscovite was separated from: (a) the Coacalco Unit (Ix 189: Lat 18°4´48.75´´, Long 98°41´43.76´´); (b) the Chicomalá Graphitic Schist Unit (Ix 46: Lat 18°2´11.02´´, Long 98°40´55.52´´); and (c) the Encinera thrust zone (Ix 42: Lat 18°1´26.40´´, Long 98°47´37.61´´).

Method

The amphibole and muscovite were separated and loaded into Al-foil packets and irradiated together with Hb3 gr (1072Ma Standard) as a neutron-fluence monitor at the McMaster Nuclear Reactor in Hamilton, Ontario Canada. Ar^{39}-Ar^{40} analyses were performed by laser step-heating techniques described by Clark et al. (1998) in Geochronology Research Laboratory of Queen´s University, Kingston, Ontario Canada.

The data are given in Table 5 and shown in Figure 3.11. All data have been corrected for blanks, mass discrimination, and neutron induced interferences. For the purposes of this paper, plateau ages are obtained when the apparent ages is obtained of at least three consecutive steps comprising a minimum of 50% of the ^{39}Ar released and that agree within 2σ error with integrated age of the plateau segment. Plateau ages are interpreted to represent the best estimate for time of cooling through a mineral´s Ar closure temperature. Errors shown in Table 1 and on the age of spectrum represent the analytical precision at ±2σ. Ca/K plots were added to show Ar release associated with reservoirs of varying chemical composition as revealed during the argon isotopic analysis of amphibole.

Results

Amphibole from Cuatlaxtecoma Unit (Ix 164, Ix 52) yielded excellent plateau ages of 344 ± 11 Ma (for steps 3-7 = 81.4% of total ^{39}Ar released, MSWD = 0.52) and 339 ± 1 Ma (for steps 3-9 = 78.4% of total ^{39}Ar released, MSWD = 1.3) (Fig. 3.11a, b). Using an assumed cooling rate of 5°C/Ma and grain sizes of 0.6 and 0.45 mm yields closure temperatures of ca. 537° C and ca. 526° C, respectively (Harrison, 1981).

Glaucophane (Ix 189) from the Coacalco Unit yielded a good plateau age of 318 ± 4 Ma, (for steps 3-8 = 63.2% of total ^{39}Ar released, MSWD = 7.1) (Fig. 3.11c). Using an assumed cooling rate of 5°C/Ma and the 0.97mm grain size yields an inferred closure temperature of ca. 556°C (Harrison, 1981). Muscovite from the Coacalco Unit yielded a slightly older plateau age of 329 ± 2 Ma (for steps 6-13 = 67.1% of total ^{39}Ar is released, MSWD = 4.7) (Fig. 3.11d). Using an assuming cooling rate of 5-4.5°C/Ma and grain size of 0.27 mm yields a closure temperature of ca. 366° C (Hames and Bowring, 1994).

Muscovite from Chicomalá Graphitic Unit (Ix 46) yielded a slightly discordant plateau age of 325 ± 2 Ma, (for steps 5-7 = 72.8% of total ^{39}Ar released, MSWD = 1.15) (Fig. 3.11e). Using an assumed cooling rate of 5°C/Ma and 0.27-0.37 mm grain size yields a closure temperature of ca. 366-376 ° C (Hames and Bowring, 1994).

Muscovite from mylonites in the Encinera thrust zone (Ix 42) has yielded a disturbed age spectrum displaying monotonically increasing ages with increasing temperature, reaching a maximum age of 335 ± 2 Ma in steps 7-12 = 22.5% of total

^{39}Ar released. Using an assumed cooling rate of 5°C/Ma and the 0.45mm grain size yields a closure temperature of ca. 382° C (Hames and Bowring, 1994).

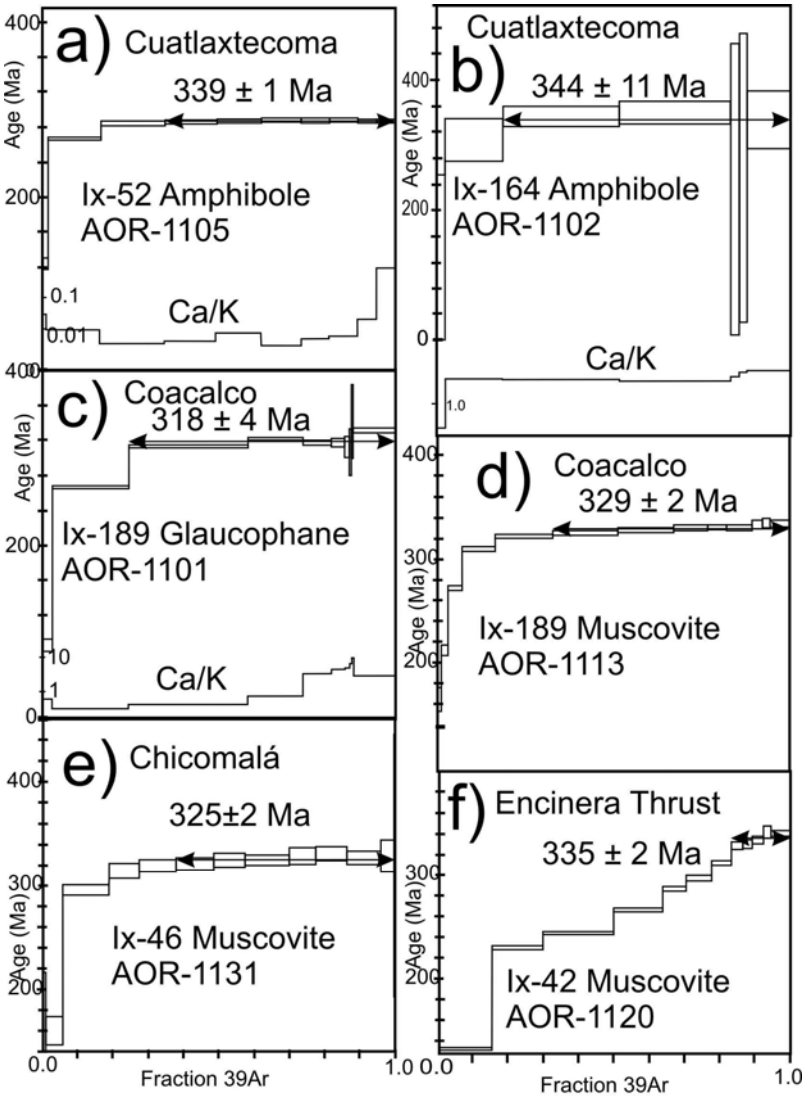

Figure 3.11 Ar^{39}-Ar^{40} apparent-age spectra showing plateau ages for amphiboles (a-c), and white mica (d-f).

Age Constraints on the tectonothermal history

The two ca. 340 Ma amphibole plateau ages in the Cuaxlaxtecoma Unit indicate cooling through ca. 550ºC and so provide a younger constraint on the time of F_1 and F_2 deformation, which took place at 440-550 °C and 9.2-16.7 Kb (near the amphibole eclogite-amphibolite facies boundary) and 560-609°C and 9.5 kb (amphibolite facies), respectively (Fig. 3.10a, Table 3). The 318 ± 4 Ma glaucophane plateau age also indicates cooling through a similar ca. 566 ºC temperature. The slightly older ca. 329 ± 2 Ma muscovite plateau age from the same blueschist sample probably reflects the

presence of some excess argon as suggested by the high initial $^{40}Ar/^{36}Ar$ (Table 5), a common feature of HP rocks (e.g. Boundy et al. 1997, Baxter et al., 2002). Thus, the ca. 318 Ma is more reliable in providing a younger constraint on F_1 and F_2 in the Coacalco Unit. This glaucophane age is within error of the 323 ± 12 Ma phengite plateau age reported by Vega-Granillo et al. (2007) from the Ixcamilpa blueschists. Together these ages indicate rapid cooling of the blueschists between ca. 566 and 350ºC. These data are consistent with the boundary between the Cuatlaxtecoma and Coacalco units being a thrust, along which the Cualaxtecoma Unit was moved upwards through the 550ºC isotherm ca. 20 my prior to passage of the underlying Coacalco blueschists through 566ºC. Similarly, the ca. 325 Ma muscovite plateau age in the Chicomala Unit provides a younger constraint on the F_2 deformation in this unit, and suggests that the eastern part of the Piaxtla Suite in the Ixcamilpa area rose through the 370ºC isotherm at approximately the same time as the Coacalco Unit.

The 335 ± 2 Ma muscovite plateau age from the Encinera thrust zone is identical within error to the 338 ± 2 Ma age of detrital muscovite in the Zumpango Unit obtained by Ortega-Obregon et al. (2009). Thus, it probably dates detrital muscovite in the mylonites of the Encinera thrust zone rather than the age of the Encinera thrust. The Encinera thrust is inferred to be of Pennsylvanian age, closely post-dating both ca. 318 Ma glaucophane age and deposition of the Mississippian Zumpango Unit (Ortega-Obregon et al., 2009). However, the Middle Permian age of the Olinalá Formation provides the only younger age constraint for the deformation.

The times of deformation in the different units in the Ixcamilpa area indicates that, although they record a similar sequence of structures, these structures formed at slightly different times and record thrusting throughout much of the Carboniferous during exhumation of the HP rocks. On the other hand, the geometric similarity of the Fb structures in the Zumpango Unit and those of F_3 in the Piaxtla Suite suggests they formed at the same time. There are two possibilities exist for the age of the major Fb and F_3 folds: (i) as they are parallel to folds deforming Mesozoic rocks east of Olinalá (García-Díaz, 2004), which are overstepped by the Late Eocene Balsas Formation, they could have been produced during the Laramide Orogeny; and (ii) as the F_3 folds are geometrically similar to Permian folds in the eastern Acatlán Complex (Morales-Gamez et al., 2009), it is possible that the F_3 folds at Ixcamilpa may also be of Permian age. Although the Sa cleavage in the Zumpango Unit is parallel to the S_2 foliation in the

Piaxtla Suite, they formed at vastly different metamorphic grades, i.e. sub-greenschist facies versus amphibolite facies. This is interpreted in terms of continuous deformation that progressed from the amphibolite facies through the greenschist facies into the sub-greenschist facies.

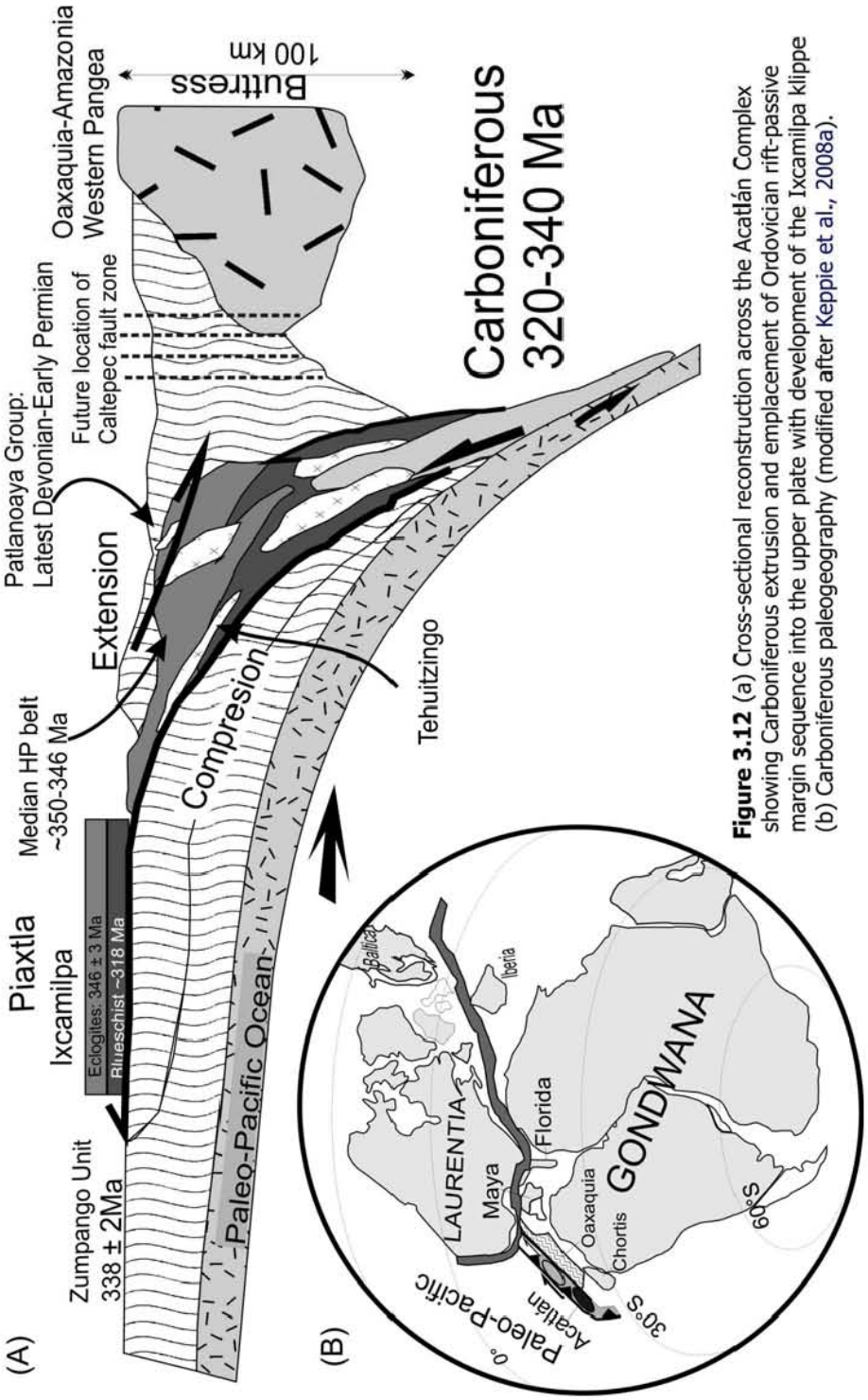

Figure 3.12 (a) Cross-sectional reconstruction across the Acatlán Complex showing Carboniferous extrusion and emplacement of Ordovician rift-passive margin sequence into the upper plate with development of the Ixcamilpa klippe (b) Carboniferous paleogeography (modified after Keppie et al., 2008a).

Discussion

From the data presented in this paper, it is clear that the HP and associated rocks of the Piaxtla Suite in the Ixcamilpa area occur in a klippe and therefore do not mark an oceanic suture as inferred by Ortega-Gutiérrez et al. (1999), Talavera Mendoza et al. (2005) and Vega-Granillo et al. (2007, 2009). Furthermore, emplacement of the klippe occurred in the Carboniferous as documented by the $^{40}Ar/^{39}Ar$ cooling ages of ca. 340 Ma in amphibole, 318 Ma in glaucophane, ca. 323 Ma in phengite, and 325 Ma in muscovite, and there is no evidence for a Late Ordovician-Early Silurian HP event as proposed by Talavera-Mendoza et al. (2005) and Vega-Granillo et al. (2009). Kinematic data presented in this paper indicate that the klippe was derived from the east and a potential root zone may occur in the median HP belt where geohronological work has yielded U-Pb zircon ages of 346 ± 3 Ma and 353 ± 1 Ma from retrogressed eclogite, and ^{40}Ar-^{39}Ar plateau ages of 344 ± 5 Ma from glaucophane, and 338 ± 3 Ma and 337 ± 2 Ma from white mica (Middleton et al., 2007; Elias et al., 2007; Keppie et al., 2010), which indicate rapid cooling between ca. 700° and 340°C. Whereas these latter ages are similar to the ca. 340 Ma amphibole ages in the Ixcamilpa area, the white mica/phengite ages are 20 my older in the median HP belt. The median HP belt has been interpreted as a steeply dipping extrusion zone (Figure 12a), which is consistent with synchronous cooling through 550-340ºC across the whole width of the zone. On the other hand, the sub-horizontal attitude of the thrust stack at Ixcamilpa may account for the progressive cooling where the higher parts cooled through ca. 550ºC at ca. 340 Ma, and the lowest thrust slice cooled through ca. 566ºC at ca. 320 Ma following some unroofing (Figure 3.10b). Further rapid unroofing is indicated by cooling through ca. 350ºC by the ca. 320 Ma phengite age (Vega-Granillo et al., 2009). The fact that the phengite defines the S_2 foliation indicates that deformation continued at ca. 320 Ma. Extrusion is also consistent with the variation in the shapes of the K-feldspars in the megacrystic granitoids: oblate in the Tecolapa granite and prolate in the Columpio del Diablo Granitoid, which are related to compressional and extensional zones within an extrusion zone, respectively (Fig. 3.7, c.f. Hudleston, 1999). In this scenario, the lower thrust slices at Ixcamilpa formed adjacent to the lower (western) side of the extrusion zone. The upper (eastern) side of the extrusion zone occurs in the Las Minas-Patlanoaya area where the listric shear fabric was dated at 344 Ma (^{40}Ar-^{39}Ar plateau ages in muscovite, Ramos-Arias et al., 2008).

Based on the detrital zircon populations (Ramos-Arias and Keppie, 2011) and rift tholeiitic nature of the mafic rocks (authors unpublished data, Ortega Obregón et al., 2009), the protoliths of the Piaxtla Suite in the Ixcamilpa area are inferred to be Ordovician a rift-passive margin sequence deposited on the periphery of Oaxaquia/Amazonia (Fig. 3.12b). This is consistent with their removal by subduction erosion (D.F. Keppie et al., 2009), followed by extrusion up along the median HP belt (c.f. Stöckhert and Gerya, 2005). That this extrusion zone occurred within the upper plate, rather than along the subduction zone, is indicated by the close correlation of Acatlán rocks on either side (Keppie et al., 2008a; Ortega-Obregon et al., 2009).

Table 1

Representative Microprobe Analyses (wt%)of mineal from Coacalco and Cuatlaxtecoma Units,

Ixcamilpa area, Acatlán Complex, Southern México

Cuatlaxtecoma Unit

	Garnet	Alamandine				Amphibole				Phengite		Plagioclase		Chlorite			Epidote		
	core	rim	rim	core	rim	Na-Ca	NaCa	Ca	Ca			Ab		Ccl	Ccl	Ccl			
	lx164-c4-5	lx164-c4-8	lx161-c1-1	lx161-c1-4	lx161-c2-26	lx161-c3-5	lx161-c3-6	lx164-c4-14	lx164-c4-15	lx164-c1-2	lx164-c1-4	lx161-c4-10	lx161-c4-11	lx161-c1-9	lx161-c1-10	lx161-c1-17	lx164-c5-19	lx164-c5-20	lx161-c2-1
SiO2	38.032	38.180	38.312	38.133	37.992	45.996	45.937	46.835	46.503	53.008	51.442	68.051	68.011	26.361	26.392	26.116	38.786	38.823	39.110
TiO2	0.075	0.223	0.141	0.168	0.140	0.258	0.263	0.190	0.228	0.174	0.181	0.000	0.000	0.034	0.052	0.025	0.060	0.113	0.098
Al2O3	19.961	20.021	20.219	20.213	20.243	14.519	14.594	10.753	10.705	31.091	31.889	19.846	19.746	21.927	22.030	21.413	26.633	26.709	28.612
FeO	27.123	26.147	27.868	27.915	28.083	18.371	18.418	20.383	20.751	2.886	2.655	0.231	0.207	0.000	0.000	0.000	9.976	10.039	8.088
MnO	3.318	3.273	3.988	3.884	3.376	0.054	0.072	0.111	0.083	0.000	0.000	0.000	0.000	25.530	25.307	25.648	0.273	0.135	0.017
MgO	0.727	0.709	1.063	1.075	1.142	8.124	8.215	8.507	8.613	2.497	2.268	0.000	0.003	0.060	0.094	0.169	0.021	0.024	0.027
CaO	11.613	12.314	9.617	9.712	10.049	8.085	8.100	9.524	9.994	0.002	0.002	0.155	0.167	16.143	16.042	16.271	23.480	23.574	23.456
Na2O	0.000	0.000	0.000	0.000	0.000	2.621	2.644	1.857	1.633	0.257	0.242	7.595	7.549	0.012	0.021	0.030	0.012	0.012	0.007
K2O	0.000	0.000	0.000	0.000	0.000	0.475	0.468	0.289	0.291	8.680	8.992	0.019	0.027	0.000	0.018	0.039	0.003	0.012	0.016
Cr2O3	0.000	0.000	0.000	0.000	0.000	0.000	0.000	0.000	0.000	0.000	0.000	0.000	0.005	0.000	0.003	0.022	0.000	0.000	0.000
NiO	0.000	0.000	0.000	0.000	0.000	0.005	0.023	0.000	0.000	0.010	0.000	0.005	0.000	0.020	0.007	0.001	0.003	0.000	0.000
F	0.000	0.000	0.000	0.000	0.000	0.000	0.000	0.000	0.000	0.006	0.000	0.000	0.000	0.001	0.000	0.005	0.000	0.018	0.000
Total	100.849	100.867	101.208	101.1	101.025	98.508	98.734	98.449	98.801	98.608	97.671	95.902	95.715	90.088	89.966	89.737	99.247	99.451	99.431
	24 oxigens					23 oxigens				11 Oxigens		32 Oxigen		14 Oxigen			12.5Oxigens		
Si	6.066	6.069	6.083	6.065	6.047	6.670	6.650	6.880	6.960	6.730	6.610	12.170	12.180	2.690	2.700	2.690	3.000	3.000	2.990
Ti	0.009	0.027	0.017	0.020	0.017	0.030	0.300	0.020	0.020	0.020	0.020	0.000	0.000	0.000	0.000	0.000	0.000	0.010	0.010
Al	3.752	3.751	3.784	3.789	3.797	2.480	2.490	1.860	1.780	4.660	4.830	4.180	4.170	2.640	2.650	2.600	2.430	2.432	2.581
Fe	3.617	3.476	3.700	3.713	3.738	2.230	2.230	2.500	2.490	0.310	0.290	0.030	0.030	2.180	2.160	2.210	0.581	0.584	0.466
Mn	0.448	0.441	0.536	0.523	0.455	0.000	0.000	0.000	0.010	0.000	0.000	0.000	0.000	0.010	0.010	0.010	0.018	0.009	0.001
Mg	0.173	0.168	0.252	0.255	0.271	1.760	1.770	1.860	1.910	0.470	0.430	0.000	0.000	2.460	2.440	2.500	0.002	0.003	0.003
Ca	1.984	2.097	1.636	1.655	1.714	1.250	1.260	1.500	1.480	0.000	0.000	0.030	0.030	0.000	0.000	0.000	1.948	1.951	1.924
Na	0.000	0.000	0.000	0.000	0.000	0.740	0.740	0.530	0.500	0.060	0.060	2.630	2.620	0.000	0.000	0.010	0.002	0.002	0.001
K	0.000	0.000	0.000	0.000	0.000	0.090	0.090	0.050	0.060	1.410	1.470	0.000	0.010	0.000	0.000	0.000	0.000	0.001	0.002
Total	16.050	16.030	16.010	16.020	16.040	15.250	15.530	15.200	15.210	13.660	13.710	19.040	19.040	9.980	9.960	10.020	7.982	7.991	7.978

Coacalco Unit

	Amphibole					Phengite			Plagioclase			Chlorite			Epidote		
	Na	Na	Na	Na-Ca	Na-Ca				Ab			Cht	Ccl	Ccl	Zo	Czo	Czo
	lx184-c6-9	lx184-c6-10	lx184-c7-10	lx287-c2-17	lx287-c3-1	lx184-c2-13	lx184-c2-7	lx184-c2-12	lx287-c2-3	lx287-c2-4	lx287-c2-5	lx184-c9-17	lx287-c4-4	lx287-c4-6	lx184-c4-10	lx184-c5-5	lx184-c5-6
SiO2	55.152	55.140	53.576	56.320	53.417	51.865	53.308	50.969	70.880	68.809	70.024	26.936	26.706	27.399	38.112	38.298	38.231
TiO2	0.000	0.000	0.052	0.000	0.031	0.126	0.142	0.126	0.343	0.000	0.000	0.000	0.021	0.006	0.007	0.000	0.003
Al2O3	9.508	9.057	9.181	7.227	4.702	26.267	25.980	26.921	19.983	19.662	19.876	19.539	20.984	20.239	23.653	23.728	24.062
FeO	19.308	17.686	20.915	18.509	18.592	5.048	4.323	4.695	0.106	0.112	0.150	0.002	0.000	0.000	13.489	12.862	12.729
MnO	0.155	0.113	0.236	0.057	0.190	0.032	0.029	0.039	0.000	0.000	0.000	28.302	22.903	23.187	0.791	0.367	0.398
MgO	6.238	7.591	6.270	8.446	11.101	2.139	2.695	2.395	0.000	0.000	0.000	0.638	0.337	0.329	0.010	0.007	0.011
CaO	0.635	0.685	1.479	0.863	5.250	0.022	0.035	0.050	0.447	0.078	0.081	14.468	18.829	17.976	22.802	23.385	23.188
Na2O	5.948	5.875	5.628	4.808	3.172	0.296	0.301	0.324	7.805	7.675	7.609	0.013	0.059	0.065	0.012	0.000	0.009
K2O	0.031	0.025	0.032	0.027	0.078	10.551	10.607	10.260	0.035	0.055	0.045	0.007	0.000	0.010	0.003	0.016	0.027
Cr2O3	0.000	0.000	0.000	0.000	0.005	0.010	0.000	0.000	0.000	0.000	0.000	0.003	0.020	0.008	0.002	0.000	0.000
NiO						0.000	0.000	0.014	0.007	0.004	0.008	0.041	0.047	0.052	0.000	0.003	0.000
F						0.000	0.000	0.000	0.026	0.000	0.003	0.002	0.003	0.012	0.001	0.000	0.001
Total	96.975	96.172	97.369	96.257	96.538	96.356	97.420	95.793	99.621	96.395	97.795	89.950	89.908	89.278	98.882	98.666	98.659
	23 Oxigens					11 oxigens			32 Oxigen			14 Oxigen			12.5 Oxigen		
Si	7.960	7.960	7.790	8.090	7.820	6.740	6.750	6.720	12.240	12.230	12.260	2.810	2.710	2.760	3.008	3.021	3.013
Ti	0.000	0.000	0.000	0.000	0.000	0.010	0.010	0.010	0.000	0.000	0.000	0.000	0.000	0.000	0.000	0.000	0.000
Al	1.610	1.540	1.630	1.220	0.810	4.330	4.330	4.430	4.070	4.120	4.100	2.400	2.510	2.440	2.200	2.206	2.235
Fe	2.330	2.140	2.430	2.230	2.280	0.660	0.560	0.630	0.020	0.020	0.020	2.470	1.940	2.040	0.801	0.764	0.755
Mn	0.020	0.010	0.030	0.010	0.020	0.000	0.000	0.000	0.000	0.000	0.000	0.060	0.030	0.030	0.053	0.025	0.027
Mg	1.340	1.630	1.360	1.810	2.420	0.410	0.510	0.470	0.000	0.000	0.000	2.250	2.850	2.740	0.001	0.001	0.001
Ca	0.100	0.010	0.190	0.130	0.820	0.000	0.000	0.010	0.080	0.010	0.020	0.000	0.010	0.010	1.928	1.977	1.958
Na	1.670	1.650	1.650	1.340	0.900	0.070	0.070	0.080	2.610	2.640	2.580	0.000	0.000	0.010	0.002	0.000	0.001
K	0.010	0.000	0.010	0.000	0.010	1.750	1.710	1.730	0.010	0.010	0.010	0.000	0.000	0.000	0.000	0.002	0.003
Total	15.040	14.940	15.090	14.830	15.080	13.970	13.940	14.080	19.030	19.030	18.990	9.990	10.050	10.030	7.993	7.995	7.994

Table 2. Calibration of geo-thermobarometric data for high pressure rocks in Ixcamilpa area.

Coacalco Blueschist path-mineral	T (°C) P (Kbar) number-range-reference	Cuatlaxtecoma Garnetiferous-Amphibolite path-mineral	T (°C) P (Kbar) number-range-reference
Co1 Na Amp-Plg Phg	[13] 287-396°C [b] [21] 10.28-12.4 Kb [g]	Cu1 Grn-Amp Phg	[12] 440-548°C [d] [10] 9.05-16.7 Kb [g]
Co2 NaCa Amp-Plg NaCa Amp	[13] 566-486°C [e] [15] 6-6.7 Kb [a]	Cu2 Na Ca Amp-Plg Amp	[10] 560-609°C [e,b] 9.5Kb
Co3 Ca Amp-Plg Ca Amp	[6] 399-419 °C [e] [15] 5-5.6 Kb [a]	Cu3 NaCa Amp-Plg	[6] 520-547°C [e] [12] 5.88 Kb [a]
Co4 Chl	[20] 330-335° C [c,f]	Cu4 Ca Amp	[10] 378-470°C [e]
		Cu5 CaAmp-Plg CaAmp	[17] 371-459° [h] [17] 3.3-4.5Kb [a]
		Cu6 Chl	[5] 356-364°C [c,f]

a-Brown, 1977; b-Blundy and Holland, 1990; c-Cathelineau, 1988; d-Graham and Powell, 1984
e-Holland and Blundy, 1994; f- Kranidiotis and MacLean, (1987); g-Massone and Schyerer, 1987; h-Spear, 1980

Table 3. Phengite Si compositions in the Coacalco blueschist and Cuatlaxtecoma garnet amphibolite plotted on the geobarometer grid of Massone and Shreyer (1987).

Point # Coacalco	Sample Si s.p.f.	P (Kb) @ 287-390°C
Ix184-c2-6	3.38	12.38
Ix184-c2-7	3.38	11.61
Ix184-c2-12	3.36	9.77
Ix184-c2-13	3.37	10.98
Ix184-c4-1	3.36	9.25
Ix184-c4-3	3.38	11.41
Ix184-c4-5	3.38	12.44
Ix184-c6-21	3.37	10.71
Ix184-c6-23	3.36	9.97
Ix184-c6-25	3.37	10.44
Ix184-c6-27	3.36	9.98
Ix184-c6-29	3.37	10.58
Ix184-c6-31	3.36	9.20
Ix184-c6-33	3.37	10.88
Ix184-c6-34	3.37	10.55
Ix184-c7-18	3.37	11.25
Ix184-c7-20	3.35	8.50
Ix184-c8-17	3.37	10.33
Ix184-c8-18	3.38	11.58
Ix184-c8-19	3.37	10.21
Ix184-c8-20	3.36	8.94

Point # Cuatlaxtecoma	Si s.p.f.	P (Kb) @ 440-550°C
Ix164-c1-11	3.37	11.32
Ix164-c2-18	3.42	16.96
Ix164-c1-13	3.40	15.52
Ix164-c1-14	3.38	12.91
Ix161-c1-1	3.36	10.35
Ix161-c1-2	3.37	11.47
Ix161-c1-13	3.35	9.05
Ix161-c2-17	3.41	16.78
Ix161-c2-18	3.36	11.09
Ix161-c2-19	3.40	16.03

Table 4. Values of K_D and temperature based on core to rim garnet analyses in the Cuatlaxtecoma Unit plotted on the geothermometer grid of Graham and Powell (1984).

Point sample	XCa,Gr	lnKD	T in °C
Ix164-c3-12$_{\mathbf{core}}$	0.322	3.11	437.95
Ix164-c3-13$_{\mathbf{core}}$	0.327	3.05	449.02
Ix164-c3-14$_{\mathbf{core}}$	0.325	2.92	465.35
Ix164-c3-15$_{\mathbf{core}}$	0.338	2.95	469.37
Ix164-c3-16$_{\mathbf{core}}$	0.343	2.90	478.71
Ix164-c3-17$_{\mathbf{core}}$	0.328	2.88	471.78
Ix164-c3-18$_{\mathbf{core}}$	0.328	2.81	483.01
Ix164-c5-5$_{\mathbf{rim}}$	0.268	2.22	536.56
Ix164-c5-4$_{\mathbf{rim}}$	0.344	2.55	532.06
Ix164-c5-3$_{\mathbf{rim}}$	0.328	2.62	511.18
Ix164-c5-2$_{\mathbf{rim}}$	0.333	2.50	533.44
Ix164-c5-1$_{\mathbf{rim}}$	0.324	2.37	548.70

Table 5 40Ar/ 39Ar

AOR-1105 Ix 52	Laser Power		Isotope Volumes								
Steps	(Watts)	^{40}Ar	^{39}Ar	38Ar	37Ar	36Ar	Ca/K	%40 Ar Atm	%*f*39Ar	40Ar*/39K	Age
1	**0.75**	270.828± 0.627	29.107±0.193	0.632±0.033	0.470±0.191	0.150±0.020	0.030	16.39	1.27	7.75±0.21	202.9±5.2
2	**2.00**	4480.779 ± 3.875	346.965 1.698	4.610 0.181	1.782 0.815	0.167 0.054	0.009	1.10	15.11	12.74 0.08	322.5± 1.8
3	**< 2.50**	5664.04±5.926	419.430 2.193	5.343 0.223	0.787 0.565	0.157 0.057	0.003	0.82	18.27	13.36 0.08	336.9 ±1.9
4	**< 2.75>**	4552.661± 4.331	336.320 1.426	4.237 0.190	0.765 0.874	0.082 0.059	0.004	0.53	14.65	13.43 0.08	338.5± 1.8
5	**< 3.00>**	3998.990 ±3.374	294.659 1.222	3.725 0.156	1.219 0.728	0.095 0.056	0.008	0.70	12.83	13.45 0.08	338.8± 1.9
6	**< 3.25>**	3497.619 ± 3.508	257.359 1.118	3.223 0.179	0.421 0.704	0.049 0.042	0.003	0.41	11.21	13.50 0.08	340.1± 1.8
7	**< 3.50>**	2492.911 ± 2.217	183.269 0.805	2.291 0.105	0.492 0.396	0.058 0.041	0.005	0.69	7.98	13.48 0.09	339.5± 2.1
8	**< 4.00>**	2468.476 ± 2.618	181.737 0.715	2.249 0.099	0.585 0.434	0.033 0.040	0.006	0.39	7.92	13.50 0.09	340.0± 2.0
9	**< 5.00>**	1715.609 ± 2.032	126.296 0.563	1.613 0.069	1.401 0.358	0.038 0.023	0.020	0.64	5.50	13.47 0.08	339.2± 1.9
10	**< 7.00>**	1649.537 ± 1.643	120.799 0.558	1.955 0.069	60.480 0.964	0.087 0.028	0.917	1.25	5.26	13.46 0.09	339.1± 2.2

J Value: 0.015363
Mass: 0.0 mg ± 0.000042
Volume 39K: 2295.94 x 1E-12 cm3 NTP Approx. % K
Integrated Age: 334.64 ± 1.10 Ma % Ca
Initial 40/36: 444.14 ± 438.55 (MSWD = 0.64, isochron between 0.37 and 2.26)
Correlation Age: 338.34 ± 3.10 Ma (65.4% of 39Ar, steps marked by >) MSWD 1.174
Plateau Age: 338.74 ± 1.14 Ma (83.6% of 39Ar, steps marked by <) Mod. err. 0.74

AOR-1102 Ix 164 Amp			Isotope Volumes								
Steps	Power	40Ar	39Ar	38Ar	37Ar	36Ar	Ca/K	%40 Ar Atm	%*f*39Ar	40Ar*/39K	Age
1	**0.75**	29.806±0.226	0.517±0.030	0.077±0.035	0.996±0.198	0.104±0.019	3.532	103.22	2.15	-1.89±10.78	-53.1±307.7
2	**2.00**	59.915 0.304	3.937 0.069	1.809 0.051	63.349 0.762	0.061 0.018	29.785	21.35	16.40	12.08 ± 1.36	306.9 ± 31.8
3	**< 2.50>**	113.056 0.342	7.918 0.085	3.675 0.078	124.671 1.415	0.056 0.017	29.138	5.28	32.97	13.65 ± 0.66	343.2 ±
4	**< 3.00>**	107.166 0.353	7.586 0.084	3.416 0.080	112.518 1.103	0.042 0.018	27.430	2.80	31.59	13.85 ± 0.74	347.8 ±17.0
5	**< 3.50>**	8.628 0.194	0.588 0.031	0.280 0.028	10.391 0.324	0.015 0.018	32.732	39.89	2.45	8.90 ± 9.2	231.0 ±224.3
6	**< 4.00>**	7.654 0.174	0.520 0.025	0.265 0.026	11.253 0.330	0.012 0.016	40.240	35.56	2.16	9.61 ± 9.17	248.3 ±221.5
7	**< 7.00>**	53.176 0.298	2.947 0.046	1.462 0.048	67.803 0.790	0.068 0.018	42.805	26.90	12.27	13.38 ± 1.89	337.1± 43.5

J Value: 0.015356
Mass: 1.0 mg ± 0.000040
Volume 39K: 802.43 x 1E-12 cm3 NTP Approx. % K
Integrated Age: 301.74 ± 1.25 Ma % Ca
Initial 40/36: 701.62 ± 276.04 (MSWD = 7.53, isochron between 0.42 and 2.15)
Correlation Age: 312.20 ± 7.04 Ma (75.7% of 39Ar, steps marked by >) MSWD 16.941
Plateau Age: 319.02 ± 1.45 Ma (75.7% of 39Ar, steps marked by <) Mod. err. 4.58

AOR-1101: IX-189 Gln			Isotope Volumes								
Steps	Power	40Ar	39Ar	38Ar	37Ar	36Ar	Ca/K	%40 Ar Atm	%*f*39Ar	40Ar*/39K	Age
1	**0.75**	168.207±0.387	22.487±0.183	0.675±0.041	7.485±0.292	0.330±0.021	0.609	57.63	2.8	3.14±0.28	85.0± 7.4
2	**2**	1835.026 1.881	172.714 0.877	2.372 0.089	29.627 0.759	0.130 0.022	0.314	1.97	21.52	10.39 0.07	267±1.6

3	**< 2.50>**	3383.162 3.591	271.252 1.364	3.501 0.157	62.492 1.235	0.097 0.050	0.422	0.69	33.8	12.36 0.08	313.5±2
4	**< 2.75>**	1608.333 1.672	124.786 0.699	1.718 0.085	50.633 0.812	0.068 0.026	0.743	0.99	15.55	12.73 0.10	322.2±2.2
5	**< 3.00>**	837.252 1.065	65.669 0.368	0.977 0.042	119.044 1.162	0.073 0.016	3.322	1.39	8.18	12.56 0.10	318.1±2.4
6	**< 3.50>**	395.214 0.668	30.434 0.228	0.465 0.041	74.829 0.833	0.066 0.017	4.507	3.34	3.79	12.54 0.19	317.8±4.5
7	**< 4.00>**	147.370 0.348	10.752 0.110	0.179 0.031	28.848 0.549	0.057 0.018	4.919	9.81	1.34	12.35 0.51	313.4 ±12.0
8	**< 5.00>**	71.148 0.312	4.477 0.067	0.104 0.029	15.900 0.384	0.062 0.017	6.516	23.95	0.56	12.09 1.14	307.2 ±26.7
9	**< 6.00>**	53.979 0.261	3.056 0.052	0.067 0.027	16.261 0.460	0.047 0.019	9.774	23.19	0.38	13.59 1.84	341.9± 42.3
10	**< 7.00>**	1343.629 1.382	96.799 0.578	1.564 0.074	151.760 1.646	0.277 0.032	2.872	5.16	12.06	13.15 0.13	331.8±2.9

J Value: 0.015356
Mass: 1.0 mg ± 0.000040
Volume 39K: 802.43 x 1E-12 cm3 NTP Approx. % K
Integrated Age: 301.74 ± 1.25 Ma % Ca
Initial 40/36: 701.62 ± 276.04 (MSWD = 7.53, isochron between 0.42 and 2.15)
Correlation Age: 312.20 ± 7.04 Ma (75.7% of 39Ar, steps marked by >) MSWD 16.941
Plateau Age: 319.02 ± 1.45 Ma (75.7% of 39Ar, steps marked by <) Mod. err. 4.58

AOR-1113: IX-189 Msc			**Isotope Volumes**								
Steps	**Power**	**40Ar**	**39Ar**	**38Ar**	**37Ar**	**36Ar**	**Ca/K**	**%40 Ar Atm**	**%ƒ39Ar**	**40Ar*/39K**	**Age**
1	**0.5**	168.607± 0.681	16.585±0.205	0.551±0.050	4.122± 1.072	0.222±0.025	0.455	38.62	0.98	6.21±0.45	164.4±11.4
2	**0.75**	288.152±0.902	33.362 0.254	0.533 0.056	5.671±1.174	0.057 0.022	0.311	5.68	1.97	8.12 0.20	211.9±5
3	**1**	723.792±1.38	67.570 0.394	0.884 0.075	8.294±1.268	0.032 0.019	0.225	1.21	4	10.55 0.11	271±2.5
4	**1.25**	1957.397±2.859	159.321 0.847	1.970 0.119	23.255±3.182	0.050 0.030	0.267	0.66	9.42	12.18 0.09	309.3±2.1
5	**1.5**	3571.342±5.973	279.161 1.409	3.464 0.222	74.929±5.921	0.091 0.059	0.491	0.58	16.51	12.69 0.09	321.2±2.2
6	**< 1.75**	4015.047±6.355	310.368 2.035	3.979 0.265	217.799±10.624	0.137 0.060	1.285	0.56	18.35	12.84 0.10	324.7±2.4
7	**< 2.00>**	3516.207±5.276	269.548 1.335	3.420 0.275	251.699 ±12.85	0.140 0.047	1.71	0.59	15.94	12.95 0.09	327.1±2
8	**< 2.25>**	2136.707±3.619	162.798 1.086	2.172 0.136	231.651±8.054	0.094 0.035	2.607	0.4	9.63	13.06 0.11	329.7±2.6
9	**< 2.50>**	1164.841±1.742	88.661 0.540	1.126 0.058	88.732±4.561	0.040 0.025	1.833	0.4	5.24	13.07 0.12	329.9±2.7
10	**< 2.69>**	1633.627±2.458	124.644 0.748	1.605 0.111	225.223 ±6.809	0.081 0.028	3.311	0.33	7.37	13.05 0.11	329.5±2.4
11	**< 2.86>**	618.324±1.405	46.753 0.404	0.656 0.069	136.686 ±4.943	0.044 0.019	5.361	0.3	2.76	13.18 0.17	332.6±3.9
12	**< 3.02>**	488.112±1.139	36.596 0.275	0.550 0.058	137.890±4.625	0.052 0.023	6.914	0.81	2.16	13.24 0.21	333.8±4.9
13	**< 7.00>**	1275.639±1.894	95.637 0.650	1.449 0.133	298.462±7.56	0.125 0.028	5.724	0.96	5.66	13.21 0.13	333.2±2.9

J Value: 0.015357
Mass: 0.0 mg ± 0.000040
Volume 39K: 1691.00 x 1E-12 cm3 NTP Approx. % K
Integrated Age: 319.28 ± 1.14 Ma % Ca
Initial 40/36: 2699.23 ±4223.45 (MSWD = 0.50, isochron between 0.37 and 2.26)
Correlation Age: 316.90 ± 22.81 Ma (48.8% of 39Ar, steps marked by >) MSWD 4.674
Plateau Age: 328.26 ± 1.30 Ma (67.1% of 39Ar, steps marked by <) Mod. err. 2.06

AOR-1131: IX-46 Msc			**Isotope Volumes**								
Steps	**Power**	**40Ar**	**39Ar**	**38Ar**	**37Ar**	**36Ar**	**Ca/K**	**%40 Ar Atm**	**%ƒ39Ar**	**40Ar*/39K**	**Age**
1	**1.80**	36.083±0.375	1.513±0.063	0.102±0.031	-0.782±-2.108	0.101±0.020	0.000	82.36	0.71	4.18±4.00	112.1±104.2
2	**2.10**	71.081 0.425	10.422 0.142	0.206 0.038	-0.062± -2.356	0.026 0.018	0.000	10.67	4.92	6.06 0.53	160.5±13.5

3	**2.40**	324.825 0.785	27.532 0.229	0.346 0.042	0.325 ± 2.304	0.016 0.017	0.022	1.41	13.00	11.60 0.21	295.7± 4.9
4	**2.50**	228.786 0.830	18.158 0.205	0.227 0.039	0.564 ± 2.608	0.011 0.016	0.057	1.41	8.58	12.39 0.30	314.2± 6.9
5	**< 2.60**	281.928 0.671	22.085 0.219	0.280 0.038	0.102 ±2.114	0.010 0.018	0.008	1.05	10.43	12.60 0.27	319.1± 6.3
6	**< 2.70**	294.428 0.838	22.891 0.284	0.284 0.041	-0.005± -2.057	0.011 0.015	0.000	1.09	10.81	12.69 0.26	321.2± 5.9
7	**< 2.80>**	243.848 0.778	18.853 0.230	0.242 0.040	0.144 ± 2.465	0.004 0.015	0.014	0.43	8.90	12.85 0.29	324.8± 6.7
8	**< 3.00>**	348.601 0.933	26.871 0.273	0.340 0.047	0.709 ± 1.849	0.010 0.017	0.048	0.82	12.69	12.84 0.23	324.5± 5.3
9	**< 3.10>**	202.808 0.746	15.418 0.194	0.195 0.038	0.105 ± 1.897	0.006 0.016	0.012	0.84	7.28	13.01 0.35	328.6 ± 8.2
10	**< 3.30>**	251.760 0.741	19.107 0.179	0.247 0.034	1.072 ± 1.708	0.003 0.017	0.103	0.34	9.02	13.10 0.30	330.7± 6.9
11	**< 3.60>**	265.755 0.729	20.282 0.203	0.266 0.040	-0.568 ±-2.059	0.009 0.016	0.000	1.05	9.58	12.94 0.27	326.8 ± 6.1
12	**< 4.00>**	103.314 0.435	7.820 0.118	0.117 0.030	0.618 ± 1.921	0.005 0.017	0.145	1.35	3.69	13.00 0.67	328.4 ± 15.5
13	**< 7.00>**	10.775 0.286	0.800 0.046	0.030 0.022	0.114 ±2.405	0.002 0.014	0.261	6.47	0.38	12.57 5.44	318.4 ±126.3

J Value: 0.015353
Mass: 0.0 mg ± 0.000040
Volume 39K: 211.75 x 1E-12 cm3 NTP Approx. % K
Integrated Age: 311.02 ± 2.34 Ma % Ca

Correlation Age: 304.82 ± 196.13 Ma (51.5% of 39Ar, steps marked by >) MSWD 1.152
Plateau Age: 324.93 ± 2.61 Ma (72.8% of 39Ar, steps marked by <) Mod. err. 2.54

AOR-1120: IX-42 Msc			**Isotope Volumes**								
Steps	**Power**	**40Ar**	**39Ar**	**38Ar**	**37Ar**	**36Ar**	**Ca/K**	**%40 Ar Atm**	**%*f*39Ar**	**40Ar*/39K**	**Age**
1	**0.50**	1317.083±2.266	226.445±1.093	3.689±0.176	3.654±1.845	0.611± 0.039	0.030	13.68	15.12	4.99±0.06	133.2±1.5
2	**0.75**	1949.657 3.364	214.848 1.135	2.720 0.151	3.719 2.020	0.129 ± 0.037	0.032	1.95	14.34	8.87 0.07	230.2 1.7
3	**1.00**	2923.877 4.149	304.307 1.605	3.744 0.214	5.373 4.026	0.145 ± 0.040	0.032	1.45	20.31	9.44 0.07	244.1 1.6
4	**1.25**	2187.542 3.121	207.997 1.112	2.514 0.178	1.394 2.077	0.089 ± 0.036	0.012	1.19	13.88	10.36 0.08	266.3 1.9
5	**1.50**	1134.223 1.620	99.803 0.565	1.252 0.087	1.215 1.148	0.043 ± 0.019	0.022	1.11	6.66	11.21 0.09	286.4 2.1
6	**1.75**	1281.182 1.708	108.304 0.644	1.331 0.111	1.851 1.324	0.053 ± 0.024	0.031	1.22	7.23	11.66 0.10	296.9 2.3
7	**2.00**	1062.128 1.706	85.440 0.486	1.065 0.079	1.137 1.207	0.029 ± 0.021	0.024	0.79	5.70	12.30 0.11	312.1 2.4
8	**< 2.25**	612.909 1.476	46.548 0.385	0.606 0.062	1.178 1.232	0.018 ± 0.018	0.046	0.83	3.11	13.03 0.16	328.9 3.7
9	**< 2.42>**	513.005 1.115	38.959 0.288	0.472 0.064	0.903 1.151	0.010 ± 0.018	0.042	0.53	2.60	13.07 0.17	329.8 4.0
10	**< 2.58>**	685.104 1.228	51.265 0.358	0.664 0.068	2.915 1.185	0.017 ± 0.020	0.104	0.68	3.42	13.24 0.15	333.9 3.4
11	**< 2.72>**	408.722 1.064	30.034 0.314	0.371 0.056	2.365 1.487	-0.003 ± -0.020	0.144	-0.05	2.00	13.59 0.25	341.7 5.7
12	**< 7.00>**	1157.688 2.015	84.172 0.495	1.236 0.081	25.656 2.311	0.067 ± 0.022	0.558	1.53	5.62	13.52 0.11	340.1 2.6

J Value: 0.015350
Mass: 1.0 mg ± 0.000042
Volume 39K: 1498.12 x 1E-12 cm3 NTP Approx. % K
Integrated Age: 255.28 ± 0.95 Ma 2.36% Ca
Initial 40/36: 1089.08 ±1035.23 (MSWD = 1.49, isochron between 0.00 and 3.00)
Correlation Age: 328.37 ± 12.39 Ma (13.6% of 39Ar, steps marked by >) MSWD 9.696
Plateau Age: 335.36 ± 1.82 Ma (16.8% of 39Ar, steps marked by <) Mod. err. 4.95

Capítulo 4

Late Paleozoic subduction and exhumation of Cambro-Ordovician passive margin and arc rocks in the northern Acatlán Complex, southern Mexico: Geochronological constraints.

Tectonophysics, doi:10.1016/j.tecto.2010.09.019, (2010)

J. Duncan Keppie a, R.D. Nance b, **M.A. Ramos-Arias** a, J.K.W. Lee c, J. Dostal d, A. Ortega-Rivera e, J.B. Murphy f

a Depto. de Geología Regional, Instituto de Geología, Universidad Nacional Autónoma de México, 04510 México, D.F., Mexico

b Dept. of Geological Sciences, 316 Clippinger Laboratories, Ohio University, Athens, OH 45701, USA

c Dept. of Geology, Queens University, Kingston, Ontario, Canada, K7L3NG

d Dept. of Geology, St. Mary's University, Halifax, Nova Scotia, Canada, B3H 3C3

e Instituto de Geología, Universidad Nacional Autónoma de México, Estación Regional del Noroeste, Apartado Postal 1039, Hermosillo, Sonora 83000, Mexico

f Dept. of Earth Sciences, St. Francis Xavier U, Antigonish, Nova Scotia, Canada, B2G 2W5

Abstract

The origin and age of high pressure (HP) rocks are crucial for paleogeographic reconstructions because they either define an oceanic suture or an extrusion zone within the upper plate. HP rocks in the San Miguel Las Minas area in the northern part of the Acatlán Complex, southern Mexico have been inferred to be of early Paleozoic age and to mark oceanic sutures. However, blueschists in the northern part of the complex have yielded Mississippian $^{40}Ar/^{39}Ar$ plateau ages of 344±5 Ma for glaucophane and 338±3 Ma and 337±2 Ma for muscovite. These ages are slightly younger than recently published ages: a U–Pb zircon age of 353±1 Ma from associated eclogite, and a 347±3 Ma muscovite age from the tectonically overlying, greenschist facies Las Minas Unit. Taken together, these data indicate rapid cooling between 700° and 340 °C in ca. 17 Myr. On the other hand, associated Ordovician Anacahuite Amphibolite cooled through ca. 500 °C at

299±6 Ma ($^{40}Ar/ ^{39}Ar$ on hornblende) suggesting a second, Permian phase of exhumation. Protoliths of the high grade rocks include Cambrian–Ordovician, rift-passive margin, psammites, pelites, and tholeiitic dykes, an Ordovician mafic intrusion (Anacahuite Amphibolite dated at 470±10 Ma: U–Pb zircon) and megacrystic granite (dated at 492±12 Ma: U–Pb zircon), and arc-related mafic rocks of unknown age. These rocks are interpreted to have been part of the upper plate rocks that was removed by subduction erosion and taken to depths between 35 and 55 km where they underwent blueschist–eclogite facies metamorphism. This was followed by rapid extrusion along a channel bounded by an easterly dipping, Mississippian, listric normal shear zone, and a thrust modified by a Permian dextral fault. Rocks above and below the extrusion zone are mainly Cambro-Ordovician rift-passive margin units, but a small vestige of the arc is preserved as dikes cutting rocks lying unconformably beneath the fossiliferous latest Devonian–Lower Permian Patlanoaya Group. Since faunal data indicate that Pangea had begun amalgamation by the Mississippian, at which time the Acatlán Complex lay 1500–2000 km south of the Ouachita collisional orogen between Gondwana and Laurentia, it is inferred that subduction and extrusion of the high pressure rocks occurred on the active western margin of Pangea.

Introduction

Understanding the origin of high pressure (HP) rocks in the Acatlán Complex of southern Mexico is crucial to Paleozoic paleogeographic reconstructions because they could represent either oceanic sutures or an extrusion zone within the complex (Keppie et al., 2010). There is currently much debate on age and tectonic significance of the HP metamorphism, with ages of HP metamorphism variously assigned to the Ordovician, Silurian and Carboniferous. This controversy has led to the assignment of the HP rocks to a variety of oceans including the Iapetus, Rheic and paleo-Pacific (Ortega-Gutiérrez et al., 1999; Talavera-Mendoza et al., 2005; Nance et al., 2006; Vega-Granillo et al., 2007; Keppie et al., 2008a; Vega-Granillo et al., 2009a,b; D.F. Keppie et al., 2009; J.D. Keppie et al., 2009). Ortega-Gutiérrez et al. (1999 and references therein) proposed that the HP rocks occurred in a nappe that was thrust eastwards over low-grade rocks during the Ordovician. This interpretation was based on the inference that earliest Silurian, megacrystic granitoids associated with the eclogites were the result of decompression

melting following the HP metamorphism. The lower intercept, U–Pb zircon age of 440±14 Ma reported for these granitoids by Ortega-Gutiérrez et al. (1999) has since been re-dated at 471±6 Ma (concordant U–Pb analysis: Sánchez-Zavala et al., 2004), implying a pre-Late Ordovician age for the HP metamorphism. This conclusion was apparently confirmed by Talavera-Mendoza et al. (2005) and Vega-Granillo et al. (2007), who proposed an Early Ordovician age (490–477 Ma) for the HP metamorphism at Mimilulco, also in the northern Acatlán Complex (Fig. 4.1), based on the inference that a 461±9 Ma granitoid post-dates the HP metamorphism. An older age limit for the HP metamorphism was provided by the 691±51 Ma age of the youngest detrital zircon cluster in the associated metasedimentary rocks of the informal El Rodeo "formation/suite" (Talavera-Mendoza et al., 2005; Vega-Granillo et al., 2007). Vega-Granillo et al. (2007) suggested a further two periods of HP metamorphism: (i) Late Ordovician–Early Silurian (ca. 458–443 Ma) at Ixcamilpa (Fig. 4.1), and (ii) Late Silurian (419–418 Ma) at Santa Cruz Organal. A 430±10 Ma $^{40}Ar/^{39}Ar$, amphibole age at Santa Cruz Organal was inferred to closely post-date the 458–443 Ma phase of HP metamorphism (Vega-Granillo et al., 2007, 2009a,b), however these data are highly discordant, probably the result of excess argon (D.F. Keppie et al., 2009; J.D. Keppie et al., 2009). On the other hand, Elías-Herrera et al. (2007) reported other ages from the Mimilulco area: (a) a 353±1 Ma U–Pb zircon age from retrogressed eclogite; (b) a 342±4 Ma $^{40}Ar/^{39}Ar$ age for glaucophane; and (c) a 342±3 Ma $^{40}Ar/^{39}Ar$ age for phengite. These data suggest that the HP metamorphism in the northern part of the Acatlán Complex is Mississippian. However, the data have only been published in abstract form.

The latter ages are consistent with a concordant U–Pb zircon age of 346±3 Ma from eclogite at San Francisco de Asis (Middleton et al., 2007; Fig. 4.1) that is inferred to date the HP metamorphism as Mississippian. Associated migmatites, interpreted as decompression melts, yielded ages between ca. 347 and 330 Ma (U–Pb SHRIMP data). Since this locality lies in the same N–S belt of HP rocks as both Mimilulco and Santa Cruz Organal, it calls into question the Early Paleozoic ages inferred for the HP metamorphism. Likewise, Ramos-Arias et al. (2008) have shown that the HP rocks at San Miguel Las Minas (Fig. 4.1) lie structurally beneath low-grade rocks that are deformed by Mississippian extensional fabrics, calling into question both the age and thrust geometry of the HP rocks.

Uncertainty in their age and tectonic significance has led to a wide variety of models that attribute the HP rocks to convergent zones in the Iapetus (e.g. Ortega-Gutiérrez et al., 1999; Talavera-Mendoza et al., 2005; Vega-Granillo et al., 2007, 2009b), Rheic (Nance et al., 2006, 2007), or paleo-Pacific (Keppie et al., 2008a) oceans. Resolution of this controversy has first-order implications for Paleozoic paleocontinental reconstructions before and after the formation of Pangea. To clarify this uncertainty, we report new geochronological and geochemical data from blueschists and associated rocks west of SanMiguel Las Minas (Fig. 4.2: Barley, 2006).

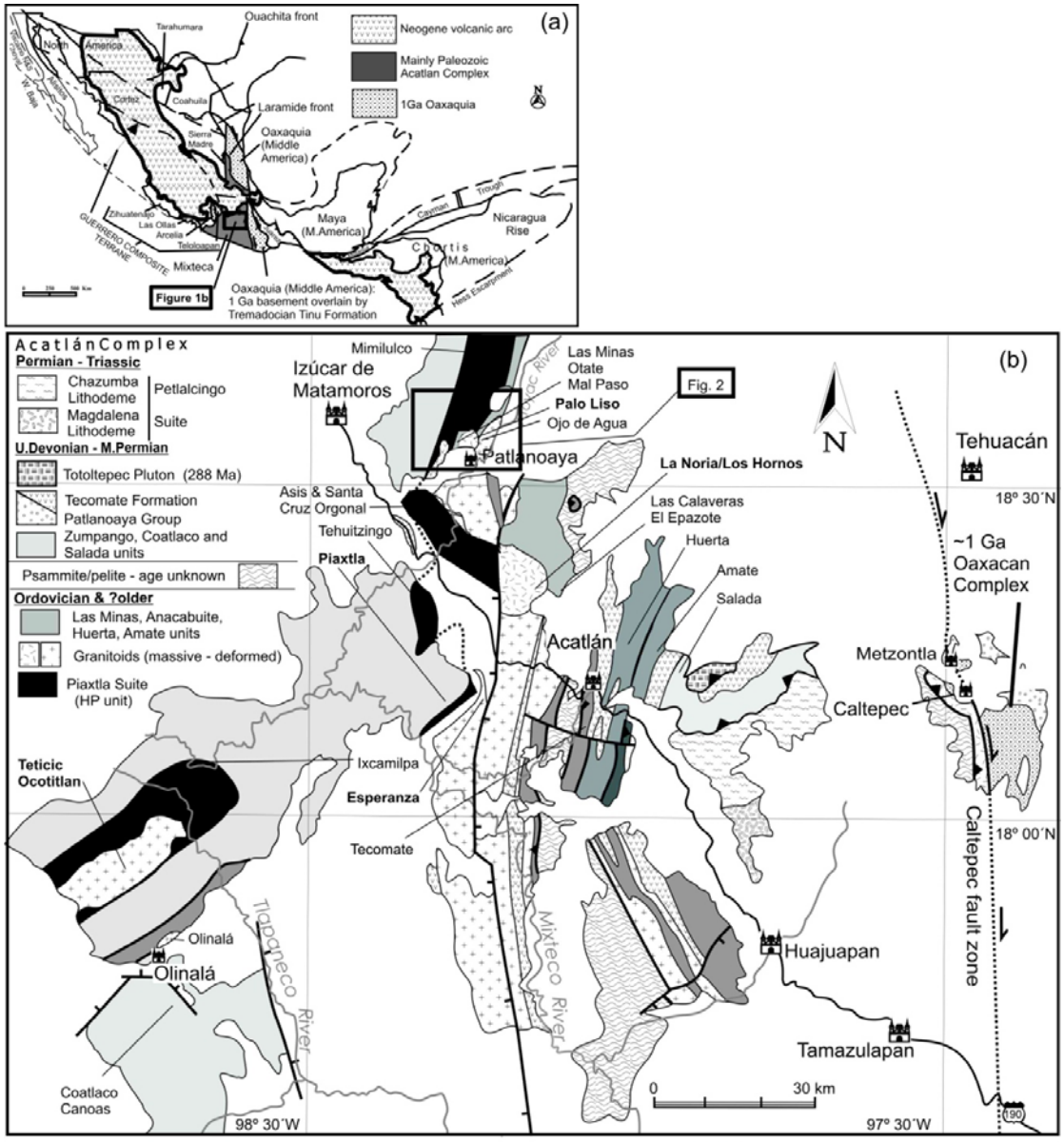

Figure 4.1 Maps of Mexico showing: (a) terranes (modified after Keppie, 2004), and (b) geological map of the Acatlán Complex (modified after Ortega-Gutiérrez et al., 1999, and Keppie et al., 2008a).

Geological setting

The Acatlán Complex (synonymous with the Mixteca Terrane) forms the largest exposed area of Paleozoic rocks in Mexico (Fig. 4.1). It is bounded along its eastern side by a Permian dextral shear zone, the Caltepec shear zone (Elias-Herrera and Ortega-Gutiérrez, 2002), east of which lies the ca. 1.0–1.3 Ga Oaxacan Complex (Keppie et al., 2003; Solari et al., 2003). That the Oaxacan Complex probably also underlies the Acatlán Complex is indicated by abundant ca. 1 Ga inherited zircons in Ordovician granitoids in the Acatlán Complex (Talavera- Mendoza et al., 2005; Miller et al., 2007; Keppie et al., 2008a). To the south of the Acatlán Complex lies the Xolapa Complex that appears to represent the roots of a Cenozoic arc built upon an Acatlán–Oaxacan continental margin (Keppie, 2004 and references therein). To the west, the Acatlán Complex is thrust over Cretaceous limestones of the Morelos Platform that probably overlie the Acatlán Complex (Keppie et al., 2008a). The northern boundary of the Acatlán Complex is obscured by the Cenozoic Trans-Mexican Volcanic Belt.

Recent multidisciplinary research has led to considerable revision and alternative models of the Paleozoic history of the Acatlán Complex (Keppie et al., 2008a, and references therein; Ortega-Obregon et al., 2009). The revised model involves at least two tectonothermal events related to opening and closing of the Rheic Ocean followed by circum-Pacific tectonic events (Fig. 4.3): (i) Cambrian(?)–Ordovician deposition of rift-passive margin sedimentary rocks on the southern flank of the Rheic Ocean accompanied by intrusion by Ordovician bimodal tholeiites and megacrystic granitoids; (ii) Latest Devonian–Permian deposition of periarc, shallow marinecontinental rocks (Vachard et al., 2000), locally associated with tholeiitic magmatism, that was synchronous with: (a) Mississippian exhumation of HP subduction-related rocks (Middleton et al., 2007), (b) Permian S-vergent thrusting and dextral shearing on N–S shear zones (Malone et al., 2002), and (c) Permian arc magmatism (Keppie et al., 2004).

The HP rocks at San Miguel Las Minas lie within the main N–S HP belt in the centre of the Acatlán Complex that is bounded on either side by poly-deformed, greenschist facies, psammite–pelite±mafic rocks (Fig. 4.1). The HP rocks are generally assigned to the Piaxtla Suite (Ortega-Gutiérrez et al., 1999; Murphy et al., 2006; Middleton et al., 2007;

Vega-Granillo et al., 2007, 2009b). The low-grade rocks have been assigned either to various informal units, such as the Cosoltepec formation (Ortega-Gutiérrez et al., 1999) and the El Rodeo "formation/ suite" (Vega-Granillo et al., 2007), or to formal lithodemic units, such as the Las Minas Unit (Ramos-Arias et al., 2008).

In the San Miguel Las Minas area, the poly-deformed, HP rocks are bounded by NNE-trending shear zones (Fig. 4.2). On the eastern side and south of the Tepetate Fault, the contact is an easterly dipping shear zone with down-dip kinematic indicators (Ramos-Arias et al., 2008). The earliest cleavage has been dated at 347±3 Ma ($^{40}Ar/^{39}Ar$ muscovite plateau age from the Las Minas Unit: Ramos-Arias et al., 2008). The Las Minas Unit is intruded by a leucogranite dike (sampled for geochronology—to be discussed below) that is deformed together with the metasedimentary rocks, and is unconformably overlain by the Otate Unit, which is intruded by the 461±2 Ma Palo Liso granite (Miller et al., 2007; Ramos-Arias et al., 2008). The eastern margin of the Palo Liso granite intrudes the Mal Paso Unit, which is overlain by the Ojo de Agua Unit (both units sampled for detrital zircons—to be discussed below). The Ojo de Agua Unit is intruded by dioritic dikes and is unconformably overlain by the latest Devonian—Early Permian Patlanoaya Group (Ramos-Arias et al., 2008). The Las Minas, Otate, Mal Paso and Ojo de Agua units have yielded Neoproterozoic–Ordovician detrital zircons (Keppie et al., 2008b). To the north of the Tepetate normal fault, a NNE-trending listric normal shear zone separates the HP rocks from the Anacahuite Amphibolite (Fig. 4.2): a felsic part of the Anacahuite Amphibolite was sampled for U–Pb geochronology. The western margin of the Anacahuite Amphibolite is cut by deformed leucocratic granitic dikes. The western margin of the HP rocks is a steeply dipping shear zone with subhorizontal slickensides and dextral kinematic indicators (Barley, 2006). The HP rocks are unconformably overlain by red beds of presumed Jurassic age that occur in a half graben within the HP rocks (Fig. 4.2).

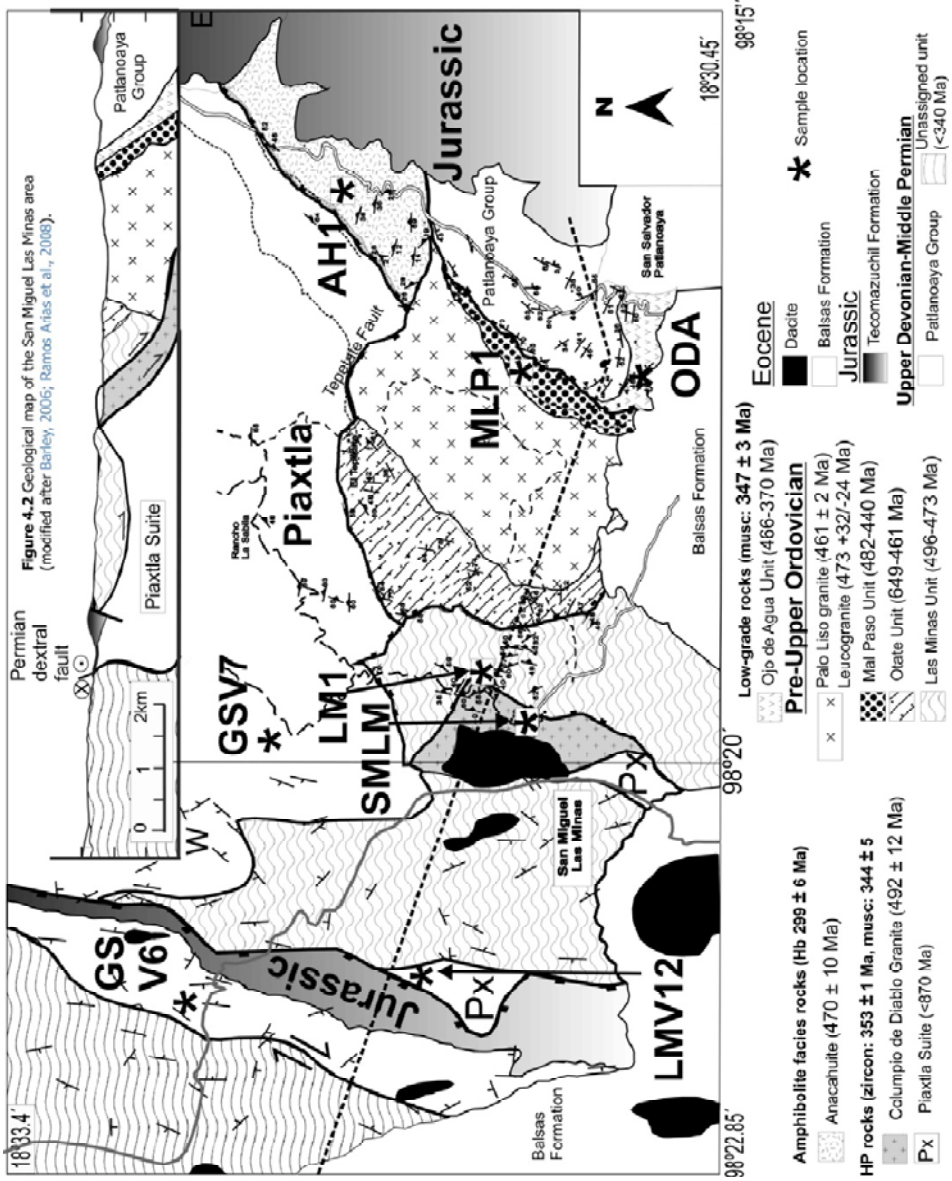

The HP Piaxtla rocks at San Miguel Las Minas consist of mica schist containing blueschist lenses, bands of amphibolite, and megacrystic granitoids, such as the San Miguel Las Minas granitoid (Barley, 2006). Several of these lithologies were sampled for U–Pb and $^{40}Ar/^{39}Ar$ geochronology (Fig. 4.2). The schists are composed of retrogressed garnets (and chlorite pseudomorphs after garnet), muscovite, and quartz. The blueschists are preserved in tectonic lenses that consist of calcic-plagioclase, glaucophane retrogressed to actinolite, lawsonite, garnet retrogressed to chlorite, epidote, muscovite, and quartz. The blueschist assemblage indicates peak temperatures and pressures of ca. 495 °C and ca. 11.5 kb (ca. 38 km depth)(Elias-Herrera et al., 2006), respectively (Fig.

4.3). On the other hand, the transitional blueschist to eclogite rocks reached ca. 550 °C and 13–13.5 kb (ca. 42 km depth)(Elías-Herrera et al., 2006). The amphibolites contain plagioclase, hornblende retrogressed to actinolite, epidote, chlorite, muscovite, and quartz. The granitoids contain orthoclase phenocrysts (partly replaced by sericite) set in a matrix of quartz, albite, orthoclase, with or without garnet, muscovite, chlorite, calcite veins, and accessory opaque minerals. The Neoproterozoic–Ordovician time of deposition of the Piaxtla Suite is constrained by the youngest detrital zircon and cross-cutting granitoids: (i) 691±51 Ma and 461±9 Ma (leucogranite), respectively, at Mimilulco (Talavera-Mendoza et al., 2005); and (ii) 705±8 Ma and ca. 470–420 Ma, respectively, at San Francisco de Asis (Murphy et al., 2006).

These high grade rocks exhibit four phases of deformation (Barley, 2006): (i) a first foliation/lineation defined by aligned amphibole in the amphibolites, and aligned glaucophane and lawsonite in the blueschists, indicative of blueschist facies metamorphism; (ii) isoclinal folds accompanied by aligned growth of muscovite, actinolite, and chlorite developed under greenschist facies metamorphic conditions; (iii) a gently dipping, crenulation cleavage that is parallel to the axial planes of shallowly ENE WNW plunging, tight-isoclinal folds formed under subgreenschist facies conditions; and (iv) NE SW plunging, upright, chevron folds and kink bands.

$^{40}Ar/^{39}Ar$ geochronology

Three samples of the HP Piaxtla Suite were collected for $^{40}Ar/^{39}Ar$ geochronology (Fig. 4.2). They are: (i) an amphibolite from which glaucophane and muscovite were separated for analysis (GSV 6: N 18 32.639″ W 098 21.441″), (ii) a garnet mica schist from which muscovite separate was separated (GSS 7: N 18 32.225″ W 098 19.984″), and (iii) a garnetiferous, amphibolitic mica schist from which a whole rock and muscovite separate were prepared (LMV 12: N 18 31.604″ W 098 21.209″).

Analytical methods

These minerals were pre-treated and concentrated by standard techniques and later selected by handpicking under a binocular microscope from fractions that ranged in size from 40 to 60 mesh at the mineral separation laboratory at ERNO—Instituto de

Geología, Universidad Nacional Autónoma de México, Hermosillo, Sonora, México. Mineral separates were loaded into Al-foil packets and irradiated together with Hb3gr (1072 Ma) as a neutron-fluence monitor at the McMaster Nuclear Reactor (Hamilton, Ontario). 40Ar/ 39Ar analyses were performed by standard laser step-heating techniques described in detail by Clark et al. (1998) at theGeochronology Research Laboratory of Queen's University, Kingston, Ontario, Canada. The data are given in Table 1 and plotted in Fig. 4.4. All data have been corrected for blanks, mass discrimination, and neutron-induced interferences. For the purpose of this paper, a plateau age is obtained when the apparent ages of at least three consecutive steps, comprising a minimum of 50% of the 39Ark released, agree within 2σ error with the integrated age of the plateau segment. Errors shown in Table 1 and on the age spectrum represent the analytical precision at ±2σ (Table 1).

Results and interpretation

Both samples from the Piaxtla Suite gave similar Mississippian plateau ages. Glaucophane (0.1×0.03 mm in size) in the amphibolites sample (GSV 6) yielded an excellent plateau age of 344±5 Ma (MSWD=1.02) for 94% of the 39Ar released (Fig. 4.4a, Table 1). Muscovite from the same sample yielded a plateau age of 338±3 Ma (MSWD=5.6) for 98% of the 39Ar released (Fig. 4.4b, Table 4.1). A similar result was obtained from muscovite (0.1×0.02 mm in size) in the garnet mica schist (sample GSS 7), which gave a plateau age of 337± 2 Ma (MSWD=5.9) for 93% of 39Ar released (Fig. 4.4c, Table 1). These data indicate cooling through ca. 470 °C for the glaucophane (Harrison et al., 1985), and ca. 340 °C for the muscovite (Hames and Bowring, 1994). Thus the data indicate rapid cooling through these temperatures between ca. 344 and 337 Ma.

The muscovite (0.05×0.01 mm in size) from the garnetiferous schist (LMV-12) yielded a hump-shaped spectrum with apparent ages defining the hump (steps 3–4) yielding an integrated age of 327± 4Ma (Fig. 4.4d, Table 1). The whole rock of the same sample yields a staircase-like spectrum with monotonically increasing ages, the upper five steps of which overlap at ca. 335 Ma (Fig. 4.4e, Table 1). These ages indicate cooling through ca. 320 °C at ca. 335 Ma.

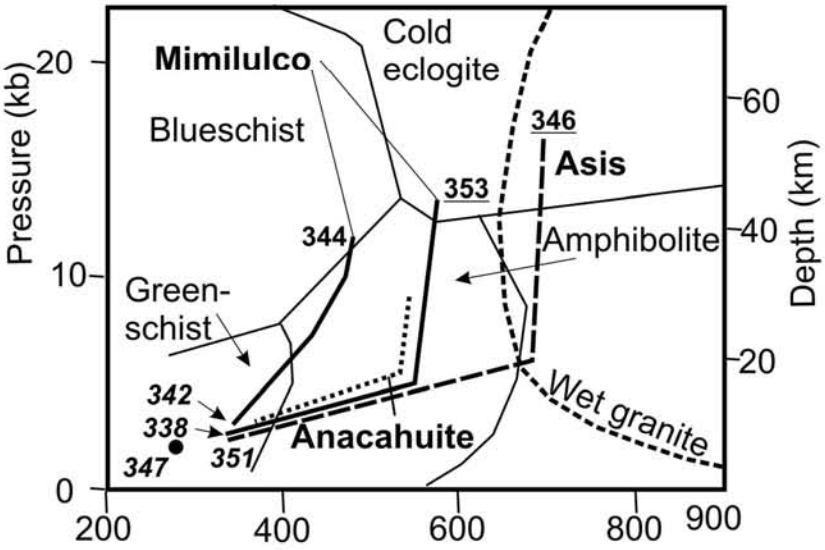

Figure 4.3 Pressure (P) - Temperature (T) graph showing the P-T paths with ages for the HP rocks in the northern part of the Acatlán Complex. Underlined numbers are U–Pb zircon ages, others are 40Ar/39Ar ages. For sources, see text.

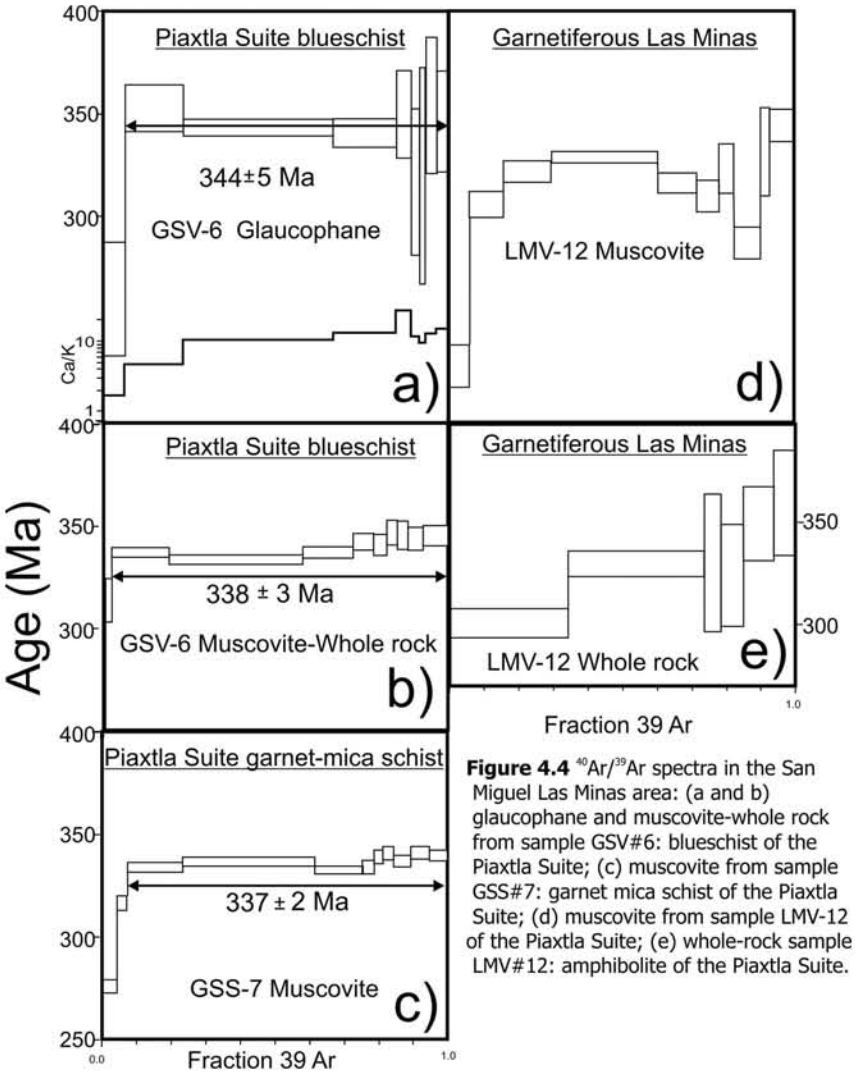

Figure 4.4 $^{40}Ar/^{39}Ar$ spectra in the San Miguel Las Minas area: (a and b) glaucophane and muscovite-whole rock from sample GSV#6: blueschist of the Piaxtla Suite; (c) muscovite from sample GSS#7: garnet mica schist of the Piaxtla Suite; (d) muscovite from sample LMV-12 of the Piaxtla Suite; (e) whole-rock sample LMV#12: amphibolite of the Piaxtla Suite.

LA-ICPMS U–Pb zircon geochronology

Several samples were collected from the San Miguel Las Minas area for LA-ICPMS analysis of zircon (Fig. 4.2): (i) a deformed megacrystic granite from the San Miguel Las Minas granitoid (SMLM: N18° 31.051′, W98° 19.733′); (ii) a felsic part of the Anacahuite Amphibolite (AH4: N18° 31.977′,W98° 16.440′); (iii) a leucogranite cutting the low-grade Las Minas Unit (LM1: N18° 31.56´,W98° 19.505′); (iv) an arkose in the Mal Paso Unit analyzed to determine if the K-feldspars were derived from the megacrystic granitoids (MLP1: N18° 31.470´, W98°17.012´); and (v) a low-grade arkose from the Ojo de Agua unit (ODA: N18° 30.351´, W98° 17.57´).

Analytical methods

The zircons were extracted using standard procedures for mineral separation (Gehrels et al., 2006). About 100 randomly selected zircons from each sample were mounted in epoxy, sanded and polished to expose the interiors of most zircon grains and also a few crystal terminations. U–Pb isotopic analyses were performed with a Micromass Isoprobe multicollector ICPMS linked to a New Wave DUV193 Excimer laser ablation system (Gehrels et al., 2006) at the University of Arizona LaserChron Center, and one sample (ODA) at the Centro de Geociencias (UNAM) in Juriquilla, Queretaro (Solari et al., 2009). The collectors are configured for simultaneous measurement of ^{204}Pb, ^{206}Pb, ^{207}Pb, ^{208}Pb, ^{232}Th, and ^{238}U. All isotope masses are measured in static mode Faraday detectors except for 204Pb, which is measured using an ion-counting channel. All analyses were conducted with a laser beam diameter of 35–50 μm operated with an output energy of ca. 32 and pulse rate of 9 Hz to yield ablation pits with a depth of ca. 15–20 μm. Each analysis consisted of one 20-second on peak blank integration with no laser firing (background) and twenty 1-second integrations on peaks with the laser firing. Any Hg contribution to the 204Pb mass position was removed by subtracting the on-peak background values. The total analysis time per zircon grain was ca. 90 s. Inter-element fractionation was monitored by analyzing fragments of a large concordant zircon crystal from Sri Lanka with a known (ID-TIMS) age of 564±4 Ma (2-sigma error). This reference zircon was analyzed once for every five unknowns. The isotopic ratios were corrected for common Pb, using the measured ^{204}Pb, assuming an initial Pb composition according to Stacey and Kramers (1975) and respective uncertainties of 1.0, 0.3, and 2.0 for

$^{206}Pb/^{204}Pb$, $^{207}Pb/^{204}Pb$, and $^{208}Pb/^{204}Pb$. The systematic error (age of standard, calibration correction from standard, composition of common Pb, and decay constant uncertainty) in the session ranged from 1.15 to 1.20% for $^{206}Pb/^{238}U$ and from 1.07 to 1.33% for $^{206}Pb/^{207}Pb$. Uranium and thorium concentrations were monitored by analyzing a NIST 610 glass. Grains for analysis were selected randomly from all sizes and morphologies present in the sample mounts, except for avoidance of grains with visible fractures, inclusions, or compositional zoning. Grains b35 μm in diameter were also avoided to ensure that each ablation pit was entirely located within a single zircon grain.

The age probability plots in this paper were constructed from the $^{206}Pb/^{238}U$ age for young (b1.3 Ga) zircon grains and the $^{206}Pb/^{207}Pb$ age for older (N1.3 Ga) zircon grains. In old zircons, analyses with N20% discordance or N10% reverse discordance are considered unreliable and were rejected. Analyses were not rejected for discordance or reverse discordance for grains that have $^{206}Pb/^{238}U$ agesb 800 Ma because of the low precision of 207Pb measurement, and hence the large errors on the $^{207}Pb/^{238}U$ age for young grains, making the geological significance of concordance and discordance difficult to assess (Gehrels et al., 2006). The $^{206}Pb/^{238}U$ age is considered robust if it belongs to a cluster of three or more zircons with similar ages (Gehrels et al., 2006). The resulting U–Pb data are shown on Tera-Wasserburg diagrams and as relative age probability curves (Fig. 4.5), which add probability distributions from all analyses from a given sample into an unique composite probability distribution. Age probability plots were constructed using IsoPlot 3.00 of Ludwig (1991). Table 2 displays a complete set of analytical U–Pb data.

Results

The San Miguel Las Minas megacrystic granite (SMLM) yielded ages ranging from 465±8 Ma to 1454±95Ma with an age of 492±12Ma for the youngest coherent group of 7 zircons (Fig. 4.5a, Table 2). On the other hand, the leucogranite (LM1) gave ages between 400±21Ma and 818±16Ma with a mean age of 473 +32/−24 Ma for the youngest coherent group of 5 igneous zircons (Fig. 4.5b, Table 2). These Cambro- Ordovician ages are inferred to date the time of intrusion. Given the errors associated with the two granitoid ages, it is possible that they represent the same intrusive event. The Neo- and Meso-proterozoic ages are inferred to be the result of inheritance from the source.

The felsic phase of the Anacahuite Amphibolite (AH4) yielded only 3 zircons, 2 of which gave ages (480±17 and 460±9 Ma: Fig. 4.5b, Table 2) that overlap at 466±3 Ma. The Anacahuite Amphibolite may be slightly younger than the granitoids, however, given the few zircons, it might also be coeval with them (Keppie et al., 2008b).

The Mal Paso arkose (MLP1) yielded ages ranging from 785±5 Ma to 1148±41 Ma with most producing populations peaks between 1058 Ma and 1243 Ma (Fig. 4.5c and d, Table 2), which corresponds to the age range of the Oaxacan Complex (Keppie et al., 2003; Solari et al., 2003). These data indicate that the K-feldspars were not derived from the erosion of the Cambro-Ordovician megacrystic granitoids, but instead were derived from the Oaxacan Complex. Somewhat younger ages were recovered from zircons in another arkose in the Mal Paso Unit (482±25 Ma, mean of three youngest zircons), with older peaks at ca. 520, 750, and 1200 Ma (Keppie et al., 2008b). The different detrital zircon populations suggest varying provenance during deposition of the Mal Paso Unit. Combining the youngest detrital zircon ages with a 440±4 Ma muscovite plateau age from hornfels in the Mal Paso Unit adjacent to the Palo Liso granitoid (Ramos-Arias et al., 2008) constrains deposition of the Mal Paso Unit to the Ordovician.

The arkose from the Ojo de Agua Unit (ODA) yielded ages ranging from 453 to 1722 Ma with major population peaks in the Cambro-Ordovician, the Ediacaran, and the Mesoproterozoic (1100–1150 Ma), and lesser peaks at 730–800 Ma and 900–980 Ma (Fig. 4.5e and f). The youngest, most concordant zircon with lowest errors has an age of 470±3 Ma, which falls within the mean of the eight youngest zircons at 471±9 Ma (Fig. 4.5e, Table 2). These data are comparable to those from a nearby sample, which yielded age population peaks at 466± 25 Ma, ca. 700 and 1100 Ma (Keppie et al., 2008b). Once again, the somewhat different age populations probably reflect variations in provenance during deposition of the Ojo de Agua Unit. These data constrain the age of deposition of the Ojo de Agua Unit to between 470 and 370 Ma (the latest Devonian base of the unconformably overlying Patlanoaya Group). They also constrain intrusion of the small dioritic intrusions to the same interval, Middle Ordovician–Upper Devonian.

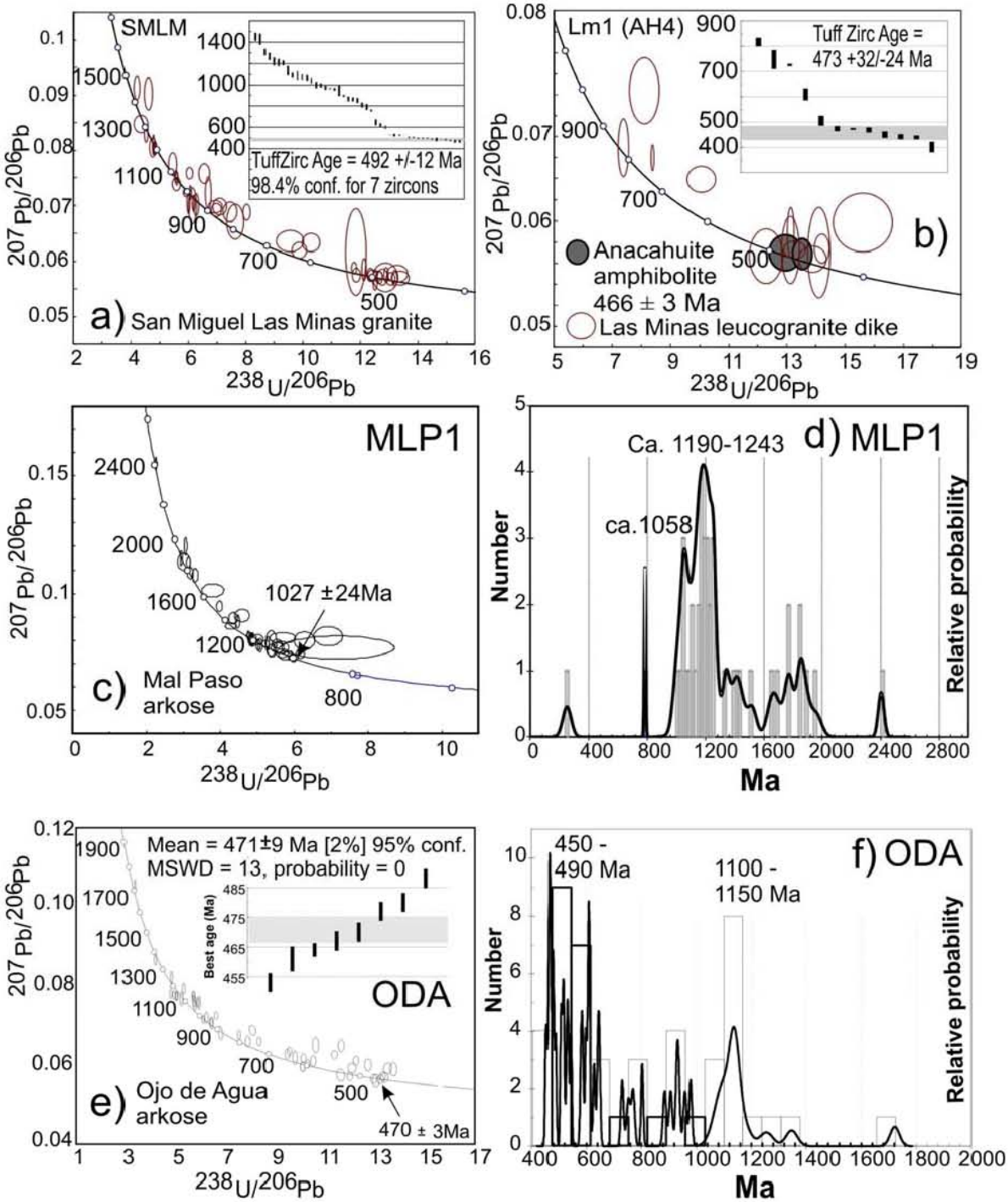

Figure 4.5. ICPMS U–Pb analyses of zircon separated from samples in the San Miguel Las Minas area plotted on Tera-Wasserburg diagrams and/or histograms: (a) deformed megacrystic granitoid, sample SMLM, San Miguel Las Minas granitoid; (b) leucogranite dike (LM1) cutting the Las Minas Unit; (c and d) arkose (MLP1) of the Mal Paso Unit; (e and f) arkose (ODA) of the Ojo de Agua Unit.

Geochemistry

Seven representative samples of the dioritic dikes that cut the Ojo de Agua Unit were analyzed for major and selected trace elements (Ba, Sr, Rb, Zr, Nb, Y, Cr, Ni, V, Pb, Zn, and Ga) by X-ray fluorescence at the Regional Geochemical Centre, Saint Mary's University, Nova Scotia. The precision and accuracy of the data have been reported by Dostal et al. (1994). The analytical error of the trace element determinations is 2–10%. Five of these samples were selected for the analysis of rare-earth elements (REE), Th, U, Hf, Zr, Nb, Ta and Y by an inductively-coupled plasma-mass spectrometer at the Memorial University of Newfoundland. The method is described by Longerich et al. (1990). The precision and accuracy of the data have beenreported by Dostal et al. (1994). The analytical error of the trace element determinations is 2–10%.

All of the rocks sampled have been modified under greenschist facies metamorphic conditions during which their chemical composition was affected. Samples yielded elevated LOI values ranging from 3.2 to 4.8, low concentrations of CaO (b1 wt.%) and highly variable Na2O all of which partly reflect these secondary processes. However, the concentrations of most major elements, high-field-strength elements (HFSE) and REE are thought to reflect primary magmatic distributions. The consistency of the compositional trends and their overall similarity to those of modern volcanic rocks suggest that the distribution of these elements reflects the original composition of the rocks. Remobilization during metamorphism is unlikely to produce such consistent results.

According to the SiO2 versus Zr/TiO2 plot (Fig. 4.6) of Winchester and Floyd (1977), which is based upon relatively immobile elements, the rocks are subalkaline with an SiO2 content ranging from 55.7 to 65.7 wt.% (LOI-free) and correspond mostly to andesites and dacites (Fig. 4.6). A slight decrease of TiO2 (Fig. 4.7) with the FeO^{+2}/MgO ratio (where FeO^{+2} equals total iron expressed as FeO) suggests that the samples have calc-alkaline characteristics, although the relatively high contents of Ti and Fe suggest that they are transitional between tholeiitic and calc-alkaline rocks (Table 3). However, their calcalkaline character is shown in the Zr–Y discrimination diagram of Ross and Bedard (2009) where the rocks plot within the calc-alkaline field (Fig. 4.8).

Chondrite-normalized REE patterns in the rocks (Fig. 4.9) are enriched in light REE (LREE) with slopes that show a range of (La/ Yb)n ratios from 6 to 13 and (La/Sm)n ca. 2.5–3. These patterns are similar to those of calc-alkaline andesites (e.g., USGS standard rock AGV-1, Guano Valley, Oregon in Fig. 4.9). However, unlike AGV-1, the patterns display small negative Eu anomalies implying fractional crystallization involving plagioclase.

The mantle normalized trace element patterns of the samples (Fig. 4.10) reveal an enrichment of large-ion-lithophile elements (LILE), such as Th, Ba, and LREE, relative to heavy REE and HFSE, and distinct troughs at Nb–Ta and Ti characteristic of subduction-related magmas. In addition, the profiles of some samples (Fig. 4.10) have negativeanomalies for Zr and Hf. Although the rocks appear to be related, the differences in the shape of the REE and trace element patterns indicate that the rocks were not derived from a homogeneous magma source by continuous fractional crystallization. The rocks were likely derived from a heterogeneous subduction-modified source. Such a tectonic environment is also implied by a Th–Hf–Ta discrimination plot of Wood (1980), where the rocks plot within the volcanic arc field (Fig. 4.11).

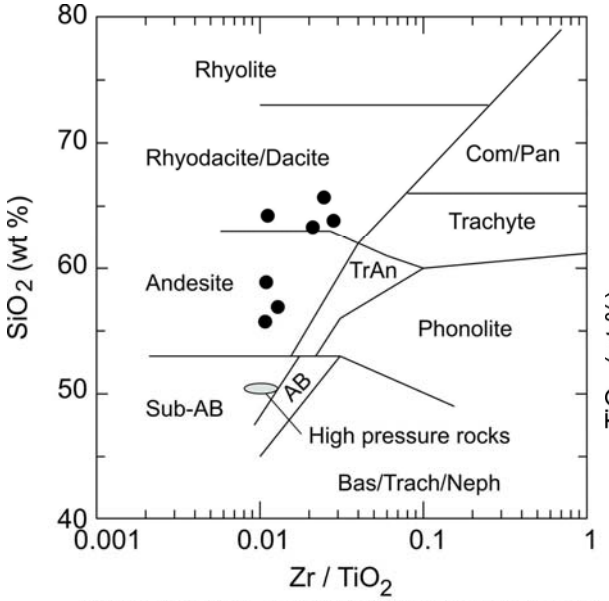

Figure 4.6 Zr/TiO_2 versus SiO_2 (wt%) diagram (based on the Winchester and Floyd 1977) for the rocks of the Ojo de Aqua Unit. Field of high pressure rocks is from Meza-Figueroa (1998).

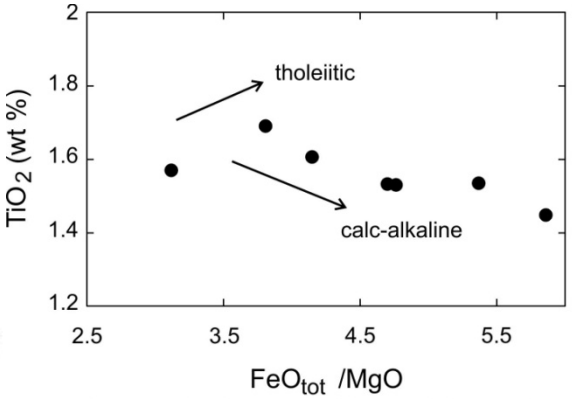

Figure 4.7 FeO_t/MgO versus TiO_2 (wt%) for the volcanic rocks of the Ojo de Aqua Unit. The lines separating the calc-alkaline and tholeiitic fields is after **Miyashiro (1974).**

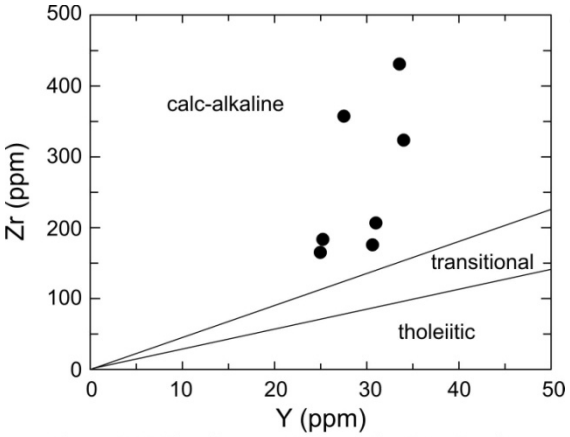

Figure 4.8 Y (ppm) versus Zr (ppm) discrimination diagram for the rocks of the Ojo de Aqua showing the boundary between calc-alkaline, transitional and tholeiitic rocks (after Ross and Bedard 2009).

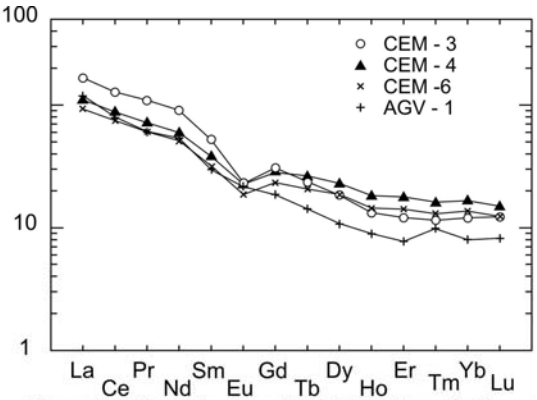

Figure 4.9 Chondrite-normalized REE patterns for the rocks of the Ojo de AquaUnit. Typical calc-alkaline andesite from the Guano Valley, Oregon (AGV-1 - USGS standard rocks; Govindaraju 1994) is shown for a comparison. Normalizing values after Sun and McDonough (1989).

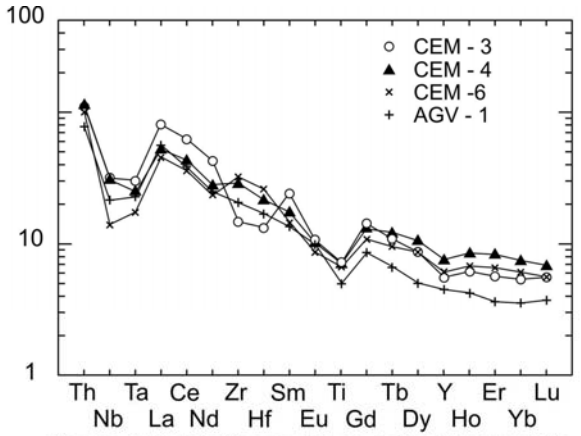

Figure 4.10 Primitive mantle-normalized incompatible trace element abundances in the rocks of the Ojo de Aqua Unit. Typical calc-alkaline andesite from the Guano Valley, Oregon (AGV-1 - USGS standard rocks; Govindaraju 1994) is shown for a comparison. Normalizing values and the element order after Sun and McDonough (1989).

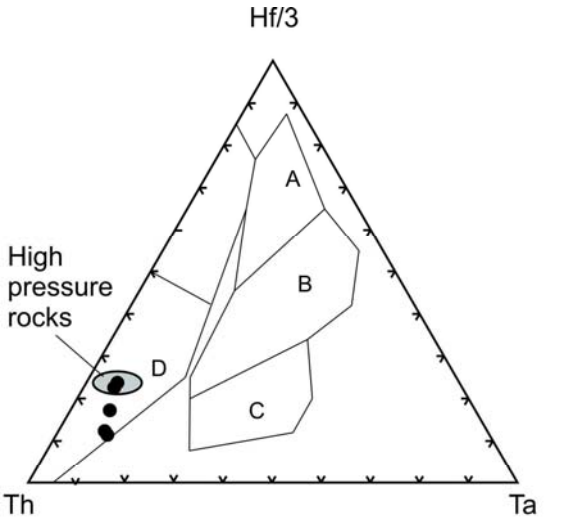

Figure 4.11 Th-Hf-Ta discrimination diagram of Wood (1980) for the rocks of the Oja de Aqua Unit. Fields: A- depleted MORB (i.e. normal MORB or N-MORB); B - enriched MORB and tholeiitic within plate basalts and differentiates; C – alkaline within plate basalts and differentiates; D – volcanic arc basalts and differentiates. Field of high pressure rocks is from Meza-Figueroa (1998).

Discussion

Time of metamorphism

The combined 353±1 MaU–Pb zircon age reported by Elías-Herrera et al. (2007) from retrogressed eclogite, the 344±5 and 338±3 Ma $^{40}Ar/^{39}Ar$ plateau ages for glaucophane and muscovite from associated blueschists, and the 337±2 Ma muscovite plateau age from adjacent garnetiferous schist indicate rapid cooling between ca. 700° and 340 °C for the rocks of the SanMiguel Las Minas area (Figs. 3 and 4). These ages are

similar to phengite ages in the HP rocks fromMimilulco (336±4 Ma and 335±2 Ma), and Piaxtla (335±4 Ma) reported by Vega-Granillo et al. (2007). The ca. 344 Ma glaucophane age is identical within error to the muscovite age (347±3 Ma) from the greenschist Las Minas Unit lying above and to the east of theHP rocks (Figs. 2 and 3: Ramos-Arias et al., 2008). It is also similar to the 346±3 Ma, concordantU–Pb zircon age from eclogite at San Francisco de Asis (Middleton et al., 2007), and phengite plateau ages from Santa Cruz Organal (345±2 Ma and 347±6 Ma: Vega-Granillo et al., 2007). Thus, on all occasions where the HP rocks have been dated directly, they have yielded Mississippian crystallization and cooling ages, which provide robust constraints on the age of HP metamorphism.

In contrast, the ca. 300 Ma hornblende cooling age for the Anacahuite Amphibolite (Ramos-Arias et al., 2008) indicates that this body was exhumed some 55 Ma later than the rocks to the south of the Tepetate Fault. Ramos-Arias et al. (2008) linked this second phase of uplift and exhumation with deposition of a conglomerate in the Patlanoaya Group.

Protoliths of the high grade rocks

The zircon data for the San Miguel Las Minas granitoid and the Anacahuite Amphibolite indicate that the both protoliths are of Cambrian–Ordovician age. The bimodal character and geochemistry of these and similar bodies led Keppie et al. (2008b) to infer that they were intruded during a rifting event at the margin of Oaxaquia. On the other hand, limited geochemistry of the eclogitic mafic rocks at Mimilulco suggests these rocks have an arc affinity (Figs. 6 and 11), but their protolith age is uncertain (Meza-Figueroa et al., 2003). The protolith age of the metasedimentary rocks of the Piaxtla Suite is bracketed between 691±51 Ma (youngest detrital zircon: Talavera-Mendoza et al., 2005) and a cross-cutting leucogranite dated at 461± 9Ma (Talavera-Mendoza et al., 2005). Thus most, if not all, of these rocks appear to have an upper plate origin.

Tectonics

In the San Miguel Las Minas area, the upper (eastern) contact between the high grade and low-grade rocks is a listric normal shear zone that was active during the

Mississippian as is indicated by the ca. 347 Ma muscovite plateau age for the earliest cleavage in the overlying greenschist facies Las Minas Unit (Ramos-Arias et al., 2008). To the west, the contact is a dextral transcurrent shear zone of inferred Permian age (Barley, 2006), the evolution of which may be related to the thermal reheating and exhumation of the Anacahuite Amphibolite at ca. 300 Ma. Such Permian motions are synchronous with dextral motions along the Caltepec Fault that forms the boundary between the Acatlán and Oaxacan complexes (Elias-Herrera and Ortega-Gutiérrez, 2002).

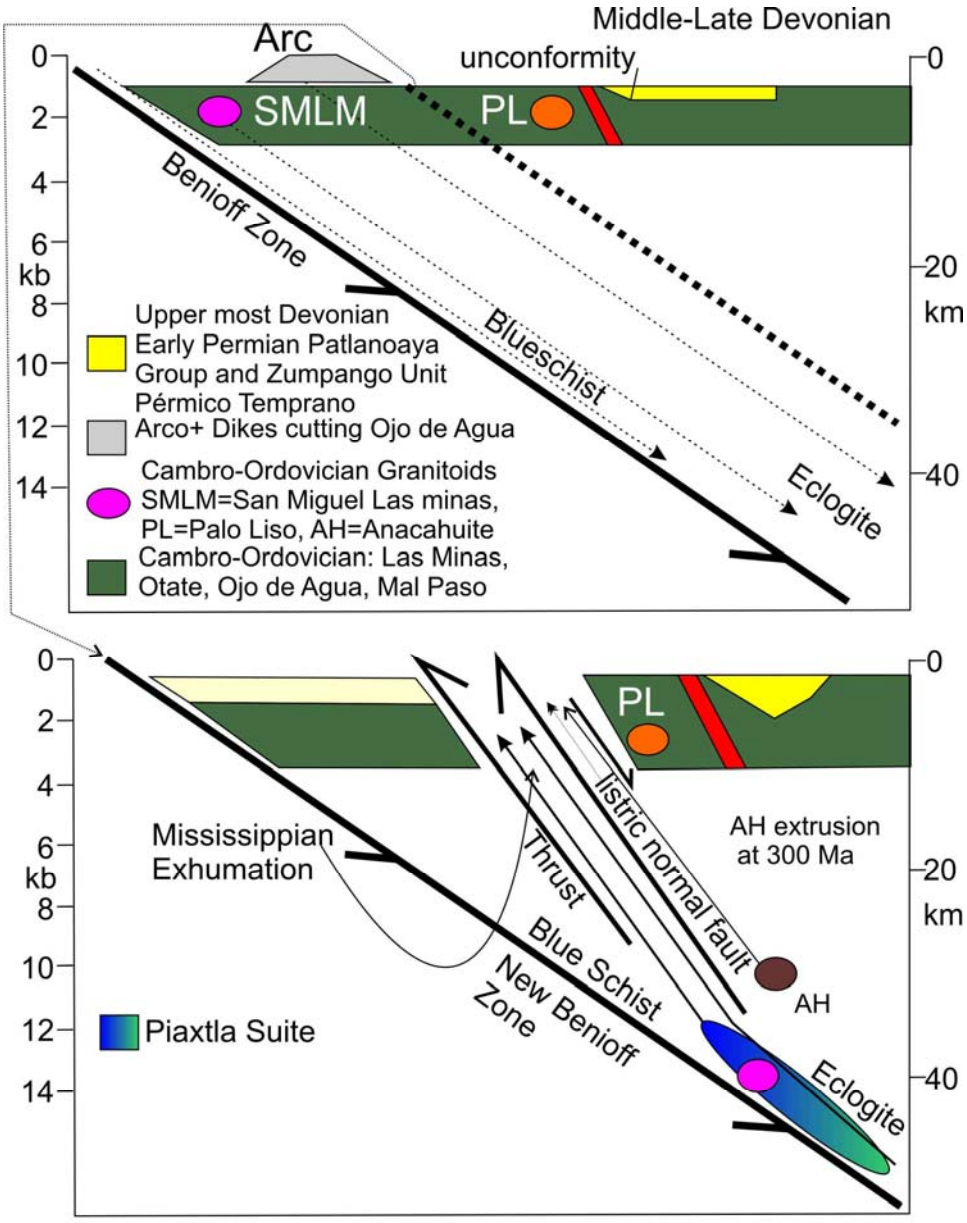

Figure. 4.12 W–E cross-section model showing: (A) subduction erosion of passive margin and arc rocks of the upper plate during the Middle-Upper Devonian; followed by (B) HP metamorphism and extrusion into the upper plate.

Along strike to the south, this Permian structure is superimposed on a W-vergent thrust (Galáz-Escanilla et al., 2009). A zone bounded below by a thrust and above by a normal fault is typical of the extrusion of HP rocks up the subduction channel (Ernst, 1988; Ernst et al., 1997; Liou et al., 2004). However, the same geometry is also present where HP rocks are extruded into the upper plate (Keppie et al., 2010). The distinction between these two scenarios dictates on whether the HP rocks represent a closed oceanand so identify a suture separating different terranes, or whether the rocks are similar on either side of the HP belt (Keppie et al., 2010), in which case no suture is implicated. In the case of the Acatlán Complex, the rocks on either side of the HP belt are similar (Keppie et al., 2008a; Ortega-Obregon et al., 2009) suggesting that the HP rocks were extruded into the upper plate (Fig. 4.12). The rift and arc protoliths of some of the HP rocks suggest that they were removed from the upper plate by subduction erosion of the leading edge of Oaxaquia. The calcalkaline volcanic rocks of the Agua de Ojo Unit may represent a vestige of the arc that was not removed by subduction erosion.

Permian arc volcanism and transtensional dextral motions between the Acatlán and Oaxacan complexes (Elias-Herrera and Ortega-Gutiérrez, 2002; Keppie et al., 2008a; Morales-Gamez et al., 2009) are synchronous with the second phase of exhumation of the high grade Anacahuite Amphibolite, which would have been facilitated by the transtensional regime.

Conclusions

Numerical models (Stöckhert and Gerya, 2005; D.F. Keppie et al., 2009) show that subduction erosion can proceed along an active ocean–continent subduction margin followed by extrusion into the upper plate. In such a setting, the Mississippian HP Piaxtla rocks are inferred to be related to subduction, extrusion and exhumation on the western margin of Pangea because Carboniferous reconstructions indicate that Pangea had begun to be amalgamated by this time (Fig. 4.13). This scenario is consistent with the presence of shallowmarine, Mid-Continent (USA), Mississippian fauna in Oaxaquia (Navarro-Santillán et al., 2002), which indicates that Pangea had already begun amalgamation by that time. Such reconstructions place the Acatlán Complex ca. 1500–2000 km south of the Ouachita Orogen, which broadly marks the location of the Rheic Ocean suture between southern

Laurentia and western Gonwana (Keppie et al., 2008a). The extrusion of HP rocks into the Acatlán Complex is indicated by the presence of the same rocks on either side of the HP belt (Keppie et al., 2008a), which implies that extrusion took place into the upper plate rather than the more common assumption that extrusion took place up along the subduction channel (Ernst et al., 1997; Ernst, 2010). This interpretation, together with the Mississippian age of extrusion, has important implications for paleogeographic reconstructions of the Acatlán Complex because it indicates that the Mimilulco–Piaxtla HP belt does not mark an oceanic suture. This conclusion simplifies paleogeographic reconstructions as it indicates that extrusion of the HP rocks took place within the continental margin of Pangea rather than involving several Paleozoic oceans. Such a mechanism may be more widespread than is currently recognized in other orogens around the world, and suggests that HP belts should be re-evaluated to determine if they represent extrusion up along the Subduction channel or into the upper plate as has been done in the Variscan belt of Europe (Keppie et al., 2010).

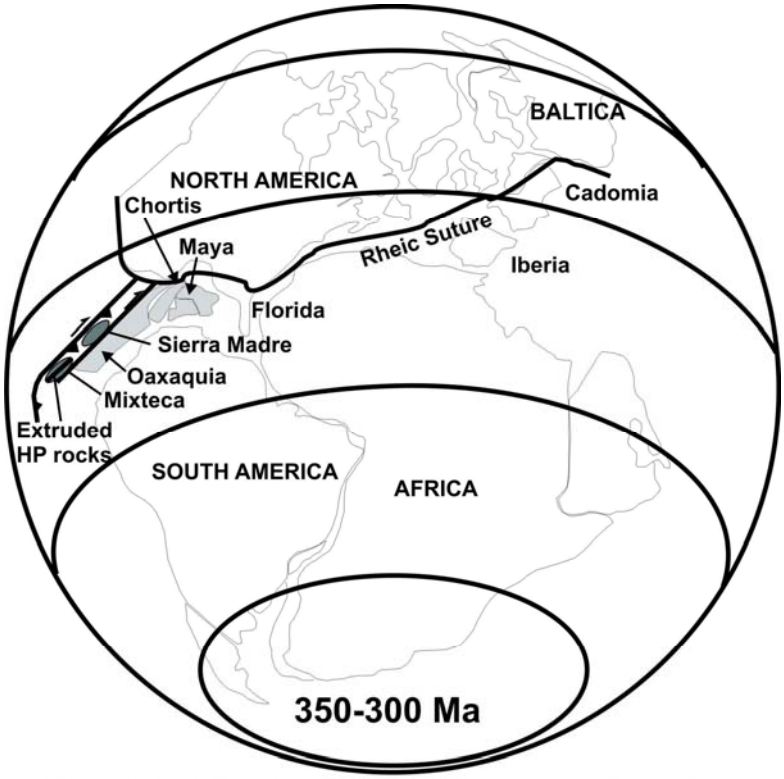

Figure 4.13 Mississippian paleogeographic reconstruction showing the Piaxtla blueschists in the active western margin of Pangea (after Keppie et al., 2008a).

Table 1
$^{40}Ar/^{39}Ar$ analyses of glaucophane and muscovite from HP rocks of the Piaxtla Suite in the northern Acatlán Complex, southern Mexico.

Steps	Laser power	Isotope volumes											Isotope correlation data		
	(Watts)	^{40}Ar	^{39}Ar	^{38}Ar	^{37}Ar	^{36}Ar	Ca/K	Cl/K	%^{40}Ar atm	f ^{39}Ar	$^{40}Ar^*/^{39}ArK$	Age	$^{36}Ar/^{40}Ar$	$^{39}Ar/^{40}Ar$	r
AOR-1035: LMV-12 Wr 80/100															
1	0.75	2.401 ± 0.009	0.067 ± 0.001	0.003 ± 0.000	0.003 ± 0.000	0.002 ± 0.000	2.396	0.007	27	34.09	26.08 ± 0.66	302.5 ± 7.1	0.000915 ± 0.000068	0.027984 ± 0.000279	0.199
2*	1.25	2.573 ± 0.010	0.077 ± 0.001	0.012 ± 0.000	0.019 ± 0.001	0.002 ± 0.000	16.503	0.031	14.06	39.12	28.84 ± 0.61	331.8 ± 6.4	0.000478 ± 0.000107	0.029793 ± 0.000410	0.515
3*	1.5	0.362 ± 0.003	0.010 ± 0.000	0.002 ± 0.000	0.004 ± 0.000	0.000 ± 0.000	19.917	0.05	16.23	5.15	28.88 ± 3.18	332.1 ± 33.4	0.000552 ± 0.000388	0.029004 ± 0.000998	0.392
4*	2	0.407 ± 0.003	0.012 ± 0.000	0.001 ± 0.000	0.006 ± 0.000	0.000 ± 0.000	30.139	0.02	11.31	6.31	28.30 ± 2.36	326.1 ± 24.9	0.000384 ± 0.000365	0.031334 ± 0.001103	0.488
5	3	0.560 ± 0.002	0.017 ± 0.000	0.002 ± 0.000	0.010 ± 0.000	0.000 ± 0.000	34.851	0.02	3.29	8.85	30.70 ± 1.74	351.2 ± 18.1	0.000113 ± 0.000281	0.031500 ± 0.000838	0.527
6	4	0.429 ± 0.003	0.013 ± 0.000	0.001 ± 0.000	0.007 ± 0.000	0.000 ± 0.000	33.44	0.02	3.93	6.47	31.66 ± 2.49	361.2 ± 25.7	0.000134 ± 0.000380	0.030341 ± 0.001036	0.55
	Total/Average	6.633 ± 0.015	0.196 ± 0.001	0.021 ± 0.001	1.638 ± 0.001	0.004 ± 0.000	15.403	0.025		100	28.78 ± 0.23	325.1 ± 2.6			
	Footnotes:	Isotope production ratios													
		($^{40}Ar/^{39}Ar$)K = 0.0302													
		($^{37}Ar/^{39}Ar$)Ca = 1416.4306													
		($^{36}Ar/^{39}Ar$)Ca = 0.3952													
		Ca/K = 1.83 × ($^{37}ArCa/^{39}ArK$)													
		J = 0.007000 ± 0.000052													
		Volume ^{39}ArK = 1.96													
		Integrated date = 325.08 ± 5.26													
		Plateau date = 331.09 ± 7.09													
		%^{39}ArK for PA = 50.59													
		Isotope correlation date = ERR													
		Initial $^{40}Ar/^{36}Ar$ ratio = ERR													
		MSWD = 0													
		%^{39}ArK for CA = 0													
AOR-1036: GSV 6 Ms Wr hp															
1	0.75	0.237 ± 0.003	0.008 ± 0.000	0.000 ± 0.000	0.001 ± 0.000	0.000 ± 0.000	0	0.003	23.62	0.41	21.74 ± 3.61	255.5 ± 39.6	0.000800 ± 0.000494	0.035115 ± 0.001222	0.283
2*	1.25	1.041 ± 0.005	0.034 ± 0.000	0.001 ± 0.000	0.001 ± 0.000	0.001 ± 0.000	0	0	9.36	1.83	27.09 ± 1.00	313.2 ± 10.6	0.000317 ± 0.000113	0.033452 ± 0.000484	0.094
3*	1.5	9.400 ± 0.024	0.313 ± 0.002	0.004 ± 0.000	0.001 ± 0.000	0.001 ± 0.000	0.037	0	2.75	16.64	29.29 ± 0.23	336.4 ± 2.4	0.000093 ± 0.000013	0.033203 ± 0.000234	0.035
4*	2	21.249 ± 0.094	0.730 ± 0.004	0.010 ± 0.001	0.002 ± 0.000	0.001 ± 0.000	0.1	0	0.91	38.8	28.97 ± 0.22	333.0 ± 2.4	0.000031 ± 0.000009	0.034204 ± 0.000252	0.043
5*	2.5	8.115 ± 0.036	0.276 ± 0.002	0.004 ± 0.000	0.003 ± 0.000	0.000 ± 0.000	0.6	0	0.7	14.67	29.29 ± 0.24	336.4 ± 2.6	0.000024 ± 0.000017	0.033903 ± 0.000251	0.074
6*	3	3.313 ± 0.014	0.111 ± 0.001	0.001 ± 0.000	0.002 ± 0.000	0.000 ± 0.000	0.51	−0	0.54	5.88	29.80 ± 0.40	341.7 ± 4.1	0.000018 ± 0.000034	0.033377 ± 0.000338	0.068
7*	3.5	2.278 ± 0.009	0.077 ± 0.001	0.001 ± 0.000	0.001 ± 0.000	0.000 ± 0.000	0.227	−0	0.16	4.07	29.63 ± 0.49	339.9 ± 5.1	0.000005 ± 0.000053	0.033694 ± 0.000374	0.14
8*	4	1.765 ± 0.007	0.058 ± 0.001	0.001 ± 0.000	0.001 ± 0.000	0.000 ± 0.000	0.239	−0	0.54	3.07	30.22 ± 0.56	346.1 ± 5.9	0.000018 ± 0.000058	0.032915 ± 0.000352	0.079
9*	5	1.740 ± 0.012	0.058 ± 0.001	0.001 ± 0.000	0.002 ± 0.000	0.000 ± 0.000	0.876	0	−0.13	3.06	30.09 ± 0.67	344.7 ± 7.0	−0.000004 ± 0.000065	0.033282 ± 0.000515	0.09
10*	6	2.465 ± 0.014	0.082 ± 0.001	0.001 ± 0.000	0.001 ± 0.000	0.000 ± 0.000	0.488	0	−0.07	4.37	29.93 ± 0.53	343.0 ± 5.6	−0.000002 ± 0.000045	0.033441 ± 0.000474	0.077
11*	7	4.069 ± 0.032	0.136 ± 0.002	0.002 ± 0.000	0.001 ± 0.000	0.000 ± 0.000	0.099	0	−0.01	7.2	30.06 ± 0.48	344.5 ± 5.0	−0.000001 ± 0.000028	0.033268 ± 0.000472	0.025
	Total/Average	55.473 ± 0.112	1.870 ± 0.006	0.024 ± 0.001	0.240 ± 0.001	0.002 ± 0.000	0.235	0		100	29.94 ± 0.06	336.2 ± 1.3			
	Footnotes:	Isotope production ratios													
		($^{40}Ar/^{39}Ar$)K = 0.0302													
		($^{37}Ar/^{39}Ar$)Ca = 1416.4306													
		($^{36}Ar/^{39}Ar$)Ca = 0.3952													
		Ca/K = 1.83 × ($^{37}ArCa/^{39}ArK$)													
		J = 0.006998 ± 0.000054													
		Volume ^{39}ArK = 18.7													
		Integrated date = 336.22 ± 2.69													
		Plateau date = 343.19 ± 3.27													
		%^{39}ArK for PA = 27.65													
		Isotope correlation date = 348.05 ± 25.49													
		Initial $^{40}Ar/^{36}Ar$ ratio = −2337.66 ± −7450.64													
		MSWD = 0.34													
		%^{39}ArK for CA = 27.65													

AOR-1037: GSV 6 Hb hp

1	0.75	1.502 ± 0.008	0.018 ± 0.000	0.007 ± 0.000	0.001 ± 0.000	0.004 ± 0.000	1.662	0.072	73.12	6.35	22.16 ± 2.53	260.0 ± 27.6	0.002477 ± 0.000151	0.012118 ± 0.000388	0.567
2*	2	2.549 ± 0.011	0.048 ± 0.001	0.008 ± 0.000	0.004 ± 0.000	0.004 ± 0.000	4.687	0.03	41.59	16.91	30.87 ± 1.09	352.7 ± 11.3	0.001409 ± 0.000091	0.018916 ± 0.000320	0.397
3*	2.5	3.927 ± 0.015	0.124 ± 0.001	0.007 ± 0.000	0.020 ± 0.001	0.001 ± 0.000	10.46	0.009	6.12	43.3	29.99 ± 0.40	343.5 ± 4.2	0.000208 ± 0.000055	0.031304 ± 0.000335	0.319
4*	3	1.613 ± 0.005	0.052 ± 0.001	0.002 ± 0.000	0.011 ± 0.000	0.001 ± 0.000	13.358	0.007	4.86	18.09	29.73 ± 0.66	340.8 ± 6.8	0.000165 ± 0.000104	0.032001 ± 0.000461	0.398
5*	3.5	0.438 ± 0.003	0.013 ± 0.000	0.001 ± 0.000	0.006 ± 0.000	0.000 ± 0.000	28.023	0.011	9.41	4.45	30.61 ± 2.03	350.0 ± 21.1	0.000319 ± 0.000306	0.029593 ± 0.000913	0.522
6*	4	0.222 ± 0.002	0.007 ± 0.000	0.000 ± 0.000	0.002 ± 0.000	0.000 ± 0.000	12.016	0.005	10.28	2.38	27.46 ± 3.37	317.0 ± 35.7	0.000348 ± 0.000515	0.032672 ± 0.001363	0.485
7*	5	0.173 ± 0.002	0.005 ± 0.000	0.000 ± 0.000	0.001 ± 0.000	0.000 ± 0.000	9.719	0.002	10.47	1.79	27.73 ± 4.95	319.9 ± 52.4	0.000355 ± 0.000663	0.032280 ± 0.001663	0.373
8*	6	0.285 ± 0.002	0.009 ± 0.000	0.000 ± 0.000	0.002 ± 0.000	0.000 ± 0.000	12.962	0.008	0.87	3.04	30.99 ± 3.19	354.0 ± 33.1	0.000030 ± 0.000434	0.031985 ± 0.001218	0.382
9*	7	0.347 ± 0.002	0.011 ± 0.000	0.001 ± 0.000	0.003 ± 0.000	0.000 ± 0.000	15.137	0.011	4.43	3.71	30.25 ± 2.35	346.3 ± 24.4	0.000151 ± 0.000343	0.031590 ± 0.001024	0.445
	Total/Average	10.912 ± 0.022	0.284 ± 0.002	0.025 ± 0.001	1.620 ± 0.001	0.009 ± 0.000	10.494	0.017		100	30.06 ± 0.19	339.1 ± 2.3			

Footnotes: Isotope production ratios
$(^{40}Ar/^{39}Ar)K = 0.0302$
$(^{37}Ar/^{39}Ar)Ca = 1416.4306$
$(^{36}Ar/^{39}Ar)Ca = 0.3952$
$Ca/K = 1.83 \times (^{37}ArCa/^{39}ArK)$
$J = 0.006995 \pm 0.000054$
Volume $^{39}ArK = 2.84$
Integrated date = 339.06 ± 4.64
Plateau date = 344.32 ± 4.53
$\%^{39}ArK$ for PA = 93.65
Isotope correlation date = 340.22 ± 10.83
Initial $^{40}Ar/^{36}Ar$ ratio = 330.67 ± 108.87
MSWD = 0.67
$\%^{39}ArK$ for CA = 93.65

AOR-1038: GSS#7 Ms hp

1	1	4.841 ± 0.015	0.177 ± 0.001	0.004 ± 0.000	0.001 ± 0.000	0.003 ± 0.000	0.068	0.002	14.01	4.03	23.62 ± 0.30	275.8 ± 3.2	0.000475 ± 0.000027	0.036394 ± 0.000321	0.045
2*	1.25	4.079 ± 0.019	0.140 ± 0.001	0.002 ± 0.000	0.001 ± 0.000	0.001 ± 0.000	0.078	0	6.08	3.19	27.44 ± 0.34	316.7 ± 3.6	0.000206 ± 0.000029	0.034223 ± 0.000316	0.076
3*	1.5	20.981 ± 0.059	0.703 ± 0.004	0.010 ± 0.001	0.001 ± 0.000	0.002 ± 0.000	0.021	0	3.15	16.03	29.04 ± 0.22	333.5 ± 2.3	0.000107 ± 0.000013	0.033350 ± 0.000222	0.039
4*	2	50.179 ± 0.177	1.676 ± 0.009	0.022 ± 0.001	0.001 ± 0.001	0.004 ± 0.000	0.008	0	2.45	38.24	29.33 ± 0.21	336.6 ± 2.2	0.000083 ± 0.000009	0.033254 ± 0.000221	0.034
5*	2.5	17.897 ± 0.060	0.608 ± 0.003	0.008 ± 0.000	0.001 ± 0.000	0.001 ± 0.000	0.006	0	2.02	13.87	28.95 ± 0.19	332.6 ± 2.0	0.000068 ± 0.000011	0.033847 ± 0.000202	0.065
6*	3	4.203 ± 0.018	0.142 ± 0.001	0.002 ± 0.000	0.001 ± 0.000	0.000 ± 0.000	0.014	0	1.74	3.24	29.08 ± 0.33	334.0 ± 3.4	0.000059 ± 0.000024	0.033789 ± 0.000321	0.063
7*	3.5	3.317 ± 0.007	0.111 ± 0.001	0.001 ± 0.000	0.001 ± 0.000	0.000 ± 0.000	0	0	1.46	2.52	29.55 ± 0.31	338.9 ± 3.3	0.000049 ± 0.000032	0.033350 ± 0.000232	0.099
8*	4	4.041 ± 0.013	0.135 ± 0.001	0.002 ± 0.000	0.001 ± 0.000	0.000 ± 0.000	0.039	0	1.17	3.07	29.73 ± 0.31	340.7 ± 3.2	0.000040 ± 0.000027	0.033245 ± 0.000273	0.097
9*	5	6.472 ± 0.023	0.219 ± 0.002	0.003 ± 0.000	0.001 ± 0.000	0.000 ± 0.000	0.043	0	0.83	5	29.35 ± 0.26	336.8 ± 2.7	0.000028 ± 0.000017	0.033791 ± 0.000274	0.08
10*	6	7.003 ± 0.038	0.234 ± 0.002	0.003 ± 0.000	0.001 ± 0.000	0.000 ± 0.000	0.017	0	0.89	5.34	29.75 ± 0.30	340.9 ± 3.1	0.000030 ± 0.000015	0.033318 ± 0.000307	0.044
11*	7	7.165 ± 0.024	0.240 ± 0.001	0.004 ± 0.000	0.001 ± 0.000	0.001 ± 0.000	0.034	0	1.14	5.47	29.61 ± 0.24	339.5 ± 2.5	0.000039 ± 0.000014	0.033389 ± 0.000237	0.051
	Total/Average	130.003 ± 0.206	4.358 ± 0.011	0.059 ± 0.002	0.045 ± 0.001	0.012 ± 0.001	0.019	0		100	29.59 ± 0.05	333.0 ± 1.3			

Footnotes: Isotope production ratios
$(^{40}Ar/^{39}Ar)K = 0.0302$
$(^{37}Ar/^{39}Ar)Ca = 1416.4306$
$(^{36}Ar/^{39}Ar)Ca = 0.3952$
$Ca/K = 1.83 \times (^{37}ArCa/^{39}ArK)$
$J = 0.006993 \pm 0.000054$
Volume $^{39}ArK = 43.58$
Integrated date = 333.02 ± 2.58
Plateau date = 337 ± 2
$\%^{39}ArK$ for PA = 21.4
Isotope correlation date = 350.40 ± 7.03
Initial $^{40}Ar/^{36}Ar$ ratio = −629.94 ± −441.29
MSWD = 5.9
$\%^{39}ArK$ for CA = 38.52

Table 2
LA-ICPMS analyses of samples from the San Miguel Las Minas area, northern Acatlán Complex, southern Mexico.

Analysis	U	^{206}Pb	U/Th	$^{206}Pb^*$	±	$^{207}Pb^*$	±	$^{206}Pb^*$	±	error	$^{206}Pb^*$	±	$^{207}Pb^*$	±	$^{206}Pb^*$	±	Best age	±	Conc
	(ppm)	^{204}Pb		$^{207}Pb^*$	(%)	$^{235}U^*$	(%)	^{238}U	(%)	corr.	$^{238}U^*$	(Ma)	^{235}U	(Ma)	$^{207}Pb^*$	(Ma)	(Ma)	(Ma)	(%)
AH4-1	569	24,940	6.1	17.5441	2.3	0.6070	4.3	0.0772	3.6	0.84	479.6	16.7	481.7	16.5	491.5	51.2	479.6	16.7	97.6
AH4-2	554	25,262	5.9	17.6044	2.0	0.5789	2.8	0.0739	2.0	0.71	459.7	8.8	463.8	10.4	484.0	43.8	459.7	8.8	95.0
AH4-3	195	19,570	13.1	13.9678	2.6	1.6320	4.8	0.1653	4.0	0.84	986.3	36.9	982.6	30.4	974.4	53.9	974.4	53.9	101.2
MLP1-3	480	95,232	1.7	15.3738	1.4	1.1619	1.5	0.1296	0.7	0.46	785.3	5.2	782.9	8.3	775.8	28.4	785.3	5.2	101.2
MLP1-8	224	53,669	4.7	13.7846	1.3	1.6718	1.9	0.1671	1.4	0.72	996.3	12.7	997.9	12.1	1001.2	26.8	1001.2	26.8	99.5
MLP1-18	188	32,008	2.5	13.6065	1.7	1.7536	2.9	0.1731	2.3	0.81	1028.9	21.9	1028.5	18.5	1027.6	34.2	1027.6	34.2	100.1
MLP1-10	154	29,383	1.3	13.4434	2.0	1.6619	2.3	0.1620	1.2	0.51	968.1	10.4	994.1	14.5	1052.0	39.7	1052.0	39.7	92.0
MLP1-5	505	118,055	1.4	13.4385	0.9	1.7546	1.5	0.1710	1.2	0.78	1017.7	10.9	1028.9	9.7	1052.7	19.0	1052.7	19.0	96.7
MLP1-21	194	64,061	1.9	13.4092	1.6	1.8128	2.6	0.1763	2.1	0.78	1046.7	20.0	1050.1	17.3	1057.1	33.0	1057.1	33.0	99.0
MLP1-25	82	37,506	1.5	13.2140	2.5	1.9337	2.9	0.1853	1.4	0.50	1095.9	14.4	1092.8	19.3	1086.6	50.2	1086.6	50.2	100.9
MLP1-41	363	68,733	2.7	13.0017	1.9	1.9130	2.8	0.1804	2.1	0.73	1069.1	20.3	1085.6	18.8	1118.9	38.3	1118.9	38.3	95.5
MLP1-42	128	19,376	3.6	12.9997	4.3	1.4767	14.7	0.1392	14.1	0.96	840.3	110.8	920.9	89.2	1119.3	85.5	1119.3	85.5	75.1
MLP1-23	154	42,637	1.2	12.9599	2.2	1.8874	3.3	0.1774	2.4	0.73	1052.8	23.0	1076.7	21.6	1125.4	44.6	1125.4	44.6	93.5
MLP1-46	285	75,891	0.8	12.8149	2.5	2.1178	2.6	0.1968	0.7	0.28	1158.3	7.8	1154.6	18.0	1147.7	49.7	1147.7	49.7	100.9
MLP1-50	224	44,660	2.1	12.8138	2.1	2.1393	2.2	0.1988	0.7	0.32	1169.0	7.5	1161.6	15.1	1147.9	41.0	1147.9	41.0	101.8
MLP1-19	143	29,036	1.6	12.7252	1.3	2.0721	1.8	0.1912	1.3	0.70	1128.1	13.0	1139.6	12.3	1161.7	25.4	1161.7	25.4	97.1
MLP1-14	158	31,721	0.6	12.7239	1.6	1.9603	2.3	0.1809	1.7	0.72	1071.9	16.3	1102.0	15.5	1161.9	31.7	1161.9	31.7	92.3
MLP1-13	36	8110	1.1	12.6892	4.5	2.0213	4.9	0.1860	1.9	0.38	1099.8	19.0	1122.7	33.4	1167.3	89.9	1167.3	89.9	94.2
MLP1-11	218	18,718	2.1	12.6837	2.5	2.0554	2.6	0.1891	0.5	0.20	1116.4	5.1	1134.1	17.5	1168.1	49.8	1168.1	49.8	95.6
MLP1-39	359	66,679	2.6	12.5098	3.0	1.7561	4.2	0.1593	3.0	0.70	953.0	26.2	1029.4	27.3	1195.4	59.4	1195.4	59.4	79.7
MLP1-45	285	63,879	3.2	12.5023	2.1	2.2610	2.6	0.2050	1.5	0.60	1202.2	16.9	1200.2	18.2	1196.6	40.9	1196.6	40.9	100.5
MLP1-38	132	30,426	1.0	12.4879	2.3	2.2765	2.3	0.2062	0.7	0.28	1208.5	7.2	1205.0	16.5	1198.9	44.4	1198.9	44.4	100.8
MLP1-16	121	31,472	1.5	12.4719	1.5	2.2791	1.9	0.2062	1.2	0.62	1208.3	12.8	1205.8	13.2	1201.4	29.0	1201.4	29.0	100.6
MLP1-6	167	47,047	1.8	12.4416	1.8	2.2154	2.8	0.1999	2.2	0.76	1174.8	23.1	1185.9	19.8	1206.2	36.1	1206.2	36.1	97.4
MLP1-7	96	27,143	0.8	12.4137	2.3	2.2786	2.3	0.2051	0.5	0.22	1202.9	5.7	1205.7	16.5	1210.7	44.9	1210.7	44.9	99.4
MLP1-29	424	89,933	2.8	12.3362	1.9	1.9661	4.5	0.1759	4.1	0.91	1044.6	39.2	1104.0	30.2	1222.9	37.1	1222.9	37.1	85.4
MLP1-9	173	47,737	2.2	12.2893	1.4	2.3172	1.5	0.2065	0.5	0.34	1210.3	5.5	1217.6	10.4	1230.4	26.9	1230.4	26.9	98.4
MLP1-47	196	5607	2.0	12.2260	3.3	1.6294	5.0	0.1445	3.7	0.75	870.0	30.4	981.6	31.4	1240.6	64.8	1240.6	64.8	70.1
MLP1-44	212	44,520	2.6	12.1718	1.5	2.3800	1.6	0.2101	0.5	0.32	1229.4	5.6	1236.6	11.2	1249.2	29.2	1249.2	29.2	98.4
MLP1-12	216	58,072	1.7	12.1343	0.7	2.3704	1.1	0.2086	0.8	0.74	1221.4	9.0	1233.7	7.8	1255.3	14.5	1255.3	14.5	97.3
MLP1-48	169	43,278	0.9	11.6174	1.1	2.7647	2.5	0.2329	2.3	0.91	1349.9	27.8	1346.1	18.8	1339.9	20.5	1339.9	20.5	100.7
MLP1-37	277	53,361	3.2	11.3706	2.1	2.7085	2.2	0.2234	0.8	0.37	1299.6	9.7	1330.8	16.5	1381.3	39.8	1381.3	39.8	94.1
MLP1-27	400	162,918	2.5	11.1892	1.8	2.8329	2.6	0.2299	1.8	0.70	1333.9	21.8	1364.3	19.4	1412.1	35.2	1412.1	35.2	94.5
MLP1-36	69	19,471	1.9	11.0364	1.9	2.7187	3.5	0.2176	2.9	0.83	1269.3	33.4	1333.6	25.9	1438.4	36.8	1438.4	36.8	88.2
MLP1-22	104	45,119	2.6	10.5800	1.6	3.2734	2.1	0.2512	1.3	0.61	1444.6	16.3	1474.8	16.0	1518.5	30.8	1518.5	30.8	95.1
MLP1-43	641	171,133	2.3	9.8640	1.8	3.6796	5.6	0.2632	5.3	0.94	1506.4	70.5	1567.0	44.4	1649.5	33.7	1649.5	33.7	91.3
MLP1-26	117	40,572	1.3	9.2833	1.8	4.4774	2.4	0.3015	1.6	0.67	1698.5	23.7	1726.8	19.6	1761.2	32.0	1761.2	32.0	96.4
MLP1-4	114	48,003	0.7	9.2116	1.4	4.6921	2.2	0.3135	1.7	0.77	1757.8	26.2	1765.8	18.6	1775.3	26.1	1775.3	26.1	99.0
MLP1-32	254	104,391	2.5	8.8538	1.3	4.9604	1.7	0.3185	1.0	0.60	1782.5	15.7	1812.6	14.2	1847.3	24.2	1847.3	24.2	96.5
MLP1-15	156	46,515	1.3	8.8173	2.1	5.1848	4.3	0.3316	3.8	0.88	1846.0	60.8	1850.1	36.8	1854.8	37.6	1854.8	37.6	99.5
MLP1-31	235	91,707	2.0	8.6899	1.8	5.3799	1.9	0.3391	0.7	0.37	1882.2	11.4	1881.7	16.4	1881.1	32.1	1881.1	32.1	100.1
MLP1-33	740	219,415	6.0	8.3343	2.1	5.4024	2.3	0.3266	0.8	0.36	1821.7	13.0	1885.2	19.6	1956.0	38.0	1956.0	38.0	93.1
MLP1-35	174	109,935	2.1	6.4510	1.2	9.4682	1.5	0.4430	0.9	0.62	2364.0	18.2	2384.5	13.6	2402.0	19.7	2402.0	19.7	98.4
SMLM-36	455	24,746	18.9	17.5472	1.9	0.5871	2.6	0.0747	1.8	0.70	464.5	8.2	469.0	9.9	491.1	41.6	464.5	8.2	94.6
SMLM-31A	422	17,888	9.0	17.2940	2.2	0.6001	3.1	0.0753	2.2	0.71	467.8	9.9	477.3	11.8	523.1	48.2	467.8	9.9	89.4
SMLM-21	507	29,530	8.3	17.5306	2.0	0.5964	2.1	0.0758	0.6	0.27	471.2	2.5	474.9	7.9	493.2	44.4	471.2	2.5	95.5
SMLM-50	305	17,892	10.2	17.5876	1.7	0.6003	2.0	0.0766	1.0	0.50	475.7	4.5	477.4	7.5	486.0	37.4	475.7	4.5	97.9
SMLM-323	426	31,780	13.2	17.3647	1.8	0.6153	1.9	0.0775	0.5	0.26	481.2	2.3	486.9	7.3	514.1	40.1	481.2	2.3	93.6
SMLM-48	203	11,794	8.6	17.5059	3.7	0.6121	4.6	0.0777	2.7	0.59	482.4	12.7	484.9	17.9	496.3	82.7	482.4	12.7	97.2
SMLM-30	273	16,700	10.6	17.4812	2.0	0.6175	2.4	0.0783	1.2	0.50	485.9	5.5	488.3	9.1	499.4	44.8	485.9	5.5	97.3
SMLM-27	357	18,370	9.6	17.4961	1.6	0.6228	1.7	0.0790	0.7	0.42	490.3	3.4	491.6	6.7	497.5	34.5	490.3	3.4	98.5
SMLM-6	499	28,526	6.8	17.4180	1.3	0.6281	1.7	0.0793	1.1	0.66	492.2	5.4	494.9	6.7	507.4	28.6	492.2	5.4	97.0
SMLM-12	247	18,122	10.6	17.6619	2.7	0.6238	2.8	0.0799	0.5	0.18	495.6	2.4	492.2	10.8	476.7	60.0	495.6	2.4	104.0
SMLM-5	541	32,944	5.9	17.4077	1.5	0.6378	1.9	0.0805	1.1	0.59	499.2	5.2	500.9	7.4	508.7	33.2	499.2	5.2	98.1

SMLM-40	450	29,510	8.8	17.3648	1.7	0.6430	1.8	0.0810	0.8	0.41	502.0	3.7	504.2	7.3	514.1	37.1	502.0	3.7	97.6	
SMLM-8	461	27,210	11.2	17.0989	2.8	0.6648	2.8	0.0824	0.5	0.18	510.7	2.5	517.6	11.4	547.9	60.3	510.7	2.5	93.2	
SMLM-42	359	21,398	35.6	17.3810	1.8	0.6687	2.1	0.0843	1.0	0.47	521.7	4.9	519.9	8.4	512.1	40.1	521.7	4.9	101.9	
SMLM-26	250	16,890	7.4	16.2105	10.3	0.7184	10.6	0.0845	2.5	0.23	522.7	12.4	549.7	45.1	663.3	221.8	522.7	12.4	78.8	
SMLM-35A	444	23,724	2.6	16.9879	1.5	0.6892	1.6	0.0849	0.6	0.37	525.4	2.9	532.3	6.6	562.1	32.2	525.4	2.9	93.5	
SMLM-9	240	23,170	7.0	15.7601	2.2	0.8518	3.3	0.0974	2.5	0.75	598.9	14.1	625.6	15.3	723.4	45.8	598.9	14.1	82.8	
SMLM-2	213	17,290	6.5	16.1225	1.9	0.8667	2.9	0.1013	2.2	0.76	622.2	12.9	633.7	13.5	675.0	40.2	622.2	12.9	92.2	
SMLM-23	170	13,188	4.5	15.7010	2.5	0.9213	4.8	0.1049	4.1	0.85	643.2	24.8	663.1	23.2	731.4	53.3	643.2	24.8	87.9	
SMLM-4	146	12,040	4.1	14.5469	1.7	1.1803	2.1	0.1245	1.2	0.58	756.6	8.9	791.5	11.7	891.1	35.9	756.6	8.9	84.9	
SMLM-19	136	14,798	1.8	14.8921	3.8	1.2117	4.9	0.1309	3.1	0.63	792.8	23.3	806.0	27.4	842.4	79.5	792.8	23.3	94.1	
SMLM-37	129	13,788	2.5	14.5194	2.1	1.2716	3.4	0.1339	2.7	0.78	810.1	20.3	833.1	19.3	895.0	43.5	810.1	20.3	90.5	
SMLM-49	176	18,448	1.8	14.3339	1.8	1.3551	3.3	0.1409	2.7	0.84	849.6	21.7	869.8	19.1	921.5	36.8	849.6	21.7	92.2	
SMLM-43	253	27,454	3.7	14.4461	1.4	1.3691	2.6	0.1434	2.2	0.84	864.1	17.4	875.8	15.0	905.4	28.6	864.1	17.4	95.4	
SMLM-28	231	33,310	5.4	14.3316	1.3	1.3861	3.2	0.1441	3.0	0.92	867.7	24.2	883.0	19.1	921.8	26.2	867.7	24.2	94.1	
SMLM-34	268	45,118	8.6	13.8454	3.4	1.4855	3.6	0.1492	1.3	0.35	896.3	10.6	924.5	21.8	992.3	68.2	896.3	10.6	90.3	
SMLM-7	161	23,032	3.5	14.1415	2.5	1.6238	2.6	0.1665	0.6	0.23	993.0	5.4	979.5	16.1	949.2	51.2	949.2	51.2	104.6	
SMLM-3	109	17,482	3.2	14.2517	2.3	1.5446	2.6	0.1597	1.2	0.44	954.8	10.2	948.3	16.1	933.3	48.1	954.8	10.2	102.3	
SMLM-22	320	35,660	3.0	14.2076	1.7	1.5700	1.8	0.1618	0.6	0.30	966.7	4.9	958.4	11.2	939.6	35.3	966.7	4.9	102.9	
SMLM-13	86	11,792	2.6	14.2839	3.7	1.5705	4.1	0.1627	1.8	0.43	971.8	15.9	958.6	25.5	928.6	76.3	971.8	15.9	104.6	
SMLM-41	338	36,290	2.7	13.8259	0.8	1.6808	1.7	0.1685	1.4	0.86	1004.1	13.3	1001.3	10.5	995.2	17.0	995.2	17.0	100.9	
SMLM-51	392	39,636	3.5	13.8150	1.4	1.6481	1.5	0.1651	0.5	0.33	985.2	4.6	988.8	9.5	996.8	28.9	996.8	28.9	98.8	
SMLM-40A	763	96,176	4.9	13.5368	1.4	1.8260	2.6	0.1793	2.2	0.85	1063.0	22.0	1054.8	17.2	1038.0	27.7	1038.0	27.7	102.4	
SMLM-47	114	16,500	2.0	13.3539	1.3	1.8489	1.4	0.1791	0.7	0.47	1061.9	6.7	1063.0	9.5	1065.4	25.5	1065.4	25.5	99.7	
SMLM-44	327	40,222	6.1	13.2827	1.3	1.8676	1.5	0.1799	0.7	0.50	1066.5	7.3	1069.7	9.7	1076.2	25.5	1076.2	25.5	99.1	
SMLM-46	336	38,812	4.0	13.1950	1.9	1.5919	3.1	0.1523	2.4	0.78	914.1	20.5	967.0	19.2	1089.4	38.7	1089.4	38.7	83.9	
SMLM-52	432	48,438	3.9	13.1872	1.1	1.7327	1.9	0.1657	1.6	0.81	988.5	14.5	1020.8	12.5	1090.6	22.8	1090.6	22.8	90.6	
SMLM-25	529	64,072	3.2	12.9033	2.2	1.9600	3.0	0.1834	2.1	0.69	1085.7	20.7	1101.9	20.1	1134.1	43.0	1134.1	43.0	95.7	
SMLM-29	143	23,888	4.1	12.4384	1.2	2.2903	1.6	0.2066	1.1	0.68	1210.7	12.0	1209.3	11.4	1206.7	23.3	1206.7	23.3	100.3	
SMLM-1	80	11,640	1.9	12.4115	1.8	2.3414	2.7	0.2108	2.0	0.75	1232.9	22.6	1224.9	19.0	1211.0	34.8	1211.0	34.8	101.8	
SMLM-39	72	11,106	2.2	12.3452	1.8	2.3374	2.0	0.2093	0.7	0.37	1225.0	8.1	1223.7	13.9	1221.5	35.7	1221.5	35.7	100.3	
SMLM-20	345	55,090	4.6	12.0405	1.5	2.5347	1.9	0.2213	1.1	0.59	1289.0	13.1	1282.1	13.9	1270.5	30.1	1270.5	30.1	101.5	
SMLM-45	296	54,246	3.2	11.7940	1.5	2.6925	4.9	0.2303	4.7	0.95	1336.1	56.5	1326.4	36.4	1310.7	29.3	1310.7	29.3	101.9	
SMLM-35	264	53,778	2.4	11.0800	2.6	2.7043	3.7	0.2173	2.7	0.72	1267.7	31.0	1329.6	27.8	1430.9	49.8	1430.9	49.8	88.6	
SMLM-10	522	79,008	2.1	10.9484	1.9	2.9998	2.9	0.2382	2.2	0.75	1377.3	26.8	1407.6	21.8	1453.6	35.8	1453.6	35.8	94.8	
LM1-2	509	5948	1.2	16.7074	3.8	0.5288	6.5	0.0641	5.4	0.82	400.4	20.8	431.0	23.0	598.3	81.7	400.4	20.8	66.9	
LM1-7	183	5024	1.5	17.4268	2.0	0.5575	2.4	0.0705	1.5	0.60	439.0	6.2	449.9	8.9	506.3	43.0	439.0	6.2	86.7	
LM1-12	75	3612	2.0	17.5432	6.1	0.5573	6.5	0.0709	2.3	0.35	441.6	9.6	449.8	23.6	491.6	134.3	441.6	9.6	89.8	
LM1-8	277	10,542	13.8	17.7383	1.8	0.5600	3.4	0.0720	2.8	0.84	448.5	12.2	451.5	12.2	467.2	40.4	448.5	12.2	96.0	
LM1-6	468	18,340	11.5	17.4531	1.2	0.5956	2.6	0.0754	2.3	0.89	468.6	10.6	474.4	10.0	503.0	26.6	468.6	10.6	93.2	
LM1-11	496	7168	3.8	16.9822	3.3	0.6181	3.3	0.0761	0.7	0.22	472.9	3.3	488.6	13.0	562.8	71.3	472.9	3.3	84.0	
LM1-9	493	19,584	5.8	17.4684	4.5	0.6017	4.9	0.0762	1.9	0.38	473.6	8.5	478.3	18.6	501.0	99.4	473.6	8.5	94.5	
LM1-10	1014	20,802	0.8	17.6393	3.7	0.6363	5.4	0.0814	3.9	0.72	504.5	18.8	500.0	21.2	479.5	82.1	504.5	18.8	105.2	
LM1-1	317	15,732	7.4	15.6441	1.6	0.8759	4.3	0.0994	4.0	0.93	610.8	23.2	638.8	20.3	739.0	33.0	610.8	23.2	82.6	
LM1-4	218	14,582	6.1	15.1513	1.5	1.0853	1.6	0.1193	0.5	0.32	726.3	3.6	746.2	8.5	806.4	31.9	726.3	3.6	90.1	
LM1-3	762	9558	7.5	13.8182	3.6	1.2308	6.3	0.1233	5.3	0.83	749.8	37.2	814.7	35.6	996.3	72.4	749.8	37.2	75.3	
LM1-5	506	45,516	6.4	14.9395	3.4	1.2491	3.9	0.1353	2.0	0.51	818.3	15.5	823.0	22.2	835.8	70.4	818.3	15.5	97.9	
ODA_46_061	134.2840578		0.284818329	0.05897	0.00106	0.59227	0.01215	0.07284	0.00049	0.38	453	3	472	8	566	39	453	3	4.025423729	
ODA_30_042	325.2938817		0.677561861	0.05915	0.00089	0.60426	0.01024	0.07408	0.00059	0.46	461	4	480	6	573	33	461	4	3.958333333	
ODA_18_028	325.285666		0.44784809	0.05683	0.0008	0.58606	0.00925	0.07476	0.00055	0.45	465	3	468	6	485	29	465	3	0.641025641	
ODA_36_050	137.8009393		0.716815047	0.05724	0.00074	0.59331	0.0084	0.07517	0.00042	0.41	467	3	473	5	501	28	467	3	1.268498943	
ODA_20_030	255.3094626		0.388745053	0.05641	0.00073	0.58874	0.00861	0.07566	0.00051	0.47	470	3	470	6	469	27	470	3	0	
ODA_44_058	256.0111947		0.251499566	0.05608	0.00107	0.59338	0.01199	0.07674	0.00053	0.33	477	3	473	8	456	42	477	3	−0.84566596	
ODA_54_070	627.361625		0.449686793	0.05649	0.00073	0.60226	0.00884	0.07726	0.00053	0.47	480	3	479	6	472	29	480	3	−0.20876827	
ODA_37_051	113.1184691		0.343615453	0.06008	0.00102	0.65089	0.01197	0.07864	0.00055	0.38	488	3	509	7	606	37	488	3	4.125736739	
ODA_6_014	207.5746554		0.220549477	0.06101	0.00079	0.68893	0.00986	0.08177	0.00049	0.43	507	3	532	6	640	27	507	3	4.69924812	
ODA_19_029	257.6427578		0.099707558	0.05884	0.00082	0.67646	0.01122	0.08284	0.00074	0.54	513	4	525	7	561	29	513	4	2.285714286	
ODA_17_027	336.6630573		0.676297138	0.05717	0.00069	0.65793	0.00895	0.08343	0.00053	0.46	517	3	513	5	498	25	517	3	−0.7797271	
ODA_49_064	349.3594128		0.112636332	0.06493	0.00103	0.76924	0.01358	0.08593	0.00061	0.4	531	4	579	8	772	33	531	4	8.29015544	
ODA_13_022	367.0943786		0.150084573	0.05748	0.00096	0.68225	0.01388	0.08609	0.00078	0.55	532	5	528	8	510	34	532	5	−0.75757576	

(continued on next page)

Table 2 (*continued*)

Analysis	U (ppm)	$^{206}Pb/^{204}Pb$	U/Th	$^{206}Pb^*/^{207}Pb^*$	± (%)	$^{207}Pb^*/^{235}U^*$	± (%)	$^{206}Pb^*/^{238}U$	± (%)	error corr.	$^{206}Pb^*/^{238}U^*$	± (Ma)	$^{207}Pb^*/^{235}U$	± (Ma)	$^{206}Pb^*/^{207}Pb^*$	± (Ma)	Best age (Ma)	± (Ma)	Conc (%)
ODA_31_044	163.8261328		0.29351077	0.06251	0.00069	0.75978	0.00979	0.08799	0.00059	0.52	544	3	574	6	692	23	544	3	5.226480836
ODA_51_067	1053.245708		0.344846612	0.0651	0.00121	0.84659	0.01837	0.09432	0.00071	0.39	581	4	623	10	778	39	581	4	6.741573034
ODA_16_026	202.6087532		0.202717633	0.06105	0.00098	0.80042	0.01379	0.09514	0.00061	0.36	586	4	597	8	641	32	586	4	1.842546064
ODA_5_012	218.189494		0.591254168	0.06027	0.00066	0.80795	0.01012	0.09717	0.00058	0.49	598	3	601	6	613	24	598	3	0.499168053
ODA_41_055	415.0545158		0.533040516	0.06173	0.00074	0.84216	0.01145	0.09888	0.00063	0.47	608	4	620	6	665	26	608	4	1.935483871
ODA_28_040	402.5462602		0.232740001	0.05956	0.00077	0.81442	0.01187	0.09914	0.00065	0.46	609	4	605	7	588	28	609	4	−0.66115702
ODA_29_041	377.3567425		0.334455991	0.05956	0.00077	0.81442	0.01187	0.09914	0.00065	0.46	609	4	605	7	588	28	609	4	−0.66115702
ODA_48_063	170.9075417		0.374108686	0.06199	0.00112	0.87283	0.01665	0.10231	0.00064	0.32	628	4	637	9	674	39	628	4	1.412872841
ODA_50_065	177.8009356		0.677929333	0.06338	0.0007	0.91542	0.01165	0.10465	0.00067	0.5	642	4	660	6	721	23	642	4	2.727272727
ODA_7_015	183.7353624		0.320917053	0.0627	0.00082	0.91424	0.01354	0.10562	0.00075	0.47	647	4	659	7	698	27	647	4	1.820940819
ODA_60_077	328.2367483		0.240336664	0.06599	0.00079	1.0905	0.01499	0.1199	0.0008	0.49	730	5	749	7	806	24	730	5	2.536715621
ODA_1_2_008	759.1948481		0.232497041	0.06887	0.00078	1.17587	0.02076	0.12383	0.00129	0.74	753	7	789	10	895	22	753	7	4.562737643
ODA_32_045	569.8799328		0.473305566	0.06607	0.00092	1.1538	0.01896	0.1268	0.00109	0.53	770	6	779	9	809	29	770	6	1.155327343
ODA_8_016	134.6270157		0.321329533	0.06768	0.00074	1.2384	0.01534	0.13266	0.00076	0.47	803	4	818	7	859	22	803	4	1.833740831
ODA_3_010	263.5171976		0.505763171	0.0681	0.00105	1.38176	0.02812	0.14716	0.00116	0.6	885	6	881	12	872	32	885	6	−0.45402951
ODA_40_053	467.914089		0.606700399	0.07256	0.00065	1.51	0.01712	0.151	0.00104	0.61	907	6	934	7	1002	18	907	6	2.890792291
ODA_59_076	313.9367068		0.156383904	0.07064	0.00106	1.5149	0.02483	0.15544	0.00103	0.4	931	6	936	10	947	30	931	6	0.534188034
ODA_4_011	685.2364436		0.882308826	0.07079	0.00071	1.5228	0.0185	0.1559	0.00108	0.56	934	6	940	7	951	20	934	6	0.638297872
ODA_9_017	174.5605098		0.375945503	0.07212	0.00094	1.595	0.02363	0.16047	0.00114	0.48	959	6	968	9	989	25	959	6	0.929752066
ODA_43_057	207.516406		0.506850079	0.07156	0.00068	1.6194	0.01811	0.16403	0.00097	0.53	979	5	978	7	973	19	979	5	−0.10224949
ODA_26_038	115.7844349		0.689840716	0.07499	0.0009	1.7977	0.0242	0.17375	0.00106	0.45	1033	6	1045	9	1068	24	1068	24	3.277153558
ODA_39_052	532.6542198		0.338209182	0.07586	0.00106	1.7657	0.02733	0.16875	0.00111	0.43	1005	6	1033	10	1091	28	1091	28	7.882676444
ODA_56_073	185.5516718		0.328058158	0.07586	0.00083	1.7837	0.02218	0.17027	0.00099	0.48	1014	5	1040	8	1091	21	1091	21	7.057745188
ODA_23_034	184.0030879		0.22835221	0.07618	0.00089	1.83351	0.02669	0.17457	0.00124	0.53	1037	7	1058	10	1100	22	1100	22	5.727272727
ODA_58_075	105.1918767		0.4164515	0.07689	0.00123	2.0313	0.03556	0.19156	0.00136	0.41	1130	7	1126	12	1118	31	1118	31	−1.07334526
ODA_15_024	185.3010178		0.239836336	0.07751	0.00085	1.8675	0.02396	0.17485	0.00115	0.52	1039	6	1070	8	1134	20	1134	20	8.377425044
ODA_27_039	883.4745416		0.378673129	0.07753	0.00068	2.128	0.02164	0.19909	0.00102	0.51	1170	5	1158	7	1135	17	1135	17	−3.08370044
ODA_25_036	181.2048996		0.38925955	0.07758	0.00085	2.1292	0.02668	0.19894	0.00119	0.49	1170	6	1158	9	1136	22	1136	22	−2.99295775
ODA_53_069	350.5061924		0.15625	0.07757	0.0007	1.8776	0.02052	0.17539	0.00109	0.56	1042	6	1073	7	1136	18	1136	18	8.274647887
ODA_21_032	149.4750029		0.37230775	0.07779	0.00074	2.179	0.02508	0.2032	0.00132	0.56	1192	7	1174	8	1142	18	1142	18	−4.37828371
ODA_45_059	259.3485008		0.268633061	0.07807	0.00078	2.2475	0.02743	0.20859	0.00146	0.57	1221	8	1196	9	1149	20	1149	20	−6.26631854
ODA_24_035	171.0360864		0.381130968	0.07933	0.00095	2.0617	0.02844	0.18837	0.00128	0.5	1113	7	1136	9	1180	22	1180	22	5.677966102
ODA_11_020	109.7252887		0.66046272	0.08241	0.00107	2.3548	0.03402	0.20745	0.00131	0.44	1215	7	1229	10	1255	24	1255	24	3.187250996
ODA_47_062	104.6336952		0.611748009	0.0864	0.00095	2.87	0.03758	0.23965	0.0017	0.54	1385	9	1374	10	1347	21	1347	21	−2.82108389
ODA_42_056	736.0129723		0.28411916	0.10545	0.00096	4.334	0.04631	0.29787	0.00167	0.52	1681	8	1700	9	1722	17	1722	17	2.380952381

Table 3
Major and trace element compositions of the igneous rocks of the Oja de Aqua Unit.

Sample		CEM-1	CEM-2	CEM-3	CEM-4	CEM-5	CEM-6	CEM-7
SiO2	%	53.71	55.950	52.46	60.84	62.160	63.15	60.74
TiO2	%	1.52	1.606	1.44	1.48	1.491	1.39	1.49
Al2O3	%	16.21	16.620	14.99	14.64	15.350	13.81	17.27
Fe2O3	%	14.99	11.840	19.02	11.40	9.980	10.54	7.42
MnO	%	0.18	0.163	0.20	0.10	0.077	0.07	0.06
MgO	%	3.25	2.800	3.59	1.91	1.910	1.62	2.14
CaO	%	0.42	0.550	0.39	0.52	0.420	0.59	0.30
Na2O	%	0.98	0.750	0.04	2.03	1.930	1.57	1.06
K2O	%	2.97	4.510	2.14	3.10	3.780	3.26	4.00
P2O5	%	0.24	0.259	0.24	0.29	0.207	0.28	0.12
L.O.I.	%	4.54	4.290	4.86	3.47	3.240	4.35	4.78
Totals		99.00	99.338	99.37	99.77	100.545	100.63	99.37
V	ppm	160.00	165.000	148.00	179.00	179.000	163.00	210.00
Cr	ppm	75.00	76.000	70.00	63.00	67.000	59.00	69.00
Co	ppm	82.00	60.000	108.00	64.00	53.000	58.00	42.00
Zr	ppm	162.00	174.000	142.00	338.00	279.000	368.00	166.00
Ba	ppm	574.00	941.000	401.00	1513.00	2487.000	1191.00	796.00
La	ppm	91.00	80.000	128.00	74.00	66.000	66.00	57.00
Nd	ppm	95.00	77.000	136.00	78.00	64.000	67.00	52.00
Ni	ppm	44.00	43.000	60.00	46.00	60.000	44.00	34.00
Cu	ppm	<4	36.000	<4	<4	<4	<4	118.00
Zn	ppm	65.00	68.000	62.00	35.00	27.000	26.00	32.00
Ga	ppm	25.00	21.000	23.00	20.00	20.000	19.00	21.00
Rb	ppm	66.00	110.000	42.00	66.00	86.000	80.00	149.00
Sr	ppm	40.00	72.000	6.00	122.00	112.000	147.00	26.00
Y	ppm	21.00	24.000	15.00	31.00	29.000	28.00	29.00
Nb	ppm	15.00	15.000	11.00	18.00	34.000	37.00	18.00
Pb	ppm	44.00	30.000	62.00	35.00	27.000	33.00	20.00
Th	ppm	25.00	19.000	32.00	22.00	20.000	22.00	20.00
U	ppm	3.00	3.000	4.00	4.00	3.000	4.00	4.00

Capítulo 5

Discusión y Conclusiones

Discusión

Los datos del área de Ixcamilpa que aquí se presentan constituyen una pieza significativa para la reconstrucción tectónica y paleogeográfica del Complejo Acatlán, dado que unifica los criterios estructurales, metamórficos y geocronológicos. Además de que divide claramente el registro geológico en dos periodos paleozoicos: (i) uno donde ocurre el depósito sedimentario e intrusión de rocas máficas y graníticas (Cámbrico tardío-Ordovícico tardío); y (ii) el tiempo en que se desarrolla la fábrica de deformación y metamorfismo de alta presión en Ixcamilpa (Devónico-Carbonífero).

El análisis geológico-estructural indica en primer lugar el origen del protolito de las rocas de alta presión, con base en una cartografía detallada y geocronología U-Pb de zircones detríticos y magmáticos, además de la correlación directa con la cartografía disponible en el sur del área. En segunda instancia se tiene los eventos de deformación y metamorfismo, gracias al análisis estructural, petrográfico-geotermobarométrico y el geocronológico por ^{39}Ar-^{40}Ar, que proporcionan un mayor entendimiento de la evolución estructural, temporalidad y ambiente potencial para la extrusión de las rocas de alta presión en el Complejo Acatlán.

Naturaleza del Protolito de las rocas de Alta Presión en Ixcamilpa

Paleozoico Temprano

La mayoría de meta-sedimentos y anfibolitas de alto grado/presión en Ixcamilpa son intrusionadas por un conjunto de diques graníticos. Es bastante evidente que las meta-sammitas de las unidades Buenavista y Zacango, con zircones detríticos más jóvenes de entre ~980 y ~654 Ma, respectivamente, son intrusionadas por el Granitoide Tecolapa de 501 ± 44Ma. De igual manera, las litologías meta-sedimentarias de las unidades Tlanipatla y Cuatlaxtecoma son intrusionadas por cuerpos graníticos que tienen correspondencia con los granitos Ocotitlán y Teticíc, 10 km hacia el sur del área, los cuales han sido fechados en 464 ±4 y 461 ±1 Ma, respectivamente (Ramírez-Espinoza, 2001; Ortega-Obregón et al., 2009). Los fechamientos realizados en lentes máficos de las unidades Tlaxco y Chicomalá en el área de Olinalá-Ixcamilpa por Ortega-Obregón (2009), y el presente estudio, han arrojado edades de entre ~473 Ma y ~446 Ma.

Las intrusiones graníticas megacristalinas y máficas tienen equivalencias temporales y geoquímicas con los intrusivos de 480-440 Ma reportados en áreas al norte y al este del Complejo Acatlán (ejemplos: los granitoides deformados Columpio del Diablo y Esperanza y sin deformar Palo Liso y La Noria). Este intervalo de tiempo concuerda con la edad de diques gabróicos en el área de Xayacatlán, cuyos zircones han sido fechados en 442±1 Ma, U-Pb (Keppie et al., 2008b). A su vez, dichos cuerpos intrusivos cortan secuencias meta-sedimentarias del Cámbrico-Ordovícico a lo largo del cinturón de Piaxtla-Mimilulco (Sánchez–Zavala et al., 2004; Talavera-Mendoza et al., 2005; Miller et al., 2006).

En las rocas de **alto grado de Ixcamilpa**, se destacan las edades de zircones detríticos mediante geocronología U-Pb, distribuidas en picos poblacionales que van del Neoproterozoico al Ordovícico:

(i) El rango de **950-1300 Ma**, se considera como procedente de Laurencia o Amazonia/Oaxaquia, no obstante, la fuente más probable es Oaxaquia, dado que incluye abundancias con posibles correspondencias de zircones para el evento Zapoteco de ~990-1000 Ma, el evento Olmeca hacia los ~1100 Ma, e inclusive rangos más viejos de entre ~1200-1300 Ma registrados en el Complejo Oaxaqueño (Keppie et al., 2003; Solari et al., 2003; Keppie y Ortega-Gutiérrez, 2009).

(ii) De igual manera, las poblaciones de entre **800-900 Ma**, refieren a una procedencia del Arco Goiás en el este de Amazonia descrito por Pimentel et al. (2000) y Laux et al. (2004).

(iii) Mientras que las edades de **500-700 Ma**, son encontradas comúnmente en el bloque de Yucatán y orógenos brasileños (Martens et al., 2010; Keppie et al., 2010b).

(iv) Por último, el intervalo de tiempo de **435-490 Ma**, es la población que presumiblemente tiene la fuente más probable en los granitoides megacristalinos ordovícicos distribuidos en el Complejo Acatlán, algunos en la margen norte de Gondwana y otros más reportados dentro del bloque Maya (Miller et al., 2006; Keppie et al., 2008a; Ortega-Obregón et al., 2008; Solari et al., 2010).

Cabe mencionar, que para la **Unidad Zumpango** fueron encontradas poblaciones de zircones de entre **356-373 Ma;** no obstante, zircones detríticos en la litología de cuarcita arrojan una edad de 310 ± 3 Ma sugiriendo que la secuencia probablemente se depositó entre el Misisípico y el Pensilvánico. Existen otros rangos poblacionales con picos en **458** y **560 Ma**, además de otras abundancias más viejas de **900** y **1200 Ma**.

Por todo lo anterior, los datos geocronológicos de U-Pb en zircones detríticos y magmáticos de rocas de alto grado en el área de Ixcamilpa, permiten definir el límite superior del depósito de la secuencia en el Ordovícico, con aporte de sedimentos de diversas fuentes en contigüidad a Amazonia y en específico a Oaxaquia (Keppie et al., 2008a).

Las rocas máficas ordovícicas del área de Ixcamilpa son idénticas a aquellas otras unidades máficas ordovícicas de Tlaxco y Zacango descritas 10 km al sur por Ortega-Obregón, (2009, 2010a) (Figura 2.4). Estas rocas exhiben firmas geoquímicas **toleíticas** y diferenciación que son características de **transición intra-placa y MORB**. Las rocas félsicas ordovícicas intrusivas distribuidas en el cinturón Ixcamilpa-Olinalá presentan una firma geoquímica calci-alcalina (Ramírez-Espinoza, 2001; Ortega-Obregón et al., 2010a). La asociación de cuerpos máficos con características toleíticas y los análisis isotópicos de Sm–Nd y ƐNd en rocas félsicas, indican que la firma calci-alcalina representa la herencia

del material fundido procedente del manto litosférico sub-continental, en su caso, el proximal Complejo Oaxaqueño de 1 Ga, (Murphy et al. 2006; Keppie et al. 2008b; y Ortega-Obregón et al., 2010a).

El conjunto de edades U-Pb de zircones detríticos y de rocas ígneas (máficas toleiticas y graníticas) del presente estudio permiten inferir que: (i) el **protolito** de las rocas de alta presión en **Ixcamilpa,** consiste en una **secuencia clástica** con zircones detríticos del **Neoproterozoico-Ordovícico**, depositada en sincronía con (ii) un **magmatismo bimodal**, dentro de un escenario de rift-margen pasivo hacia el **Cámbrico-Ordovícico medio** (Figura 5.1). Esta historia es compatible con el nacimiento del Océano Réico en el borde norte de Gondwana (Figura 5.1b, c, d) (Murphy et al., 2006; Keppie et al., 2008a; Morales-Gámez et al., 2008). Se puede agregar, que existe una estrecha afinidad litológica de las rocas de Ixcamilpa con rocas del cinturón intermedio de Piaxtla-Mimilulco, lo cual se traduce en un mismo protolito para ambos cinturones.

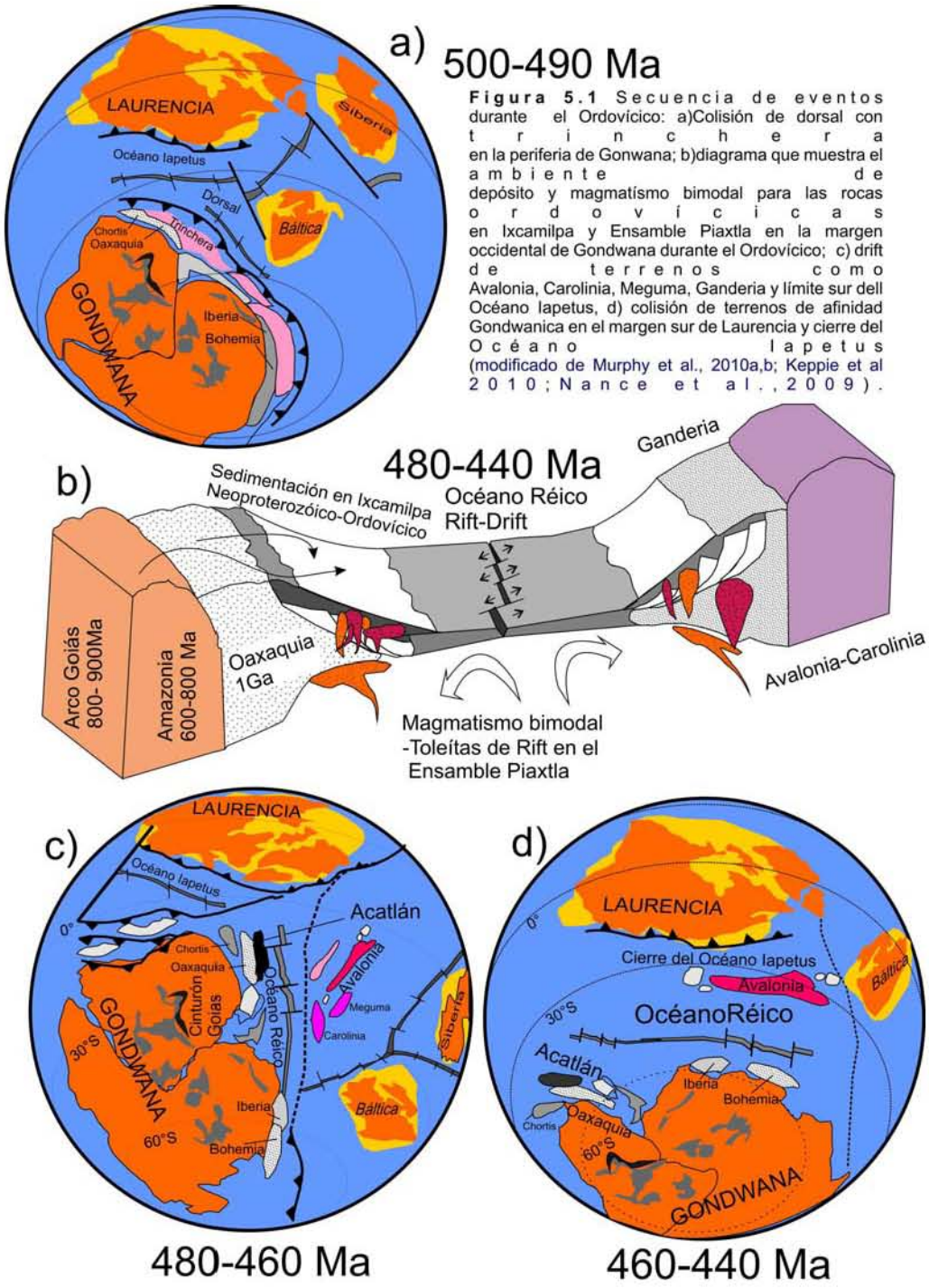

Figura 5.1 Secuencia de eventos durante el Ordovícico: a)Colisión de dorsal con trinchera en la periferia de Gonwana; b)diagrama que muestra el ambiente de depósito y magmatísmo bimodal para las rocas ordovícicas en Ixcamilpa y Ensamble Piaxtla en la margen occidental de Gondwana durante el Ordovícico; c) drift de terrenos como Avalonia, Carolinia, Meguma, Ganderia y límite sur dell Océano Iapetus, d) colisión de terrenos de afinidad Gondwanica en el margen sur de Laurencia y cierre del Océano Iapetus (modificado de Murphy et al., 2010a,b; Keppie et al 2010; Nance et al., 2009).

Estructura y metamorfismo en Ixcamilpa

Paleozoico Tardío

El modelo propuesto en el presente trabajo contrasta con la interpretación de tres periodos de actividad tectonotermal en el Complejo Acatlán por Talavera-Mendoza et al. (2005) y Vega-Granillo et al. (2007, 2009). A continuación se describe el arreglo general primero en el área de Ixcamilpa, y posteriormente se detallan algunas equivalencias estructurales y temporales a lo largo del Complejo Acatlán. El arreglo estructural en Ixcamilpa consiste de seis piezas de grado medio-alto (en facies de esquisto azul-anfibolita eclogita), que fueron imbricadas durante las primeras dos etapas de deformación (Figura 3.2). Las piezas de alto grado cabalgan en conjunto a la Unidad Zumpango de bajo grado (en facies de esquisto verde) y exhiben tres fases de acortamiento bajo un régimen dúctil (Figura 3.3):

1) una foliación penetrativa, $\mathbf{S_1}$, subparalela a un plegamiento isoclinal $\mathbf{F_1}$, ambas orientadas NE/30-50°;

2) estas estructuras han sido replegadas en forma cerrada, asimétrica y recumbente, $\mathbf{F_2}$, con transposición de $\mathbf{S_1}$ en $\mathbf{S_{1/2}}$, ambas estructuras tienen orientación NE/40. Los indicadores cinemáticos (σ, δ, peces de mica, contenidos en la primera foliación S_1 y pliegues F_2, tanto en litología granítica, anfibolítica y meta-sedimentaria) denotan cizalla inversa con cima al NW;

3) las estructuras dúctiles más tardías afectan a todas las unidades Paleozoicas, y presentan geometría de pliegues sinformes y antiformes, abiertos y sub-verticales, con ejes de pliegues buzando al ~SW/20°.

Las observaciones petrográficas y los análisis geo-termobarométricos en las fábricas minerales de unidades de alta presión, Coacalco y Cuatlaxtecoma indican que:

i) La primera foliación, S_1, en la Unidad Coacalco se genera en el campo de facies de esquisto azul, con posterior ingreso en el campo de facies de epidota-anfibolita, al pasar de los 566 a 350°C, obteniéndose una edad en glaucofano de 318 ± 4 Ma en ^{40}Ar-^{39}Ar; para finalmente entrar en facies de esquisto verde (Figura 3.10, ver pasos PT de *Co*). Dicha edad es bastante similar a aquella reportada por Vega-

Granillo et al. (2009) en rocas de alto grado de Ixcamilpa, arrojando una meseta de ^{40}Ar-^{39}Ar en 323 ± 12 Ma para fengita.

ii) Por su parte, la Unidad Cuatlaxtecoma tiene metamorfismo en el campo de anfibolita-eclogita, muy posiblemente en la transición de F_1 a F_2 (deformación y geotermobarometría de granate, Capítulo 3, Figura 3.9); con retrogresión posterior en facies de epidota-anfibolita. Fueron obtenidas dos edades de ~340 Ma, por medio de sistema ^{40}Ar-^{39}Ar, que indica el enfriamiento del anfíbol de 609 a 550°C. Por último, las rocas entran en el campo de facies de esquisto verde (Figura 3.10, ver pasos PT de *Cu*).

Se infiere que el cabalgamiento de las rocas de alta presión sobre la Unidad Zumpango ocurrió entre los ~335 Ma y la edad de enfriamiento de glaucófano en la Unidad Coacalco en ~318 Ma; existen zircones detríticos más jóvenes con 322 ± 5 Ma, extraídos de una muestra dentro de la zona de cabalgadura La Encinera. Además, se obtuvo un fechamiento dentro de la zona de cizalla para muscovita, resultando una meseta de 335 ± 2 Ma (^{40}Ar-^{39}Ar), la cual es idéntica a la edad de meseta obtenida en muscovita detrítica para la Unidad Zumpango por Ortega-Obregón et al. (2009) en 338 ± 2 Ma.

La imbricación de varias piezas bajo condiciones metamórficas de entre ~600° a ~350°C, puede interpretarse como una deformación progresiva durante el desarrollo de la fábrica $S_{1/2}$ y plegamiento F_1-F_2; en la cual la Unidad Cuatlaxtecoma en facies de eclogita-anfibolita se desplazó dúctil y progresivamente hasta posicionarse en el mismo nivel estructural de la Unidad Coacalco en facies de esquisto azul. Por su parte, las curvas P-T-t construidas en Ixcamilpa definen trayectorias similares a los patrones construidos en las áreas de Mimilulco, (Meza-Figueroa., 2003), en Las Minas (Elías-Herrera et al., 2006; Keppie et la., 2010b) y San Francisco de Asís (Middleton et al., 2006) (Figura 3.10); inclusive, observaciones petrológicas dentro de los Granitoides Esperanza (Reyes Salas, 2003) definen picos metamórficos en 16 kbar y 720° C, con posterior retrogresión hacia presiones de 12 kbar y temperaturas entre 500-450° C; trayecto bastante similar al observado en San Francisco de Asís.

Las observaciones en conjunto son consistentes con una potencial celda de flujo durante tiempos del Devónico-Carbonífero posicionada entre los ~45 y 20 km. En primer lugar, porque las gráficas P-T-t expresan la cercanía relativa de los niveles corticales desde los cuales las rocas fueron extruidas. Y en segundo término, la gama de edades ^{40}Ar-^{39}Ar para mica y anfíbol en la fábrica de la retrogresión, se expanden entre los 360-320 Ma y exhiben en su mayoría la secuencia de enfriamiento de ~700-600-550-350°C. Este hecho, restringe hasta el momento la posibilidad de plantear la sobreposición de un grado metamórfico mayor en el Ensamble Piaxtla.

El intervalo de tiempo en el Carbonífero de entre ~340 Ma y ~318-320 Ma, muy posiblemente acota el levantamiento del ensamble de alta presión en Ixcamilpa desde los ~40 hacia los ~17-20 km de profundidad. El análisis geotermobarométrico arroja una tasa de enfriamiento de 10-12.5 °C/Ma, una tasa de extrusión promedio del 1.1 km/Ma y gradiente P-T de 11.33-16.6 °C/km. En suma, las trayectorias PT de Coacalco y Cuatlaxtecoma (Figura 3.10), son curvas similares a las descritas en los cinturones de Nueva Caledonia y Sanbagawa (Ernst, 1988; Ernst y Liou, 2008; Agard et al., 2009).

La disposición estructural y distribución metamórfica en Ixcamilpa son una secuencia típica encontrada en cinturones de alta presión en el mundo (Ejemplo: Japón y el oeste de los Alpes: Ernst 1975). Expondría un ejemplo de doblamiento de las isogradas "congeladas", de tal forma que se produce el plegamiento e imbricación del material posicionado a mayor profundidad y temperatura (Figura 1.2) (Searle y Rex, 1989, Harrison et al., 1999; Beaumont et al., 2004).

Una vez conformado el Ensamble Piaxtla en Ixcamilpa, las rocas de alto grado pudieron continuar ascendiendo de manera progresiva durante F_2 hacia un nivel más superficial. Estas características son compatibles con la geometría del canal de extrusión donde las isógradas metamórficas tienden a ser plegadas pasiva y asimétricamente, de igual manera como sucede para el modelo de vorticidad con componentes Couette + Poiseuille (Figura 5.2) (Searle y Rex, 1989; Grujic et al., 2002; Jamieson et al., 1996, 2004; Godín et al., 2006).

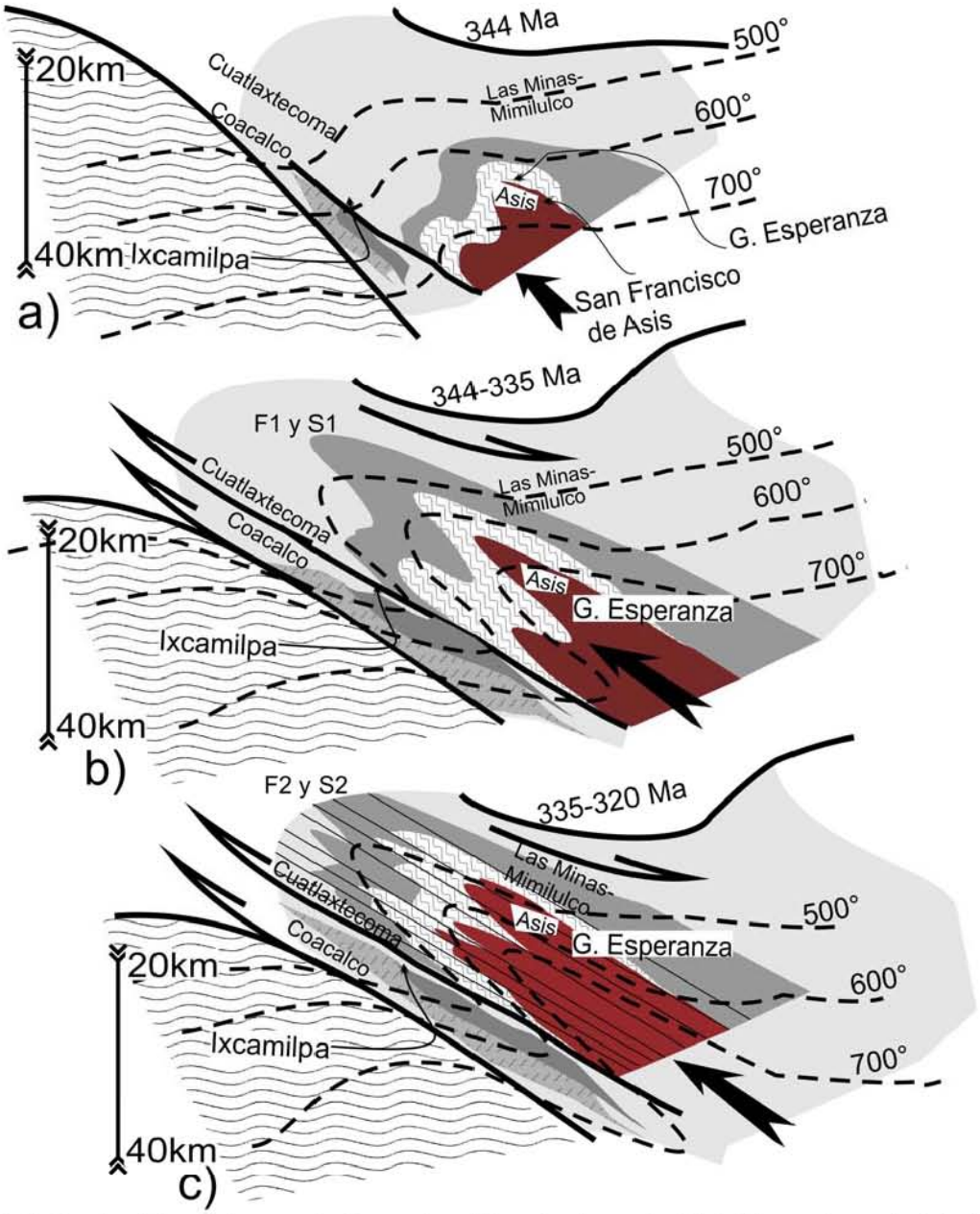

Figura 5.2 Evolución del canal de extrusión desde: a) 344 Ma; etapa inicial del emplazamiento de la secuencia de rift-margen pasivo; en seguida, b) 344-335 Ma físicamente ocurre el plegameinto F1 y foliación S1, se pliegan e imbrican las isogradas "congeladas", tal y como sucede en el modelo de flujo por dos componentes Couette + Poisseuille, donde las velocidades internas del canal de extrusión son diferentes (basado en Godin et al., 2006 y más referencias) y las predicciones hechas por los modelos de Searle y Rex (1989); Beaumont et al.,(2004). Para c) 335-320 Ma, durante el ascenso del material en el canal se produce un fallamiento discreto, por lo cual el plegamiento pasivo tiene a lugar, las isogradas "congeladas" (paragénesis metaestables) son afectadas por la última fábrica de retrogresión (facies de esquisto verde) posicionando rocas que estaban a mayor profundidad y temperatura en contiguidad con rocas en facies de menor grado, estas zonas de cizalla discretas funcionan como envolventes para la segunda fábrica de deformación progresiva F2 y S2.

La estructura en Ixcamilpa es considerada la raíz de una napa activa durante el Carbonífero con cima hacia el NW, preservada como una estructura sinforme que ha sido truncada conformando un *klippe*, el cual tiene un rol en un contexto de escala regional, con complementos estructurales, metamórficos y geocronológicos en las rocas de alto grado a lo largo del Complejo Acatlán (Figura 5.3):

I) En el cinturón intermedio de Piaxtla-Mimilulco, se toman en cuenta las mesetas de enfriamiento ^{40}Ar-^{39}Ar: en el área de Las Minas, dos edades para glaucófano, 342 ± 1 Ma, por Elías-Herrara et al. (2007) y otra de 344 ± 5 Ma, por Keppie et al (2010b); en el área de Santa Cruz Organal, ~345-348 Ma en fengita, por Vega Granillo et al. (2007); y en el área tipo de Piaxtla, ~342-344 Ma en anfíbol, por Keppie et al. (2011, en prensa). Estas edades constriñen el tiempo cuando rocas del Ensamble Piaxtla alcanzaron la mayor profundidad con un retroceso subsecuente hacia a la superficie.

II) Las edades de U-Pb en zircón de ~345 y 353 ±1 Ma en las áreas de Mimilulco y San Francisco de Asís por Elías, et al. (2006) y Middleton et al. (2006), respectivamente, definen el tiempo para el desarrollo de una estructura de rampa transtensional con cima hacia el E-NE. Son interpretadas como el límite más viejo de eclogitización y descompresión súbita hacia facies de anfibolita-eclogita (de 16 a 5 Kbar, en 700°C), acompañada por migmatización parcial.

III) El transecto Las Minas-Patlanoaya exhibe características de arreglo lístrico con cima hacia el E y elipsoide prolada en el granitoide Columpio del Diablo que denota su carácter extensivo. Dichas estructuras se formaron en facies de esquisto verde hacia los ~344 Ma (Ramos-Arias, 2007; Ramos-Arias et al., 2008). A esta estructura le sobreyace el depósito de la Formación Cerro Puntiagudo del Devónico tardío (Struniano) y base del Grupo Patlanoaya que no presenta deformación penetrativa (Vachard et al., 2004; Ramos-Arias et al., 2008). El límite hacia el oeste es una zona de cizalla dextral sub-vertical que yuxtapone a rocas de alta presión con metasedimentos de bajo grado (Barley, 2006). Las características de cabalgadura en Ixcamilpa y las de fallamiento normal en Patlanoaya, concuerdan con el modelo de un canal de extrusión de cizalla inversa en la base y cizalla normal en la cima (Platt et al., 1993; Grujic et al., 1996; Chemenda et al., 1996; Hynes, 2002).

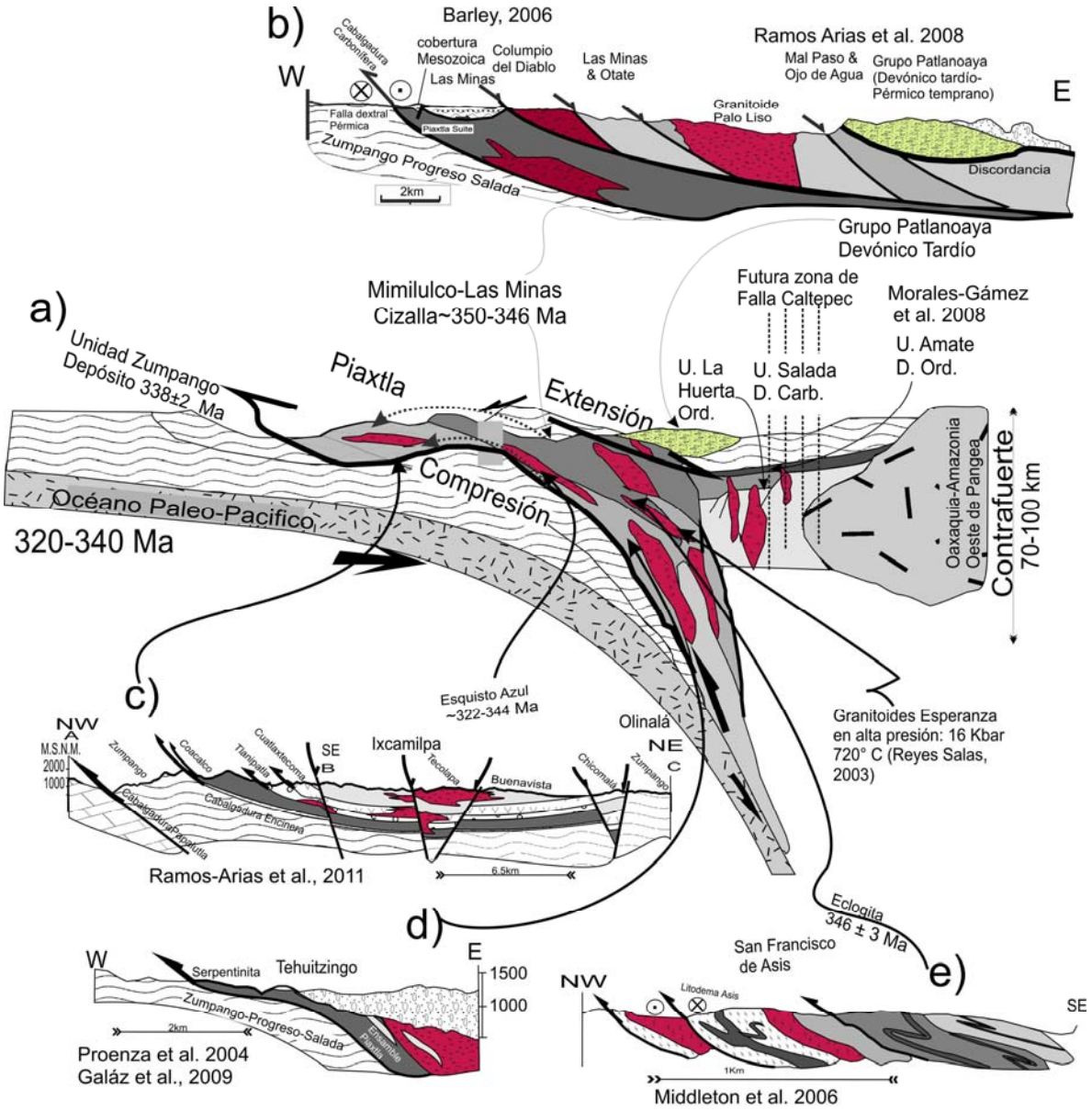

Figure 5.3 a) Correlación de unidades y modelo de extrusión para las rocas de alta presión con base en secciones y datos disponibles en: b) Sección de fallamiento lístrico en el área de Las Minas-Patlanoaya (Barley, 2006; Ramos Arias et al., 2008); c) raíz de la napa en el área de Ixcamilpa (trabajo presente); d) serpentinita en el área de Tehuitzingo, en una rampa de cabalgadura, (Proenza et al., 2004; Galáz et al., 2009). e) Disposición estructural en el área de San Francico de Asís, con el reporte de eclogitas (Middleton et al., 2006); Otros datos son tomados de localidad tipo del Granioide Esperanza (Reyes - Salas, 2003), y el área de Xayacatlán (Morales-Gámez et al., 2008), muestra el depósito de la Unidad Salada en el Carbonífero, por encima de las unidades ordovícicas de La Huerta y Amate.

Se tiene el reporte de rocas máficas eclogitizadas en el área de Mimilulco, con afinidad geoquímica de arco, aunque con edad de protolito incierta (Meza-Figueroa et al., 2003). Se le suma la existencia de material ultramáfico serpentinizado y cromititas, con lentes en facies de eclogita-anfibolita en el área de Tehuitzingo (Figura 5.3d) (Proenza et al., 2004). La presencia de firmas de afinidad calci-alcalina en rocas máficas de Mimilulco y

Tehuitzingo inmersas en rocas de alto grado de Piaxtla, implicaría la existencia de relictos de un arco, que pudo haberse erigido sobre la secuencia ordovícica de rift-margen pasivo, posiblemente durante las etapas iniciales de la subducción en un extremo de Oaxaquia, (Devónico tardío-Carbonífero temprano) (Figura 5.4a).

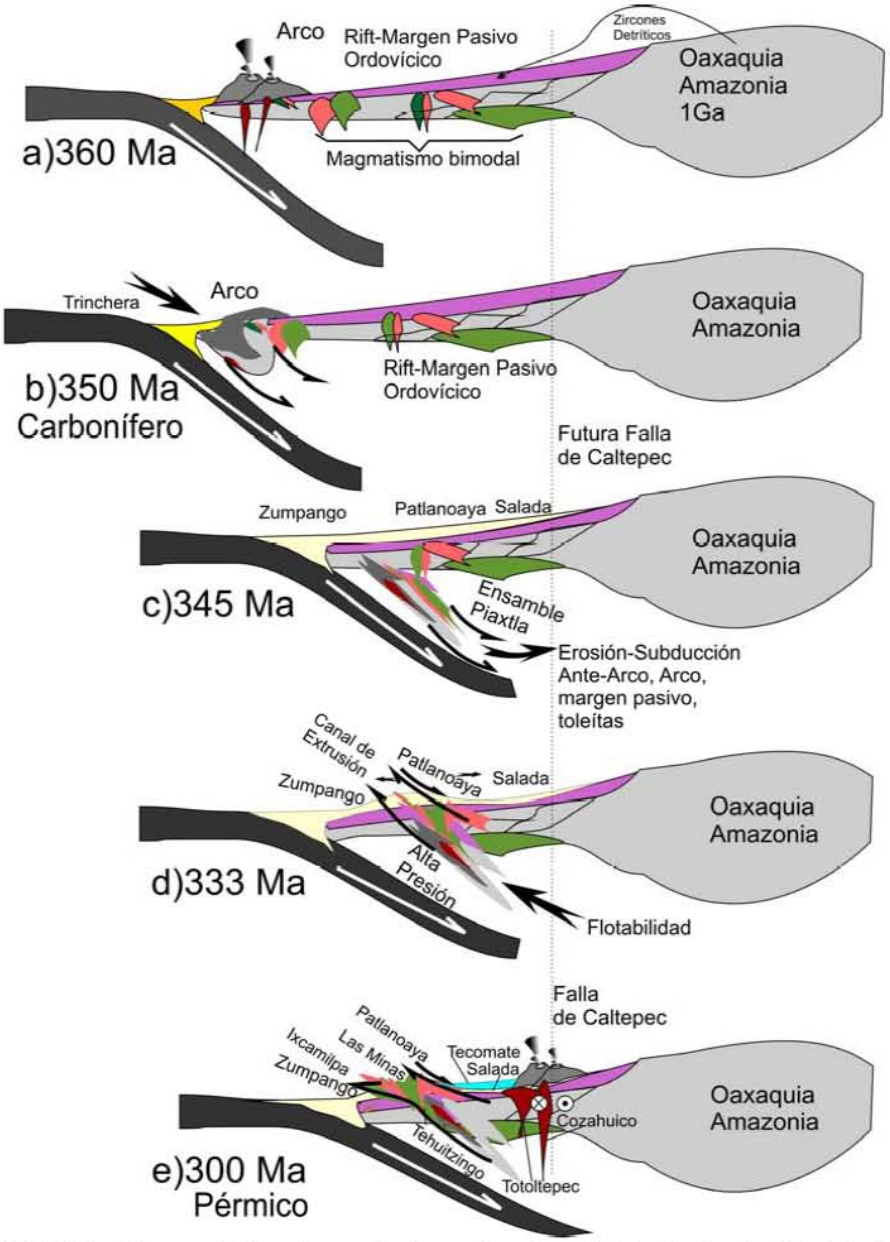

Figura 5.4 Ciclo tectónico para el orígen de rocas de alta presión en el Complejo Acatlán durante el Devónico-Carbonífero; a) inicio de la subducción, con desarrollo de un arco. b) el arco entra en el tracto de subdución, por el proceso de Erosión - Subducción y también piezas del margen pasivo, c) en seguida, las piezas se posicionan por debajo de la corteza superior y se produce la fábrica metamórfica en alta presión; d) el material liviano de la secuencia de margen pasivo y la potencial serpentinización de la cuña del manto detonan la flotabilidad y emplazamiento en la corteza superior; e) restitución del arco Pérmico en la margen activa, ya en convergencia dextral con el Océano paleo-Pacífico, en esta etapa se genera el cabalgamiento del frente del canal de extrusión sobre la Unidad Zumpango (Modificado de Keppie et al., 2008a, b, 2010a, b)

Los protolitos (en su mayoría) de rift-margen pasivo y remanentes de arco en las rocas del Ensamble Piaxtla y la celda de flujo de rocas de alta presión de Ixcamilpa, son consistentes con la remoción del arco por el proceso de subducción-erosión (Keppie D.F. et al., 2009). Seguida por la inmersión y desacople de la zona de subducción, para posteriormente posicionarse por debajo de la corteza superior y emplazarse como un cinturón intermedio (Stöckhert and Gerya, 2005).

El cinturón de extrusión de alta presión está limitado en ambos lados por rocas con una estrecha correlación en el Complejo Acatlán: unidades Zumpango, Progreso, Coatlaco y Salada con zircones detríticos del Devónico-Carbonífero (Morales-Gámez et al., 2008; Grodzicki et al., 2008; Ortega-Obregón et al., 2009; Keppie et al., 2008a, 2010b). De tal manera que es aplicable el modelo de extrusión en la intraplaca como variante de colisión oceánica Tipo Pacífico (Liou et al., 2004; Keppie et al., 2010 a, b). Además de posicionar la subducción en el borde oeste de Gondwana (Oaxaquia/Amazonia) como contrafuerte continental (Figura 5.5a).

Los datos que aquí se presentan, simplifican de manera significativa la evolución estructural del Ensamble Piaxtla en el Paleozoico en su porción occidental, permite correlacionar los dos cinturones de alto grado/presión en el Complejo Acatlán (Ixcamilpa-Olinalá, Piaxtla-Mimilulco) y le confieren un modelo de extrusión de rocas de alta presión de Tipo Pacífico con variante de Intraplaca (Liou et al., 2004; Keppie et al., 2010a).

El ciclo tectónico de rocas de alta presión en el Complejo Acatlán puede completarse en el Devónico-Carbonífero de la siguiente manera (Figura 5.4):

a) 365-350 Ma: una subducción debajo de la corteza atenuada de Oaxaquia produce un arco con depósito en la periferia (zircones detríticos jóvenes del Carbonífero de ~365 Ma en rocas de alto grado) (Figura 5.4 a-b).

b) 350-345 Ma: en el inicio del ciclo, los protolitos cámbrico-ordovícicos de ambiente de rift-margen pasivo y los remanentes de protolitos del arco devónico, fueron arrancados en conjunto de la corteza superior y sumergidos en la subducción por el proceso de erosión-subducción. De esta manera, se produce una celda de flujo posicionada entre los 20-45 km, generándose las rocas de alta

presión en Ixcamilpa en facies de esquito azul, anfibolita-eclogita y anfibolita. De tal manera que se infiere un engrosamiento cortical con reflejo directo en la extensión y depósito sedimentario en el área de Patlanoaya (Figura 5.4 c).

c) 345-310Ma: El ciclo finaliza durante el Misisípico con el retorno y emplazamiento en la corteza superior del Ensamble Piaxtla hasta posicionarse de forma somera (20-17 km), donde el frente del canal de extrusión cabalga a la Unidad Zumpango, produciéndose en conjunto las últimas fábricas de retrogresión en facies de esquisto verde (Figura 5.4 d).

d) 310-280 Ma: la disposición estructural que tiene el Complejo Acatlán se completa con la restitución del arco Pérmico, con una convergencia oblícua-dextral bajo la dinámica del Océano paleo-Pacífico (Figura 5.4 e).

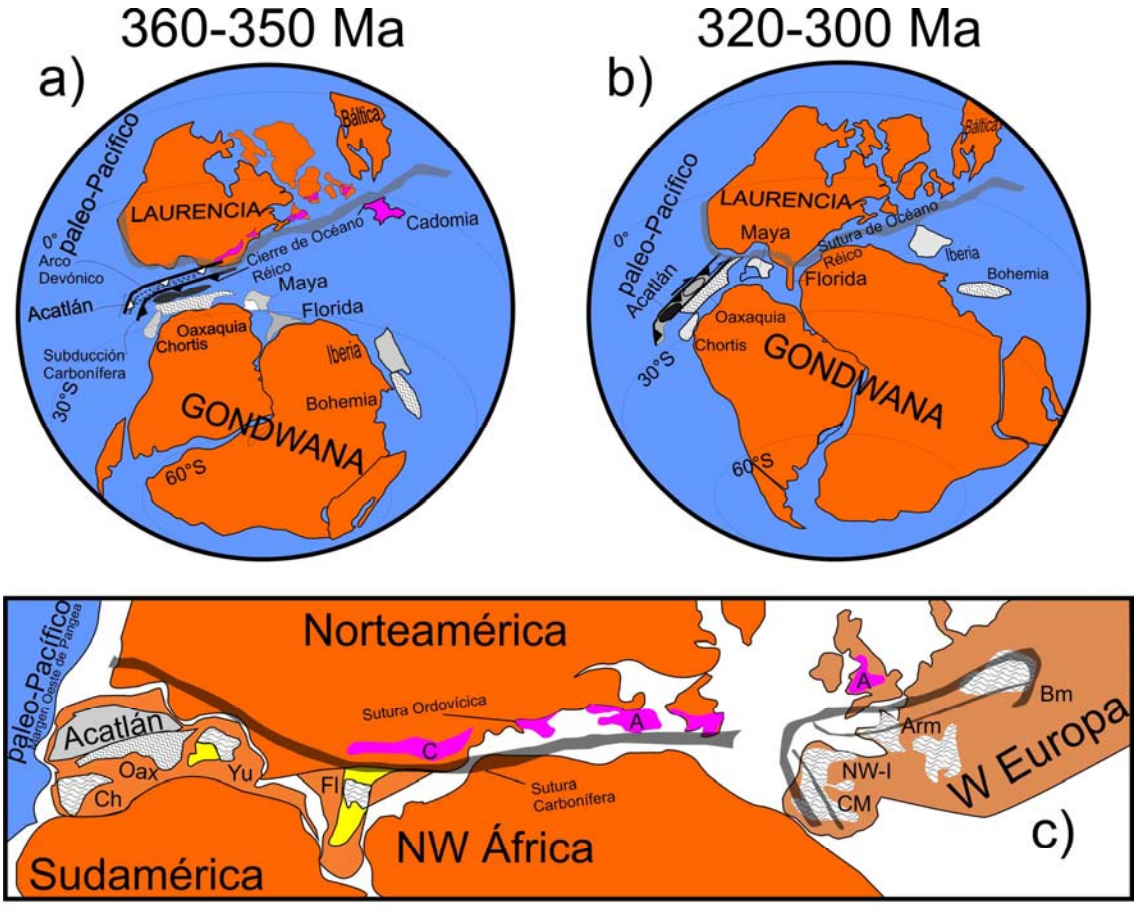

Figura 5.5 Esquemas de paleogeografía; a)subducción en la margen noroeste de Gondwana, el arco del Devónico es erosionado por subducción y se genera una nueva zona de subducción en el Carbonífero, b) cierre del Océano Réico y ensamble de Pangea, posición mas occidental del Complejo Acatlán; c) sutura Variscana del Misisípico, entre los continentes Laurencia, Sudamérica, África y Europa; y la presencia de micro terrenos Ch=Chortis, Oax=Oaxaquia, Yu=Yucatán, Fl= Florida, y el Complejo Acatlán en la margen oeste de Pangea; C=Carolinia, A=Avalonia, NW-I=Nororeste de Iberia, Arm=Armoricia, Bm=Bohemia (modificado de Keppie et al., 2008a, 2008b; Nance y Linnemann, 2007)

En una escala continental-regional, la posición paleogeográfica (Ordovícico-Pérmico) del Complejo Acatlán se asume en yuxtaposición con el noroeste de Gondwana. El proceso de subducción y extrusión de rocas de alta presión en Ixcamilpa son equivalentes en tiempo Misisípico para el cierre del Océano Réico en Iberia y Bohemia. Por tanto, se interpreta que el Complejo Acatlán queda bajo la influencia de la Orogenia Variscana-Alleghaniana en su porción más occidental (Figura 5.5c) (Linnemann et al., 2007; Arenas et al., 2007; Martínez Catalán et al., 2007; Nance et al., 2010; Murphy et al., 2010a, b; Keppie et al., 2010a).

La última etapa de deformación en el Paleozoico tardío, está directamente relacionada al desplazamiento transcurrente dextral descrito en el límite de terrenos Mixteca y Oaxaqueño. Corresponde a la etapa final del ensamble de Pangea, una vez que ha cambiado al régimen de convergencia oblicua del Océano paleo-Pacífico (Figuras 5.4e y 5.5b) (Elías-Herrera y Ortega-Gutiérrez, 2002; Keppie et al., 2004; Keppie et al., 2008a).

Es posible inferir un gradiente decreciente de la cizalla dextral desde el este del Complejo Acatlán, el cual tiene su expresión en: i) la intrusión dinámica del Granito Cozahuico en la Falla de Caltepec (Elías Herrera y Ortega-Gutiérrez 2002); ii) la imbricación y enorme elongación NE-SW de piezas eminentemente pérmicas, como la Formación Tecomate y el Granito Totoltepec (Malone et al., 2004; Morales Gámez et al., 2009); y iii) el estilo del plegamiento sub-vertical, sinforme y kilométrico en el Grupo Patlanoaya y porción oeste en Olinalá e Ixcamilpa (Ramírez-Espinoza, 2001; Ramos Arias et al., 2008). En el área de Ixcamilpa, una vez que el frente del canal de extrusión posicionó las rocas de alta presión por encima de la Unidad Zumpango, fueron plegándose en conjunto en una estructura sinforme (Figura 5.3), que a su vez fue truncada configurando un *klippe*. Este hecho explica la aparente división cartográfica entre el cinturón del oeste de Ixcamilpa-Olinalá y el cinturón intermedio de Piaxtla-Mimilulco (Ramos Arias et al., 2011).

La configuración actual y distribución de unidades metamórficas en Ixcamilpa está afectada por fallas frágiles cenozoicas orientadas NE-SW que tienen un movimiento lateral-dextral. Muy posiblemente aprovechan los contrastes litológicos producidos por las

primeras fábricas de imbricación carbonífera y truncan el plegamiento sinforme kilométrico. Es evidente que existe un movimiento transtensional, con arreglo de falla escalonado y antitético orientado NE-SW (ver roseta de fallamiento frágil, Figura 3.2), a su vez que existe otro sistema E-W frágil que evidencia una extensión N-S.

Conclusiones

- Los protolitos graníticos y de rocas máficas en Ixcamilpa se originaron en el Ordovícico; corresponden geocronológica, geoquímica y litológicamente a las rocas graníticas y meta-basitas distribuidas en el cinturón intermedio de Piaxtla-Mimilulco, por lo cual se infiere un mismo protolito para ambos cinturones.

- La distribución de poblaciones de zircones detríticos para rocas metasedimentarias en Ixcamilpa hace posible definir el límite superior del depósito en el Ordovícico; además de que las rocas detríticas tienen una afinidad amazónica y un aporte considerable de Oaxaquia. Por tanto, es posible posicionar el desarrollo del protolito del Ensamble Piaxtla en el borde noroeste de Gondwana.

- El protolito de las rocas de alta presión en Ixcamilpa, consiste en una secuencia clástica con zircones detríticos del Neoproterozoico-Ordovícico, que posiblemente se depositó en sincronía con un magmatismo bimodal, dentro de un escenario de rift-margen pasivo hacia el Cámbrico-Ordovícico medio.

- El arreglo estructural en Ixcamilpa consiste de seis piezas de grado medio-alto (bajo condiciones metamórficas de esquisto azul, eclogita-anfibolita y anfibolita), que fueron imbricadas dúctilmente durante las primeras dos etapas de deformación (F_1-F_2, $S_{1/2}$).

- La estructura en Ixcamilpa es considerada la raíz de una napa activa durante el Carbonífero (344-320 Ma) con cima hacia el NW, preservada como una estructura sinforme que ha sido truncada conformando un *klippe*, tiene correspondencia estructural y temporal con una zona de cizalla listrica en el este del cinturón Piaxtla-Mimilulco durante el Misisípico, lo cual define una geometría de una zona de extrusión con falla normal en la cima y falla inversa en la base.

- El análisis geotermobarométrico en rocas de alta presión de Ixcamilpa confrontado con otros análisis para rocas de alta presión dentro del Ensamble Piaxtla, describen pasos P-T-t que expresan la cercanía relativa de los niveles corticales desde los cuales las rocas fueron extruidas y son consistentes con una potencial celda de flujo durante tiempos del Devónico-Carbonífero posicionada entre los ~45 y 20 km.

- El frente del canal de extrusión posicionó las rocas de alta presión por encima de la Unidad Zumpango, subsecuentemente se generó el plegamiento abierto subvertical y kilométrico F_3, en régimen dúctil frágil, conformando una estructura sinforme.

- El área de Ixcamilpa está afectada por fallas frágiles cenozoicas orientadas NE-SW que tienen un movimiento lateral-dextral y truncan el plegamiento sinforme kilométrico, configurando la disposición actual del cinturón Ixcamilpa-Olinalá y el Complejo Acatlán en general.

Bibliografía

Agard P., Yamato P., Jolivet L. and Burov E., 2009, Exhumation of oceanic Blueschist and eclogites in subduction zones: Timing and mechanisms. Earth- Science Reviews, Vol. 92, 53-79.

Arenas, R., Martínez Catalán, JR., Sánchez Martínez, S., Díaz Garcia, F., Abati, J., Fernández-Suárez, J., Andonaegui, P., Gómez-Barreiro, J., 2007. Paleozoic ophiolites in the Variscan suture of Galicia (northwest Spain): distribution, characteristics, and meaning. In: Hatcher Jr., R.D., Carlson, M.P., McBride, J.H., Martínez Catalán, J.R. (Eds.), 4-D Framework of Continental Crust: Geological Society of America Memoir Vol. 200, p. 425–444. doi:10.1130/2007.1200(22).

Banno, S., Sakai, C., and Higashino, T., 1986, Pressure-temperature trajectory of the Sanbagawa metamorphism deduced from garnet zoning: Lithos, Vol. 19, p. 51-63.

Barley, J. 2006. Polyphase deformation in San Miguel Las Minas, Northern Acatlán Complex, Southern México: Tesis de Maestría, Faculty of the Arts and Sciences of Ohio University.

Baxter, E.F., DePaolo, D.J., and Renne, P.R., 2002, Spatially Correlated Anomalous 40Ar/39Ar "Age" Variations About a Lithologic Contact near Simplon Pass, Switzerland: A Mechanistic Explanation for Excess Ar. Geochimica et Cosmochimica Acta, Vol. 66, p. 1067-1083.

Beaumont, C., Jamieson, R. A., Nguyen, M.H. and Medvedev, S., 2004, Crustal channel flows: 1. Numerical models with applications to the tectonics of the Himalayan-Tibetan orogen. Journal of Geophysical Research. Vol. 109, B06406, doi:10.1029/2003JB002809.

Blenkinsop, T., 2000, Deformation Microstructures and mechanisms in mineral and rocks. Klewer Academic Publishers, 150 p.

Blundy, J. D., and Holland, T. J. B., 1990, Calcic amphibole equilibria and a new amphibole-plagioclase geothermometer: Contributions to Mineralogy and Petrology, Vol. 104, p. 208-24.

Boundy, T.M., Hall, C.M., Li, Essene, E.J., and Halliday, A.N., 1997, Fine-scale isotopic heterogeneities and fluids in the deep crust: a $^{40}Ar/^{39}Ar$ laser ablation and TEM study of muscovites from a granulite-eclogite transition zone: Earth and Planetary Science Letters, Vol. 148, p. 223-242.

Brown, E.H., 1977, The crossite content of Ca-amphibole as a guide to pressure of metamorphism: Journal of Petrology, v. 18, p. 53–72.

Burov, E. B., Jolivet, L.,Le Pouthiet, L., Poliakov, A., 2001, A thermomechanical model of exhumation of Hp and UHP metamorphic rocks in alpine mountain belts. Tectonophysics, Vol. 342, 113-136.

Campa, M.F., and Coney P. J., 1983, Tectono-stratigraphic terranes and mineral distributions in México. Canadian Journal of Earth Science, Vol. 20, p. 1040-1051.

Castro, A., Gerya, T.V., 2007. Magmatic implications of mantle wedge plumes: experimental study. Lithos 79, 229–250.

Cathelineau, M., 1988, Cation site occupancy in chlorites and illites as a function of temperature: Clay Minerals, Vol. 23, p. 471–485, doi:10.1180/claymin.

Cerca, M., Ferrari, L., López-Martínez, M., Martiny, B., and Iriondo, A., 2006, Late Cretaceous shortening and early Tertiary shearing in the central Sierra Madre del Sur, southern Mexico: Insights into the evolution of the Caribbean–North American plate interaction: Tectonics, Vol. 26, TC3007, doi: 10.1029/2006TC001981.

Chemenda, A., Yang, R., Hsieh, C.-H., Groholsky, A., 1997. Evolutionary model for the Taiwan collision based on physical modelling. Tectonophysics, Vol. 274, 253–274.

Clark, A.H., Archibald, D.A., Lee, A.W., Farrar, E., and Hodgson, C.J., 1998, Laser Probe $^{40}Ar/^{39}Ar$ ages of early- and late-stage alteration assemblages, Rosario porphyry copper-molybdenum deposit, Collahuasi District, I Region, Chile: Economic Geology, Vol. 93, p. 326–337.

Cocks, L.R.M., Torsvik, T.H., 2002. Earth geography from 500 to 400 million years ago: a faunal and paleomagnetic review. Journal of the Geological Society of London, Vol. 159, p. 531–544.

Currie, C.A., Beaumont, C., Huismans, R.S., 2007. The fate of subducted sediments: a case for backarc intrusion and underplating. Geology, Vol. 35, No.12, p. 1111–1114.

Davis, G.H., and Reynolds, S.J., 2000, Structural geology of rocks and regions, 2nd edition, John Wiley and Sons, New York, USA., 800 p.

De Cserna, Z., Ortega-Gutiérrez F., and Palacios-Nieto M., 1980, Reconocimiento geológico de la parte central de la cuenca del alto Río Balsas, estados de Guerrero y Puebla, *in* Sociedad Geológica Mexicana, Libro Guía de la excursión geológica a la parte central de la cuenca del alto Rio Balsas, paper presented at V Convención Geológica Nacional, Soc. Geol. Mex., México, D. F. Boletín Instituto de Geología, Vol. 62, p. 1-76.

De la Cruz-Vargas, J.C. 2004, Geoquímica de esquistos azules y eclogitoides del Complejo Acatlán: Evidencia de una zona de subducción del Paleozoico en el Sur de México: Tesis de Maestría, Universidad de Sonora, Hermosillo, Sonora, México.

Dostal, J., Dupuy, C., and Caby, R. 1994. Geochemistry of the Neoproterozoic Tilemsi belt of Iforas (Mali, Sahara): a crustal section of an oceanic island arc. Precambrian Research, Vol. 65, p. 55-69.

Elías-Herrera Elías-Herrera, M., Ortega-Gutiérrez, F., Macias-Romo, C., Reyes-Salas, M., Sánchez-Zavala, J.L., Aparicio-Aparicio, D. 2006. Blueschist in the Acatlán Complex, southern México: new insights and tectonothermal implications. Geos, Vol. 26, No.1, p. 190.

Elías-Herrera, M., Ortega-Gutiérrez, F., Sánchez Zavala, J.L., Iriondo, A., and Ortega-Rivera, A., 2007, Conflicting stratigraphic and geochronological data from the Acatlán Complex: "Ordovician" granite intrude metamorphic and sedimentary rocks of Devonian-Permian age: Eos Transactions AGU, Vol. 88. No. 23, Joint Assembly Suppl., Abstract, T41A-12.

Elías-Herrera, M., y Ortega-Gutiérrez, F. 2002. Caltepec fault zone: an Early Permian dextral transpressional boundary between the Proterozoic Oaxacan and Paleozoic Acatlán Complexes, southern Mexico, and regional implications. Tectonics, Vol. 21, No. 3, doi:10.1029/2000TC001278.

Ernst, W. G., Tsujimori, T., Zhang, R. Y., and Liou, J. G., 2008. Permo-Triassic orogeny and metallogenesis along the East Asian margin: subduction-zone metamorphism, crustal accretion, and exhumation: in Spencer, J. E., and Titley, S. R. (Eds.), Ore, p. 151-180.

Ernst, W.G. 1975. Systematic of large-scale tectonics and age progressions in Alpine and circum-Pacific blueschist belts. Tectonophysics, Vol. 26, p. 229-246.

Ernst, W.G. and Liou, J.G., 2008, High- and ultrahigh-pressure metamorphism: Past results and future prospects: American Mineralogist, Vol. 93, p. 1771-1786.

Ernst, W.G., 1988. Tectonic histories of subduction zones inferred from retrograde blueschist P–T paths. Geology, Vol. 16, p. 1081–1084.

Ernst, W.G., Maruyama, S., and Wallis, S., 1997, Buoyancy-driven, rapid exhumation of ultrahigh-pressure metamorphosed continental crust: Proceedings of the National Academy of Science, Vol. 94, p. 9532-9537.

Farfán-Panamá, J.L., 1998, Caracterización petrotectónica de los granitoides del Complejo Acatlán en las regiones de Tehuitzingo, Puebla y Olinalá, Guerrero. Tesis de Licenciatura, Escuela Regional de Ciencias de la Tierra, Universidad Autónoma de Guerrero.

Fortey, R.A., Cocks, L.R.M., 2003. Palaeontological evidence bearing on global Ordovician–Silurian continental reconstructions. Earth Science Reviews, Vol. 61, p. 245–307.

Galáz G., Keppie, J.D., Solari L. 2009. Complejo Acatlán en el area de Tehuitzingo, estado de Puebla, sur de México: Evidencias de su evolución tectónica. Reunión Anual 2009. Libro de resúmenes, Unión Geofísica Mexicana, Vol. 29, No. 1, p. 48.

García-Díaz, J.L., 2004, Etude Geologique de la Sierra Madre del Sur aux environts de Chilcpancingo et D'Olinalá, Gro. Une contribution a la connaissance de lévolution géodynamique de la mafrgen pacifique du Mexique depuis le Jurassique: Tesis de Doctorado, Ecole Doctorale de L´Universite de Savoie, France.

Gehrels, G., Valencia, V., Pullen, A. 2006. Detrital zircon geochronology by laser ablation multicollector ICPMS at the Arizona LaserChron Center, *in* Olszewski , T., ed., Geochronology: Emerging opportunities. Paleontology Society Papers, Vol. 12, p. 67–76.

Gerya, T., Stockhert, B., Perchuck, A., 2002. Exhumation of high-pressure metamorphic rocks in a subduction channel: a numerical simulation. Tectonics, Vol. 21, No.6, p. 227–236.

Geyra and Stöckhert, 2006. Two-dimensional numerical modeling of tectonic and metamorphic histories at active continental margins Int J Earth Sci (Geol Rundsch) (2006), Vol. 95, p. 250–274.

Gillis, R.J., Gehrels, G.E., Ruiz, J., Flores de Dios González, L.A. 2005. Detrital zircon provenance of Cambrian–Ordovician and Carboniferous strata of the Oaxaca terrane, southern Mexico. Sedimentary Geology, Vol. 182, p. 87–100.

Godin L., Grujic D., Law R.D. and Searle M.P. (2006) Channel Flow, Ductile extrusion and exhumation in Continental Collision Zones. Geological Society London, Special Publications, Vol. 268, p. 1-23.

Govindaraju, K. 1994. 1994 compilation of working values and sample description for 383 geostandards. Geostandards Newsletter, Vol. 18, p. 1-158.

Graham, C.M., and Powell, R., 1984, A garnet-hornblende geothermometer: Calibration, testing, and application to the Pelona Schist, Southern California: Journal of Metamorphic Geology, Vol. 2, p. 13–21, doi: 10.1111/ j.1525-1314.1984.tb00282.x.

Grodzicki, K.R., Nance, R.D., Keppie, J.D., Dostal, J., y Murphy, J.B., 2008. Structural, geochemical and geochronological analysis of metasedimentary and metavolcanic rocks of the Coatlaco area, Acatlán Complex, southern Mexico. In: Pereira, M.F., Bozkurt, E., Quesada, C., Strachan, R. (Eds.), In The Foundations and Birth of the Rheic Ocean: Avalonian–Cadomian Orogenic Processes and Early Palaeozoic Rifting at the North-Gondwana Margin. Tectonophysics.

Grujic, D., Casey, M., Davidson, C., Hollister, L. S., Kündig, R., Pavlis, T. & Schmid, S. 1996. Ductile extrusion of the Higher Himalayan Crystalline in Bhutan: evidence from quartz microfabrics. Tectonophysics, Vol. 260, p. 21–43.

Grujic, D., Hollister, L. & Parrish, R. 2002. Himalayan metamorphic sequence as an orogenic channel: insight from Bhutan. Earth and Planetary Science Letters, Vol. 198, p. 177–191.

Hames, W.H., and Bowring, S.A., 1994, An empirical evolution of the argon diffusion geometry in muscovite: Earth and Planetary Science Letters, Vol. 124, p. 161-167.

Harrison, T. M., Grove, M., Lovera, O. M., Catlos, E. J. y D'Andrea, J. 1999. The origin of Himalayan anatexis and inverted metamorphism: Models and constraints. Journal of Asian Earth Sciences, Vol. 17, p. 755–772.

Harrison, T.M., 1981, Diffusion of ^{40}Ar in hornblende: Contributions to Mineralogy and Petrology, Vol. 78, p. 324-331.

Hermanns, R.L. 1994. Der paläozoiche Acatlán-Komplex bei Olinala, Mexiko: Metamorphose-facies, geochemie von metabasalten und deformationgeschichte. Tesis de Licenciatura. Universität Tübingen, Germany.

Hinojosa-Prieto, H., Nance, R.D., Keppie, J.D., Dostal, J., Ortega-Rivera, A., and Lee, J.K.W., in review, Ordovician and Late Paleozoic–Early Mesozoic tectonothermal history of the La Noria area, northern Acatlán Complex, southern Mexico: record of convergence in the Rheic and paleo-Pacific Oceans, in The Foundations and Birth of the Rheic Ocean: Avalonian– Cadomian orogenic processes and Early Palaeozoic rifting at the north- Gondwana margin, M. F. Pereira, E. Bozkurt, C. Quesada & R. Strachan (eds), Tectonophysics

Holland, T., and Blundy, J., 1994, Non-ideal interactions in calcic amphiboles and their bearing on amphibole-plagioclase thermometry: Contributions to Mineralogy and Petrology, Vol. 116, p. 433-47.

Houseman G. A. and England P.C. (1986), Finite strain calculations of continental deformation. I. Method and general results for convergent zones, J. Geophys. Res., Vol. 91, p. 3651-3663.

Hudleston, P., 1999, Strain compatibility and shear zones: is there a problem?: Journal of Structural Geology, Vol. 21, p. 923-932.

Hynes A. (2002) Encouranging the extrusion of deep-crustal rocks in collisional zones. Mineralogical Magazine, February Vol. 66, No.1, p. 5-24.

Jamieson, R. A., Beaumont, C., Hamilton, J. y Fullsack, P., 1996. Tectonic assembly of inverted metamorphic sequences. Geology, Vol. 24, p. 839–854.

Jamieson, R. A., Beaumont, C., Medvedev, S. y Nguyen, M. H., 2004. Crustal channel flows: 2. Numerical models with implications for metamorphism in the Himalayan-Tibetan Orogen. Journal of Geophysical Research, Vol. 109. DOI: 10.1029/2003JB002811.

Jeffries, T., Fernández-Suárez, J., Corfu, F., Gutiérrez Alonso, G. 2003. Advances in U-Pb geochronology using a frequency quintupled Nd:YAG based laser ablation system (lambda = 213 nm) and quadrupole based ICP-MS. Journal of Analytical Atomic Spectrometry, Vol. 18, p. 847–855, doi: 10.1039/b300929g.

Jessup, M. J., Law, R. D., Searle, M. P. y Hubbard, M. S. 2006. Structural evolution and vorticity of flow during extrusion and exhumation of the Greater Himalayan Slab, Mount Everest massif, Tibet/Nepal: implications for orogen-scale flow partitioning. In: LAW, R. D., SEARLE, M. P. & GODIN, L. (eds) Channel Flow, Ductile Extrusion and Exhumation in Continental Collision Zones. Geological Society, London, Special Publications, Vol. 268, p. 379–414.

Keppie J. D., Nance R.D., Lee J.K.W., Dostal J., y Ortega-Rivera A., 2011, en prensa. Constraints on the subduction erosion/extrusion cycle in the Paleozoic Acatlán Complex of southern Mexico: geochemistry and geochronology of the type Piaxtla Suite. Kranidiotis, P., and MacLean, W. H., 1987, Systematics of chlorite alteration at the Phelps Dodge massive sulfide deposit, Matagami, Quebec: Economic Geology, Vol. 82, p. 1898–1911.

Keppie J.D. y Ortega-Gutierrez F. 2009. 1.3-0.9 Ga Oaxaquia (Mexico): remnant of an arc/backarc on the northern margin of Amazonia. Journal of South American Earth Sciences, Vol. 29, p. 21-27. doi:10.1016/j.jsames.2009.07.001.

Keppie J.D., 2004, Terranes of México revisited: a 1.3 billion year odyssey. International Geology Review. Vol. 46, p. 765-794.

Keppie, D.F., Currie, C.A., and Warren, C., 2009, Subduction erosion modes: comparing finite element numerical models with the geological record: Earth and Planetary Science Letters, Vol. 287, p. 241–254.

Keppie, J.D., 2004, Terranes of Mexico revisited: a 1.3 billion year odyssey. International Geology Review, Vol. 46, p. 83–100.

Keppie, J.D., Dostal, J., Cameron, K.L., Solari, L.A., Ortega- Gutiérrez, F., and Lopez, R., 2003, Geochronology and geochemistry of Grenvillian igneous suites in the northern Oaxacan Complex, southern México: Tectonic implications: Precambrian Research, Vol. 120, p. 365–389.

Keppie, J.D., Dostal, J., Miller, B.V., Ramos-Arias, M.A., Morales-Gamez, M., Nance, R.D., Murphy, J.B., Ortega-Rivera, A., Lee, J.W.K., Housh, T., Cooper, P. 2008b. Ordovician-earliest Silurian rift tholeiites in the Acatlán Complex, southern Mexico: Evidence of rifting on the southern margin of the Rheic Ocean. Tectonophysics, Vol. 461, p. 130–156, doi: 10.1016/ j.tecto.2008.01.010.

Keppie, J.D., Dostal, J., Murphy, J. B., Nance, R. D. 2008a. Synthesis and tectonic interpretation of the westernmost Paleozoic Variscan orogen in southern Mexico: From rifted Rheic margin to active Pacific margin. Tectonophysics, Vol. 461, p. 277–290.

Keppie, J.D., Nance R.D., Ramos-Arias M.A., Lee J.K.W., Dostal J., Ortega-Rivera A., and Murphy J.B., 2010b. Late Paleozoic subduction and exhumation of Cambro-Ordovician passive margin and arc rocks in the northern Acatlán Complex, southern Mexico: Geochronological constraints. Tectonophysics, Vol. 495, p. 213-229, doi:10.1016/j.tecto.2010.09.019.

Keppie, J.D., Nance, R.D., Murphy, J.B., and Dostal, J. in press. Comment on “Structural and tectonic evolution of the Acatlán Complex, southern Mexico: Its role in the collisional history of Laurentia and Gondwana”by R.Vega-Granillo et al. Tectonics, Vol. 28, TC4008, doi:10.1029/2007TC002159.

Keppie, J.D., Nance, R.D., Murphy, J.B., and Dostal, J., 2010a. The high-pressure Iberian-Czech belt in the Variscan orogen: extrusion into the upper (Gondwanan) plate? Gondwana Research, Vol.17, p. 306-316, doi:10.1016/j.gr.2009.08.007.

Keppie, J.D., Nance, R.D., Murphy, J.B., Miller, B.V., Dostal, J., Ortega-Rivera, A. 2009. Pressure-temperature-time evolution of high pressure rocks of the Acatlán Complex (southern Mexico): Implications for the evolution of the Iapetus and Rheic oceans: Discussion. Geological Society of America Bulletin. Vol. 121: 1456-1459, doi:10.1130/B26356.1.

Landing, E., Keppie, J.D., and Westrop, 2007, Terminal Cambrian and lowest Ordovician of Mexican West Gondwana—biotas and sequence stratigraphy of the Tiñu Formation: Geological Magazine.

Laux J. H., Pimentel M.M., Dantas E.L., Armstrong R., Armele A. A. A.Nilson. 2004. Mafic magmatism associated with the Goiás magmatic arc in the Anicuns region, Goiás, central Brazil: Sm–Nd isotopes and new ID-TIMS and SHIMP U–Pb data. Journal of South American Earth Sciences, Vol. 16, p. 599–614.

Leake, B.E., Woolley, A.R., Birch, W.D., Burke, E.A.J., Ferraris, G., Girce, J.D., Hawthorne, F.C., Kisch, H.J., Krivovichiev, V. G., Schumacher, J.C., Stepehenson, N.C.N., and Whittaker, E.J.W., 2003, Nomenclature of amphiboles: additions and revisions to the International Mineralogical Association’s 1997 recommendations: The Canadian Mineralogist, Vol. 41, p. 1355-1362.

Linnemann, U., Gerdes, A., Drost, K., Buschmann, B., 2007. The continuum between Cadomian orogenesis and opening of the Rheic Ocean: constraints from LA-ICP-MS U–Pb zircon dating and analysis of plate-tectonic setting (Saxo-Thuringian zone, northeastern Bohemian Massif, Germany). In: Linnemann, U., Nance, R.D., Kraft, P., Zulauf, G. (Eds.), The Evolution of the Rheic Ocean: From Avalonian–Cadomian Active Margin to Alleghenian–Variscan Collision, Vol. 423. Geological Society of America Special Paper, p. 61–96. doi:10.1130/2007.2423(03).

Linnemann, U., McNaughton, N.J., Romer, R.L., Gehmlich, M., Drost, K., Tonk, C., 2004. West African provenance for Saxo-Thuringia (Bohemian Massif): did Armorica ever leave pre-Pangean Gondwana?—U/Pb-SHRIMP zircon evidence and the Ndisotopic record. Int. J. Earth Sci., Vol. 93, p. 683–705.

Liou, J.G., Tsujimori T., Zhang R.Y., Katayama I. and Murayama S. 2004. Global UHP Metamorphism and Continental Subduction/Collision: The Himalayan Model. International Geology Review, Vol. 46, p. 1-27.

Longerich, H. P., Jenner, G. A., Fryer, B. J., and Jackson, S. E. 1990. Inductively coupled plasma-mass spectrometric analysis of geological samples: A critical evaluation based on case studies. Chemical Geology, Vol. 83, p. 105-118.

Ludwig, K.R. 1991. ISOPLOT: A plotting and regression program for radiogenic-isotope data; version 2.53: U.S. Geological Survey Open-File Microsoft excel, Berkeley Geochronology Center Report, Special Publication No. 4a.

Malone, J.W., Nance, R.D., Keppie, J.D., Dostal, J., 2002. Deformational history of part of the Acatlán Complex: Late Ordovician–Early Silurian and Early Permian orogenesis in southern Mexico. Journal of South American Earth Sciences, Vol. 15, p. 511–524.

Mancktelow, N. S. 1995. Nonlithostatic pressure during sediment subduction and the development and exhumation of high pressure metamorphic rocks. Journal of Geophysical Research – Solid Earth, Vol. 100, p. 571–583.

Marshak, S. and Mitra, G., 1988, Basic Methods of Structural Geology, Prentice Hall, USA, 446 p.

Martens U., Weber B., Valencia V. A. 2010. U/Pb geochronology of Devonian and older Paleozoic beds in the southeastern Maya block, Central America: Its affinity with peri-Gondwanan terranes.GSA Bulletin, Vol. 122, No. 5/6, p. 815–829.

Martínez Catalán, J.R., Arenas, R., Díaz García, F., Gómez-Barreiro, J., González Cuadra, P., Abati, J., Castiñeiras, P., Fernández-Suárez, J., Sánchez Martínez, S., Andonaegui, P., González Clavijo, E., Díez Montes, A., Rubio Pascual, F.J., Valle Aguado, B., 2007. Space and time in the tectonic evolution of the northwestern IberianMassif: implications for the comprehension of the Variscan belt. In: Hatcher Jr., R.D., Carlson,M.P.,McBride, J.H., Martínez Catalán, J.R. (Eds.), 4-D Framework of Continental Crust: Geological Society of America Memoir, Vol. 200. doi:10.1130/2007.1200(21).

Massone, H.J., and Schreyer, W., 1987, Phengite geobarometry based on the limiting assemblage with K-feldspar, phlogopite, and quartz: Contributions to Mineralogy and Petrology, Vol. 96, p. 212–224.

Meza-Figueroa, D. M. 1998. Geochemistry and characterization of intermediate temperature eclogites from the Acatlán Complex, southern Mexico. Tesis de Doctorado, University of Arizona, USA.

Meza-Figueroa, D., Ruiz, J., Talavera-Mendoza, O., and Ortega-Gutiérrez, F., 2003, Tectonometamorphic evolution of the Acatlán Complex eclogites (southern México): Canadian Journal of Earth Sciences, Vol. 40, p. 27–44.

Middleton, M., J.D., Murphy, J.B., Miller, B.V., Nance, R.D., Ortega-Rivera, A., Lee, J.K.W. 2007. P-T-t constraints on exhumation following subduction in the Rheic Ocean from eclogitic rocks in the Acatlán Complex of southern México. *In* The evolution of the Rheic Ocean: from Avalonian-Cadomian active margin to Alleghenian-Variscan collision. *Edited by* U. Linnemann, R.D. Nance, G. Zulaf, and P. Kraft. Geological Society of America Special Paper Vol. 423, p. 437–452, doi: 10.1130/2007.2423(24).

Miller, B.V., Dostal, J., Keppie, J.D., Nance, R.D., Ortega-Rivera, A., Lee, J.K.W. 2007. Ordovician calc-alkaline granitoids in the Acatlán Complex, southern Mexico: geochemical and geochronological evidence for either rifting or subduction along the Gondwanan margin of the Rheic Ocean. *In* The evolution of the Rheic Ocean: from Avalonian-Cadomian active margin to Alleghenian-Variscan collision. *Edited by* U. Linnemann, R.D. Nance, G. Zulaf, and P. Kraft. Geological Society of America, Special Paper, Vol. 423, p. 465–475.

Miyashiro, A., 1961. Evolution of metamorphic belts. Journal of Petrology, Vol. 2, 277–311.

Miyashiro, A., 1967. Orogeny, regional metamorphism, and magmatism in the Japanese islands. Medd. fra Dansk Geol. Forening, Vol. 17, p. 390–446.

Morales-Gamez, M, Keppie J.D., Dostal J. 2009a. Carboniferous tholeiitic dikes in the Salada unit, Acatlán Complex, southern Mexico: a record of extension on western margin of Pangea. Revista Mexicana de Ciencias Geológicas, Vol. 26, No. 1, p. 133-142.

Morales-Gámez, M., Keppie, J. D., Lee, J. K., and Ortega-Rivera, A., 2009b, Palaeozoic structures in the Xayacatlán area, Acatlán Complex, southern México: transtensional rift- and subduction-related deformation along the margin of Oaxaquia. International Geology Review, Vol. 51, No. 4, p.279–303.

Morales-Gámez, M., Keppie, J.D., Norman, M. 2008. Ordovician–Silurian rift passive margin on the Mexican margin of the Rheic Ocean overlain by Permian periarc rocks: evidence from the Acatlán Complex, southern Mexico. Tectonophysics, Vol. 461, p. 291–310, doi: 10.1016/j.tecto.2008.01.014

Murphy J. B., Keppie J. D., Nance R. D., y Dostal J., 2010b, Comparative evolution of the Iapetus and Rheic Oceans: A North America perspective Gondwana Research, Vol. 17, p. 482–499.

Murphy J. B.. Cousens B. L, Braid J. A, Strachan R. A., Dostal J., Keppie J. D., y Nance R. D., 2010a, Highly depleted oceanic lithosphere in the Rheic Ocean: Implications for Paleozoic plate reconstructions Lithos.

Murphy, J.B., Gutierrez-Alonso, G., Nance, R.D., Fernandez-Suarez, J., Keppie, J.D., Quesada, C., Strachan, R.A., Dostal, J., 2006a. Origin of the Rheic Ocean: rifting along a Neoproterozoic suture?, Geology, Vol. 34, p. 325–328.

Murphy, J.B., Keppie, J.D., Nance, R.D., Miller, B.V.,,Dostal, J., Middleton, M., Fernandez-Suarez, J., Jeffries , T.E., Storey, C.D. 2006b. Geochemistry and U-Pb protolith ages of eclogitic rocks of the Asis Lithodeme, Piaxtla Suite, Acatlán Complex, southern Mexico: Tectonothermal activity along the southern margin of the Rheic Ocean. Geological Society of London, Vol. 163, No. 4, p. 683–695, doi: 10.1144/0016-764905-108.

Nance, R.D., Fernández-Suárez, J., Keppie, J.D., Storey, C., and Jeffries, T.E., 2007a, Provenance of the Granjeno Schist, Ciudad Victoria, Mexico: Detrital zircon U-Pb age constraints and implications for Paleozoic paleogeography, *in* U. Linnemann, R.D. Nance, G. Zulaf and P. Kraft (eds.), The Geology of Peri-Gondwana: The Avalonian-Cadomian Belt, Adjoining Cratona and the Rheic Ocean: Geological Society of America, Special Paper, Vol. 423, p. 437-452.

Nance, R.D., Gutiérrez-Alonso, G., Keppie, J.D., Linnemann, U., Murphy, J.B., Quesada, C., Strachan, R.A., Woodcock, N., 2010. Evolution of the Rheic Ocean. Gondwana Res., Vol. 17, p. 194–222.

Nance, R.D., Linnemann, U., 2008. The Rheic Ocean: origin, evolution and significance. GSA Today 18 (12), 4–12. Nance, R.D., Keppie, J.D., Miller, B.V., Murphy, J.B. and Dostal, J., 2009. Palaeozoic palaeogeography of Mexico: Constraints from detrital zircon age data. Geological Society of London Special Publication, Vol. 327, p. 239–269.

Nance, R.D., Miller, B.V., Keppie, J.D., Murphy, J.B., Dostal, J. 2006a. Acatlán Complex, southern Mexico: Record spanning the assembly and breakup of Pangea. Geology, Vol. 34, p. 857–860, doi: 10.1130/G22642.1.

Nance, R.D., Miller, B.V., Keppie, J.D., Murphy, J.B., Dostal, J., 2006b. The Acatlán Complex, southern Mexico: record of Pangea assembly to breakup. Geology, Vol. 34, p. 857–860.

Nance, R.D., Miller, B.V., Keppie, J.D., Murphy, J.B., Dostal, J. 2007b. Vestige of the Rheic Ocean in North America: the Acatlán Complex of southern Mexico. *In* The evolution of the Rheic Ocean: from Avalonian-Cadomian active margin to Alleghenian-Variscan collision. *Edited by* U. Linnemann, R.D. Nance, G. Zulaf, and P. Kraft. Geological Society of America Special Paper, Vol. 423, p. 4437–4452.

Navarro-Santillán, D., Sour-Tovar, F., and Centeno-García, E., 2002, Lower Mississippian (Osagean) barchiopods from the Santiago Formation, Oaxaca, México: stratigraphic and tectonic implications: J. South Amer. Earth Sci., Vol. 15, p. 327-336.

Ortega Gutiérrez, F., 1974, Nota prelimitar sobre las eclogitas de Acatlán, Puebla. Boletín de la Sociedad Geológica Mexicana. Vol. 25, p. 1-6.

Ortega-Gutierrez, F. 1978. Estratigrafía del Complejo Acatlán en la Región de la Mixteca Baja, Estado de Puebla, Universidad Nacional Autónoma de México, Instituto de Geología Revista, 2, 112-131.Ortega-Gutiérrez, F., 1981, Metamorphic belts of southern México and their tectonic significance: Geofísica Internacional, Vol. 20, No. 3, p. 177–202.

Ortega-Gutiérrez, F., Elías-Herrera, M., Reyes-Salas, M.,Macias-Romo, C., and López, R., 1999, Late Ordovician– Early Silurian continental collision orogeny in southern Mexico and its bearing on Gondwana-Laurentia connections: Geology, Vol. 27, p. 719–722.

Ortega-Obregón, C., Keppie, J.D., Murphy, J.B., Lee, J.K., and Ortega-Rivera, A., 2009, Geology and geochronology of Paleozoic rocks in western Acatlán Complex, southern Mexico: evidence for contiguity across an extruded high-pressure belt and constraints on Paleozoic reconstructions: Geological Society of America Bulletin, Vol. 121, p. 1678-1694, doi:10.1130/B26597.1.

Ortega-Obregon, C., Murphy J.B., and Keppie J.D., 2010, Geochemistry and Sm–Nd isotopic systematics of Ediacaran–Ordovician, sedimentary and bimodal igneous rocks in the western Acatlán Complex, southern Mexico: Evidence, Lithos, Vol. 114, No. 1-2, p. 155-167.

Ortega-Obregón, C., Solari, L.A., Keppie, J.D., Ortega- Gutiérrez, F., Solé, J., and Morán, S., 2008, Middle–Late Ordovician magmatism and Late Cretaceous collision in the southern Maya block, Rabinal-Salamá area, central Guatemala: Implications for North America–Caribbean plate tectonics: Geological Society of America Bulletin, Vol. 120, p. 556–570, doi: 10.1130/ B26238.1.

Passchier, C.W., and Trouw, R.A.J., 1996, Microtectonics. Springer, Germany. 289 p.

Pimentel, M.M., Fuck, R.A., Jost, H., Ferreira Fihlo, C.F., Araújo, S.M. 2000. The basement of the Brasilia fold belt and the Goiás magmatic arc. *In* Tectonic Evolution of South America. Edited by U.G. Cordani, E.J. Milani, A. Thomaz Fihlo, and D.A. Campos, D.A. 31st International Geological Congress, Rio de Janeiro, p. 195–230.

Platt J.P. (1993) Exhumation of high pressure rocks; a review of concepts and processes. Rerra Nova, Vol. 5, p.119-133.

Pollock, J.C., Hibbard, J.P., Sylvester, P.J., 2009. Early Ordovician rifting of Avalonia and birth of the Rheic Ocean: U–Pb detrital zircon constraints from Newfoundland. Journal of the Geological Society, London, Vol. 166, p. 501–515.

Proenza, J.A., Ortega-Gutiérrez, F., Camprubi, A., Trilla, J., Elías-Herrera, M., Reyes-Salas, M. 2004. Paleozoic serpentinite-enclosed chromitites from Tehuatzingo (Acatlán Complex, southern Mexico): a petrological and study. Journal of South American Earth Sciences, Vol. 16, p. 649–666

Quesada, C., 1990. Precambrian terranes in the Iberian Variscan foldbelt. In: Strachan, R.A., Taylor, G.K. (Eds.), Avalonian and Cadomian Geology of the North Atlantic. Glasgow, Blackie and Son, p. 109–133.

Ramírez-Espinoza, J., 2001, Tectono-magmatic evolution of the Paleozoic Acatlán Complex in southern Mexico and its correlation with the Appalachian system: Tesis de Doctorado, Arizona University, USA.

Ramos-Arias, M. A., 2007, Análisis Estructural en el área de San Miguel Las Minas-San salvador Patlanoaya, Puebla, dentro del Complejo Acatlán, Sur de México. Tesis de Maestría. UNAM, México.

Ramos-Arias, M.A., Keppie, J.D., Lee, J.K.W., Ortega-Rivera, A., 2011, en prensa. A Carboniferous high pressure/grade klippe in the western Acatlán Complex (southern Mexico): implications for tectonothermal development and Pangean paleogeography. International Geology Review.

Ramos-Arias, M.A., Keppie, J.D., Ortega-Rivera, A., and Lee, J.W.K., 2008, Extensional late Paleozoic deformation on the western margin of Pangea, Patlanoaya area, Acatlán Complex, southern México: Tectonophysics, Vol. 448, p. 60–76.

Ramos-Arias, M.A., y Keppie, J.D., 2011, U–Pb Neoproterozoic–Ordovician protolith age constraints for high- to medium-pressure rocks thrust over low-grade metamorphic rocks in the Ixcamilpa area, Acatlán Complex, southern Mexico: Canadian Journal of Earth Sciences, Vol. 48, p. 45-61.

Ramsay, J.G., 1967, Folding and Fracturing of Rocks. McGraw- Hill, New York, USA.

Reyes-Salas, A. M., 2003, Mineralogía y Petrología de los Granitoides Esperanza del Complejo Acatlán, Sur de México. Tesis de Doctorado, Universidad Autónoma del Estado de Morelos.

Ring U., Brandon, M.T., Willet, S.D. and Lister, G.S.,1999, Exhumation Processes, *in* Ring, U, Brandon, M. T., Lister, G.S and Willet, S.D., eds., Exhumation Processes: Normal Faulting, Ductile Flow and erosion: Geological Society London. Special Publications, Vol. 154, p. 1-27.

Ross, P.S. and Bedard, J.H. 2009. Magmatic affinity of modern and ancient subalkaline volcanic rocks determined from trace-element discrimination diagrams. Canadian Journal of Earth Sciences, Vol. 46, p. 823-839.

Sánchez-García, T., Bellido, F., Quesada, C., 2003. Geodynamic setting and geochemical signatures of Cambrian–Ordovician rift-related igneous rocks (Ossa-Morena Zone, SW Iberia). Tectonophysics, Vol. 365, p. 233–255.

Sánchez-Zavala, J.L., Ortega-Gutiérrez, F., Keppie, J.D., Jenner, G.A., Belousova, E., 2004. Ordovician and Mesoproterozoic zircon from the Tecomate Formation and Esperanza granitoid, Acatlán Complex, southern Mexico: local provenance in the Acatlán and Oaxacan complexes. International Geology Review, Vol. 46, p. 1005–1021.

Searle, M. P. & Rex, A. J. 1989. Thermal model for the Zanskar Himalaya. Journal of Metamorphic Geology, Vol. 7, p. 127–134.

Sedlock R.L., Ortega-Gutiérrez, F. and Speed, R.C., 1993, Tectonostratigraphic Terranes and Tectonic Evolution of México. Geol. Soc. Am. Special Paper, Vol. 278. pp. 153.

Solari L.A., Gómez-Tuena, A., Bernal, J. P., Pérez-Arvizu, O., Tanner, M. 2009. U-Pb Zircon Geochronology with an Integrated LA-ICP-MS Microanalytical Workstation: Achievements in Precision and Accuracy. Geostandards and Geoanalytical Research, Vol. 34, No. 1, p. 5-18.

Solari, L.A., Keppie, J.D., Ortega-Gutiérrez, F., Cameron, K.L., Lopez, R., Hames, W.E., 2003. 990 Ma and 1,100 Ma Grenvillian tectonothermal events in the northern Oaxacan Complex, southern Mexico: roots of an orogen. Tectonophysics, Vol. 365, p. 257–282.

Solari, L.A., Ortega-Gutiérrez, F., Elías-Herrera, M., Gómez-Tuena, A., Schaaf, P., 2010. Refining the age of magmatism in the Altos Cuchumatanes, western Guatemala, by LA-ICPMS, and tectonic implications. International Geology Review, Vol. 52, No. 9, p. 977-998.

Spear, F.S., 1980, NaSi-CaAl exchange equilibrium between plagioclase and amphibole: Contributions to Mineralogy and Petology, Vol. 72, p. 33–41.

Spear, F.S., 1995, Metamorphic phase equilibria and Pressure-Temperature-Time Paths: Mineralogical Society of América, Washington D.C., 799 p.

Stacey, J.S., and Kramers, J.D., 1975. Aproximation of terrestrial lead isotope evolution by a two-stage model. Earth and Planetary Science Letters, Vol. 26, p. 207-221.

Stöckhert, B., and Gerya, T.V., 2005, Pre-collisional high pressure metamorphism and nappe tectonics at active continental margins: a numerical simulation: Terra Nova, Vol. 17, p. 102–110.

Sun, S. S., and McDonough, W. F. 1989. Chemical and isotopic systematics of oceanic basalts: implications for mantle composition and processes. In Magmatism in the Ocean Basins. Edited by A. D. Saunders and M. J. Norry. Geological Society London, Special Publication, Vol. 42, p. 313-345.

Talavera-Mendoza, O., Ruiz, J., Gehrels, G.E., Meza-Figueroa, D.M., Vega- Granillo, R., and Campa-Uranga, M.F., 2005, U–Pb geochronology of the Acatlán Complex and implications for the Paleozoic paleogeography and tectonic evolution of southern Mexico: Earth and Planetary Science Letters, Vol. 235, p. 682–699.

Tolson, G. 2005, La Falla Chacalapa en el sur de Oaxaca: Boletin Sociedad Geolóica Mexicana, Vol. LVII, No. 1, p. 111 – 122.

Torres De León, R. 2001. Estructuras del Terreno Mixteca, en el área comprendida entre la cabalgadura de Papalutla y el sinclinorio Olinalá, Estado de Guerrero. Tesis Licenciatura, Escuela Regional de Ciencias de la Tierra, Universidad Autónoma de Guerrero.

Torres-de León, R., 2005, Análisis Estructural y Caracterización Petrográfica de Unidades Miloníticas en el Área de La Venta, Estado de Guerrero: Implicaciones Tectónicas: Tesis de Maestría, Universidad Nacional Autónoma de México, Posgrado en Ciencias de la Tierra.

Turcotte, D. L. y Schubert, G. 2002. Geodynamics. Cambridge University Press, Cambridge.

Vachard, D., Flores de Dios, A., Buitrón, B., 2004. Guadalupian and Lopingian (Middle and Late Permian) deposits from Mexico and Guatemala, a review with new data. Geobios, Vol. 37, p. 99–115.

van Staal, C.R., Dewey, J.F., Mac Niocaill, C., McKerrow, W.S., 1998. The Cambrian– Silurian tectonic evolution of the Northern Appalachians and British Caledonides: history of a complex, west and southwest Pacific-type segment of Iapetus. In: Blundell, D., Scott, A.C. (Eds.), Lyell: The Past is the Key to the Present. Geological Society of London Special Publication, Vol. 143, p. 199–242

Vega Granillo, R., Calmus T., Meza-Figueroa, D., Ruiz, J., Talavera-Mendoza, O. and López-Martínez, M., 2009, Structural and tectonic evolution of the Acatlán Complex, southern México: Its role in Collisional history of Laurentia and Gondwana. Tectonics, v. 28, TC4008, doi:10.1029/2007TC002159.

Vega-Granillo, R., Talavera-Mendoza, O., Meza-Figueroa, D., Ruiz, J., Gehrels, G.E., López-Martínez, M., and de La Cruz-Vargas, J.C. 2009a. Pressure-temperature-time evolution of Paleozoic high-pressure rocks of the Acatlán Complex (southern Mexico): implications for the evolution of the Iapetus and Rheic Oceans, Reply. Geological Society of America Bulletin, Vol. 121, p. 1460–1464; doi: 10.1130/B26514.1.

Vega-Granillo, R., Talavera-Mendoza, O., Meza-Figueroa,D., Ruiz, J., Gehrels, G.E., López-Martínez, M., and de La Cruz-Vargas, J.C., 2007, Pressure-temperature-time evolution of Paleozoic high-pressure rocks of the Acatlán Complex (southern Mexico): Implications for the evolution of the Iapetus and Rheic Oceans: Geological Society of America Bulletin, Vol. 119, p. 1249–1264.

Vernon, R.H., and Clarke, G.L., 2008, Principles of Metamorphic Petrology. Cambridge University Press, 446 p.

von Huene, R., y Scholl, D.W., 1991. Observations at convergent margins concerning sediment subduction, subduction erosion, and the growth of continental crust. Rev. Geophys. Vol. 29, No.3, p. 279–316.

von Raumer, J., Stampfli, G., Borel, G., Bussy, F., 2002. Organization of pre-Variscan basement areas at the north-Gondwanan margin. International Journal of Earth Sciences, Vol. 91, p. 32–52.

Warren, C., Beaumont, C., y Jamieson, R., 2008b. Modelling tectonic styles and ultra-high pressure (UHP) rock exhumation during the transition from oceanic subduction to continental collision. Earth Planet. Sci. Lett. No. 1–2, p. 129–145.

Will T., Okrusch, M., Schmaé, E., and Chen, D. G., 1998, Phase relations in the greenschist-blueschist-amphibolite-eclogite facies in the system Na_2O-CaO-FeO-MgO-Al_2O_3-SiO_2-H_2O (NCFMASH), with application to metamorphic rocks from Samos, Greece: Contributions to Mineralogy and Petrology, Vol. 132, p. 85-102.

Winchester, J. A. and Floyd, P. A. 1977. Geochemical discrimination of different magma series and their differentiation products using immobile elements. Chemical Geology, Vol. 20, p. 325-343.

Winchester, J.A., Pharaoh, T.C., Verniers, J., 2002. Palaeozoic amalgamation of Central Europe: an introduction and synthesis of new results from recent geological and geophysical investigations. In: Verniers, J. (Ed.), Palaeozoic amalgamation of Central Europe: Geological Society of London Special Publication, Vol. 201, p. 1–18.

Wood, D. A. 1980. The application of a Th–Hf–Ta diagram to problems of tectonomagmatic classification and to establishing the nature of crustal contamination of basaltic lavas of the British Tertiary volcanic province. Earth and Planetary Science Letters, Vol. 50, p. 11–30.

Table _1____. U-Pb geochronologic analyses. (UTM coordinates is on Nad 27 for México)

				Isotope ratios								Apparent ages (Ma)							
Analysis	U (ppm)	206Pb 204Pb	U/Th	206Pb* 207Pb*	± (%)	207Pb* 235U*	± (%)	206Pb* 238U	± (%)	error corr.	206Pb* 238U*	± (Ma)	207Pb* 235U	± (Ma)	206Pb* 207Pb*	± (Ma)	Best age (Ma)	± (Ma)	Conc (%)
Ix 45 UTM LAT0533648, LONG1994241																			
IX45-3	80	3350	27.0	18.2185	18.6	0.4078	18.6	0.0539	0.8	0.04	338.3	2.5	347.3	54.7	407.7	418.4	338.3	2.5	83.0
IX45-4	38	7986	1.3	17.8896	26.2	0.5181	26.4	0.0672	3.2	0.12	419.4	12.8	423.9	91.6	448.3	591.0	419.4	12.8	93.6
IX45-5	57	2646	0.8	14.5777	18.8	0.6446	19.2	0.0682	3.8	0.20	425.0	15.8	505.2	76.6	886.7	392.1	425.0	15.8	47.9
IX45-23	133	4078	1.3	17.5733	2.6	0.5502	3.9	0.0701	2.9	0.74	436.9	12.2	445.1	14.1	487.8	58.1	436.9	12.2	89.6
IX45-1	326	55554	22.8	17.8425	2.1	0.5533	3.1	0.0716	2.3	0.75	445.8	10.0	447.2	11.2	454.2	46.0	445.8	10.0	98.1
IX45-13	163	39822	7.4	15.8536	2.3	0.8172	2.6	0.0940	1.3	0.51	578.9	7.4	606.5	12.0	710.8	48.2	578.9	7.4	81.4
IX45-28	89	20298	3.4	13.8788	3.8	1.5537	3.9	0.1564	0.6	0.16	936.7	5.5	952.0	23.8	987.4	77.5	987.4	77.5	94.9
IX45-26	173	121236	7.9	13.7514	1.6	1.3674	2.1	0.1364	1.4	0.65	824.1	10.6	875.0	12.3	1006.1	32.1	1006.1	32.1	81.9
IX45-16	82	20650	3.7	13.4600	2.1	1.5949	2.7	0.1557	1.7	0.63	932.8	14.6	968.2	16.8	1049.5	42.3	1049.5	42.3	88.9
IX45-22	211	30700	7.3	13.1246	1.8	1.7154	4.9	0.1633	4.6	0.93	975.0	41.2	1014.3	31.5	1100.1	36.6	1100.1	36.6	88.6
IX45-20	408	125288	6.1	13.1219	1.9	1.8231	2.7	0.1735	2.0	0.71	1031.4	18.7	1053.8	18.0	1100.6	38.4	1100.6	38.4	93.7
IX45-17	74	40894	4.5	13.0825	3.1	1.9060	3.5	0.1809	1.5	0.43	1071.6	14.7	1083.2	23.2	1106.5	62.9	1106.5	62.9	96.8
IX45-14	92	106130	3.8	13.0111	2.9	1.9197	3.6	0.1812	2.0	0.56	1073.3	19.7	1088.0	23.7	1117.5	58.7	1117.5	58.7	96.0
IX45-30	124	36002	2.9	12.9503	2.4	2.0263	3.3	0.1903	2.2	0.69	1123.1	23.1	1124.4	22.2	1126.8	47.5	1126.8	47.5	99.7
IX45-18	126	23930	3.1	12.9040	0.9	1.8551	2.2	0.1736	2.1	0.92	1032.0	19.6	1065.2	14.8	1133.9	17.5	1133.9	17.5	91.0
IX45-38	91	56588	3.8	12.8215	2.3	2.0694	2.9	0.1924	1.8	0.61	1134.5	18.2	1138.7	19.8	1146.7	45.6	1146.7	45.6	98.9
IX45-34	549	85076	5.9	12.8136	0.8	2.0308	1.8	0.1887	1.6	0.89	1114.5	16.4	1125.9	12.2	1147.9	15.9	1147.9	15.9	97.1
IX45-19	92	41694	3.3	12.8004	2.2	2.1475	2.3	0.1994	0.6	0.26	1171.9	6.3	1164.2	16.0	1150.0	44.3	1150.0	44.3	101.9
IX45-36	954	28892	2.5	12.7633	2.1	1.7810	2.6	0.1649	1.5	0.56	983.8	13.2	1038.6	16.7	1155.7	42.1	1155.7	42.1	85.1
IX45-37	83	15406	4.4	12.7011	1.4	2.1474	1.5	0.1978	0.5	0.33	1163.6	5.3	1164.2	10.4	1165.4	28.1	1165.4	28.1	99.8
IX45-2	79	29802	3.0	12.6945	2.4	2.1814	2.8	0.2008	1.4	0.50	1179.8	15.1	1175.1	19.6	1166.4	48.4	1166.4	48.4	101.1
IX45-35	85	15370	2.9	12.6891	3.0	2.1396	3.4	0.1969	1.6	0.46	1158.7	16.5	1161.7	23.5	1167.3	59.9	1167.3	59.9	99.3
IX45-27	136	49272	2.5	12.6625	2.3	2.2577	3.8	0.2073	3.0	0.80	1214.7	33.5	1199.2	26.7	1171.5	45.0	1171.5	45.0	103.7
IX45-33	69	28450	6.0	12.6564	2.3	2.1747	3.0	0.1996	2.0	0.65	1173.3	21.2	1173.0	21.2	1172.4	45.9	1172.4	45.9	100.1
IX45-7	77	9318	1.9	12.6396	3.5	2.0598	3.7	0.1888	1.2	0.32	1115.0	12.1	1135.6	25.1	1175.1	68.7	1175.1	68.7	94.9
IX45-29	391	123986	4.0	12.6097	1.3	2.1370	1.9	0.1954	1.3	0.72	1150.8	14.1	1160.9	12.9	1179.8	25.5	1179.8	25.5	97.5
IX45-24	698	64924	4.1	12.4341	3.2	2.1129	3.9	0.1905	2.1	0.55	1124.3	22.1	1153.0	26.7	1207.4	63.4	1207.4	63.4	93.1
IX45-32	310	63636	4.2	12.3646	1.8	2.2995	1.9	0.2062	0.5	0.27	1208.6	5.6	1212.1	13.4	1218.4	36.0	1218.4	36.0	99.2
IX45-8	171	52142	2.7	11.9699	1.5	2.1111	1.7	0.1833	0.7	0.43	1084.8	7.4	1152.4	11.8	1281.9	30.0	1281.9	30.0	84.6
IX45-11	255	51762	2.5	11.8002	1.7	2.5090	2.8	0.2147	2.2	0.80	1254.0	25.5	1274.7	20.2	1309.7	32.2	1309.7	32.2	95.7
IX45-25	830	34866	2.0	11.6735	3.4	2.4737	4.3	0.2094	2.6	0.60	1225.8	28.8	1264.4	30.9	1330.6	66.0	1330.6	66.0	92.1
IX45-10	142	32620	2.0	11.4063	2.3	2.8120	2.3	0.2326	0.5	0.21	1348.2	6.1	1358.7	17.5	1375.3	43.9	1375.3	43.9	98.0
IX45-12	834	87922	3.6	11.4009	1.7	2.9371	2.2	0.2429	1.3	0.60	1401.5	16.4	1391.5	16.5	1376.2	33.5	1376.2	33.5	101.8
IX45-31	484	51520	1.8	11.0325	1.5	2.8437	2.4	0.2275	1.9	0.77	1321.6	22.2	1367.2	18.1	1439.1	29.0	1439.1	29.0	91.8
IX45-15	166	210040	3.4	10.8344	1.1	3.2692	1.6	0.2569	1.2	0.73	1473.9	15.4	1473.8	12.4	1473.5	20.7	1473.5	20.7	100.0
IX45-21	208	74108	3.1	9.5421	1.4	4.2537	1.5	0.2944	0.6	0.36	1663.4	8.2	1684.5	12.7	1710.8	26.5	1710.8	26.5	97.2
IX45-9	118	81104	3.2	6.2128	2.6	10.3834	3.8	0.4679	2.7	0.72	2474.2	55.9	2469.6	35.1	2465.7	44.4	2465.7	44.4	100.3
Ix 46 UTM LAT 0533648, LONG 1994241																			
IX46-16A	123	7194	3.9	19.7474	7.8	0.4405	8.4	0.0631	3.1	0.36	394.4	11.7	370.6	26.0	224.5	180.2	394.4	11.7	175.7
IX46-16	115	5166	4.0	18.4816	13.2	0.4812	13.5	0.0645	2.8	0.21	402.9	11.0	398.9	44.5	375.5	297.6	402.9	11.0	107.3
IX46-31	183	8678	4.2	18.2072	4.1	0.5499	4.8	0.0726	2.6	0.53	451.9	11.1	445.0	17.5	409.1	92.2	451.9	11.1	110.5
IX46-14A	527	33594	2.6	17.9501	2.4	0.5805	3.8	0.0756	2.9	0.77	469.6	13.2	464.8	14.2	440.8	54.2	469.6	13.2	106.5
IX46-25	205	11996	1.7	17.8658	1.8	0.6015	2.0	0.0779	1.0	0.47	483.8	4.4	478.2	7.7	451.3	39.9	483.8	4.4	107.2
IX46-14	683	49726	1.6	17.5096	1.1	0.6144	1.7	0.0780	1.4	0.78	484.3	6.3	486.3	6.7	495.8	23.8	484.3	6.3	97.7
IX46-29	609	28536	13.4	17.7735	2.5	0.6059	2.6	0.0781	0.6	0.22	484.8	2.7	480.9	10.0	462.8	56.5	484.8	2.7	104.7
IX46-24	231	17830	2.4	17.8982	3.6	0.6061	3.8	0.0787	1.2	0.31	488.2	5.5	481.1	14.7	447.2	81.0	488.2	5.5	109.2
IX46-5	150	45706	1.5	17.5395	5.5	0.6253	6.0	0.0795	2.4	0.40	493.4	11.4	493.1	23.4	492.1	121.0	493.4	11.4	100.3
IX46-30	236	16144	1.6	17.5314	4.7	0.6606	4.7	0.0840	0.7	0.14	519.9	3.3	515.0	19.0	493.1	102.9	519.9	3.3	105.4
IX46-11	84	10046	2.3	18.2092	6.4	0.6513	6.6	0.0860	1.6	0.24	531.9	8.0	509.3	26.3	408.8	142.5	531.9	8.0	130.1
IX46-26	187	23588	3.7	16.1437	1.6	0.8673	3.2	0.1015	2.8	0.88	623.4	16.9	634.1	15.3	672.2	33.6	623.4	16.9	92.7
IX46-3	300	41240	5.2	15.1975	3.7	0.9767	5.4	0.1076	3.9	0.73	659.1	24.6	691.9	27.0	800.0	77.2	659.1	24.6	82.4
IX46-18	126	6970	1.5	16.0969	1.6	0.9500	2.6	0.1109	2.1	0.79	678.0	13.3	678.1	12.9	678.3	34.4	678.0	13.3	100.0
IX46-26A	115	41168	2.6	15.2514	1.2	1.1905	1.3	0.1317	0.5	0.40	797.4	3.9	796.2	7.3	792.6	25.4	797.4	3.9	100.6
IX46-17	137	16218	3.7	13.4459	2.1	1.8458	2.6	0.1800	1.5	0.59	1067.0	14.8	1061.9	16.9	1051.6	41.8	1051.6	41.8	101.5
IX46-20	238	42206	4.2	13.4113	2.1	1.8052	2.6	0.1756	1.5	0.58	1042.8	14.3	1047.3	16.9	1056.8	42.6	1056.8	42.6	98.7
IX46-6	145	23696	1.3	13.3337	1.9	1.7866	2.5	0.1728	1.6	0.65	1027.4	15.4	1040.6	16.1	1068.5	37.6	1068.5	37.6	96.2
IX46-19	144	8790	1.8	13.2624	4.6	1.7774	5.6	0.1710	3.1	0.55	1017.4	29.1	1037.2	36.2	1079.2	93.0	1079.2	93.0	94.3
IX46-21	112	20782	2.2	13.2531	1.8	1.7710	2.2	0.1702	1.3	0.58	1013.4	11.7	1034.9	14.1	1080.6	35.6	1080.6	35.6	93.8
IX46-19A	145	14744	1.3	13.1645	2.4	1.8059	2.6	0.1724	1.0	0.38	1025.5	9.3	1047.6	16.9	1094.1	47.9	1094.1	47.9	93.7
IX46-1	261	78452	2.8	13.1571	1.1	1.8388	1.9	0.1755	1.6	0.83	1042.2	15.0	1059.4	12.4	1095.2	21.2	1095.2	21.2	95.2
IX46-12	84	8204	2.6	13.0738	4.7	1.5450	9.4	0.1465	8.2	0.87	881.3	67.1	948.5	58.1	1107.9	94.2	1107.9	94.2	79.5
IX46-7	237	66162	1.8	12.5645	2.3	2.2478	3.1	0.2048	2.1	0.67	1201.2	22.9	1196.1	22.1	1186.9	46.3	1186.9	46.3	101.2

Analysis	U (ppm)	206Pb 204Pb	U/Th	206Pb* 207Pb*	± (%)	207Pb* 235U*	± (%)	206Pb* 238U	± (%)	error corr.	206Pb* 238U*	± (Ma)	207Pb* 235U	± (Ma)	206Pb* 207Pb*	± (Ma)	Best age (Ma)	± (Ma)	Conc (%)
IX46-8	193	60638	1.9	12.5612	1.9	2.1224	2.2	0.1934	1.2	0.53	1139.5	12.4	1156.1	15.4	1187.4	37.2	1187.4	37.2	96.0
IX46-22	58	15662	3.7	12.4836	2.6	2.1988	3.1	0.1991	1.8	0.58	1170.4	19.3	1180.7	21.8	1199.6	50.4	1199.6	50.4	97.6
IX46-23	347	51742	2.7	12.3765	2.1	2.2705	2.6	0.2038	1.5	0.57	1195.8	15.9	1203.2	18.0	1216.5	41.3	1216.5	41.3	98.3
IX46-2A	90	34716	1.5	12.0166	3.4	2.3570	4.7	0.2054	3.3	0.70	1204.4	36.5	1229.7	33.7	1274.3	65.8	1274.3	65.8	94.5
IX46-2	169	7276	2.6	9.6567	1.7	2.8774	2.1	0.2015	1.3	0.61	1183.5	13.8	1376.0	15.8	1688.8	30.6	1688.8	30.6	70.1
IX46-32	137	1212	1.7	9.4048	42.3	0.7016	43.1	0.0479	8.5	0.20	301.4	25.1	539.8	182.5	1737.4	814.7	1737.4	814.7	17.3
IX46-27	767	15516	9.3	8.7483	2.5	4.0524	3.6	0.2571	2.7	0.73	1475.1	34.9	1644.8	29.6	1869.0	45.0	1869.0	45.0	78.9
IX46-13	120	28420	0.9	8.3052	1.4	5.9472	1.5	0.3582	0.6	0.40	1973.8	10.2	1968.1	12.9	1962.2	24.3	1962.2	24.3	100.6
IX46-9	233	95208	2.8	6.1425	7.2	9.9979	8.7	0.4454	4.9	0.56	2374.8	96.6	2434.6	80.0	2484.9	120.9	2484.9	120.9	95.6
IX46-10	324	204658	8.9	5.5819	2.1	12.5925	2.9	0.5098	2.0	0.68	2655.8	43.1	2649.7	27.3	2645.0	35.2	2645.0	35.2	100.4
Ix 48 UTM: LAT 0530777, LONG 1991472																			
IX48-7	1048	15760	20.3	14.6487	1.9	1.0856	2.8	0.1153	2.0	0.72	703.7	13.4	746.4	14.8	876.6	40.1	€ 703.67	€ 13.40	80.3
IX48-6	429	77456	9.4	13.9782	3.0	1.5774	3.3	0.1599	1.5	0.45	956.3	13.2	961.4	20.8	972.9	61.0	€ 956.32	€ 13.24	98.3
IX48-35	553	191244	4.3	13.5533	1.3	1.7099	1.7	0.1681	1.1	0.63	1001.5	10.0	1012.2	11.0	1035.5	27.1	€ 1,035.52	€ 27.10	96.7
IX48-26	480	49762	3.2	13.5073	2.2	1.7713	3.3	0.1735	2.5	0.74	1031.5	23.5	1035.0	21.6	1042.4	45.0	€ 1,042.38	€ 45.03	99.0
IX48-19	191	53130	11.0	13.3582	1.6	1.7316	2.0	0.1678	1.2	0.58	999.7	10.7	1020.3	12.8	1064.8	32.4	1064.8	32.4	93.9
IX48-28	197	45062	1.7	13.3196	2.2	1.9056	2.6	0.1841	1.4	0.55	1089.3	14.4	1083.0	17.6	1070.6	44.4	1070.6	44.4	101.7
IX48-46	117	29434	2.8	13.2838	2.6	1.8404	2.6	0.1773	0.5	0.19	1052.3	4.9	1060.0	17.1	1076.0	51.3	1076.0	51.3	97.8
IX48-27	126	38030	2.7	13.1499	1.3	1.9487	1.7	0.1858	1.0	0.61	1098.9	10.3	1098.0	11.3	1096.3	26.8	1096.3	26.8	100.2
IX48-30	237	59986	2.7	13.1404	1.3	1.9301	2.9	0.1839	2.6	0.90	1088.5	25.8	1091.6	19.3	1097.7	25.7	1097.7	25.7	99.2
IX48-39	235	60808	2.9	12.7109	1.7	2.0726	1.8	0.1911	0.7	0.38	1127.2	7.1	1139.8	12.4	1163.9	33.1	1163.9	33.1	96.8
IX48-44	105	21576	3.4	12.6813	2.8	2.1202	2.9	0.1950	0.6	0.20	1148.4	6.0	1155.4	20.0	1168.5	56.2	1168.5	56.2	98.3
IX48-16	145	67410	3.6	12.6541	2.9	1.9165	3.2	0.1759	1.3	0.42	1044.5	12.9	1086.9	21.1	1172.8	56.7	1172.8	56.7	89.1
IX48-38	342	75030	3.5	12.6072	1.4	2.1531	3.2	0.1969	2.9	0.90	1158.5	30.3	1166.0	22.0	1180.1	27.3	1180.1	27.3	98.2
IX48-4	346	99064	5.2	12.6059	1.3	2.0357	1.5	0.1861	0.9	0.58	1100.3	9.0	1127.5	10.5	1180.3	24.9	1180.3	24.9	93.2
IX48-47	244	56032	1.5	12.6049	1.7	2.2400	1.9	0.2048	0.8	0.45	1200.9	9.1	1193.7	13.0	1180.5	32.8	1180.5	32.8	101.7
IX48-14	191	110388	1.4	12.5914	1.6	2.1550	1.9	0.1968	0.9	0.49	1158.1	9.9	1166.6	13.1	1182.6	32.4	1182.6	32.4	97.9
IX48-20	663	234290	3.8	12.5853	2.0	2.1215	2.2	0.1936	1.0	0.45	1141.1	10.2	1155.8	15.1	1183.6	38.7	1183.6	38.7	96.4
IX48-5	390	148404	2.4	12.4951	1.7	2.0647	1.8	0.1871	0.6	0.32	1105.7	5.9	1137.2	12.5	1197.8	34.3	1197.8	34.3	92.3
IX48-11	329	9904	4.4	12.4942	3.0	1.8687	3.1	0.1693	0.9	0.29	1008.5	8.6	1070.1	20.7	1197.9	58.9	1197.9	58.9	84.2
IX48-36	341	66854	4.5	12.4927	0.9	2.1134	1.5	0.1915	1.3	0.83	1129.4	13.2	1153.2	10.6	1198.1	17.0	1198.1	17.0	94.3
IX48-43	193	71198	5.7	12.4880	1.8	2.1902	2.3	0.1984	1.5	0.63	1166.6	15.8	1177.9	16.3	1198.9	35.8	1198.9	35.8	97.3
IX48-41	234	34728	1.9	12.4194	1.9	2.1840	2.3	0.1967	1.2	0.54	1157.7	13.0	1176.0	15.8	1209.7	37.4	1209.7	37.4	95.7
IX48-1112	174	45362	1.8	12.4147	2.3	2.2820	2.4	0.2055	0.8	0.32	1204.6	8.6	1206.7	17.3	1210.5	45.7	1210.5	45.7	99.5
IX48-17	95	44360	3.4	12.4128	2.4	2.2125	2.8	0.1992	1.3	0.47	1170.9	13.9	1185.0	19.3	1210.8	47.9	1210.8	47.9	96.7
IX48-42	356	103294	7.2	12.3623	1.1	2.2039	1.7	0.1976	1.3	0.76	1162.4	13.6	1182.3	11.8	1218.8	21.6	1218.8	21.6	95.4
IX48-13	77	21860	3.0	12.3227	2.1	2.3202	3.3	0.2074	2.6	0.77	1214.8	28.3	1218.5	23.6	1225.1	41.7	1225.1	41.7	99.2
IX48-15	152	50596	3.3	12.2617	1.1	2.1732	1.3	0.1933	0.6	0.44	1139.0	5.8	1172.5	8.8	1234.9	22.2	1234.9	22.2	92.2
IX48-37	592	154598	3.8	12.2591	1.0	2.2973	1.4	0.2043	1.1	0.73	1198.1	11.5	1211.5	10.2	1235.3	19.2	1235.3	19.2	97.0
IX48-18	237	67592	4.4	11.9650	3.2	2.5228	4.2	0.2189	2.7	0.64	1276.2	30.8	1278.6	30.3	1282.7	62.6	1282.7	62.6	99.5
IX48-29	175	49384	2.8	11.8952	1.1	2.5060	1.8	0.2162	1.5	0.81	1261.8	16.7	1273.8	13.1	1294.1	20.7	1294.1	20.7	97.5
IX48-31	591	125858	4.1	11.8324	1.9	2.6060	2.1	0.2236	0.8	0.38	1301.1	9.4	1302.3	15.4	1304.4	37.7	1304.4	37.7	99.7
IX48-21	303	91192	5.8	11.8195	2.3	2.4364	2.5	0.2089	1.0	0.41	1222.7	11.4	1253.4	17.9	1306.5	44.1	1306.5	44.1	93.6
IX48-23	202	64064	2.6	11.7148	2.2	2.6934	2.9	0.2288	2.0	0.67	1328.4	23.4	1326.6	21.7	1323.8	42.2	1323.8	42.2	100.4
IX48-8	96	27476	3.9	11.6599	2.9	2.6737	3.0	0.2261	0.5	0.17	1314.0	5.9	1321.2	22.0	1332.9	56.7	1332.9	56.7	98.6
IX48-40	136	44764	3.2	11.5677	1.1	2.6519	1.7	0.2225	1.3	0.77	1295.0	15.4	1315.2	12.5	1348.2	20.9	1348.2	20.9	96.1
IX48-2	241	61510	3.0	11.3539	1.5	2.9046	2.0	0.2392	1.2	0.62	1382.4	15.2	1383.1	14.8	1384.1	29.4	1384.1	29.4	99.9
IX48-48	256	25110	4.8	10.9871	1.5	3.1125	2.2	0.2480	1.6	0.73	1428.2	20.6	1435.8	16.8	1446.9	28.3	1446.9	28.3	98.7
IX48-10	387	104714	3.1	10.5594	3.2	3.5056	3.6	0.2685	1.7	0.46	1533.1	22.8	1528.5	28.7	1522.1	60.9	1522.1	60.9	100.7
IX48-1	188	115354	2.2	10.5425	2.8	3.5389	3.5	0.2706	2.1	0.60	1543.8	28.6	1536.0	27.5	1525.2	52.4	1525.2	52.4	101.2
IX48-3	179	101096	4.4	10.4767	2.3	3.3624	2.6	0.2555	1.2	0.47	1466.7	15.9	1495.7	20.2	1537.0	42.9	1537.0	42.9	95.4
IX48-34	205	68308	4.0	10.1668	3.6	3.4543	3.6	0.2547	0.5	0.14	1462.7	6.5	1516.9	28.6	1593.2	67.1	1593.2	67.1	91.8
IX48-323	275	128994	3.6	9.9988	5.3	3.4246	7.3	0.2483	5.1	0.69	1429.9	65.1	1510.0	57.8	1624.3	98.7	1624.3	98.7	88.0
IX51-5	136	16656	4.1	13.4190	1.3	1.4304	3.4	0.1392	3.2	0.93	840.2	25.2	901.7	20.5	1055.6	25.3	840.2	25.2	79.6
IX51-11	194	33642	16.9	14.1719	1.8	1.5895	2.2	0.1634	1.3	0.60	975.5	12.1	966.1	13.9	944.7	36.3	975.5	12.1	103.3
IX51-8	1075	32598	6.3	13.9382	1.7	1.6090	2.5	0.1627	1.8	0.74	971.5	16.6	973.7	15.6	978.7	34.1	978.7	34.1	99.3
IX51-23	750	130736	31.1	13.8119	1.1	1.6950	1.4	0.1698	0.9	0.65	1011.0	8.7	1006.7	9.2	997.2	22.1	997.2	22.1	101.4
IX51-10	236	26568	1.9	13.7371	2.2	1.6345	3.1	0.1628	2.2	0.70	972.6	19.8	983.6	19.7	1008.2	45.4	1008.2	45.4	96.5
IX51-38	979	161052	5.6	13.4777	1.2	1.8097	1.3	0.1769	0.6	0.46	1050.0	5.7	1049.0	8.5	1046.8	23.2	1046.8	23.2	100.3
IX51-22	748	122882	3.1	13.3990	2.0	1.8467	2.1	0.1795	0.5	0.24	1064.0	4.9	1062.3	13.5	1058.6	40.1	1058.6	40.1	100.5
IX51-48	972	138776	34.6	13.3652	1.3	1.6998	2.0	0.1648	1.5	0.76	983.2	13.9	1008.5	12.8	1063.7	26.4	1063.7	26.4	92.4
IX51-22	93	14146	2.0	13.3056	1.5	1.8635	1.9	0.1798	1.2	0.61	1066.1	11.6	1068.2	12.7	1072.7	30.5	1072.7	30.5	99.4
IX51-42	228	32178	3.2	13.1748	2.1	1.9860	2.4	0.1898	1.1	0.46	1120.1	11.4	1110.8	16.3	1092.5	42.9	1092.5	42.9	102.5
IX51-2	544	47342	3.6	13.0810	2.0	1.8443	3.7	0.1750	3.1	0.84	1039.5	29.9	1061.4	24.5	1106.8	40.6	1106.8	40.6	93.9
IX51-24A	451	66850	23.4	13.0762	1.2	1.9634	1.4	0.1862	0.7	0.52	1100.8	7.5	1103.1	9.7	1107.5	24.6	1107.5	24.6	99.4
IX51-13	657	34914	5.8	12.7996	1.5	1.9906	2.6	0.1848	2.1	0.82	1093.1	21.4	1112.3	17.7	1150.1	30.0	1150.1	30.0	95.0
IX51-49	136	9338	4.3	12.7712	2.3	2.0091	3.4	0.1861	2.5	0.74	1100.2	25.5	1118.6	23.2	1154.5	45.9	1154.5	45.9	95.3

Analysis	U (ppm)	206Pb 204Pb	U/Th	206Pb* 207Pb*	± (%)	207Pb* 235U*	± (%)	206Pb* 238U	± (%)	error corr.	206Pb* 238U*	± (Ma)	207Pb* 235U	± (Ma)	206Pb* 207Pb*	± (Ma)	Best age (Ma)	± (Ma)	Conc (%)
IX51-25	148	23178	1.4	12.7119	1.5	2.1970	1.7	0.2026	0.7	0.39	1189.0	7.1	1180.1	11.5	1163.7	30.1	1163.7	30.1	102.2
IX51-30	291	83548	2.9	12.6223	2.0	2.1692	2.2	0.1986	0.9	0.41	1167.7	9.7	1171.2	15.5	1177.8	40.1	1177.8	40.1	99.1
IX51-49	128	14700	2.3	12.5935	1.2	2.2079	2.2	0.2017	1.9	0.85	1184.2	20.6	1183.5	15.5	1182.3	22.8	1182.3	22.8	100.2
IX51-1	224	34018	2.9	12.5764	1.9	2.2341	1.9	0.2038	0.5	0.26	1195.6	5.5	1191.8	13.6	1185.0	37.0	1185.0	37.0	100.9
IX51-47	117	24736	2.4	12.5756	1.7	2.2054	2.2	0.2011	1.4	0.64	1181.5	15.4	1182.8	15.6	1185.1	33.9	1185.1	33.9	99.7
IX51-46	296	44304	2.9	12.5419	1.3	2.2407	1.8	0.2038	1.3	0.70	1195.8	14.0	1193.9	12.8	1190.4	25.5	1190.4	25.5	100.5
IX51-20	205	17276	2.1	12.5337	2.5	2.2842	2.5	0.2076	0.5	0.20	1216.2	5.5	1207.4	17.9	1191.7	49.1	1191.7	49.1	102.1
IX51-37	151	24052	2.3	12.5170	1.8	2.2521	2.4	0.2045	1.6	0.66	1199.2	17.3	1197.4	16.8	1194.3	35.3	1194.3	35.3	100.4
IX51-27	93	15880	1.9	12.5108	1.9	2.2793	2.4	0.2068	1.5	0.62	1211.9	16.5	1205.9	16.9	1195.3	37.2	1195.3	37.2	101.4
IX51-15	116	18802	1.9	12.5068	1.8	2.3142	1.9	0.2099	0.6	0.32	1228.4	6.7	1216.7	13.5	1195.9	35.6	1195.9	35.6	102.7
IX51-19	273	41800	10.4	12.4494	2.2	2.3548	3.0	0.2126	2.0	0.66	1242.7	22.0	1229.0	21.2	1205.0	44.2	1205.0	44.2	103.1
IX51-18	434	64898	3.6	12.4351	1.3	2.2710	1.6	0.2048	0.9	0.56	1201.1	9.5	1203.3	11.0	1207.3	25.4	1207.3	25.4	99.5
IX51-24	340	31560	2.4	12.4161	1.1	2.2490	2.2	0.2025	1.9	0.86	1188.8	20.3	1196.5	15.4	1210.3	22.3	1210.3	22.3	98.2
IX51-43	429	54338	3.0	12.3816	2.2	2.1578	2.4	0.1938	0.9	0.39	1141.8	9.6	1167.6	16.4	1215.8	42.9	1215.8	42.9	93.9
IX51-31	74	13260	4.8	12.3795	2.3	2.3486	2.6	0.2109	1.2	0.47	1233.5	13.7	1227.1	18.6	1216.1	45.4	1216.1	45.4	101.4
IX51-19	390	66612	3.9	12.3284	1.6	2.3164	2.5	0.2071	1.9	0.77	1213.4	21.3	1217.3	17.8	1224.2	31.4	1224.2	31.4	99.1
IX51-32	83	18178	1.7	12.3281	2.0	2.3809	2.2	0.2129	0.7	0.34	1244.2	8.4	1236.9	15.6	1224.2	40.3	1224.2	40.3	101.6
IX51-42	280	49492	3.6	12.3165	1.0	2.2642	4.8	0.2023	4.7	0.98	1187.4	51.2	1201.2	34.0	1226.1	19.7	1226.1	19.7	96.8
IX51-33	152	47498	2.7	12.3095	1.3	2.3594	1.7	0.2106	1.1	0.65	1232.2	12.2	1230.4	12.0	1227.2	25.0	1227.2	25.0	100.4
IX51-5	835	107214	1.3	12.2978	1.9	2.3491	2.1	0.2095	0.9	0.43	1226.3	10.2	1227.3	15.2	1229.1	37.9	1229.1	37.9	99.8
IX51-30	271	32730	3.5	12.2879	1.8	2.1903	4.2	0.1952	3.8	0.90	1149.5	40.0	1177.9	29.4	1230.7	35.8	1230.7	35.8	93.4
IX51-1	630	81704	2.6	12.2763	1.7	2.3669	2.2	0.2107	1.4	0.64	1232.8	15.7	1232.7	15.7	1232.5	33.3	1232.5	33.3	100.0
IX51-32	240	30312	1.6	12.2732	1.2	2.3736	2.0	0.2113	1.6	0.80	1235.6	18.0	1234.7	14.3	1233.0	23.8	1233.0	23.8	100.2
IX51-36	562	89426	4.0	12.2638	1.9	2.3823	2.2	0.2119	1.1	0.51	1238.9	12.5	1237.3	15.5	1234.5	36.5	1234.5	36.5	100.4
IX51-41	274	32990	2.7	12.1696	2.7	2.3643	2.7	0.2087	0.5	0.18	1221.8	5.6	1231.9	19.5	1249.6	52.7	1249.6	52.7	97.8
IX51-4	153	20036	2.0	12.1684	1.5	2.4306	2.2	0.2145	1.6	0.72	1252.8	18.0	1251.7	15.7	1249.8	29.6	1249.8	29.6	100.2
IX51-35	886	83596	8.9	12.0102	1.2	2.3191	3.5	0.2020	3.3	0.94	1186.1	35.3	1218.2	24.7	1275.4	23.4	1275.4	23.4	93.0
IX51-29	403	84006	3.0	12.0007	0.9	2.4614	2.5	0.2142	2.3	0.93	1251.3	25.9	1260.8	17.8	1276.9	17.9	1276.9	17.9	98.0
IX51-29	165	21268	3.7	11.9615	2.1	2.3866	2.2	0.2070	0.5	0.23	1213.0	5.5	1238.6	15.7	1283.3	41.5	1283.3	41.5	94.5
IX51-10	615	26900	3.0	11.8625	2.0	2.0890	8.6	0.1797	8.4	0.97	1065.5	82.4	1145.2	59.2	1299.4	37.9	1299.4	37.9	82.0
IX51-7	284	30262	6.6	11.8387	3.2	2.4415	5.3	0.2096	4.2	0.80	1226.9	47.0	1254.9	38.1	1303.3	62.0	1303.3	62.0	94.1
IX51-13	1015	54004	7.4	11.7762	1.2	2.5006	1.9	0.2136	1.5	0.78	1247.8	17.2	1272.2	14.1	1313.6	23.7	1313.6	23.7	95.0
IX51-4	123	49884	1.3	11.7398	3.9	2.6522	4.3	0.2258	1.8	0.42	1312.6	21.5	1315.3	31.7	1319.6	75.4	1319.6	75.4	99.5
IX51-18	163	26530	1.9	11.7394	1.8	2.6870	2.0	0.2288	0.9	0.46	1328.1	10.9	1324.9	14.7	1319.7	34.2	1319.7	34.2	100.6
IX51-34	983	53818	3.0	11.7372	1.1	2.5561	1.9	0.2176	1.6	0.81	1269.1	18.1	1288.2	14.2	1320.1	22.1	1320.1	22.1	96.1
IX51-6	172	2818	2.6	11.6491	5.8	2.2001	6.1	0.1859	1.8	0.30	1099.0	18.4	1181.1	42.6	1334.6	112.8	1334.6	112.8	82.3
IX51-28	164	15914	2.9	11.6264	1.4	2.0904	5.4	0.1763	5.2	0.97	1046.5	50.6	1145.7	37.2	1338.4	26.8	1338.4	26.8	78.2
IX51-45	767	20596	7.4	11.6209	1.8	2.5402	2.1	0.2141	1.0	0.48	1250.6	11.4	1283.6	15.2	1339.3	35.3	1339.3	35.3	93.4
IX51-25	157	41472	1.4	11.5647	1.5	2.6944	1.6	0.2260	0.6	0.38	1313.5	7.0	1326.9	11.6	1348.7	28.0	1348.7	28.0	97.4
IX51-14	453	83668	2.7	11.5496	2.0	2.7975	2.2	0.2343	0.7	0.34	1357.2	9.1	1354.9	16.1	1351.2	39.0	1351.2	39.0	100.4
IX51-12	935	42398	3.7	11.5400	3.8	2.1493	4.0	0.1799	1.2	0.30	1066.3	11.6	1164.8	27.6	1352.8	73.5	1352.8	73.5	78.8
IX51-7	267	81288	3.8	11.5335	1.3	2.8237	1.6	0.2362	0.9	0.59	1366.9	11.5	1361.8	11.8	1353.9	24.5	1353.9	24.5	101.0
IX51-44	158	31910	2.7	11.4857	1.5	2.8438	1.6	0.2369	0.6	0.36	1370.5	7.2	1367.2	12.0	1361.9	28.6	1361.9	28.6	100.6
IX51-35	866	98276	4.1	11.4825	1.2	2.8018	3.3	0.2333	3.1	0.94	1351.9	37.8	1356.0	24.8	1362.5	22.5	1362.5	22.5	99.2
IX51-34	313	33228	2.1	11.4714	1.2	2.7341	1.6	0.2275	1.1	0.69	1321.2	13.4	1337.8	12.1	1364.3	22.9	1364.3	22.9	96.8
IX51-37	644	89476	12.9	11.4092	1.4	2.8898	1.5	0.2391	0.5	0.34	1382.1	6.2	1379.3	11.1	1374.8	26.5	1374.8	26.5	100.5
IX51-40	147	18740	1.6	11.2826	2.4	2.6110	2.8	0.2137	1.5	0.52	1248.3	16.6	1303.7	20.4	1396.2	45.4	1396.2	45.4	89.4
IX51-16	858	109566	3.6	11.2763	1.7	2.9892	1.8	0.2445	0.7	0.39	1409.9	9.0	1404.9	13.9	1397.3	32.4	1397.3	32.4	100.9
IX51-21	244	54648	1.9	11.2124	2.5	3.0150	2.5	0.2452	0.5	0.20	1413.6	6.3	1411.4	19.4	1408.2	47.7	1408.2	47.7	100.4
IX51-46	265	24668	4.0	11.1903	3.1	2.8206	3.4	0.2289	1.5	0.43	1328.8	17.7	1361.0	25.5	1411.9	58.8	1411.9	58.8	94.1
IX51-31	618	147050	15.2	11.0953	2.1	3.0890	2.2	0.2486	0.8	0.37	1431.1	10.7	1430.0	17.3	1428.2	39.9	1428.2	39.9	100.2
IX51-23	297	30288	4.4	11.0269	0.6	2.8695	1.6	0.2295	1.4	0.93	1331.8	17.3	1374.0	11.7	1440.0	11.1	1440.0	11.1	92.5
IX51-17	186	30040	2.8	10.9417	0.7	3.1354	2.5	0.2488	2.4	0.96	1432.4	30.3	1441.4	19.0	1454.8	13.6	1454.8	13.6	98.5
IX51-3	157	17384	2.2	10.8805	2.6	3.1698	3.2	0.2501	1.8	0.56	1439.2	23.0	1449.8	24.6	1465.5	50.1	1465.5	50.1	98.2
IX51-45	386	46722	4.7	10.8690	2.0	3.0682	3.2	0.2419	2.4	0.77	1396.4	30.4	1424.8	24.2	1467.5	38.6	1467.5	38.6	95.2
IX51-2	410	89342	2.5	10.8466	1.7	3.3275	1.9	0.2618	0.8	0.43	1498.9	11.0	1487.5	14.8	1471.4	32.5	1471.4	32.5	101.9
IX51-51	729	52880	13.8	10.7297	3.3	2.7887	5.0	0.2170	3.8	0.76	1266.1	43.2	1352.5	37.2	1491.9	61.5	1491.9	61.5	84.9
IX51-9	354	27094	3.3	10.7015	2.4	3.4690	4.4	0.2692	3.6	0.83	1537.0	49.4	1520.2	34.3	1496.9	46.0	1496.9	46.0	102.7
IX51-40	731	53458	2.8	10.6821	1.1	2.8719	1.9	0.2225	1.6	0.82	1295.1	18.2	1374.6	14.3	1500.3	20.8	1500.3	20.8	86.3
IX51-12	567	57708	3.8	10.5462	1.4	3.4108	1.5	0.2609	0.5	0.34	1494.4	6.7	1506.9	11.5	1524.5	25.8	1524.5	25.8	98.0
IX51-3	193	50426	2.6	10.4788	4.8	3.4577	5.0	0.2628	1.2	0.25	1504.1	16.5	1517.6	39.1	1536.6	90.6	1536.6	90.6	97.9
IX51-47	213	52808	3.7	10.4750	2.7	3.3031	3.7	0.2509	2.5	0.68	1443.3	32.7	1481.8	29.1	1537.3	51.6	1537.3	51.6	93.9
IX51-39	345	87306	3.3	10.4475	1.5	3.4338	1.6	0.2602	0.7	0.42	1490.8	9.1	1512.2	12.6	1542.2	27.3	1542.2	27.3	96.7
IX51-14	789	49264	4.8	10.4366	1.3	3.4213	2.5	0.2590	2.2	0.86	1484.6	28.6	1509.3	19.7	1544.2	24.1	1544.2	24.1	96.1
IX51-28	668	103188	2.6	10.4323	2.8	3.6378	3.1	0.2752	1.3	0.43	1567.4	18.6	1557.8	24.6	1544.9	52.3	1544.9	52.3	101.5
IX51-26	479	39572	4.4	10.4286	1.8	3.5197	2.7	0.2662	2.0	0.75	1521.6	27.0	1531.7	21.0	1545.6	32.9	1545.6	32.9	98.4
IX51-9	755	87888	5.9	10.3762	1.8	3.6270	2.0	0.2730	1.0	0.47	1555.8	13.3	1555.5	16.3	1555.1	34.0	1555.1	34.0	100.0
IX51-87	283	63104	2.9	10.3123	1.6	3.7277	2.4	0.2788	1.7	0.73	1585.3	24.3	1577.3	19.1	1566.6	30.7	1566.6	30.7	101.2
IX51-27	102	39196	1.7	10.2830	2.3	3.6839	2.4	0.2747	0.8	0.32	1564.8	10.7	1567.9	19.3	1572.0	42.9	1572.0	42.9	99.5
IX51-15	303	88722	4.2	10.1197	0.9	3.8878	1.1	0.2853	0.5	0.47	1618.2	7.2	1611.1	8.5	1601.9	17.4	1601.9	17.4	101.0

Analysis	U (ppm)	206Pb 204Pb	U/Th	206Pb* 207Pb*	± (%)	207Pb* 235U*	± (%)	206Pb* 238U	± (%)	error corr.	206Pb* 238U*	± (Ma)	207Pb* 235U	± (Ma)	206Pb* 207Pb*	± (Ma)	Best age (Ma)	± (Ma)	Conc (%)
IX51-41	995	169774	8.6	10.0884	1.5	3.7954	1.8	0.2777	1.0	0.53	1579.8	13.3	1591.8	14.3	1607.7	28.1	1607.7	28.1	98.3
IX51-20	316	49570	3.9	10.0674	2.6	3.8128	2.9	0.2784	1.1	0.39	1583.3	15.4	1595.5	22.9	1611.6	49.0	1611.6	49.0	98.2
IX51-50	139	23474	4.1	10.0499	1.8	3.6155	2.6	0.2635	1.8	0.71	1507.9	24.6	1552.9	20.6	1614.8	34.1	1614.8	34.1	93.4
IX51-50	335	76960	1.5	9.9805	0.8	3.9037	1.2	0.2826	1.0	0.77	1604.3	13.5	1614.4	10.0	1627.7	14.7	1627.7	14.7	98.6
IX51-11	85	19898	1.1	9.9009	1.8	4.0619	2.0	0.2917	0.7	0.37	1649.9	10.6	1646.7	16.0	1642.6	33.9	1642.6	33.9	100.4
IX51-17	275	43336	2.3	9.8567	1.3	4.1387	2.4	0.2959	2.1	0.85	1670.8	30.2	1662.0	19.7	1650.9	23.4	1650.9	23.4	101.2
IX51-48	248	71976	3.0	9.8532	1.1	4.0548	2.0	0.2898	1.7	0.83	1640.4	24.0	1645.3	16.2	1651.5	20.4	1651.5	20.4	99.3
IX51-43	203	54246	2.7	9.7037	0.8	4.1222	1.0	0.2901	0.6	0.64	1642.1	9.0	1658.7	8.0	1679.8	13.9	1679.8	13.9	97.8
IX51-26	487	70754	1.3	9.6635	1.4	4.2124	1.6	0.2952	0.8	0.52	1667.6	12.0	1676.4	13.0	1687.5	24.9	1687.5	24.9	98.8
IX51-44	234	62182	2.7	9.5499	1.6	4.1216	1.6	0.2855	0.5	0.30	1618.9	7.2	1658.6	13.5	1709.3	28.9	1709.3	28.9	94.7
IX51-38	134	34784	1.8	9.0654	1.4	4.8890	1.5	0.3214	0.5	0.33	1796.8	7.8	1800.4	12.7	1804.5	25.8	1804.5	25.8	99.6
IX51-6	124	13662	1.2	8.8742	1.5	5.0939	3.0	0.3279	2.6	0.87	1828.0	41.2	1835.1	25.3	1843.2	26.7	1843.2	26.7	99.2
Ix 51 UTM LAT 0530777, LONG 1991472																			
Ix 52 UTM LAT 0527946 LONG 1994353																			
IX52-1	430	2448	2.1	14.6461	4.6	0.5845	4.7	0.0621	1.0	0.22	388.3	3.9	467.3	17.5	877.0	94.3	388.3	3.9	44.3
IX52-4	393	16300	2.1	15.8017	4.1	0.6679	5.1	0.0765	3.1	0.60	475.5	14.0	519.4	20.8	717.8	87.2	475.5	14.0	66.2
IX52-3	97	12408	2.6	15.3380	16.3	0.8176	16.4	0.0910	2.1	0.13	561.2	11.1	606.7	75.1	780.7	344.5	561.2	11.1	71.9
IX52-2	244	15994	3.4	13.2820	3.9	0.8811	7.2	0.0849	6.1	0.84	525.2	30.8	641.6	34.4	1076.3	78.1	1076.3	78.1	48.8
IX52-5	69	31086	3.6	12.5096	2.3	2.1924	3.3	0.1989	2.4	0.72	1169.5	25.3	1178.6	23.0	1195.5	45.3	1195.5	45.3	97.8
IX52-7	218	83458	6.2	12.2908	1.8	2.0617	2.3	0.1838	1.5	0.65	1087.6	15.3	1136.2	16.1	1230.2	34.9	1230.2	34.9	88.4
IX52-6	224	75654	7.0	10.9274	2.7	2.7932	5.3	0.2214	4.5	0.86	1289.1	52.8	1353.7	39.5	1457.3	51.9	1457.3	51.9	88.5
IX54-26	81	7386	1.8	17.6477	4.3	0.5924	4.3	0.0758	0.6	0.14	471.1	2.6	472.4	16.2	478.5	94.1	471.1	2.6	98.5
IX54-3	173	7886	1.5	18.0670	4.3	0.5803	4.3	0.0760	0.5	0.12	472.4	2.3	464.6	16.0	426.3	94.9	472.4	2.3	110.8
IX54-1	230	9512	2.7	16.1146	6.9	0.7012	7.3	0.0820	2.3	0.32	507.8	11.4	539.5	30.6	676.0	148.2	507.8	11.4	75.1
IX54-25	165	8010	5.9	14.5560	6.8	0.8563	7.3	0.0904	2.8	0.39	557.9	15.2	628.1	34.3	889.7	139.6	557.9	15.2	62.7
IX54-10	116	13580	3.3	15.8482	4.5	0.8064	5.4	0.0927	3.0	0.55	571.4	16.3	600.4	24.5	711.5	95.9	571.4	16.3	80.3
IX54-28	282	33436	4.7	14.4408	1.4	1.3579	2.2	0.1422	1.7	0.76	857.2	13.3	871.0	12.8	906.1	29.3	906.1	29.3	94.6
IX54-48	93	15240	3.2	14.4084	3.7	1.5140	3.9	0.1582	1.2	0.30	946.8	10.2	936.1	23.6	910.7	75.8	910.7	75.8	104.0
IX54-14	49	9272	2.9	14.3284	4.1	1.5584	4.2	0.1619	1.0	0.24	967.6	9.0	953.8	26.2	922.2	84.8	922.2	84.8	104.9
IX54-56	1344	93842	4.0	14.2858	1.7	1.5362	1.9	0.1592	0.7	0.40	952.2	6.6	945.0	11.4	928.3	34.9	928.3	34.9	102.6
IX54-9	904	92424	5.9	14.2357	1.0	1.5403	3.1	0.1590	2.9	0.94	951.4	25.7	946.6	18.9	935.6	20.9	935.6	20.9	101.7
IX54-24	93	18998	3.2	14.2003	3.4	1.5787	3.6	0.1626	1.1	0.31	971.1	10.0	961.8	22.4	940.7	70.1	940.7	70.1	103.2
IX54-34	120	16548	1.6	14.1443	1.6	1.4573	1.7	0.1495	0.6	0.33	898.1	4.8	912.9	10.3	948.8	33.2	948.8	33.2	94.7
IX54-55	362	38630	42.2	14.1324	1.0	1.5194	1.8	0.1557	1.5	0.84	933.0	13.3	938.2	11.2	950.5	20.3	950.5	20.3	98.2
IX54-19	1209	119830	41.5	14.1277	1.7	1.4217	2.3	0.1457	1.6	0.68	876.7	12.8	898.1	13.6	951.2	34.2	951.2	34.2	92.2
IX54-12	407	83572	5.4	13.7217	1.5	1.5603	2.2	0.1553	1.6	0.74	930.5	13.9	954.6	13.4	1010.5	29.6	1010.5	29.6	92.1
IX54-18	117	27272	4.0	13.6805	1.3	1.7017	1.4	0.1688	0.5	0.36	1005.7	4.7	1009.2	9.0	1016.6	26.6	1016.6	26.6	98.9
IX54-20	443	15794	2.5	13.4798	2.5	1.7540	2.8	0.1715	1.2	0.44	1020.2	11.5	1028.6	18.1	1046.5	50.8	1046.5	50.8	97.5
IX54-54	175	24976	1.6	12.9419	1.8	2.0842	2.3	0.1956	1.5	0.64	1151.8	15.4	1143.6	15.7	1128.1	35.1	1128.1	35.1	102.1
IX54-35	163	36956	3.2	12.6925	2.0	2.1140	2.1	0.1946	0.7	0.32	1146.2	7.0	1153.4	14.3	1166.8	38.9	1166.8	38.9	98.2
IX54-39	51	5034	1.9	12.6892	2.8	2.2216	3.4	0.2045	2.0	0.59	1199.2	22.3	1187.9	24.1	1167.3	55.0	1167.3	55.0	102.7
IX54-27	101	38548	3.0	12.6666	2.1	2.1258	2.1	0.1953	0.5	0.23	1150.0	5.3	1157.2	14.8	1170.9	41.2	1170.9	41.2	98.2
IX54-23	64	14962	1.8	12.6576	1.5	2.1616	1.6	0.1984	0.7	0.44	1166.9	7.6	1168.8	11.3	1172.3	28.9	1172.3	28.9	99.5
IX54-53	188	33202	3.7	12.6004	1.0	2.1431	1.2	0.1958	0.5	0.43	1153.0	5.3	1162.8	8.0	1181.2	20.6	1181.2	20.6	97.6
IX54-43	114	24300	3.7	12.5952	0.6	2.2051	2.1	0.2014	2.0	0.96	1183.0	21.7	1182.6	14.6	1182.0	11.8	1182.0	11.8	100.1
IX54-11	161	51074	4.5	12.5441	5.0	1.9982	11.1	0.1818	10.0	0.89	1076.8	98.9	1114.9	75.5	1190.1	98.2	1190.1	98.2	90.5
IX54-45	290	55490	15.4	12.5176	1.8	1.8680	5.8	0.1696	5.5	0.95	1009.9	51.3	1069.8	38.2	1194.2	35.5	1194.2	35.5	84.6
IX54-30	131	23208	2.1	12.5115	2.6	2.1225	2.9	0.1926	1.3	0.43	1135.4	13.0	1156.1	20.2	1195.2	52.1	1195.2	52.1	95.0
IX54-22A	39	17280	5.1	12.4918	5.0	2.1973	5.2	0.1991	1.1	0.21	1170.4	11.7	1180.2	36.0	1198.3	99.4	1198.3	99.4	97.7
IX54-17	246	36778	1.8	12.4649	2.0	2.2959	2.1	0.2076	0.5	0.26	1215.8	6.0	1211.0	14.8	1202.5	39.9	1202.5	39.9	101.1
IX54-40	336	68298	2.5	12.4311	1.7	2.3499	3.4	0.2119	2.9	0.87	1238.8	32.9	1227.5	24.0	1207.9	33.3	1207.9	33.3	102.6
IX54-49	61	13044	1.9	12.3694	3.0	2.3870	3.2	0.2141	0.9	0.30	1250.8	10.7	1238.7	22.7	1217.7	59.5	1217.7	59.5	102.7
IX54-44	142	32362	4.2	12.3274	4.2	2.1743	4.3	0.1944	1.2	0.27	1145.1	12.5	1172.8	30.3	1224.3	82.2	1224.3	82.2	93.5
IX54-21	51	12852	2.0	12.3208	3.2	2.4369	3.4	0.2178	1.2	0.35	1270.0	13.8	1253.6	24.5	1225.4	62.4	1225.4	62.4	103.6
IX54-6	34	11932	1.3	12.2373	3.2	2.5124	3.3	0.2230	0.9	0.27	1297.6	10.6	1275.6	24.3	1238.8	63.2	1238.8	63.2	104.8
IX54-32	206	51548	5.7	12.2272	1.4	2.3359	1.6	0.2071	0.7	0.44	1213.6	7.7	1223.3	11.2	1240.4	27.7	1240.4	27.7	97.8
IX54-33	348	74148	7.7	12.1740	1.5	2.3089	1.6	0.2039	0.5	0.32	1196.0	5.5	1215.0	11.1	1248.9	29.0	1248.9	29.0	95.8
IX54-31	404	73540	5.1	12.1462	1.2	2.4538	1.3	0.2162	0.5	0.40	1261.6	5.7	1258.6	9.0	1253.4	22.5	1253.4	22.5	100.7
IX54-47	207	48418	5.5	12.1448	1.9	2.3760	2.7	0.2093	2.0	0.72	1225.0	22.0	1235.4	19.6	1253.6	37.2	1253.6	37.2	97.7
IX54-15	179	36364	4.3	12.0703	1.6	2.4687	3.2	0.2161	2.9	0.88	1261.3	32.6	1262.9	23.5	1265.6	30.5	1265.6	30.5	99.7
IX54-13	92	22408	1.4	11.8660	1.6	2.5771	2.5	0.2218	1.9	0.75	1291.3	21.6	1294.2	18.0	1298.9	31.3	1298.9	31.3	99.4
IX54-29	200	36688	3.6	11.8464	1.5	2.5030	2.1	0.2151	1.5	0.72	1255.7	17.1	1272.9	15.2	1302.1	28.4	1302.1	28.4	96.4
IX54-8	137	47314	1.9	11.6802	1.2	2.7172	2.1	0.2302	1.7	0.82	1335.4	20.6	1333.2	15.5	1329.5	23.0	1329.5	23.0	100.4
IX54-4	155	62042	0.8	11.5292	1.6	2.8193	1.7	0.2357	0.5	0.30	1364.5	6.1	1360.7	12.6	1354.6	31.1	1354.6	31.1	100.7
IX54-58	252	24302	3.8	11.3891	0.8	2.7166	5.2	0.2244	5.2	0.99	1305.1	61.1	1333.0	38.8	1378.2	14.9	1378.2	14.9	94.7
IX54-42	213	57512	8.1	11.1978	1.6	2.7957	2.4	0.2270	1.8	0.75	1319.0	21.1	1354.4	17.7	1410.7	30.1	1410.7	30.1	93.5
IX54-7	129	29924	4.0	11.0789	3.2	2.7684	8.7	0.2224	8.1	0.93	1294.8	95.0	1347.0	65.0	1431.1	60.5	1431.1	60.5	90.5
IX54-37	272	27952	5.0	10.6786	0.9	3.3066	1.3	0.2561	1.0	0.77	1469.8	13.5	1482.6	10.5	1501.0	16.2	1501.0	16.2	97.9

Analysis	U (ppm)	206Pb 204Pb	U/Th	206Pb* 207Pb*	± (%)	207Pb* 235U*	± (%)	206Pb* 238U	± (%)	error corr.	206Pb* 238U*	± (Ma)	207Pb* 235U	± (Ma)	206Pb* 207Pb*	± (Ma)	Best age (Ma)	± (Ma)	Conc (%)
IX54-16	550	64654	3.1	10.6647	1.0	3.4102	1.2	0.2638	0.6	0.53	1509.1	8.5	1506.7	9.4	1503.4	19.1	1503.4	19.1	100.4
IX54-38	317	53456	2.3	10.6432	1.5	3.4584	1.7	0.2670	0.7	0.45	1525.4	10.1	1517.8	13.0	1507.2	28.0	1507.2	28.0	101.2
IX54-2	77	6182	3.1	10.5552	2.8	3.6038	2.9	0.2759	0.9	0.29	1570.6	12.0	1550.4	23.3	1522.9	52.8	1522.9	52.8	103.1
IX54-5	194	76574	1.2	8.7483	0.8	5.2630	1.8	0.3339	1.6	0.89	1857.4	25.5	1862.9	15.2	1869.0	14.6	1869.0	14.6	99.4
IX54-52	67	31182	1.3	5.1795	1.3	14.0629	2.0	0.5283	1.6	0.77	2734.2	34.5	2754.0	19.1	2768.5	21.0	2768.5	21.0	98.8
Ix 54 UTM: LAT 0527798, LONG 1994172																			
Ix 56 UTM: LAT 0519032, LONG 1990538																			
IX56-83	295	17846	1.5	18.2374	4.1	0.4265	4.1	0.0564	0.7	0.17	353.7	2.4	360.7	12.5	405.4	90.8	353.7	2.4	87.3
IX56-51	292	15688	1.2	18.4650	2.8	0.4447	3.7	0.0596	2.4	0.66	372.9	8.7	373.6	11.4	377.5	62.0	372.9	8.7	98.8
IX56-50	208	9970	5.1	17.5507	4.2	0.5792	6.2	0.0737	4.6	0.74	458.6	20.5	464.0	23.3	490.7	92.2	458.6	20.5	93.5
IX56-57	270	16266	2.6	17.4645	3.2	0.6209	5.8	0.0787	4.9	0.83	488.1	22.8	490.4	22.6	501.5	70.6	488.1	22.8	97.3
IX56-27	192	16228	1.6	17.5332	3.4	0.6279	3.7	0.0798	1.4	0.38	495.2	6.6	494.8	14.4	492.8	75.0	495.2	6.6	100.5
IX56-3	240	18676	1.8	16.9436	2.5	0.6585	4.0	0.0809	3.2	0.79	501.6	15.4	513.7	16.3	567.8	54.1	501.6	15.4	88.3
IX56-9	126	7598	1.5	17.9317	4.7	0.6257	4.9	0.0814	1.2	0.25	504.3	5.8	493.4	19.1	443.1	105.3	504.3	5.8	113.8
IX56-22	191	11228	0.4	17.3465	3.3	0.6496	3.9	0.0817	2.1	0.54	506.4	10.2	508.2	15.5	516.4	71.6	506.4	10.2	98.1
IX56-43	166	11028	2.3	17.6594	2.7	0.6445	3.0	0.0825	1.3	0.44	511.3	6.3	505.1	11.7	477.0	58.7	511.3	6.3	107.2
IX56-44	563	51798	5.8	17.1462	2.0	0.6725	2.1	0.0836	0.5	0.24	517.8	2.5	522.3	8.4	541.9	43.5	517.8	2.5	95.5
IX56-39	237	18320	4.4	17.1428	1.6	0.6767	2.2	0.0841	1.5	0.68	520.8	7.5	524.8	9.1	542.3	35.7	520.8	7.5	96.0
IX56-256	184	16100	3.1	17.5913	2.8	0.6611	3.0	0.0843	1.0	0.32	522.0	4.9	515.3	12.2	485.6	62.9	522.0	4.9	107.5
IX56-10	143	8762	2.0	17.0563	7.3	0.6880	7.4	0.0851	1.4	0.19	526.5	7.2	531.6	30.8	553.4	159.4	526.5	7.2	95.1
IX56-16	242	14560	0.7	17.4089	2.2	0.6759	2.5	0.0853	1.3	0.51	527.9	6.4	524.3	10.2	508.5	47.4	527.9	6.4	103.8
IX56-76	829	82054	2.9	17.2405	1.5	0.6850	2.4	0.0857	1.8	0.78	529.8	9.3	529.8	9.7	529.9	32.4	529.8	9.3	100.0
IX56-80	632	114524	7.2	17.2786	2.3	0.6859	2.5	0.0860	1.1	0.43	531.6	5.5	530.3	10.3	525.0	49.6	531.6	5.5	101.2
IX56-30	284	22718	5.8	17.3941	2.4	0.6829	2.8	0.0862	1.4	0.51	532.8	7.3	528.6	11.4	510.4	51.9	532.8	7.3	104.4
IX56-7	573	39466	3.8	17.2878	1.0	0.6894	1.4	0.0864	1.0	0.71	534.4	5.0	532.4	5.7	523.8	21.5	534.4	5.0	102.0
IX56-1	240	19090	2.3	17.1963	3.0	0.6933	4.0	0.0865	2.6	0.65	534.6	13.4	534.8	16.6	535.5	66.1	534.6	13.4	99.8
IX56-22	463	31158	2.6	17.2644	1.4	0.6936	1.8	0.0869	1.2	0.65	536.9	6.2	535.0	7.6	526.9	30.4	536.9	6.2	101.9
IX56-26	140	11904	1.4	17.5440	8.5	0.6834	8.9	0.0870	2.7	0.30	537.5	13.7	528.8	36.5	491.5	186.7	537.5	13.7	109.4
IX56-50	266	21204	2.1	17.2730	3.3	0.6957	3.7	0.0872	1.7	0.47	538.7	8.9	536.2	15.5	525.7	72.0	538.7	8.9	102.5
IX56-43	274	16252	1.1	17.1566	2.2	0.7022	2.3	0.0874	0.5	0.22	540.0	2.6	540.1	9.6	540.6	48.9	540.0	2.6	99.9
IX56-61	1920	5576	59.3	17.1091	3.5	0.7057	4.0	0.0876	1.8	0.46	541.2	9.4	542.2	16.7	546.6	77.1	541.2	9.4	99.0
IX56-28	27	6320	1.3	18.1614	16.9	0.6649	17.0	0.0876	2.2	0.13	541.2	11.4	517.6	69.1	414.7	379.7	541.2	11.4	130.5
IX56-11	105	8210	1.7	17.5513	4.3	0.6890	5.1	0.0877	2.7	0.53	542.0	14.0	532.2	21.0	490.6	94.5	542.0	14.0	110.5
IX56-42	193	14610	0.5	17.5617	2.9	0.6931	3.1	0.0883	1.2	0.37	545.3	6.1	534.6	13.0	489.3	64.2	545.3	6.1	111.5
IX56-47	66	10306	38.7	17.6381	4.2	0.6927	4.5	0.0886	1.8	0.40	547.3	9.5	534.4	18.9	479.7	92.2	547.3	9.5	114.1
IX56-42	276	25008	1.9	17.2117	2.1	0.7115	2.2	0.0888	0.7	0.31	548.5	3.6	545.6	9.2	533.5	45.1	548.5	3.6	102.8
IX56-51	114	8174	1.2	17.1005	4.5	0.7241	4.6	0.0898	0.6	0.13	554.4	3.1	553.1	19.4	547.7	98.8	554.4	3.1	101.2
IX56-8	167	13132	3.1	16.9862	3.0	0.7292	3.3	0.0898	1.4	0.42	554.5	7.3	556.1	13.9	562.3	64.4	554.5	7.3	98.6
IX56-41	80	7390	0.9	17.0677	4.5	0.7356	4.6	0.0911	1.0	0.21	561.8	5.2	559.9	19.8	551.9	98.3	561.8	5.2	101.8
IX56-11	72	5674	1.7	17.3558	5.0	0.7282	5.1	0.0917	1.2	0.23	565.4	6.5	555.5	21.9	515.2	109.3	565.4	6.5	109.7
IX56-29	86	6356	3.7	17.0530	2.6	0.7434	2.8	0.0919	0.8	0.29	567.0	4.4	564.4	12.0	553.8	57.7	567.0	4.4	102.4
IX56-75	123	31042	4.3	17.4092	4.4	0.7303	4.5	0.0922	1.0	0.23	568.6	5.6	556.8	19.3	508.5	96.5	568.6	5.6	111.8
IX56-5	135	8736	2.4	16.8365	2.0	0.7607	2.8	0.0929	2.0	0.69	572.6	10.8	574.4	12.5	581.6	44.4	572.6	10.8	98.5
IX56-6	121	13860	1.9	16.6911	5.0	0.7759	5.0	0.0939	0.8	0.16	578.7	4.5	583.1	22.3	600.4	107.7	578.7	4.5	96.4
IX56-77	531	47644	4.7	16.7594	2.9	0.7777	3.5	0.0945	2.0	0.56	582.2	11.0	584.1	15.7	591.6	63.8	582.2	11.0	98.4
IX56-53	462	27978	19.1	16.8443	2.5	0.7780	2.8	0.0950	1.3	0.45	585.3	7.1	584.4	12.5	580.6	54.5	585.3	7.1	100.8
IX56-17	276	48128	2.6	16.8246	2.5	0.7791	3.2	0.0951	2.0	0.62	585.4	11.0	585.0	14.1	583.1	53.9	585.4	11.0	100.4
IX56-27	114	27516	1.6	17.2893	5.3	0.7609	5.5	0.0954	1.5	0.26	587.5	8.2	574.5	24.3	523.7	117.4	587.5	8.2	112.2
IX56-46	129	14396	1.9	16.9897	3.0	0.7866	3.2	0.0969	0.9	0.28	596.4	5.0	589.3	14.1	561.9	66.0	596.4	5.0	106.1
IX56-20	431	39464	5.4	16.7872	1.7	0.7970	3.1	0.0970	2.6	0.84	597.1	14.6	595.2	13.7	588.0	36.1	597.1	14.6	101.5
IX56-19	443	27812	17.6	16.8028	2.1	0.8100	2.5	0.0987	1.3	0.52	606.9	7.5	602.5	11.3	586.0	46.1	606.9	7.5	103.6
IX56-21	341	25976	176.0	16.4903	1.9	0.8339	2.1	0.0997	0.8	0.39	612.9	4.7	615.8	9.7	626.5	41.8	612.9	4.7	97.8
IX56-5	197	30278	0.8	16.8090	2.5	0.8195	3.0	0.0999	1.6	0.52	613.8	9.1	607.8	13.6	585.2	55.1	613.8	9.1	104.9
IX56-13	34	3182	457.9	16.5873	2.2	0.8399	3.8	0.1010	3.1	0.81	620.5	18.1	619.1	17.6	613.9	48.3	620.5	18.1	101.1
IX56-44	220	17662	2.0	16.7025	2.3	0.8432	3.1	0.1021	2.2	0.69	627.0	12.8	620.9	14.6	598.9	49.4	627.0	12.8	104.7
IX56-25	66	13060	1.6	16.5364	1.5	0.8560	1.9	0.1027	1.2	0.61	630.0	7.1	627.9	9.0	620.5	32.9	630.0	7.1	101.5
IX56-36	558	26834	3.6	16.5514	2.4	0.8644	2.6	0.1038	1.0	0.38	636.5	5.8	632.5	12.1	618.6	51.2	636.5	5.8	102.9
IX56-39	255	59726	4.5	16.1371	2.6	0.8981	3.2	0.1051	1.9	0.58	644.3	11.4	650.7	15.5	673.0	56.4	644.3	11.4	95.7
IX56-10	140	19670	4.1	16.0494	3.2	0.9139	3.6	0.1064	1.7	0.47	651.7	10.4	659.1	17.4	684.7	67.6	651.7	10.4	95.2
IX56-15	314	15958	1.3	15.9188	2.8	0.9269	3.2	0.1070	1.5	0.46	655.4	9.2	666.0	15.7	702.1	60.6	655.4	9.2	93.3
IX56-19	154	15742	2.5	16.3499	2.2	0.9064	2.5	0.1075	1.3	0.51	658.1	7.9	655.1	12.1	645.0	46.3	658.1	7.9	102.0
IX56-67	180	72822	1.6	16.4000	2.1	0.9153	2.3	0.1089	0.9	0.38	666.2	5.4	659.9	11.0	638.4	45.2	666.2	5.4	104.4
IX56-40	210	41086	2.3	16.2120	1.7	0.9516	2.4	0.1119	1.7	0.70	683.7	10.9	678.9	11.8	663.1	36.5	683.7	10.9	103.1
IX56-73	494	64904	2.2	15.7557	0.8	1.0421	1.1	0.1191	0.8	0.67	725.3	5.2	725.0	5.9	724.0	18.0	725.3	5.2	100.2
IX56-58	311	32562	2.5	15.2066	2.3	1.1063	3.1	0.1220	2.1	0.67	742.1	14.9	756.4	16.8	798.8	48.8	742.1	14.9	92.9
IX56-12	116	12818	1.0	15.3587	1.9	1.1066	2.1	0.1233	0.8	0.37	749.3	5.5	756.5	11.2	777.9	40.9	749.3	5.5	96.3
IX56-31	475	57918	1.0	15.2371	1.9	1.1957	3.2	0.1321	2.6	0.80	800.0	19.2	798.6	17.6	794.5	39.9	800.0	19.2	100.7
IX56-18	238	47906	1.1	15.2746	3.6	1.2106	3.9	0.1341	1.4	0.36	811.3	10.6	805.5	21.5	789.4	75.9	811.3	10.6	102.8
IX56-41	247	40710	2.8	14.4190	2.5	1.3098	3.7	0.1370	2.8	0.74	827.6	21.4	850.1	21.5	909.2	51.6	827.6	21.4	91.0

Analysis	U (ppm)	206Pb 204Pb	U/Th	206Pb* 207Pb*	± (%)	207Pb* 235U*	± (%)	206Pb* 238U	± (%)	error corr.	206Pb* 238U*	± (Ma)	207Pb* 235U	± (Ma)	206Pb* 207Pb*	± (Ma)	Best age (Ma)	± (Ma)	Conc (%)
IX56-14	131	20932	1.5	14.7696	2.2	1.3617	2.4	0.1459	1.1	0.45	877.7	8.9	872.6	14.1	859.6	44.9	877.7	8.9	102.1
IX56-49	76	8074	2.5	14.5816	3.6	1.2718	3.7	0.1345	1.2	0.32	813.5	9.1	833.2	21.3	886.1	73.5	886.1	73.5	91.8
IX56-72	328	112666	2.9	14.4149	1.6	1.4454	3.9	0.1511	3.5	0.91	907.2	29.8	908.0	23.1	909.8	32.3	909.8	32.3	99.7
IX56-36	148	35070	8.3	13.8789	4.3	1.5228	4.5	0.1533	1.6	0.34	919.3	13.3	939.6	27.8	987.4	86.8	919.3	13.3	93.1
IX56-32	468	139216	2.3	14.0481	3.1	1.5768	3.5	0.1607	1.8	0.50	960.4	15.7	961.1	21.9	962.7	62.5	960.4	15.7	99.8
IX56-30	319	88592	1.3	13.9875	4.0	1.6509	4.2	0.1675	1.2	0.28	998.2	11.0	989.9	26.5	971.5	82.0	971.5	82.0	102.7
IX56-13	597	54328	2.3	13.9810	1.3	1.5866	1.6	0.1609	1.0	0.59	961.7	8.6	965.0	10.1	972.5	26.5	972.5	26.5	98.9
IX56-28	266	23110	3.6	13.8819	1.6	1.5138	4.2	0.1524	3.9	0.93	914.5	33.5	936.0	25.9	986.9	31.8	986.9	31.8	92.7
IX56-49	91	15206	1.0	13.8357	1.8	1.6891	2.1	0.1695	1.0	0.50	1009.3	9.6	1004.4	13.1	993.7	36.3	993.7	36.3	101.6
IX56-25	84	11068	1.9	13.8103	2.3	1.6310	2.4	0.1634	0.9	0.36	975.5	7.9	982.3	15.3	997.5	46.0	997.5	46.0	97.8
IX56-45	142	28404	1.7	13.7961	1.9	1.6628	2.4	0.1664	1.4	0.60	992.1	13.1	994.5	15.2	999.5	39.1	999.5	39.1	99.3
IX56-52	322	41612	3.0	13.7807	2.1	1.5277	4.3	0.1527	3.7	0.87	916.0	31.8	941.6	26.3	1001.8	43.5	1001.8	43.5	91.4
IX56-31	179	21046	2.2	13.7796	1.4	1.6467	2.7	0.1646	2.3	0.85	982.1	21.1	988.3	17.2	1002.0	29.0	1002.0	29.0	98.0
IX56-78	1084	24556	3.0	13.6242	3.2	1.2525	5.5	0.1238	4.5	0.82	752.2	32.1	824.5	31.2	1025.0	64.0	1025.0	64.0	73.4
IX56-6	201	23038	3.7	13.5769	1.8	1.7858	2.1	0.1758	1.0	0.50	1044.2	10.0	1040.3	13.5	1032.0	36.1	1032.0	36.1	101.2
IX56-70	91	120646	2.4	13.5539	3.1	1.8395	3.2	0.1808	0.5	0.16	1071.5	4.9	1059.7	20.9	1035.4	63.3	1035.4	63.3	103.5
IX56-33	72	6014	4.5	13.4579	3.2	1.5810	3.3	0.1543	1.0	0.30	925.1	8.5	962.8	20.6	1049.8	63.7	1049.8	63.7	88.1
IX56-34	69	8100	0.7	13.4578	2.9	1.8430	3.1	0.1799	1.1	0.37	1066.3	11.2	1060.9	20.3	1049.8	57.7	1049.8	57.7	101.6
IX56-33	187	19324	2.8	13.4237	3.3	1.7775	4.1	0.1731	2.5	0.60	1028.9	23.6	1037.3	26.9	1054.9	66.6	1054.9	66.6	97.5
IX56-15	234	26942	5.5	13.3252	2.5	1.7538	3.9	0.1695	3.0	0.77	1009.3	27.8	1028.6	25.1	1069.8	50.1	1069.8	50.1	94.4
IX56-45	135	22100	1.6	13.3151	1.9	1.8230	1.9	0.1760	0.5	0.27	1045.3	5.1	1053.8	12.8	1071.3	37.6	1071.3	37.6	97.6
IX56-64	102	42768	2.1	13.2934	1.7	1.9258	2.0	0.1857	1.1	0.56	1097.9	11.4	1090.1	13.4	1074.6	33.4	1074.6	33.4	102.2
IX56-79	114	20756	1.0	13.2340	4.3	1.7921	4.5	0.1720	1.3	0.29	1023.2	12.3	1042.6	29.3	1083.5	86.3	1083.5	86.3	94.4
IX56-38	751	97462	3.6	13.2130	3.8	1.7794	4.0	0.1705	1.2	0.30	1015.0	11.4	1038.0	26.0	1086.7	76.4	1086.7	76.4	93.4
IX56-16	134	49140	0.9	13.2112	3.0	2.0213	3.1	0.1937	0.6	0.18	1141.2	5.9	1122.7	20.8	1087.0	60.2	1087.0	60.2	105.0
IX56-81	547	116396	2.7	13.1876	1.9	1.8783	2.2	0.1796	1.1	0.51	1065.1	11.1	1073.5	14.7	1090.5	38.3	1090.5	38.3	97.7
IX56-55	234	17692	2.6	13.1167	1.6	1.9449	2.1	0.1850	1.4	0.66	1094.3	14.2	1096.7	14.4	1101.3	32.4	1101.3	32.4	99.4
IX56-29	89	25286	0.9	13.0636	2.8	2.0643	2.9	0.1956	0.7	0.26	1151.5	7.8	1137.0	19.8	1109.4	55.9	1109.4	55.9	103.8
IX56-84	206	11776	3.9	13.0323	4.7	1.9391	4.8	0.1833	1.1	0.23	1084.9	10.8	1094.7	32.2	1114.2	93.4	1114.2	93.4	97.4
IX56-74	155	19456	1.8	12.9864	1.3	2.0023	1.5	0.1886	0.6	0.41	1113.7	6.2	1116.3	10.0	1121.3	26.8	1121.3	26.8	99.3
IX56-17	655	80254	5.8	12.8719	1.1	1.9131	1.8	0.1786	1.4	0.80	1059.3	14.0	1085.7	12.0	1138.9	21.7	1138.9	21.7	93.0
IX56-52	316	72206	2.3	12.7564	3.2	2.0121	3.4	0.1862	1.2	0.35	1100.5	11.9	1119.6	23.0	1156.8	63.1	1156.8	63.1	95.1
IX56-37	702	201114	5.0	12.7440	2.8	2.1842	3.7	0.2019	2.5	0.67	1185.4	27.3	1176.0	26.0	1158.7	54.7	1158.7	54.7	102.3
IX56-9	398	55542	1.5	12.7243	2.2	2.1475	2.4	0.1982	0.9	0.38	1165.6	9.9	1164.3	16.8	1161.8	44.4	1161.8	44.4	100.3
IX56-35	203	7164	3.6	12.7190	5.2	1.7961	6.9	0.1657	4.6	0.66	988.3	41.8	1044.0	45.1	1162.6	103.0	1162.6	103.0	85.0
IX56-4	258	39466	4.3	12.4573	5.1	1.9575	5.7	0.1769	2.7	0.46	1049.8	25.7	1101.0	38.6	1203.7	100.3	1203.7	100.3	87.2
IX56-21	157	50054	2.1	12.1222	2.1	2.4612	2.1	0.2164	0.5	0.23	1262.7	5.7	1260.7	15.5	1257.3	40.7	1257.3	40.7	100.4
IX56-14	224	36992	1.8	11.6465	1.6	2.6085	5.1	0.2203	4.8	0.95	1283.7	56.0	1303.0	37.1	1335.1	30.2	1335.1	30.2	96.2
IX56-8	72	17082	2.6	11.5253	1.1	2.6694	2.8	0.2231	2.5	0.92	1298.4	29.6	1320.0	20.3	1355.3	21.3	1355.3	21.3	95.8
IX56-46	183	29378	2.2	11.2677	0.9	2.9685	1.0	0.2426	0.5	0.52	1400.2	6.7	1399.6	7.7	1398.7	16.5	1398.7	16.5	100.1
IX56-20	109	16248	2.7	10.2038	2.8	3.4328	2.9	0.2540	0.7	0.26	1459.3	9.5	1511.9	22.5	1586.4	51.6	1586.4	51.6	92.0
IX56-66	94	70268	2.2	9.8135	2.6	4.2103	2.7	0.2997	0.7	0.27	1689.6	10.9	1676.0	22.3	1659.0	48.6	1659.0	48.6	101.8
IX56-60	531	35362	1.4	9.3943	1.1	4.5707	1.4	0.3114	1.0	0.67	1747.7	14.5	1743.9	11.9	1739.4	19.5	1739.4	19.5	100.5
IX56-35	518	185112	1.3	9.3206	2.4	4.7162	3.6	0.3188	2.7	0.74	1783.9	41.5	1770.1	30.0	1753.9	43.7	1753.9	43.7	101.7
IX56-23	62	15324	1.4	9.0155	2.1	5.0107	2.3	0.3276	0.7	0.32	1826.9	11.6	1821.1	19.1	1814.5	38.7	1814.5	38.7	100.7
IX56-69	99	43048	1.4	8.8868	1.9	4.7086	2.4	0.3035	1.5	0.60	1708.6	21.9	1768.8	20.4	1840.6	35.2	1840.6	35.2	92.8
IX56-24	224	120282	3.5	8.4423	2.1	5.8250	3.4	0.3567	2.7	0.78	1966.3	45.6	1950.1	29.8	1933.0	38.3	1933.0	38.3	101.7
IX56-82	231	177016	2.3	8.1772	1.7	5.4273	2.9	0.3219	2.4	0.82	1798.9	36.9	1889.2	24.6	1989.9	29.3	1989.9	29.3	90.4
IX56-7	222	48072	2.4	8.1003	2.0	6.1990	2.4	0.3642	1.4	0.57	2002.0	23.4	2004.3	20.8	2006.7	34.6	2006.7	34.6	99.8
IX56-18	180	46868	2.7	7.8493	0.8	6.6470	1.8	0.3784	1.6	0.89	2068.8	28.3	2065.6	15.9	2062.4	14.7	2062.4	14.7	100.3
IX56-3	484	53308	2.7	5.5510	1.6	9.9776	2.1	0.4017	1.3	0.63	2176.8	24.0	2432.7	19.0	2654.2	26.4	2654.2	26.4	82.0
IX56-4	101	35678	2.3	5.3558	0.9	12.9825	1.9	0.5043	1.7	0.88	2632.2	36.3	2678.4	18.1	2713.4	15.2	2713.4	15.2	97.0
IX56-32	149	28202	2.1	5.2834	1.2	12.5704	1.9	0.4817	1.4	0.77	2534.6	30.0	2648.0	17.4	2735.8	19.4	2735.8	19.4	92.6
IX56-1	435	227336	1.4	4.8756	2.2	16.0126	3.1	0.5662	2.2	0.71	2892.3	52.0	2877.5	30.1	2867.2	36.1	2867.2	36.1	100.9
IX56-48	219	75358	3.0	4.7580	1.9	15.3990	2.5	0.5314	1.6	0.65	2747.3	36.2	2840.2	23.8	2906.9	30.8	2906.9	30.8	94.5
IX56-2	136	73872	0.9	4.2981	2.2	19.8225	3.4	0.6179	2.7	0.78	3101.6	66.2	3082.7	33.4	3070.4	34.5	3070.4	34.5	101.0
IX56-65	768	245052	2.0	4.1172	1.1	19.7808	2.5	0.5907	2.3	0.91	2992.1	54.6	3080.7	24.3	3139.0	17.0	3139.0	17.0	95.3
x 57 UTM: LAT 0519478, LONG 1989744																			
IX57-33	150	18234	5.1	14.3294	1.6	1.2611	2.3	0.1311	1.6	0.69	793.9	11.7	828.4	12.8	922.1	33.5	793.9	11.7	86.1
IX57-7	152	14914	3.7	14.4138	3.0	1.3893	3.2	0.1452	1.0	0.30	874.2	7.9	884.4	18.9	910.0	62.7	874.2	7.9	96.1
IX57-28	286	47712	1.8	14.4066	1.8	1.4053	2.1	0.1468	1.2	0.56	883.2	9.9	891.2	12.7	911.0	36.7	883.2	9.9	97.0
IX57-44	354	21094	3.0	13.8957	2.0	1.5003	2.3	0.1512	1.0	0.45	907.7	8.7	930.5	13.9	985.0	41.5	907.7	8.7	92.2
IX57-25	247	21530	2.9	14.1937	1.4	1.4724	1.6	0.1516	0.9	0.52	909.8	7.2	919.1	9.9	941.6	28.9	909.8	7.2	96.6
IX57-5	591	96504	13.1	14.0373	2.4	1.5006	2.6	0.1528	1.0	0.37	916.5	8.1	930.6	15.8	964.3	49.4	916.5	8.1	95.0
IX57-32	959	100042	9.7	14.4344	3.6	1.4847	4.2	0.1554	2.1	0.50	931.3	18.0	924.1	25.3	907.0	74.6	931.3	18.0	102.7
IX57-17	346	51464	1.7	13.9961	1.3	1.5492	2.0	0.1573	1.5	0.76	941.5	13.0	950.2	12.1	970.3	26.2	941.5	13.0	97.0
IX57-31	205	45934	2.7	13.9642	0.9	1.5832	1.9	0.1603	1.7	0.89	958.7	15.4	963.6	12.1	974.9	18.2	958.7	15.4	98.3
IX57-4	212	25524	4.0	13.7642	2.1	1.6419	2.2	0.1639	0.6	0.27	978.4	5.5	986.4	14.1	1004.2	43.5	1004.2	43.5	97.4
IX57-1	331	47504	1.4	13.5037	1.8	1.7865	4.4	0.1750	4.0	0.91	1039.4	38.5	1040.6	28.7	1042.9	37.2	1042.9	37.2	99.7
IX57-13	346	75904	4.9	13.4898	2.5	1.6282	3.0	0.1593	1.7	0.57	952.9	15.1	981.2	19.0	1045.0	50.1	1045.0	50.1	91.2

Analysis	U (ppm)	206Pb 204Pb	U/Th	206Pb* 207Pb*	± (%)	207Pb* 235U*	± (%)	206Pb* 238U	± (%)	error corr.	206Pb* 238U*	± (Ma)	207Pb* 235U	± (Ma)	206Pb* 207Pb*	± (Ma)	Best age (Ma)	± (Ma)	Conc (%)
IX57-20	143	26702	2.6	13.3555	2.3	1.9057	2.4	0.1846	0.7	0.28	1092.0	6.8	1083.1	16.0	1065.2	46.3	1065.2	46.3	102.5
IX57-15A	148	26384	2.0	13.1203	1.8	1.7264	2.3	0.1643	1.4	0.62	980.5	12.7	1018.4	14.5	1100.8	35.3	1100.8	35.3	89.1
IX57-18	68	16758	2.2	13.0063	2.9	1.8033	3.3	0.1701	1.7	0.52	1012.7	16.2	1046.6	21.8	1118.3	57.0	1118.3	57.0	90.6
IX57-8	55	19432	3.7	12.8628	2.9	2.0120	3.1	0.1877	1.0	0.31	1108.9	9.7	1119.6	21.0	1140.3	58.6	1140.3	58.6	97.2
IX57-15	360	97342	3.6	12.8525	1.4	1.9817	1.8	0.1847	1.1	0.62	1092.7	11.0	1109.3	11.8	1141.9	27.2	1141.9	27.2	95.7
IX57-11	212	72256	2.5	12.8246	1.4	1.9312	2.4	0.1796	1.9	0.81	1064.9	18.8	1092.0	15.9	1146.2	27.7	1146.2	27.7	92.9
IX57-22	141	27496	2.6	12.8203	1.6	2.1209	1.8	0.1972	0.8	0.43	1160.3	8.0	1155.6	12.1	1146.9	31.6	1146.9	31.6	101.2
IX57-30	116	21132	3.8	12.8158	1.1	2.0039	2.6	0.1863	2.4	0.91	1101.1	23.8	1116.8	17.5	1147.6	21.0	1147.6	21.0	95.9
IX57-14	43	17834	2.8	12.8102	3.2	1.9657	3.2	0.1826	0.5	0.16	1081.3	5.0	1103.8	21.6	1148.4	63.0	1148.4	63.0	94.2
IX57-19	437	80026	4.9	12.7725	2.4	2.0874	2.4	0.1934	0.6	0.24	1139.6	6.1	1144.7	16.8	1154.3	47.0	1154.3	47.0	98.7
IX57-16	225	55082	5.6	12.7604	2.2	1.9928	2.5	0.1844	1.3	0.51	1091.1	12.9	1113.1	17.1	1156.2	43.3	1156.2	43.3	94.4
IX57-12	327	56172	3.8	12.6995	1.7	2.0351	1.9	0.1874	0.8	0.44	1107.5	8.5	1127.3	12.9	1165.7	33.7	1165.7	33.7	95.0
IX57-3	149	29826	2.8	12.5883	2.0	2.2457	2.1	0.2050	0.6	0.28	1202.3	6.5	1195.4	14.9	1183.1	40.1	1183.1	40.1	101.6
IX57-42	237	54764	3.6	12.5790	1.5	2.1280	1.9	0.1941	1.2	0.61	1143.7	12.1	1157.9	13.1	1184.6	29.9	1184.6	29.9	96.6
IX57-10	155	21378	2.8	12.4133	1.2	2.2236	1.4	0.2002	0.8	0.52	1176.3	8.1	1188.5	10.1	1210.7	24.3	1210.7	24.3	97.2
IX57-48	228	29306	4.0	12.4040	3.5	2.1246	4.1	0.1911	2.2	0.53	1127.5	22.4	1156.8	28.3	1212.2	68.5	1212.2	68.5	93.0
IX57-38	226	42084	2.5	12.3970	2.4	2.3272	3.2	0.2092	2.1	0.66	1224.8	23.4	1220.6	22.7	1213.3	47.5	1213.3	47.5	100.9
IX57-26	415	104178	2.8	12.3931	1.5	1.9141	4.5	0.1720	4.3	0.94	1023.4	40.5	1086.0	30.2	1213.9	29.3	1213.9	29.3	84.3
IX57-39	146	32294	1.8	12.3318	2.2	2.3270	2.4	0.2081	0.8	0.34	1218.8	9.0	1220.6	16.9	1223.6	44.1	1223.6	44.1	99.6
IX57-27	95	28168	2.5	12.2631	1.7	2.2225	2.0	0.1977	1.0	0.49	1162.8	10.4	1188.2	13.9	1234.6	33.8	1234.6	33.8	94.2
IX57-46	135	31932	3.9	12.0927	2.0	2.3647	2.7	0.2074	1.7	0.65	1214.9	19.2	1232.0	19.0	1262.0	39.5	1262.0	39.5	96.3
IX57-23	88	31360	1.4	12.0473	2.0	2.3379	2.1	0.2043	0.5	0.24	1198.2	5.5	1223.9	14.7	1269.3	39.1	1269.3	39.1	94.4
IX57-40	152	32456	1.9	12.0203	2.4	2.4616	2.9	0.2146	1.6	0.57	1253.3	18.7	1260.8	20.8	1273.7	46.3	1273.7	46.3	98.4
IX57-45	164	31340	3.8	12.0184	3.4	2.2870	4.6	0.1993	3.1	0.67	1171.8	33.1	1208.3	32.5	1274.1	66.5	1274.1	66.5	92.0
IX57-47	149	31938	3.3	12.0118	2.8	2.3823	3.1	0.2075	1.3	0.42	1215.7	14.5	1237.3	22.3	1275.1	55.2	1275.1	55.2	95.3
IX57-9	254	53290	4.6	11.7871	1.5	2.4300	2.7	0.2077	2.2	0.82	1216.7	24.4	1251.5	19.3	1311.8	29.7	1311.8	29.7	92.8
IX57-37	94	6724	1.3	11.7557	6.4	2.6392	6.6	0.2250	1.6	0.23	1308.3	18.4	1311.6	48.7	1317.0	124.7	1317.0	124.7	99.3
IX57-21	315	77852	2.7	11.5086	1.7	2.6057	1.8	0.2175	0.6	0.33	1268.6	6.8	1302.3	13.2	1358.1	32.8	1358.1	32.8	93.4
IX57-35	280	81980	10.0	11.4604	1.2	2.6531	1.9	0.2205	1.4	0.75	1284.6	16.3	1315.5	13.7	1366.2	23.7	1366.2	23.7	94.0
IX57-41	325	23006	5.8	11.1663	4.4	2.9331	4.5	0.2375	0.6	0.13	1373.9	7.4	1390.5	33.9	1416.0	84.9	1416.0	84.9	97.0
IX57-29	141	45930	3.5	11.0501	2.0	3.1490	2.4	0.2524	1.3	0.55	1450.7	17.3	1444.8	18.6	1436.0	38.4	1436.0	38.4	101.0
IX57-6	165	41728	3.6	10.8664	1.7	3.0587	1.8	0.2411	0.6	0.33	1392.2	7.6	1422.4	14.0	1467.9	32.7	1467.9	32.7	94.8
IX57-36A	117	36318	3.5	10.8526	2.4	3.2106	2.6	0.2527	1.1	0.43	1452.4	14.4	1459.7	20.2	1470.3	44.8	1470.3	44.8	98.8
IX57-43	158	55140	3.6	10.4575	2.1	3.3439	2.5	0.2536	1.5	0.57	1457.1	18.9	1491.4	19.8	1540.4	38.9	1540.4	38.9	94.6
IX57-24	428	90416	2.6	10.3907	1.4	3.4933	1.7	0.2633	1.0	0.58	1506.5	13.3	1525.7	13.5	1552.5	26.3	1552.5	26.3	97.0
IX57-2	106	21652	1.7	10.2158	1.6	3.7538	1.8	0.2781	0.8	0.47	1581.9	11.8	1582.9	14.4	1584.2	29.6	1584.2	29.6	99.9
Ix 63 UTM: LAT 0521927 LONG 1992600			Barranca Grande sample close to Los Laureles Dacite of ~61 Ma (Ortega-Obregón et al., 2009 and present paper)																
IX63-2	514	80454	7.2	14.1227	2.4	1.5980	2.5	0.1637	0.5	0.20	977.2	4.5	969.4	15.4	951.9	49.3	977.2	4.5	102.7
IX63-91	1099	10900	11.2	21.0112	5.8	0.0627	6.1	0.0096	1.8	0.29	61.3	1.1	61.8	3.6	79.1	137.7	61.3	1.1	77.6
IX63-97A	726	19680	10.3	20.9380	6.9	0.0631	8.2	0.0096	4.4	0.54	61.5	2.7	62.1	4.9	87.4	164.3	61.5	2.7	70.3
IX63-8	473	4846	12.8	21.1923	4.8	0.0627	5.1	0.0096	1.9	0.36	61.8	1.2	61.8	3.1	58.7	114.4	61.8	1.2	105.3
IX63-97	655	13286	9.3	18.3599	5.6	0.0915	7.5	0.0122	5.1	0.67	78.1	3.9	88.9	6.4	390.4	125.4	78.1	3.9	20.0
IX63-55	614	37760	2.4	18.9156	2.6	0.3745	3.1	0.0514	1.7	0.55	322.9	5.4	322.9	8.7	323.1	59.7	322.9	5.4	99.9
IX63-9	261	10122	1.5	18.3751	5.0	0.4039	5.2	0.0538	1.2	0.24	337.9	4.1	344.4	15.1	388.5	113.1	337.9	4.1	87.0
IX63-69A	680	63802	3.2	18.5941	1.7	0.4185	2.1	0.0564	1.2	0.57	354.0	4.1	355.0	6.2	361.8	38.0	354.0	4.1	97.8
IX63-69	593	234288	3.0	18.6192	3.1	0.4198	3.2	0.0567	0.7	0.23	355.4	2.5	355.9	9.5	358.8	69.5	355.4	2.5	99.1
IX63-85	170	29530	2.7	18.7731	2.8	0.4335	3.0	0.0590	0.9	0.30	369.7	3.2	365.7	9.1	340.2	63.8	369.7	3.2	108.7
IX63-58	675	27496	2.3	18.5919	2.7	0.4466	2.9	0.0602	1.2	0.42	377.0	4.5	374.9	9.2	362.1	59.8	377.0	4.5	104.1
IX63-29	352	19298	2.5	18.4375	3.1	0.4524	3.3	0.0605	1.2	0.37	378.7	4.6	379.0	10.6	380.9	69.7	378.7	4.6	99.4
IX63-10	270	9318	2.6	18.5378	3.0	0.4561	3.3	0.0613	1.4	0.43	383.7	5.3	381.6	10.5	368.7	67.2	383.7	5.3	104.1
IX63-35	569	217104	3.3	17.8498	1.3	0.4757	2.7	0.0616	2.3	0.86	385.2	8.6	395.1	8.7	453.3	29.8	385.2	8.6	85.0
IX63-38	149	17946	1.4	18.2110	2.6	0.5504	3.1	0.0727	1.7	0.54	452.4	7.4	445.2	11.3	408.6	58.9	452.4	7.4	110.7
IX63-96	132	16774	1.9	18.0668	5.2	0.5883	5.4	0.0771	1.5	0.28	478.7	6.9	469.8	20.2	426.4	115.2	478.7	6.9	112.3
IX63-61	596	34382	3.2	17.4974	2.6	0.6155	3.0	0.0781	1.5	0.49	484.9	6.8	487.1	11.5	497.4	57.4	484.9	6.8	97.5
IX63-82	821	157870	2.8	17.0348	2.2	0.6465	2.3	0.0799	0.7	0.30	495.4	3.3	506.3	9.2	556.1	48.2	495.4	3.3	89.1
IX63-22	173	11610	1.2	17.7095	3.2	0.6227	3.6	0.0800	1.5	0.42	496.0	7.2	491.5	13.9	470.8	71.9	496.0	7.2	105.4
IX63-45	237	30130	2.0	17.7519	3.5	0.6328	3.7	0.0815	1.0	0.27	504.9	4.8	497.8	14.4	465.5	78.3	504.9	4.8	108.5
IX63-53	241	25348	15.9	17.0561	2.6	0.6673	3.0	0.0826	1.4	0.48	511.3	7.0	519.1	12.1	553.4	57.1	511.3	7.0	92.4
IX63-36	595	52450	13.4	16.8281	1.8	0.6778	4.2	0.0827	3.7	0.90	512.4	18.4	525.4	17.0	582.7	39.2	512.4	18.4	87.9
IX63-99	463	40158	2.5	17.4455	2.8	0.6596	4.3	0.0835	3.2	0.74	516.7	15.7	514.4	17.2	503.9	62.7	516.7	15.7	102.6
IX63-73	172	115800	1.0	17.0552	3.1	0.6822	3.4	0.0844	1.5	0.43	522.2	7.3	528.1	13.9	553.5	66.6	522.2	7.3	94.4
IX63-100	167	19428	1.9	16.8371	10.6	0.7088	10.6	0.0866	0.7	0.06	535.1	3.4	544.0	44.7	581.5	230.7	535.1	3.4	92.0
IX63-64	231	11818	3.0	16.6120	3.7	0.7198	4.4	0.0867	2.5	0.56	536.2	12.6	550.6	18.7	610.7	79.0	536.2	12.6	87.8
IX63-11	343	23802	14.7	16.3999	1.2	0.7316	1.7	0.0870	1.2	0.71	537.9	6.3	557.5	7.4	638.4	26.1	537.9	6.3	84.3
IX63-12	181	11748	2.8	16.9634	2.4	0.7134	2.8	0.0878	1.4	0.49	542.3	7.1	546.8	11.8	565.2	52.8	542.3	7.1	95.9
IX63-43	188	19122	0.8	17.1293	3.2	0.7144	4.0	0.0888	2.4	0.60	548.2	12.7	547.4	17.0	544.0	69.8	548.2	12.7	100.8
IX63-19	288	34874	0.4	16.6151	3.2	0.7399	3.6	0.0892	1.5	0.43	550.5	8.1	562.3	15.4	610.3	69.3	550.5	8.1	90.2
IX63-90	97	83432	1.8	17.1687	5.7	0.7186	6.1	0.0895	2.2	0.36	552.4	11.8	549.8	26.0	539.0	125.1	552.4	11.8	102.5

Analysis	U (ppm)	206Pb 204Pb	U/Th	206Pb* 207Pb*	± (%)	207Pb* 235U*	± (%)	206Pb* 238U	± (%)	error corr.	206Pb* 238U*	± (Ma)	207Pb* 235U	± (Ma)	206Pb* 207Pb*	± (Ma)	Best age (Ma)	± (Ma)	Conc (%)
IX63-16	371	23422	1.3	17.0505	2.6	0.7260	2.7	0.0898	0.8	0.31	554.2	4.4	554.2	11.5	554.1	56.1	554.2	4.4	100.0
IX63-21	65	4090	0.5	16.3488	8.3	0.7612	8.3	0.0903	0.9	0.11	557.1	4.7	574.7	36.6	645.1	178.3	557.1	4.7	86.4
IX63-84	55	37874	0.6	16.9598	9.6	0.7356	10.4	0.0905	4.1	0.39	558.4	22.0	559.9	44.9	565.7	209.2	558.4	22.0	98.7
IX63-67	530	225768	5.2	16.9424	1.9	0.7375	2.6	0.0906	1.8	0.70	559.2	9.8	560.9	11.3	568.0	40.9	559.2	9.8	98.5
IX63-83	205	19750	2.6	16.8983	2.2	0.7446	2.6	0.0913	1.4	0.52	563.0	7.3	565.1	11.3	573.6	48.5	563.0	7.3	98.1
IX63-95A	39	2912	0.5	16.0557	4.7	0.7840	6.8	0.0913	4.9	0.72	563.2	26.4	587.8	30.4	683.9	101.2	563.2	26.4	82.4
IX63-39	497	88378	1.0	17.2722	2.2	0.7289	2.6	0.0913	1.3	0.51	563.3	7.1	555.9	11.1	525.8	48.7	563.3	7.1	107.1
IX63-56	384	35754	5.1	17.1793	2.7	0.7343	2.9	0.0915	1.1	0.38	564.4	6.1	559.1	12.6	537.7	59.4	564.4	6.1	105.0
IX63-93	149	18380	3.3	17.1416	5.5	0.7363	5.5	0.0915	1.0	0.18	564.6	5.4	560.2	23.9	542.5	119.3	564.6	5.4	104.1
IX63-23	386	37112	2.3	16.8888	2.9	0.7500	4.2	0.0919	3.1	0.73	566.5	16.8	568.2	18.3	574.8	62.1	566.5	16.8	98.6
IX63-44	417	48352	15.3	17.1117	2.8	0.7475	3.5	0.0928	2.0	0.58	571.9	11.0	566.8	15.1	546.3	62.1	571.9	11.0	104.7
IX63-24	535	35412	5.4	17.0971	2.4	0.7536	2.4	0.0934	0.5	0.21	575.9	2.8	570.3	10.5	548.2	51.4	575.9	2.8	105.1
IX63-28	148	17518	1.3	17.0609	2.9	0.7600	3.4	0.0940	1.8	0.54	579.4	10.2	574.0	14.9	552.8	62.5	579.4	10.2	104.8
IX63-4	963	87608	13.4	16.7067	1.5	0.7820	1.8	0.0948	0.9	0.53	583.6	5.2	586.6	7.9	598.4	32.5	583.6	5.2	97.5
IX63-41	335	31148	3.6	16.9916	2.8	0.7714	3.1	0.0951	1.4	0.46	585.4	8.0	580.6	13.8	561.6	60.2	585.4	8.0	104.2
IX63-37	392	64186	24.9	17.0059	2.2	0.7759	2.9	0.0957	1.9	0.66	589.2	10.8	583.2	12.9	559.8	47.8	589.2	10.8	105.2
IX63-71	652	101760	21.8	16.1384	2.1	0.8258	2.7	0.0967	1.8	0.65	594.8	10.2	611.3	12.6	672.9	44.3	594.8	10.2	88.4
IX63-48	847	45058	2.5	16.8877	1.6	0.7943	1.7	0.0973	0.5	0.30	598.5	2.9	593.6	7.6	575.0	34.9	598.5	2.9	104.1
IX63-81	208	51706	2.3	15.3907	1.4	0.8755	1.5	0.0977	0.5	0.34	601.1	3.0	638.6	7.1	773.5	29.8	601.1	3.0	77.7
IX63-62	119	13194	2.7	16.3606	1.2	0.8309	2.0	0.0986	1.6	0.81	606.1	9.5	614.1	9.4	643.6	26.0	606.1	9.5	94.2
IX63-30	181	14710	1.0	15.8373	2.2	0.8702	2.8	0.1000	1.7	0.61	614.1	9.9	635.7	13.1	713.0	46.4	614.1	9.9	86.1
IX63-94	257	21550	4.6	16.1545	2.6	0.8615	3.7	0.1009	2.6	0.70	619.9	15.2	630.9	17.3	670.7	56.3	619.9	15.2	92.4
IX63-3	287	21496	1.2	16.6506	1.6	0.8403	3.0	0.1015	2.5	0.84	623.0	14.9	619.3	13.8	605.6	34.7	623.0	14.9	102.9
IX63-57	323	23552	17.0	15.8451	1.1	0.8920	1.4	0.1025	0.8	0.59	629.1	5.0	647.4	6.8	712.0	24.4	629.1	5.0	88.4
IX63-52	575	52424	27.8	16.0119	2.6	0.8835	3.5	0.1026	2.3	0.66	629.7	13.7	642.9	16.5	689.7	55.7	629.7	13.7	91.3
IX63-13	102	8380	1.8	16.1612	1.8	0.8758	2.0	0.1027	0.8	0.39	630.0	4.6	638.7	9.3	669.8	38.7	630.0	4.6	94.0
IX63-50	286	30468	3.4	16.4295	2.5	0.8705	2.5	0.1037	0.5	0.20	636.2	3.0	635.8	12.0	634.5	53.4	636.2	3.0	100.3
IX63-65	100	9474	2.9	16.3754	2.0	0.8818	2.9	0.1047	2.1	0.72	642.0	12.6	641.9	13.6	641.6	42.5	642.0	12.6	100.1
IX63-27	287	28720	2.0	15.8249	2.5	0.9262	3.2	0.1063	2.0	0.62	651.2	12.1	665.6	15.5	714.7	53.1	651.2	12.1	91.1
IX63-54	209	49586	2.6	15.9857	2.4	0.9186	2.5	0.1065	0.7	0.28	652.4	4.3	661.6	12.3	693.2	51.6	652.4	4.3	94.1
IX63-78	174	29246	2.3	15.1891	3.5	0.9759	3.8	0.1075	1.5	0.39	658.2	9.1	691.5	19.0	801.2	73.0	658.2	9.1	82.2
IX63-66	102	37310	1.0	16.1311	1.1	0.9386	1.2	0.1098	0.5	0.41	671.6	3.2	672.1	6.0	673.8	23.7	671.6	3.2	99.7
IX63-31	99	8354	0.7	15.9858	1.8	0.9675	2.0	0.1122	0.9	0.47	685.4	6.0	687.2	9.9	693.1	37.6	685.4	6.0	98.9
IX63-70	106	71516	2.4	14.3666	4.0	1.0943	4.1	0.1140	1.0	0.24	696.0	6.6	750.6	21.7	916.8	81.8	696.0	6.6	75.9
IX63-42	124	13038	4.8	15.9132	1.6	0.9994	1.9	0.1153	0.9	0.47	703.7	5.9	703.5	9.4	702.9	34.7	703.7	5.9	100.1
IX63-60	216	20788	8.2	14.7943	3.2	1.1255	3.4	0.1208	1.1	0.32	735.0	7.7	765.6	18.4	856.1	67.1	735.0	7.7	85.9
IX63-68	277	141306	3.3	14.1575	3.1	1.2231	7.1	0.1256	6.4	0.90	762.7	45.8	811.2	39.5	946.8	62.7	762.7	45.8	80.5
IX63-77	46	17508	2.4	14.5617	1.3	1.2021	2.8	0.1270	2.5	0.88	770.5	18.1	801.5	15.6	888.9	27.3	770.5	18.1	86.7
IX63-40	233	24984	2.5	15.1699	1.8	1.2343	2.0	0.1358	0.8	0.39	820.9	6.1	816.3	11.2	803.8	38.6	820.9	6.1	102.1
IX63-75	378	31248	3.6	15.2221	2.3	1.2487	2.4	0.1379	0.7	0.28	832.5	5.4	822.8	13.8	796.6	49.2	832.5	5.4	104.5
IX63-18	170	36624	1.7	13.7782	2.6	1.4234	4.4	0.1422	3.6	0.81	857.3	29.1	898.8	26.5	1002.2	52.5	857.3	29.1	85.5
IX63-74	493	59248	4.5	13.9310	3.4	1.5072	4.1	0.1523	2.3	0.56	913.8	19.3	933.3	24.8	979.8	68.5	913.8	19.3	93.3
IX63-59	56	7980	2.3	13.7227	2.4	1.7603	2.5	0.1752	0.6	0.22	1040.7	5.3	1031.0	16.2	1010.4	49.6	1010.4	49.6	103.0
IX63-51	97	19798	3.5	13.4095	2.6	1.8732	3.2	0.1822	1.9	0.58	1078.8	18.5	1071.6	21.2	1057.1	52.3	1057.1	52.3	102.1
IX63-72	179	343142	1.7	13.3693	1.7	1.6708	1.9	0.1620	0.8	0.40	967.9	6.8	997.5	12.1	1063.1	35.0	1063.1	35.0	91.0
IX63-34	125	59594	4.2	13.2224	2.7	1.7855	3.2	0.1712	1.7	0.53	1018.8	16.1	1040.2	20.9	1085.3	54.6	1085.3	54.6	93.9
IX63-7	231	12532	3.2	13.2156	2.8	1.7483	3.5	0.1676	2.1	0.60	998.7	19.5	1026.5	22.9	1086.3	57.0	1086.3	57.0	91.9
IX63-32	79	14694	2.6	13.2141	3.1	1.7615	3.6	0.1688	1.9	0.52	1005.6	17.5	1031.4	23.5	1086.5	62.1	1086.5	62.1	92.5
IX63-20	277	44322	5.9	13.1955	2.4	1.8963	2.5	0.1815	0.7	0.26	1075.1	6.4	1079.8	16.7	1089.3	48.6	1089.3	48.6	98.7
IX63-88	217	86274	3.6	13.1287	1.5	1.8882	1.7	0.1798	0.7	0.43	1065.8	7.2	1076.9	11.3	1099.5	30.8	1099.5	30.8	96.9
IX63-33	176	53432	3.6	13.0944	2.4	1.9162	2.6	0.1820	1.0	0.38	1077.8	9.7	1086.7	17.1	1104.8	47.2	1104.8	47.2	97.6
IX63-46	1035	165046	1.7	13.0791	2.2	1.9016	3.5	0.1804	2.7	0.78	1069.1	26.7	1081.6	23.0	1107.1	43.0	1107.1	43.0	96.6
IX63-98	45	11370	3.0	13.0408	1.4	1.9569	1.7	0.1851	0.9	0.55	1094.7	9.4	1100.8	11.4	1112.9	28.1	1112.9	28.1	98.4
IX63-92	346	60002	6.1	12.9848	2.0	1.8906	2.2	0.1780	0.9	0.41	1056.3	8.7	1077.8	14.3	1121.5	39.1	1121.5	39.1	94.2
IX63-86	347	107404	2.1	12.9168	2.0	2.0470	2.2	0.1918	0.8	0.35	1130.9	8.0	1131.3	14.8	1132.0	40.5	1132.0	40.5	99.9
IX63-6	131	22128	2.0	12.3574	2.4	2.2656	2.7	0.2031	1.2	0.45	1191.7	13.4	1201.6	19.2	1219.6	47.8	1219.6	47.8	97.7
IX63-95	384	69744	13.9	12.0696	2.7	1.9182	7.0	0.1679	6.4	0.92	1000.6	59.3	1087.4	46.4	1265.7	52.9	1265.7	52.9	79.1
IX63-87	37	33764	1.0	11.6510	4.5	2.6280	4.6	0.2221	0.7	0.15	1292.8	8.1	1308.5	33.8	1334.3	88.0	1334.3	88.0	96.9
IX63-89	64	36626	2.3	10.7545	1.4	3.2581	1.6	0.2541	0.9	0.55	1459.7	11.9	1471.1	12.8	1487.5	26.0	1487.5	26.0	98.1
IX63-80	177	73236	3.0	9.9006	2.1	3.3513	2.4	0.2406	1.2	0.50	1390.0	15.3	1493.1	18.9	1642.6	38.8	1642.6	38.8	84.6
IX63-5	629	88064	6.5	9.3835	2.0	4.1241	2.7	0.2807	1.9	0.69	1594.7	26.7	1659.1	22.4	1741.5	36.3	1741.5	36.3	91.6
IX63-76	255	95706	2.1	9.1511	2.9	4.8055	3.7	0.3189	2.4	0.64	1784.6	37.6	1785.9	31.5	1787.4	52.3	1787.4	52.3	99.8
IX63-17	399	87388	8.1	7.9929	1.1	6.3338	2.5	0.3672	2.2	0.90	2016.1	38.6	2023.1	21.6	2030.4	18.6	2030.4	18.6	99.3
IX63-63	165	41088	3.7	7.8215	2.4	5.9613	2.7	0.3382	1.3	0.47	1877.9	20.5	1970.2	23.3	2068.6	41.6	2068.6	41.6	90.8
IX63-15	201	63142	1.6	7.7932	1.5	6.5856	1.7	0.3722	0.7	0.40	2039.9	11.7	2057.4	14.6	2075.0	26.8	2075.0	26.8	98.3
IX63-14	171	37050	1.0	7.7137	1.3	6.7339	1.7	0.3767	1.2	0.67	2061.0	20.6	2077.1	15.5	2093.1	22.9	2093.1	22.9	98.5
IX63-49	121	16978	3.2	5.8804	2.5	9.6080	2.6	0.4098	0.8	0.30	2213.9	14.6	2397.9	24.1	2558.2	41.9	2558.2	41.9	86.5
IX63-47	441	106976	3.2	5.6486	2.5	12.2285	3.0	0.5010	1.6	0.53	2617.9	34.2	2622.1	28.0	2625.3	41.9	2625.3	41.9	99.7
IX63-26	288	93392	1.6	5.1366	5.9	14.0126	6.0	0.5220	1.2	0.21	2707.8	27.4	2750.6	57.1	2782.1	96.6	2782.1	96.6	97.3

Analysis	U (ppm)	206Pb 204Pb	U/Th	206Pb* 207Pb*	± (%)	207Pb* 235U*	± (%)	206Pb* 238U	± (%)	error corr.	206Pb* 238U*	± (Ma)	207Pb* 235U	± (Ma)	206Pb* 207Pb*	± (Ma)	Best age (Ma)	± (Ma)	Conc (%)
Tecolapa LAT 17° 58.305´, LONG 98° 45.949´																			
TLAP1-77	208	12971	8.2	17.7109	1.2	0.6130	1.9	0.0787	1.5	0.77	488.6	6.9	485.4	7.4	470.6	27.0	488.6	6.9	
TLAP1-36	93	5144	5.0	17.2037	1.7	0.6512	2.3	0.0812	1.6	0.69	503.6	7.8	509.2	9.3	534.5	36.7	503.6	7.8	
TLAP1-12	181	22355	4.5	17.0595	1.4	0.6925	2.7	0.0857	2.3	0.85	529.9	11.9	534.3	11.4	552.9	31.2	529.9	11.9	
TLAP1-18	243	13037	2.3	17.1672	1.5	0.6951	1.8	0.0866	1.0	0.57	535.1	5.1	535.9	7.4	539.2	31.9	535.1	5.1	
TLAP1-23	236	15182	5.2	15.9793	2.7	0.7712	2.9	0.0894	1.0	0.35	551.9	5.3	580.5	12.8	694.0	57.9	551.9	5.3	
TLAP1-33	245	18411	6.0	15.9860	1.2	0.8041	1.6	0.0932	1.0	0.63	574.6	5.5	599.1	7.2	693.1	26.4	574.6	5.5	
TLAP1-28	127	8558	4.7	15.4570	2.2	1.0831	3.3	0.1214	2.5	0.76	738.7	17.5	745.1	17.5	764.4	45.5	738.7	17.5	
TLAP1-81	87	7787	3.4	15.2594	1.3	1.1760	1.8	0.1302	1.2	0.67	788.7	8.8	789.5	9.7	791.5	27.4	788.7	8.8	
TLAP1-64	80	8774	4.5	15.2704	1.6	1.1797	2.2	0.1307	1.6	0.70	791.6	11.6	791.2	12.3	790.0	33.9	791.6	11.6	
TLAP1-49	404	40925	1.8	14.8171	1.0	1.2313	2.1	0.1323	1.9	0.88	801.1	14.2	814.9	11.9	852.9	20.9	801.1	14.2	
TLAP1-46	460	49195	3.4	15.2555	3.7	1.2210	4.2	0.1351	2.0	0.48	816.8	15.3	810.2	23.3	792.0	77.0	816.8	15.3	
TLAP1-38	309	23149	5.3	14.6981	1.9	1.2930	2.9	0.1378	2.2	0.75	832.4	16.9	842.6	16.5	869.6	39.7	832.4	16.9	
TLAP1-35	169	9718	3.0	13.4079	4.1	1.4204	5.8	0.1381	4.1	0.71	834.0	32.2	897.5	34.6	1057.3	82.3	834.0	32.2	
TLAP1-41	774	47299	1.7	14.7289	1.7	1.3655	2.0	0.1459	1.0	0.51	877.7	8.2	874.2	11.5	865.3	35.1	877.7	8.2	
TLAP1-47	175	21196	2.6	13.5230	1.2	1.5016	2.2	0.1473	1.8	0.83	885.7	15.0	931.0	13.3	1040.0	24.4	885.7	15.0	
TLAP1-6	218	18219	4.7	13.8238	1.2	1.4808	4.4	0.1485	4.2	0.96	892.4	35.1	922.6	26.6	995.5	25.2	892.4	35.1	
TLAP1-83	135	39814	3.5	14.1861	1.9	1.4543	2.2	0.1496	1.1	0.49	898.9	9.0	911.7	13.1	942.7	38.7	898.9	9.0	
TLAP1-90	272	19909	1.1	12.9269	1.0	1.6001	2.3	0.1500	2.0	0.89	901.1	17.0	970.3	14.1	1130.4	20.3	901.1	17.0	
TLAP1-100	326	34425	3.9	13.4500	1.6	1.5394	1.9	0.1502	1.0	0.52	901.9	8.4	946.3	11.9	1051.0	33.2	901.9	8.4	
TLAP1-16	190	16862	1.4	14.2165	1.4	1.4583	1.8	0.1504	1.2	0.64	903.0	9.9	913.3	11.0	938.3	28.7	903.0	9.9	
TLAP1-37	57	8591	5.0	14.3609	1.9	1.4490	2.3	0.1509	1.2	0.52	906.1	10.1	909.5	13.7	917.5	40.1	906.1	10.1	
TLAP1-30	118	16874	5.2	13.8947	1.7	1.4983	2.2	0.1510	1.4	0.62	906.5	11.6	929.7	13.4	985.1	34.8	906.5	11.6	
TLAP1-27	71	10706	4.2	14.2101	1.8	1.5130	2.0	0.1559	1.0	0.49	934.1	8.7	935.6	12.4	939.2	36.1	934.1	8.7	
TLAP1-42	234	15958	2.6	12.4607	1.7	1.7524	3.6	0.1584	3.2	0.89	947.7	28.5	1028.1	23.6	1203.2	33.3	947.7	28.5	
TLAP1-98	342	45796	4.3	13.9021	2.0	1.5886	2.6	0.1602	1.7	0.64	957.7	15.0	965.7	16.5	984.0	41.6	957.7	15.0	
TLAP1-86	469	59963	5.9	13.7792	1.6	1.6064	1.9	0.1605	1.0	0.54	959.8	8.9	972.7	11.7	1002.0	31.9	959.8	8.9	
TLAP1-40	469	41096	2.3	14.0820	1.3	1.6031	1.8	0.1637	1.2	0.69	977.5	11.1	971.4	11.0	957.8	25.9	977.5	11.1	
TLAP1-99	107	21982	3.7	12.5495	1.1	1.8216	2.0	0.1658	1.7	0.84	988.9	15.8	1053.2	13.4	1189.2	22.0	988.9	15.8	
TLAP1-63	192	22482	2.3	13.3482	1.0	1.7213	1.6	0.1666	1.3	0.78	993.5	11.5	1016.5	10.3	1066.2	20.1	993.5	11.5	
TLAP1-82	351	37460	0.8	13.8515	1.7	1.6640	2.3	0.1672	1.5	0.67	996.5	14.2	994.9	14.7	991.4	35.1	996.5	14.2	
TLAP1-76	72	12481	1.5	13.6481	1.3	1.7050	1.8	0.1688	1.3	0.69	1005.3	11.7	1010.4	11.7	1021.4	26.8	1005.3	11.7	
TLAP1-61	340	49056	8.0	13.5456	1.1	1.7277	2.7	0.1697	2.4	0.91	1010.6	22.4	1018.9	17.1	1036.7	22.8	1010.6	22.4	
TLAP1-91	30	3856	2.3	13.5245	2.6	1.7567	2.8	0.1723	1.0	0.36	1024.9	9.5	1029.7	18.0	1039.8	52.4	1024.9	9.5	
TLAP1-19	415	44894	11.0	13.0812	1.3	1.8198	1.7	0.1727	1.2	0.67	1026.7	10.9	1052.6	11.2	1106.7	25.4	1026.7	10.9	
TLAP1-62	349	55091	3.9	13.4317	1.5	1.7788	1.8	0.1733	1.0	0.55	1030.2	9.5	1037.7	11.7	1053.7	30.3	1030.2	9.5	
TLAP1-9	86	13072	1.7	13.4550	1.4	1.7835	3.4	0.1740	3.1	0.90	1034.3	29.2	1039.5	22.0	1050.2	29.1	1034.3	29.2	
TLAP1-57	253	47082	4.1	13.0504	1.3	1.8449	2.0	0.1746	1.5	0.77	1037.5	14.8	1061.6	13.2	1111.5	25.5	1037.5	14.8	
TLAP1-94	186	19018	4.3	12.8203	1.8	1.8794	4.9	0.1747	4.5	0.93	1038.2	43.2	1073.8	32.2	1146.9	36.5	1038.2	43.2	
TLAP1-60	18	6610	1.7	12.9148	4.9	1.8870	5.0	0.1768	1.0	0.20	1049.2	9.7	1076.5	33.3	1132.3	97.9	1049.2	9.7	
TLAP1-55	207	56721	1.9	13.3268	1.0	1.8383	2.2	0.1777	2.0	0.89	1054.3	19.4	1059.2	14.7	1069.5	20.6	1054.3	19.4	
TLAP1-67	286	27570	4.1	13.0971	1.3	1.8831	2.5	0.1789	2.2	0.87	1060.8	21.2	1075.2	16.6	1104.3	25.0	1060.8	21.2	
TLAP1-73	56	14970	1.5	13.2298	1.6	1.8723	1.8	0.1796	1.0	0.54	1065.1	9.8	1071.3	12.2	1084.1	31.1	1065.1	9.8	
TLAP1-3	119	17274	2.2	12.7584	2.0	1.9651	2.2	0.1818	1.0	0.46	1077.0	9.9	1103.6	14.8	1156.5	38.7	1077.0	9.9	
TLAP1-59	126	17299	2.7	12.7199	1.4	1.9817	1.7	0.1828	1.0	0.57	1082.3	10.0	1109.3	11.8	1162.5	28.3	1082.3	10.0	
TLAP1-50	151	21086	1.8	12.8337	2.7	1.9743	3.2	0.1838	1.7	0.52	1087.5	16.8	1106.8	21.6	1144.8	54.3	1087.5	16.8	
TLAP1-70	400	105325	3.1	13.0601	1.0	1.9483	1.4	0.1845	1.0	0.71	1091.8	10.0	1097.9	9.5	1110.0	20.0	1091.8	10.0	
TLAP1-25	157	11405	4.2	12.7948	1.4	2.0170	1.7	0.1872	1.0	0.59	1106.0	10.2	1121.3	11.6	1150.8	27.5	1106.0	10.2	
TLAP1-89	224	29813	1.6	12.8955	1.0	2.0147	1.4	0.1884	1.0	0.71	1112.9	10.2	1120.5	9.6	1135.3	20.0	1112.9	10.2	
TLAP1-2	309	61918	4.2	13.1466	1.1	2.0174	1.6	0.1924	1.1	0.72	1134.1	11.9	1121.4	10.8	1096.8	22.0	1134.1	11.9	
TLAP1-92	324	128971	3.2	12.7385	1.2	2.0875	1.5	0.1929	1.0	0.65	1136.9	10.4	1144.7	10.6	1159.6	23.5	1136.9	10.4	
TLAP1-93	90	12847	2.4	12.3895	1.4	2.1545	1.8	0.1936	1.2	0.65	1140.8	12.5	1166.5	12.8	1214.5	27.6	1140.8	12.5	
TLAP1-20	844	59942	2.7	12.6435	2.1	2.1287	3.3	0.1952	2.5	0.76	1149.5	26.2	1158.1	22.7	1174.4	42.4	1149.5	26.2	
TLAP1-26	53	7100	4.1	12.6564	2.2	2.1327	2.7	0.1958	1.6	0.59	1152.5	17.0	1159.4	19.0	1172.4	43.9	1152.5	17.0	
TLAP1-97	151	37781	4.4	12.5470	1.1	2.1539	1.5	0.1960	1.0	0.66	1153.8	10.6	1166.3	10.4	1189.6	22.2	1153.8	10.6	
TLAP1-71	270	34422	4.6	12.7995	1.2	2.1171	1.6	0.1965	1.0	0.65	1156.7	10.6	1154.4	10.7	1150.1	23.5	1156.7	10.6	
TLAP1-66	165	48615	2.9	12.6261	2.1	2.1482	3.1	0.1967	2.2	0.72	1157.7	23.6	1164.5	21.4	1177.1	42.4	1157.7	23.6	
TLAP1-10	773	123106	5.3	12.8826	1.0	2.1059	1.4	0.1968	1.0	0.71	1157.9	10.6	1150.7	9.7	1137.3	19.9	1157.9	10.6	
TLAP1-17	418	49907	5.9	12.8571	1.7	2.1109	1.9	0.1968	1.0	0.52	1158.3	10.6	1152.4	13.3	1141.2	32.8	1158.3	10.6	
TLAP1-88	205	35929	2.9	12.7260	1.0	2.1662	1.4	0.1999	1.0	0.71	1175.0	10.7	1170.3	9.8	1161.5	19.9	1175.0	10.7	
TLAP1-15	113	21950	3.6	12.3338	1.2	2.2353	1.6	0.2000	1.0	0.63	1175.1	10.7	1192.2	11.2	1223.3	24.3	1175.1	10.7	
TLAP1-65	140	23385	2.5	12.7671	1.5	2.1743	1.8	0.2013	1.0	0.55	1182.4	10.8	1172.8	12.7	1155.1	30.4	1182.4	10.8	
TLAP1-14	463	103447	5.9	12.6496	1.3	2.1952	1.7	0.2014	1.2	0.68	1182.8	12.8	1179.5	12.1	1173.5	25.3	1182.8	12.8	
TLAP1-22	170	23223	4.0	12.3821	1.9	2.2471	2.3	0.2018	1.2	0.53	1185.0	13.3	1195.9	16.2	1215.6	38.3	1185.0	13.3	
TLAP1-5	280	30196	3.3	11.6003	1.0	2.4089	1.8	0.2027	1.5	0.83	1189.6	16.5	1245.2	13.1	1342.8	19.4	1189.6	16.5	
TLAP1-79	171	5613	1.2	11.7279	1.5	2.3835	1.9	0.2027	1.2	0.60	1190.0	12.5	1237.7	13.8	1321.6	30.0	1190.0	12.5	
TLAP1-69	287	50400	3.5	12.4161	2.8	2.2543	3.0	0.2030	1.0	0.34	1191.4	10.9	1198.1	21.0	1210.2	55.3	1191.4	10.9	
TLAP1-39	137	15606	5.2	12.2652	1.9	2.2867	2.1	0.2034	1.0	0.47	1193.6	10.9	1208.2	14.9	1234.3	36.4	1193.6	10.9	
TLAP1-58	641	93792	3.0	12.8676	1.3	2.1809	1.6	0.2035	1.0	0.61	1194.3	10.9	1175.0	11.4	1139.6	25.7	1194.3	10.9	
TLAP1-4	61	9707	3.3	12.3225	1.9	2.2938	2.2	0.2050	1.0	0.46	1202.1	11.0	1210.4	15.4	1225.1	38.0	1202.1	11.0	

Analysis	U (ppm)	206Pb 204Pb	U/Th	206Pb* 207Pb*	± (%)	207Pb* 235U*	± (%)	206Pb* 238U	± (%)	error corr.	206Pb* 238U*	± (Ma)	207Pb* 235U	± (Ma)	206Pb* 207Pb*	± (Ma)	Best age (Ma)	± (Ma)	Conc (%)
TLAP1-96	101	18292	3.3	12.4299	2.2	2.2940	2.4	0.2068	1.0	0.41	1211.7	11.0	1210.4	17.2	1208.1	43.7	1211.7	11.0	
TLAP1-8	572	57209	5.8	12.7020	1.4	2.2496	1.8	0.2072	1.0	0.57	1214.1	11.1	1196.7	12.3	1165.3	28.5	1214.1	11.1	
TLAP1-34	634	116515	3.1	12.4731	1.1	2.2990	1.5	0.2080	1.0	0.67	1218.0	11.1	1212.0	10.5	1201.2	21.7	1218.0	11.1	
TLAP1-78	431	63312	1.6	12.3828	1.0	2.3209	2.0	0.2084	1.8	0.87	1220.5	19.5	1218.7	14.3	1215.5	19.7	1220.5	19.5	
TLAP1-72	77	12019	3.6	12.1244	2.3	2.3806	2.8	0.2093	1.5	0.56	1225.3	17.2	1236.8	19.8	1256.9	44.9	1225.3	17.2	
TLAP1-85	223	31291	3.5	12.5835	2.7	2.2942	3.2	0.2094	1.7	0.53	1225.5	18.6	1210.5	22.5	1183.8	53.4	1225.5	18.6	
TLAP1-1	175	54054	6.4	12.0610	1.2	2.4006	2.7	0.2100	2.4	0.88	1228.8	26.4	1242.8	19.1	1267.1	24.3	1228.8	26.4	
TLAP1-45	370	47743	2.2	12.3861	1.3	2.3925	1.7	0.2149	1.0	0.60	1255.0	11.4	1240.4	11.9	1215.0	26.2	1255.0	11.4	
TLAP1-11	353	78362	2.8	12.2524	1.2	2.4424	1.6	0.2170	1.0	0.63	1266.2	11.5	1255.2	11.4	1236.3	24.0	1266.2	11.5	
TLAP1-95	146	16620	4.3	11.7419	1.2	2.5508	1.9	0.2172	1.4	0.77	1267.2	16.5	1286.7	13.6	1319.3	23.0	1267.2	16.5	
TLAP1-87	253	51704	1.8	11.7457	4.4	2.5919	5.1	0.2208	2.5	0.49	1286.1	28.9	1298.3	37.3	1318.7	86.1	1286.1	28.9	
TLAP1-52	31	5428	0.8	11.8294	2.1	2.5922	2.3	0.2224	1.0	0.44	1294.5	11.7	1298.4	16.8	1304.9	39.9	1294.5	11.7	
TLAP1-54	480	92969	2.5	11.9077	1.0	2.5778	1.4	0.2226	1.0	0.71	1295.7	11.7	1294.3	10.4	1292.1	19.5	1295.7	11.7	
TLAP1-29	227	29272	2.0	11.7584	1.2	2.6166	1.6	0.2231	1.0	0.63	1298.5	11.8	1305.3	11.7	1316.6	24.1	1298.5	11.8	
TLAP1-68	172	16328	1.4	11.7776	1.0	2.6420	1.4	0.2257	1.0	0.70	1311.8	11.9	1312.4	10.5	1313.4	19.6	1311.8	11.9	
TLAP1-13	257	50878	1.9	11.7324	1.3	2.6905	1.8	0.2289	1.2	0.67	1329.0	14.2	1325.9	13.0	1320.8	25.3	1329.0	14.2	
TLAP1-53	402	28354	1.3	11.4705	3.2	2.7833	3.3	0.2315	1.0	0.30	1342.6	12.1	1351.1	25.0	1364.5	61.5	1342.6	12.1	
TLAP1-32	453	66681	3.3	11.5802	1.0	2.7796	1.9	0.2334	1.6	0.84	1352.6	19.3	1350.1	14.0	1346.1	19.3	1352.6	19.3	
TLAP1-56	367	139485	2.4	11.8540	1.0	2.7329	1.4	0.2350	1.0	0.71	1360.4	12.3	1337.4	10.5	1300.8	19.4	1360.4	12.3	
TLAP1-7	194	23303	1.8	11.2106	2.2	2.9906	4.5	0.2432	3.9	0.87	1403.1	49.3	1405.2	34.2	1408.5	42.6	1403.1	49.3	
TLAP1-44	71	16109	4.7	10.8807	2.6	3.1262	2.8	0.2467	1.0	0.36	1421.5	12.8	1439.2	21.2	1465.4	48.8	1421.5	12.8	
TLAP1-51	289	59000	1.3	11.0696	1.0	3.1476	1.6	0.2527	1.3	0.79	1452.4	16.6	1444.4	12.5	1432.7	19.1	1452.4	16.6	
TLAP1-43	130	24324	4.1	10.4979	1.9	3.6346	2.2	0.2767	1.0	0.46	1574.9	14.0	1557.1	17.3	1533.1	36.4	1574.9	14.0	
TLAP1-31	373	73497	2.1	10.3022	1.0	3.7084	2.8	0.2771	2.6	0.94	1576.7	36.9	1573.2	22.6	1568.5	18.7	1576.7	36.9	
TLAP1-74	184	59074	2.9	9.2795	1.3	4.4581	1.9	0.3000	1.5	0.76	1691.5	22.0	1723.2	16.1	1762.0	22.9	1691.5	22.0	
TLAP1-75	87	16325	1.4	9.6676	1.3	4.2822	1.8	0.3002	1.3	0.71	1692.5	19.1	1689.9	14.9	1686.7	23.7	1692.5	19.1	
TLAP1-84	392	63091	7.3	9.1632	1.0	4.5945	1.7	0.3053	1.4	0.80	1717.7	20.8	1748.3	14.4	1785.0	19.0	1717.7	20.8	
Ix 190 UTM LAT 0537153, LONG 19878908																			
Zircon_19_029	959.9	289.5	0.3	0.05204	0.00102	0.35295	0.00906	0.04919	0.00053	0.67	310	3	307	7	287	40	310	3	99.0
Zircon_33_046	193.9	255.6	1.2	0.05277	0.00116	0.39886	0.00956	0.05481	0.00052	0.4	344	3	341	7	319	45	344	3	
Zircon_55_070	340.8	299.0	0.8	0.05401	0.00381	0.43715	0.03321	0.0587	0.00053	0.22	368	3	368	23	371	152	368	3	
Zircon_88_109	469.2	204.3	0.4	0.05613	0.00073	0.46066	0.00691	0.0595	0.00045	0.5	373	3	385	5	458	28	373	3	
Zircon_60_076	200.4	180.6	0.8	0.05788	0.0011	0.51296	0.0104	0.06426	0.00046	0.35	401	3	420	7	525	39	401	3	
Zircon_5_012	1218.5	360.2	0.3	0.05879	0.00059	0.63271	0.01089	0.0781	0.00109	0.81	485	7	498	7	559	21	485	7	102.6
Zircon_96_119	393.4	134.3	0.3	0.06116	0.0008	0.66071	0.01005	0.07847	0.00062	0.51	487	4	515	6	645	27	487	4	105.4
Zircon_46_060	268.3	217.6	0.7	0.05854	0.00076	0.63944	0.00932	0.07922	0.00052	0.45	491	3	502	6	550	27	491	3	102.2
Zircon_10_018	217.6	114.9	0.5	0.05818	0.00087	0.66847	0.01121	0.08331	0.00062	0.45	516	4	520	7	537	31	516	4	100.8
Zircon_85_105	137.1	68.7	0.5	0.05874	0.00094	0.68214	0.01249	0.08423	0.00075	0.49	521	4	528	8	558	33	521	4	101.3
Zircon_38_051	140.5	183.7	1.2	0.06286	0.00107	0.73126	0.01365	0.0848	0.00065	0.41	525	4	557	8	704	32	525	4	105.7
Zircon_56_072	554.5	227.1	0.4	0.06001	0.00078	0.70789	0.01123	0.08552	0.00078	0.57	529	5	543	7	604	26	529	5	102.6
Zircon_50_064	141.7	94.1	0.6	0.0602	0.00102	0.71665	0.01326	0.08612	0.00063	0.4	533	4	549	8	611	34	533	4	102.9
Zircon_34_047	396.1	204.2	0.5	0.06071	0.00091	0.72332	0.01197	0.08668	0.00061	0.42	536	4	553	7	629	29	536	4	103.1
Zircon_76_095	688.8	28.8	0.0	0.05842	0.0007	0.70211	0.00975	0.08714	0.00061	0.51	539	4	540	6	546	25	539	4	100.2
Zircon_8_016	317.0	106.7	0.3	0.05263	0.00063	0.63371	0.00887	0.08736	0.00063	0.52	540	4	498	6	313	26	540	4	91.6
Zircon_87_108	204.2	116.3	0.5	0.0595	0.00107	0.7203	0.01399	0.08779	0.00064	0.38	542	4	551	8	585	37	542	4	101.6
Zircon_90_111	408.7	56.3	0.1	0.05897	0.00077	0.71892	0.01224	0.08845	0.00097	0.64	546	6	550	7	566	27	546	6	100.7
Zircon_77_096	488.0	4.5	0.0	0.05769	0.00069	0.7194	0.01026	0.09047	0.0007	0.54	558	4	550	6	518	25	558	4	98.5
Zircon_2_009	231.9	786.0	3.1	0.05914	0.00077	0.74046	0.01146	0.09073	0.00076	0.54	560	4	563	7	572	25	560	4	100.5
Zircon_13_022	184.4	143.2	0.7	0.06265	0.001	0.79873	0.01422	0.09253	0.00072	0.44	570	4	596	8	696	32	570	4	104.4
Zircon_41_054	289.5	207.3	0.6	0.06093	0.00091	0.77909	0.01405	0.09296	0.00093	0.56	573	5	585	8	637	30	573	5	102.1
Zircon_7_015	262.4	79.2	0.3	0.05581	0.00073	0.71905	0.01069	0.09357	0.00067	0.48	577	4	550	6	445	28	577	4	95.1
Zircon_63_080	632.6	180.5	0.3	0.06335	0.00109	0.82205	0.01934	0.09411	0.00106	0.67	580	6	609	11	720	35	580	6	104.8
Zircon_100_123	317.3	239.0	0.7	0.06295	0.00082	0.81896	0.01263	0.09449	0.00078	0.54	582	5	607	7	707	26	582	5	104.1
Zircon_74_092	292.8	133.2	0.4	0.05999	0.0012	0.78508	0.01709	0.09482	0.00082	0.39	584	5	588	10	603	42	584	5	100.7
Zircon_66_084	298.6	382.7	1.2	0.05908	0.00083	0.77494	0.01231	0.09508	0.00071	0.47	586	4	583	7	570	29	586	4	99.5
Zircon_59_075	849.7	48.3	0.1	0.06151	0.00069	0.81817	0.01226	0.09647	0.00076	0.61	594	4	607	7	657	23	594	4	102.1
Zircon_24_035	319.7	203.5	0.6	0.05964	0.00072	0.80444	0.01138	0.09786	0.00073	0.52	602	4	599	6	591	23	602	4	99.5
Zircon_91_113	322.7	73.1	0.2	0.05941	0.00097	0.80409	0.01971	0.09816	0.00131	0.68	604	8	599	11	582	34	604	8	99.2
Zircon_40_053	337.1	108.5	0.3	0.06059	0.00073	0.82905	0.0121	0.09919	0.00082	0.56	610	5	613	7	625	24	610	5	100.5
Zircon_39_052	73.4	35.1	0.4	0.06487	0.00136	0.89461	0.02121	0.09945	0.00109	0.47	611	6	649	11	770	42	611	6	105.9
Zircon_65_082	346.0	307.6	0.8	0.0602	0.00072	0.83733	0.01212	0.10065	0.00082	0.56	618	5	618	7	611	25	618	5	100.0
Zircon_72_090	1232.7	240.3	0.2	0.06247	0.00062	0.88311	0.01249	0.10189	0.00102	0.71	625	6	643	7	690	20	625	6	102.8
Zircon_9_017	250.2	131.6	0.5	0.0548	0.00077	0.77907	0.01284	0.10308	0.0009	0.52	632	5	585	7	404	30	632	5	92.0
Zircon_82_102	136.5	40.8	0.3	0.0602	0.00096	0.91263	0.01825	0.10988	0.00132	0.6	672	8	658	10	611	33	672	8	97.9
Zircon_99_122	283.1	70.3	0.2	0.06364	0.00095	0.97942	0.01656	0.11183	0.00087	0.47	683	5	693	8	730	30	683	5	101.4
Zircon_4_011	404.0	66.1	0.1	0.06524	0.00072	1.0281	0.01335	0.11411	0.00079	0.53	697	5	718	7	782	22	697	5	102.9
Zircon_35_048	514.3	164.7	0.3	0.06527	0.00072	1.0517	0.01791	0.1158	0.00151	0.76	706	9	730	9	783	21	706	9	103.3
Zircon_81_101	63.4	44.6	0.6	0.06427	0.00135	1.026	0.02321	0.11568	0.00097	0.37	706	6	717	12	751	43	706	6	101.5

Mean = 362±39
Wtd by data-pt
MSWD = 107, p

Analysis	U (ppm)	206Pb 204Pb	U/Th	206Pb* 207Pb*	± (%)	207Pb* 235U*	± (%)	206Pb* 238U	± (%)	error corr.	206Pb* 238U*	± (Ma)	207Pb* 235U	± (Ma)	206Pb* 207Pb*	± (Ma)	Best age (Ma)	± (Ma)	Conc (%)
Zircon_70_088	579.4	143.9	0.2	0.06568	0.00072	1.0552	0.01429	0.11625	0.00092	0.59	709	5	731	7	796	22	709	5	103.0
Zircon_64_081	379.2	50.6	0.1	0.06395	0.00077	1.0624	0.0166	0.12045	0.0012	0.64	733	7	735	8	740	25	733	7	100.3
Zircon_79_098	542.6	93.1	0.2	0.06547	0.00072	1.1155	0.0146	0.12349	0.00088	0.54	751	5	761	7	789	22	751	5	101.3
Zircon_45_058	560.7	138.1	0.2	0.06336	0.00093	1.08376	0.02338	0.12406	0.00131	0.74	754	8	745	11	720	29	754	8	98.8
Zircon_57_073	823.1	170.7	0.2	0.06488	0.00087	1.11032	0.02238	0.12412	0.0013	0.74	754	7	758	11	770	26	754	7	100.5
Zircon_78_097	262.9	104.3	0.4	0.06803	0.00095	1.1804	0.01927	0.1259	0.00106	0.52	764	6	791	9	869	28	764	6	103.4
Zircon_93_115	198.9	51.0	0.2	0.06475	0.00091	1.2345	0.02198	0.13858	0.00152	0.61	837	9	816	10	766	28	837	9	97.4
Zircon_51_066	422.8	122.4	0.3	0.06771	0.001	1.30465	0.02663	0.13975	0.00128	0.69	843	7	848	12	860	29	843	7	100.6
Zircon_61_078	403.7	121.5	0.3	0.06609	0.00073	1.3029	0.0172	0.14305	0.00104	0.55	862	6	847	8	809	22	862	6	98.2
Zircon_21_032	859.6	304.5	0.3	0.06886	0.00069	1.4036	0.01842	0.14789	0.00126	0.65	889	7	890	8	895	19	889	7	100.1
Zircon_27_039	418.8	188.5	0.4	0.0702	0.00077	1.4585	0.02374	0.15027	0.0018	0.74	902	10	913	10	934	20	902	10	101.2
Zircon_23_034	644.8	54.8	0.1	0.07014	0.00069	1.4946	0.01838	0.15447	0.00113	0.6	926	6	928	7	932	18	926	6	100.2
Zircon_28_040	337.7	279.4	0.7	0.07167	0.00086	1.5487	0.02217	0.15656	0.00122	0.55	938	7	950	9	977	22	938	7	101.3
Zircon_73_091	616.2	167.7	0.2	0.07262	0.0008	1.5684	0.02171	0.15664	0.00132	0.61	938	7	958	9	1003	22	938	7	102.1
Zircon_18_028	381.3	164.4	0.4	0.07316	0.0008	1.6182	0.02881	0.1606	0.00225	0.79	960	12	977	11	1018	20	960	12	101.7
Zircon_49_063	374.2	86.6	0.2	0.07241	0.0008	1.6217	0.02097	0.16237	0.0011	0.52	970	6	979	8	997	21	970	6	100.9
Zircon_97_120	302.4	192.0	0.6	0.07185	0.00079	1.7211	0.02263	0.17371	0.00125	0.55	1033	7	1016	8	982	21	982	21	98.3
Zircon_43_056	360.7	56.0	0.1	0.07221	0.0014	1.69521	0.03794	0.17027	0.00107	0.48	1014	6	1007	14	992	37	992	37	99.3
Zircon_44_057	324.8	62.4	0.2	0.07225	0.00079	1.7814	0.02476	0.17879	0.00152	0.62	1060	8	1039	9	993	21	993	21	98.0
Zircon_89_110	246.6	96.3	0.4	0.07228	0.0008	1.7428	0.02591	0.17476	0.00175	0.67	1038	10	1025	10	994	21	994	21	98.7
Zircon_14_023	332.7	126.1	0.3	0.071	0.00078	1.6446	0.02227	0.1679	0.00133	0.58	1001	7	987	9	957	21	1001	7	98.6
Zircon_22_033	252.5	94.0	0.3	0.07292	0.0008	1.7083	0.02274	0.16977	0.00127	0.57	1011	7	1012	9	1012	20	1012	20	100.1
Zircon_80_099	428.4	104.5	0.2	0.07299	0.0008	1.7275	0.03644	0.17116	0.00308	0.85	1018	17	1019	14	1014	21	1014	21	100.1
Zircon_11_020	784.7	210.2	0.2	0.07354	0.00073	1.6749	0.02252	0.16511	0.0015	0.67	985	8	999	9	1029	19	1029	19	101.4
Zircon_62_079	274.2	197.9	0.7	0.07379	0.00089	1.798	0.02489	0.17668	0.00122	0.49	1049	7	1045	9	1036	23	1036	23	99.6
Zircon_30_042	116.4	47.2	0.4	0.07423	0.00096	1.9213	0.02819	0.18778	0.00128	0.47	1109	7	1089	10	1048	23	1048	23	98.2
Zircon_25_036	220.5	94.8	0.4	0.07445	0.00089	1.814	0.02548	0.17667	0.00129	0.53	1049	7	1051	9	1054	22	1054	22	100.2
Zircon_54_069	259.8	246.5	0.9	0.0754	0.0009	1.7888	0.02662	0.17197	0.00151	0.6	1023	8	1041	10	1079	22	1079	22	101.7
Zircon_36_049	158.6	56.1	0.3	0.07565	0.00098	1.7449	0.02862	0.16738	0.00167	0.61	998	9	1025	11	1086	23	1086	23	102.6
Zircon_92_114	107.7	69.1	0.6	0.07569	0.00114	2.0898	0.03767	0.20138	0.00201	0.55	1183	11	1145	12	1087	29	1087	29	96.7
Zircon_32_045	139.4	136.2	0.9	0.07907	0.00087	2.2197	0.02894	0.20339	0.00142	0.54	1194	8	1187	9	1174	20	1174	20	99.4
Zircon_84_104	338.6	82.9	0.2	0.07928	0.00087	2.1019	0.02922	0.19164	0.00163	0.61	1130	9	1149	10	1179	21	1179	21	101.7
Zircon_37_050	237.5	82.0	0.3	0.0863	0.00135	2.51849	0.04775	0.21167	0.00156	0.56	1238	8	1277	14	1345	27	1345	27	103.1
Zircon_16_026	59.8	48.1	0.7	0.08683	0.00156	2.3866	0.04814	0.19984	0.00182	0.45	1174	10	1239	14	1357	31	1357	31	105.2
Zircon_20_030	307.5	334.7	1.0	0.08958	0.00099	3.0571	0.04105	0.24732	0.0019	0.57	1425	10	1422	10	1417	19	1417	19	99.8
Zircon_83_103	285.7	97.4	0.3	0.09522	0.00105	3.3568	0.05464	0.25475	0.00306	0.74	1463	16	1494	13	1532	20	1532	20	102.1
Zircon_31_044	829.4	55.4	0.1	0.10054	0.001	3.2224	0.04534	0.23185	0.00232	0.71	1344	12	1463	11	1634	17	1634	17	108.1
Zircon_26_038	468.8	361.8	0.7	0.10436	0.00104	4.0513	0.0556	0.28097	0.00264	0.69	1596	13	1645	11	1703	16	1703	16	103.0
Zircon_42_055	314.4	177.4	0.5	0.1066	0.00175	4.26511	0.09344	0.29019	0.00253	0.62	1642	13	1687	18	1742	28	1742	28	102.7
Zircon_IX193_1_00	72.1	74.6	0.9	0.11225	0.00135	5.0495	0.072	0.32611	0.00251	0.54	1819	12	1828	12	1836	21	1836	21	100.5
Zircon_71_089	395.8	283.7	0.6	0.11771	0.00129	4.9894	0.06757	0.3079	0.00243	0.59	1730	12	1818	11	1922	19	1922	19	104.8
Zircon_69_087	318.7	111.4	0.3	0.11805	0.00118	5.0822	0.07555	0.31219	0.00343	0.74	1751	17	1833	13	1927	17	1927	17	104.5
Zircon_75_093	238.7	169.4	0.6	0.11859	0.00119	5.7131	0.06909	0.34937	0.00238	0.56	1932	11	1933	10	1935	17	1935	17	100.1
Zircon_95_117	82.1	193.3	2.1	0.11948	0.00143	5.7534	0.0877	0.34951	0.00329	0.62	1932	16	1939	13	1948	20	1948	20	100.4
Zircon_48_062	104.2	6.0	0.1	0.1214	0.00158	4.7006	0.07681	0.2794	0.00277	0.6	1588	14	1767	14	1977	22	1977	22	110.1
Zircon_52_067	486.0	200.7	0.4	0.12734	0.00155	6.02449	0.10349	0.34313	0.00287	0.65	1902	14	1979	15	2062	20	2062	20	103.9
Zircon_17_027	505.6	303.1	0.5	0.1383	0.00187	7.56111	0.13498	0.39651	0.00316	0.63	2153	15	2180	16	2206	21	2206	21	101.2
Zircon_67_085	208.9	112.1	0.5	0.13943	0.00139	6.162	0.08208	0.32031	0.00282	0.66	1791	14	1999	12	2220	17	2220	17	110.4
Zircon_29_041	117.5	74.7	0.6	0.17655	0.00194	12.14683	0.19049	0.499	0.00435	0.59	2609	19	2616	15	2621	17	2621	17	100.3
Zircon_15_024	316.5	192.5	0.5	0.18311	0.00219	12.31653	0.18662	0.48784	0.00324	0.55	2561	14	2629	14	2681	18	2681	18	102.6
Zircon_68_086	276.6	47.5	0.2	0.18433	0.00177	11.566	0.13474	0.45455	0.003	0.57	2415	13	2570	11	2692	15	2692	15	106.0
Zircon_53_068	499.2	64.8	0.1	0.18754	0.00186	12.754	0.20841	0.49268	0.0064	0.79	2582	28	2662	15	2721	16	2721	16	103.0
Zircon_94_116	157.5	75.5	0.4	0.19103	0.00183	13.411	0.15777	0.50891	0.00346	0.58	2652	15	2709	11	2751	15	2751	15	102.1
Zircon_47_061	346.0	274.9	0.7	0.26864	0.0025	24.757	0.29891	0.66848	0.00515	0.64	3300	20	3299	12	3298	14	3298	14	100.0
Ix 280 UTM: LAT 0520929, LONG 1989265																			
Zircon_39_051	927.3	455.3	0.4	0.06248	0.00106	0.56532	0.01282	0.06587	0.00099	0.66	411	6	455	8	691	32	411	6	109.7
Zircon_68_084	369.9	169.0	0.4	0.05939	0.00274	0.54015	0.02878	0.06596	0.00099	0.51	412	6	439	19	581	100	412	6	106.2
Zircon_30_040	330.4	153.6	0.4	0.06087	0.0043	0.55518	0.04185	0.06615	0.00075	0.28	413	5	448	27	635	136	413	5	107.8
Zircon_22_031	507.4	320.6	0.6	0.05831	0.0007	0.55012	0.00896	0.06855	0.00075	0.68	427	5	445	6	541	25	427	5	104.0
Zircon_25_034	863.1	318.0	0.3	0.06259	0.00218	0.59637	0.02484	0.06911	0.00081	0.65	431	5	475	16	694	72	431	5	109.3
Zircon_8_015	569.6	448.6	0.7	0.05825	0.00076	0.55736	0.01238	0.0696	0.00125	0.81	434	8	450	8	539	28	434	8	103.6
Zircon_31_042	561.8	253.3	0.4	0.05561	0.00311	0.53764	0.03399	0.07012	0.0011	0.46	437	7	437	22	437	111	437	7	100.0
Zircon_44_057	253.9	180.8	0.6	0.05933	0.00967	0.57855	0.09903	0.07072	0.00114	0.14	441	7	464	64	579	322	441	7	105.0
Zircon_7_014	233.9	164.3	0.6	0.05827	0.00266	0.56874	0.02935	0.0708	0.00077	0.54	441	5	457	19	540	100	441	5	103.5
Zircon_42_055	868.0	421.2	0.4	0.06034	0.00203	0.60079	0.02511	0.07222	0.00105	0.55	450	6	478	16	616	64	450	6	105.9
Zircon_18_027	433.6	280.9	0.6	0.05885	0.00077	0.59251	0.00901	0.07336	0.00058	0.51	456	3	472	6	562	28	456	3	103.4
Zircon_66_082	377.8	112.1	0.3	0.06194	0.00195	0.62576	0.02217	0.07327	0.00069	0.52	456	4	493	14	672	60	456	4	107.5
Zircon_4_011	205.3	50.3	0.2	0.0587	0.001	0.59633	0.01133	0.07384	0.00063	0.44	459	4	475	7	556	33	459	4	103.4
Zircon_38_050	335.9	227.1	0.6	0.05821	0.00099	0.60888	0.01233	0.07613	0.00084	0.54	473	5	483	8	538	33	473	5	102.1

Analysis	U (ppm)	206Pb 204Pb	U/Th	206Pb* 207Pb*	± (%)	207Pb* 235U*	± (%)	206Pb* 238U	± (%)	error corr.	206Pb* 238U*	± (Ma)	207Pb* 235U	± (Ma)	206Pb* 207Pb*	± (Ma)	Best age (Ma)	± (Ma)	Conc (%)
Zircon_IX280_1_008	178.9	81.8	0.4	0.05484	0.00104	0.57464	0.01196	0.07636	0.00065	0.41	474	4	461	8	406	42	474	4	97.2
Zircon_2_009	301.6	152.8	0.5	0.05814	0.00087	0.62425	0.01102	0.07813	0.00073	0.53	485	4	493	7	535	32	485	4	101.6
Zircon_73_090	533.9	131.9	0.2	0.05862	0.00161	0.635	0.0209	0.07857	0.00097	0.6	488	6	499	13	553	59	488	6	102.2
Zircon_64_079	268.2	139.3	0.5	0.06027	0.00096	0.6528	0.01192	0.07875	0.00069	0.49	489	4	510	7	613	30	489	4	104.1
Zircon_16_025	350.9	385.2	1.0	0.05869	0.00117	0.63972	0.01383	0.07891	0.00065	0.39	490	4	502	9	556	42	490	4	102.4
Zircon_70_086	798.3	340.6	0.4	0.06542	0.00786	0.71278	0.08903	0.07902	0.0009	0.2	490	5	546	53	788	264	490	5	110.3
Zircon_43_056	441.1	327.8	0.7	0.0574	0.0008	0.63202	0.01069	0.08001	0.00076	0.57	496	5	497	7	507	27	496	5	100.2
Zircon_40_052	272.5	132.6	0.4	0.06241	0.00106	0.6902	0.01334	0.0809	0.00074	0.48	501	4	533	8	688	32	501	4	106.0
Zircon_72_089	351.4	167.5	0.4	0.05891	0.00118	0.65807	0.01502	0.08108	0.00089	0.48	503	5	513	9	564	43	503	5	101.9
Zircon_74_091	444.7	239.2	0.5	0.06162	0.00092	0.70042	0.01225	0.08233	0.00074	0.52	510	4	539	7	661	32	510	4	105.4
Zircon_51_066	324.4	411.0	1.2	0.06378	0.00466	0.72664	0.05801	0.08262	0.00117	0.23	512	7	555	34	734	138	512	7	107.7
Zircon_55_070	141.3	104.0	0.7	0.06226	0.00156	0.71635	0.02019	0.08385	0.00109	0.46	519	6	549	12	683	47	519	6	105.5
Zircon_52_067	216.0	27.8	0.1	0.05983	0.00096	0.69289	0.01269	0.08423	0.00075	0.48	521	4	535	8	597	31	521	4	102.6
Zircon_62_078	226.5	208.9	0.8	0.06074	0.01242	0.72223	0.15744	0.08623	0.00206	0.2	533	12	552	93	630	399	533	12	103.4
Zircon_59_075	939.7	50.2	0.0	0.06151	0.00094	0.75374	0.01558	0.08887	0.00105	0.68	549	6	570	9	657	29	549	6	103.7
Zircon_3_010	298.4	261.6	0.8	0.05805	0.00081	0.72232	0.01214	0.09046	0.00084	0.56	558	5	552	7	532	27	558	5	98.9
Zircon_26_036	416.4	591.3	1.3	0.06753	0.00088	0.84607	0.01377	0.09113	0.00089	0.6	562	5	622	8	854	26	562	5	109.6
Zircon_12_020	111.8	54.1	0.4	0.05933	0.00119	0.74277	0.01695	0.09125	0.001	0.48	563	6	564	10	579	42	563	6	100.2
Zircon_24_033	383.0	340.0	0.8	0.05885	0.003	0.76898	0.04445	0.09476	0.00107	0.48	584	6	579	26	562	107	584	6	99.1
Zircon_19_028	371.4	106.4	0.3	0.06025	0.00118	0.79076	0.01942	0.09518	0.00092	0.57	586	5	592	11	613	41	586	5	101.0
Zircon_6_013	719.2	113.7	0.1	0.06116	0.00073	0.80203	0.01198	0.09529	0.00085	0.6	587	5	598	7	645	23	587	5	101.8
Zircon_46_060	333.3	78.6	0.2	0.06429	0.00084	0.85312	0.0163	0.09627	0.00135	0.73	593	8	626	9	751	24	593	8	105.3
Zircon_54_069	375.6	301.7	0.7	0.05827	0.00087	0.77795	0.01341	0.09748	0.00083	0.5	600	5	584	8	540	29	600	5	97.3
Zircon_41_054	413.1	30.2	0.1	0.06284	0.00147	0.87826	0.02407	0.10137	0.0012	0.54	622	7	640	13	703	44	622	7	102.8
Zircon_65_080	49.2	53.8	1.0	0.06561	0.00184	0.91659	0.02869	0.10187	0.00143	0.44	625	8	661	15	794	52	625	8	105.4
Zircon_71_088	280.4	54.2	0.2	0.06222	0.00144	0.90462	0.02448	0.10545	0.00107	0.53	646	6	654	13	682	49	646	6	101.2
Zircon_17_026	124.6	132.3	1.0	0.06739	0.00108	0.99577	0.01781	0.10788	0.00086	0.44	660	5	702	9	850	32	660	5	106.0
Zircon_27_037	336.0	538.5	1.5	0.06591	0.00079	1.0835	0.01692	0.11936	0.00119	0.64	727	7	745	8	804	22	727	7	102.4
Zircon_47_061	561.4	274.7	0.4	0.06423	0.00196	1.15106	0.04839	0.12997	0.00217	0.8	788	12	778	23	749	57	788	12	98.7
Zircon_53_068	120.9	145.3	1.1	0.07051	0.00371	1.34465	0.08193	0.1383	0.0018	0.46	835	10	865	35	943	96	835	10	103.5
Zircon_67_083	241.8	98.8	0.4	0.06818	0.00156	1.33106	0.03811	0.14159	0.00147	0.64	854	8	859	17	874	47	854	8	100.6
Zircon_60_076	191.1	184.8	0.9	0.07496	0.00135	1.5509	0.03735	0.15031	0.0024	0.66	903	13	951	15	1067	32	903	13	105.0
Zircon_36_048	347.0	121.1	0.3	0.07049	0.00092	1.5246	0.02319	0.15698	0.00124	0.51	940	7	940	9	943	24	940	7	100.0
Zircon_11_019	173.5	158.0	0.8	0.08808	0.00106	2.8968	0.04194	0.23888	0.00193	0.56	1381	10	1381	11	1384	22	1384	22	100.0
Zircon_34_045	385.7	585.3	1.4	0.09393	0.00418	3.33491	0.17681	0.25749	0.00304	0.64	1477	16	1489	41	1507	75	1507	75	100.8
Zircon_28_038	253.3	111.6	0.4	0.0941	0.00222	2.60313	0.08118	0.20062	0.00256	0.68	1179	14	1302	23	1510	39	1510	39	109.4
Zircon_23_032	454.3	212.2	0.4	0.09424	0.00222	2.76464	0.09351	0.21276	0.00316	0.79	1243	17	1346	25	1513	43	1513	43	107.7
Zircon_69_085	190.7	106.1	0.5	0.09557	0.00124	3.246	0.05528	0.24617	0.00271	0.65	1419	14	1468	13	1539	24	1539	24	103.3
Zircon_15_023	231.1	125.5	0.5	0.09805	0.00202	3.51492	0.11529	0.26001	0.00434	0.8	1490	22	1531	26	1587	37	1587	37	102.7
Zircon_35_046	794.5	240.3	0.3	0.10467	0.00201	2.59367	0.10333	0.17972	0.00476	0.91	1065	26	1299	29	1708	31	1708	31	118.0